DIMETHYLSULPHIDE AND AMMONIA IN REMOTE MARINE REGIONS - AN ATLANTIC MERIDIONAL TRANSECT STUDY

Thomas G. Bell

A thesis presented to the School of Environmental Sciences, University of East Anglia, in candidature for the degree of Doctor of Philosophy

September 2006

ABSTRACT

The NERC Atlantic Meridional Transect (AMT) programme involves a biannual UK-Falklands research transect and has facilitated detailed study of the Atlantic's oligotrophic gyres. Dimethylsulphide (DMS) and dimethylsulphoniopropionate (dissolved and particulate, DMSPd and DMSPp) were depth profiled on cruises throughout 2001-03 (AMT-12, -13 and -14) and combined with data previously collected by Conor McKee (AMT-5 and -9). Ambient surface DMS concentrations were low (1.0 nM mean; 0.01 – 13.4 nM range), while fluxes were variable (0.4 – 12.2 µmol m^{-2} day^{-1}). The dataset was interpreted in conjunction with ancillary data such as accessory pigments, carbon fixation rates, bacterial numbers and DMSP-lyase activity as available. As expected, DMS and DMSPp correlated poorly with an indicator of biomass (chlorophyll *a*). However, significant positive correlations with carbon fixation rates (primary production) were observed. When divided into biogeochemical provinces (Longhurst, 1995) it became clear that such regions are not homogeneous and caution should be exercised when extrapolating measured data to these scales. When compared with values from predictive models, measured surface DMS concentrations were found to be lower. During AMT-14, the *in vitro* activity of the enzyme responsible for DMS production (DMSP-lyase) was often substantially higher at the surface compared to the chlorophyll maximum. These results provide some support for the proposed protective role of DMS and related parameters during periods of oxidative stress.

Atmospheric gas (ammonia, NH_3) and aerosol measurements were made throughout AMT-12, -13 and -14. Results suggest that the NH_3 flux is finely balanced between *in* and *out* of the ocean in low latitudes (flux range between -7.3 and 24.8 µmol m^{-2} day^{-1}). The potential for a flux out of the ocean is surprising given the low seawater ammonium concentrations in such regions. The submicron ammonium to non-sea-salt sulphate (NH_4^+:$nssSO_4^{2-}$) ratio in remote marine aerosol was consistently greater than 1:1 (i.e. between partially and fully neutralised). However, little correlation was apparent between DMS and NH_3 for either sea-to-air fluxes or oceanic concentrations. Studies from around the globe consistently produce a mean NH_4^+:$nssSO_4^{2-}$ aerosol ratio between 1:1 and 2:1, but the degree of variation in individual samples suggests that it may be driven purely by variations in source strength of NH_3 and $nssSO_4^{2-}$.

LIST OF CONTENTS

LIST OF TABLES

LIST OF FIGURES

ACKNOWLEDGEMENTS

Supervision is easy to say but a lot more difficult and time-consuming to carry out. I thank my supervisors Gill Malin, Tim Jickells, Alex Baker and Peter Liss, for providing so much help and encouragement with unrivalled enthusiasm, even when it was the fifth time I'd arrived at their office door that afternoon! Thank you all for your immense patience and good humour – it's kept me interested even when I felt like I wasn't.

One of the reasons this department works well is that graduate students don't feel they are locked away from other researchers. I have been helped by so many people for so little in return that it blows my mind. Thank you to Michael Steinke and Sue Turner, especially for your tireless patience teaching me how to operate the purge and trap system. Thanks to Alastair Grant for invaluable advice on the various statistics I did and did not use. With Jamie Kettle I enjoyed many complex theoretical discussions that have been invaluable – thank you, I followed at least half of them! Thank you also to Manuela Martino and Keith Weston for helpful information and advice.

I also thank my peers – those beginning, those ending and those who have finished their PhDs. Susa Kadner, Claire Hughes and Louise Darroch – my laboratory buddies and major source of information and help during the first couple of years. Martin Johnson, a true academic inspiration and enthusiastic colleague throughout the past 4 years – I hope we can continue to work together. Andy Hind, my UEA AMT buddy – how different the cruises would have been without you! I will never be able to think about elephants and tea in the same way. I've had many office mates, but a particular thank you to Rosie Chance (a welcome new face and lab mate just when I needed it), Manfredi Manizza, Rose Chambers, Anne Hulse, Pete Brown and Claire Powell for informative discussions and for providing many hours of entertainment when we should have been working! Thank you to Gareth Lee for his help and support, both in the laboratory and out of it. I'm always confident that if there's a way round any problem, he'll find it no matter what the cost! Thank you also to the rest of ENV technical and computing support – you all do a great job.

Throughout the AMT cruises, I would have achieved very little had it not been for the hard working, helpful and fun-loving army of scientists and crew aboard each cruise. In particular Alex Poulton, Carol Robinson and Patrick Holligan – thank you for everything.

I thank my parents and sister for providing the belief that I really *can* whenever I've begun to think *I can't* throughout my entire life. Finally, Hannah – thank you for being you, always doing the right thing by me and supporting every aspect of my life over the past 5 years. You've lived this as much as I have and I owe it to you that I've made it through to the end. I'm so excited about our future together.

1 Introduction

There are a number of sulphur and nitrogen compounds involved in important processes within the lower atmosphere and surface ocean. For many years, oceanic emissions of dimethylsulphide (DMS, a biogenic trace gas) to the atmosphere have been recognised to be of potential climatic significance (Charlson et al., 1987). In addition, the supply of sulphur to the terrestrial sphere has been shown to influence the quality and yield of plants and crops such as wheat (Zhao et al., 1999). Meanwhile, in areas of the surface ocean where nitrogen is limiting, the flux of gaseous ammonia ($NH_{3(g)}$) in or out of the ocean may have significant impacts upon atmospheric chemistry and biological production in the ocean.

At a basic level, theoretical links between nitrogen and sulphur cycles are apparent. Should the flux of NH_3 have an impact on biological production in certain areas, then oceanic DMS emissions are also likely to be affected. A proportion of DMS oxidised in the atmosphere influences cloud formation by forming cloud condensation nuclei (CCN) and thereby affects the amount of solar radiation reaching the earth's surface (Twomey, 1977). The phytoplanktonic production of DMS and potential climatic feedback is known as the CLAW hypothesis, so named after the initials of the authors of the original paper – Charlson, Lovelock, Andreae and Warren (1987). Once acidic aerosol droplets are formed, they scavenge basic material such as $NH_{3(g)}$ from the atmosphere, forming either partially neutralised, NH_4HSO_4, or fully neutralised, $(NH_4)_2SO_4$, ammonium sulphate. The nitrogen and sulphur cycles are primarily driven by biological activity in the surface ocean while redox chemistry plays a role in both atmosphere and ocean. It is clear that this cannot be summarised in one paragraph, but the examples above impart an idea of how the elements' pathways may be entwined.

In addition to theory, analytical evidence has been produced suggesting a real link between the cycles. Atmospheric aerosol measurements from the central Pacific Ocean demonstrated a consistent particulate NH_4^+ to non sea-salt sulphate ($nssSO_4^{2-}$) mean molar ratio close to one (Quinn et al., 1990). The authors suggest that the consistency of this ratio might indicate a relationship between the factors controlling the production of NH_3 and $nssSO_4^{2-}$ (derived from DMS oxidation) in remote marine environments. Although no direct correlation between seawater DMS and NH_3 was found, fluxes were out of the ocean for both chemical species and approximately the same order of magnitude (Quinn et al.,

1990). A potential relationship is attractive when considered in the context of its theoretical impact on the CLAW hypothesis as ammonium-sulphate-H_2O particles demonstrate enhanced nucleation rates relative to sulphate-H_2O particles (Coffman and Hegg, 1995; Korhonen et al., 1999). This is the driving force behind my PhD research.

The following sections detail the chemistry and physics behind the sea-air gas exchange and flux of $NH_{3(g)}$ and DMS (Section 1.1), the biological processes influencing sulphurous and nitrogenous compounds in the surface ocean, and the chemistry dictating atmospheric aerosol composition and acidity in remote regions (encompassed in Sections 1.2 & 1.3). Finally, this chapter will bring together the nitrogen and sulphur cycles (Section 1.4), before introducing the programme that was integral to this study and outlining my PhD research (Section 1.5).

1.1 Air-Sea Gas Exchange

Both DMS and NH_3 cross the air-sea interface in gaseous form and it is therefore important to outline current understanding of this process. Gas exchange theory employs the premise that, if there is a concentration gradient between two regions, the flux will be towards the region of lowest concentration and away from the region of highest concentration. However, the ocean-atmosphere interface is not as simple due to the phase change between the two regions (water and air). At the molecular scale, there is a theoretical point where any movement of gases across the air-sea interface is via molecular processes. The interfacial layers either side of the interface are considered to provide the main resistance to gas transport while the main body of fluid (or air) is well mixed (Liss and Slater, 1974). This theory is represented by the 'thin film model' (Figure 1.1).

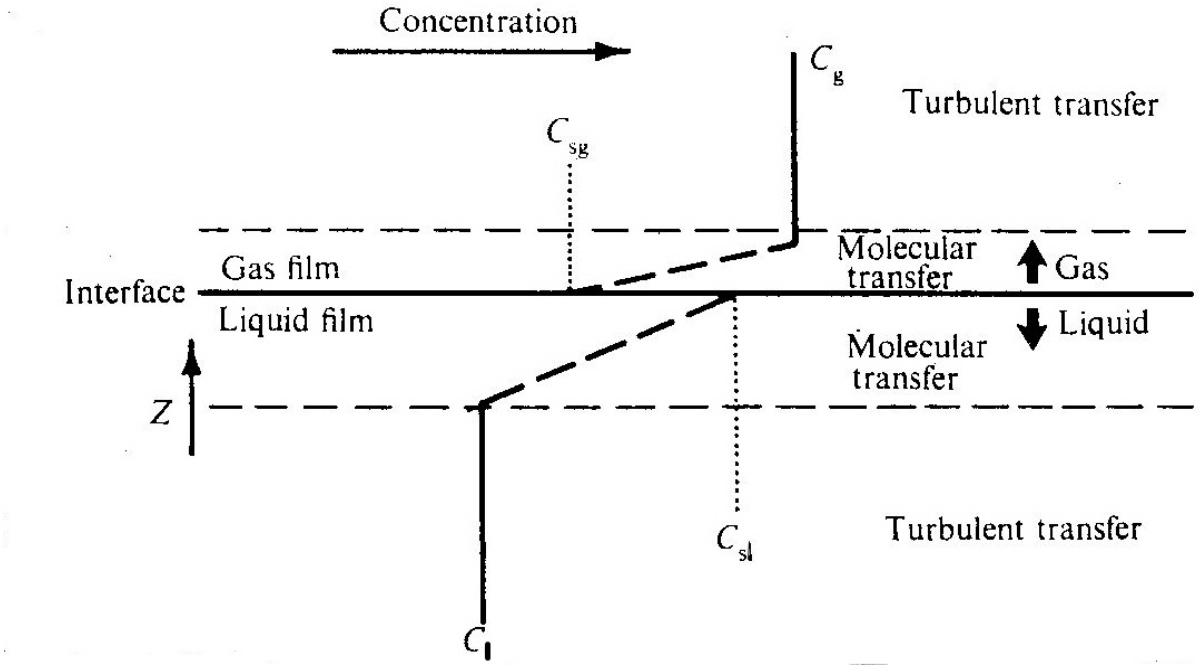

Figure 1.1 Thin film model of a gas-liquid interface (figure taken from Liss and Slater, 1974).

Using this model, Liss and Slater (1974) derive an equation for gas exchange between the ocean and atmosphere that many authors have used as a basis for calculating gas fluxes:

$$F = k.\Delta c$$

Equation 1.1

where F is the flux of gas through the layer; Δc is the concentration difference across the layer and k is termed the transfer velocity. k has dimensions of velocity and is a measure of the flux of gas per unit concentration gradient. k depends on a number of factors, the

most important being the degree of turbulence on both sides of the interface and the chemical reactivity of the gas (Liss and Slater, 1974). Whilst near-surface turbulence in both the atmosphere and the ocean is a major control on air-sea gas exchange kinetics, it is difficult to quantify and measure. It is easier to measure an environmental parameter that influences near-surface turbulence and from this make parameterisations in order to relate it to the exchange constant (*k*). The easiest environmental parameter to measure is wind speed as it can be predicted using satellite data and therefore enables global estimates of air-sea fluxes. Other potential controls on near-surface turbulence are surface currents, convective overturning and, if the water column is shallow enough, bottom friction.

Equation 1.1 can be displayed in more detail if Henry's law is included. Henry's law states that, for an air-water interface at equilibrium, the ratio of a compound's concentration in the gas phase $[A]_G$ over its concentration in the liquid phase $[A]_L$ is equal to a constant, H_C. This can be re-written with either $[A]_G$ or $[A]_L$ as the subject:

$$[A]_G = H_C.[A]_L$$

Equation 1.2

$$[A]_L = \frac{[A]_G}{H_C}$$

Equation 1.3

H_C varies with temperature and the relationship is different for every gaseous compound; the temperature-dependent relationships for NH_3 (Dasgupta and Dong, 1986) and DMS (Dacey et al., 1984) are displayed below (T represents temperature in °K):

$$H_{NH_3} = 10^{\left(\frac{4092}{T} - 9.70\right)}$$ where H has units of moles litre^{-1} atm^{-1}

Equation 1.4

$$H_{DMS} = e^{\left(\frac{-3547}{T} + 12.64\right)}$$ where H has units of atm litre moles^{-1}

Equation 1.5

The form of *Equation 1.4* needs to be adjusted for two factors. The H_C for NH_3 presented by Dasgupta and Dong (1986) has units of moles litre^{-1} atm^{-1} and is in the form [liquid]/[gas]. In order to be used in the flux calculation (see *Equation 1.8* later), the H_C

for NH_3 must be unitless and in the form [gas]/[liquid]. The following correction factors must therefore be used:

- Firstly, *Equation 1.4* must be multiplied by the ideal gas volume for one mole (V_m). This varies with temperature (T) as per the following equation:

$$V_m = 22.41 \times \left(\frac{T}{273} \right)$$

Equation 1.6

  where V_m has units of litre^{-1} and T has units of °K.
- Secondly, *Equation 1.4* must be inversed to get it into the form [liquid]/[gas] (sometimes called the Ostwald solubility coefficient).

The H_{DMS} presented by Dacey et al. (1984) and displayed in *Equation 1.5* also needs to be adjusted so that it is unitless. This is a lot easier as it simply involves dividing H_{DMS} by *Equation 1.6*.

H_C for DMS has been shown to vary linearly with sodium chloride concentration at a fixed temperature although the authors do not provide an equation (Wong and Wang, 1997). This supports the findings of Dacey et al. (1984) who showed that DMS solubility is 16-19% lower in seawater relative to distilled water over the temperature range measured. While H_C for NH_3 is also likely to vary with salinity in a similar manner, there is little information within the literature concerning the nature of the relationship. Gibb (1994), McKee (2001) and Johnson (2004) all used the statement that gases are 20% less soluble in seawater (Stumm and Morgan, 1981) to correct H_C for their NH_3 flux calculations. This has previously proven confusing as it is not H_C that is 20% reduced, but rather the concentration of gas in seawater. The liquid concentration must therefore be multiplied by 0.8 to reduce it by 20%. When H_C is in the [liquid]/[gas] form, it must be multiplied by 0.8; however, when H_C is in the [gas]/[liquid] form, it must be multiplied by 1.25 (i.e. 1 divided by 0.8). This salinity correction approach can also be applied to the H_C value for DMS, but the value of 1.25 should be corrected slightly according to the experimental findings of Dacey et al. (1984), which would mean multiplying the H_C for DMS by between 1.19 and 1.23.

Air-sea exchange of NH_3 is controlled by a number of different parameters. Quinn *et al.*, (1996) attempted to assess the sensitivity of their calculated NH_3 flux to variations in these parameters; they found that the atmospheric and seawater concentrations of NH_3 had the

greatest influence on the flux. Seawater temperature had a less pronounced influence, while salinity, seawater pH and the exchange velocity each had a minimal influence (Quinn et al., 1996). It should be noted that pH would actually have a substantial impact on the flux were seawater not buffered to changes in pH. More recent work corroborated the conclusions of Quinn et al. (1996) and showed that within natural ranges and when equilibrium concentrations are fixed, temperature has the greatest influence relative to salinity and pH on equilibrium $NH_{3(g)}$ concentrations, with pH of secondary importance (Johnson, 2004).

Either *Equation 1.2* or *Equation 1.3* can be incorporated into *Equation 1.1* and Figure 1.1 to describe the flux of a gas across the air-sea interface (see Figure 1.2a&b). NH_3 is a highly soluble gas, so it is the gas phase side of the flux that controls its exchange velocity (k). There is essentially no concentration gradient at the very surface of the ocean (i.e. $C_{SL} = C_L$) because NH_3 dissolves so easily. Contrastingly, DMS is only moderately soluble and the liquid phase side is therefore the dominant control on the exchange velocity, k (i.e. no difference between C_{SG} and C_G). Measurements of the H_C for DMS have confirmed this (Dacey et al., 1984; Wong and Wang, 1997). However, as DMS is rapidly oxidised in the atmosphere and its dominant source is the ocean, concentrations in surface seawater are up to three orders of magnitude higher than the overlying atmosphere (Putaud and Nguyen, 1996). As a result, most flux calculations assume that $[A]_G$ is negligible and only use measured seawater concentrations (Quinn et al., 1990).

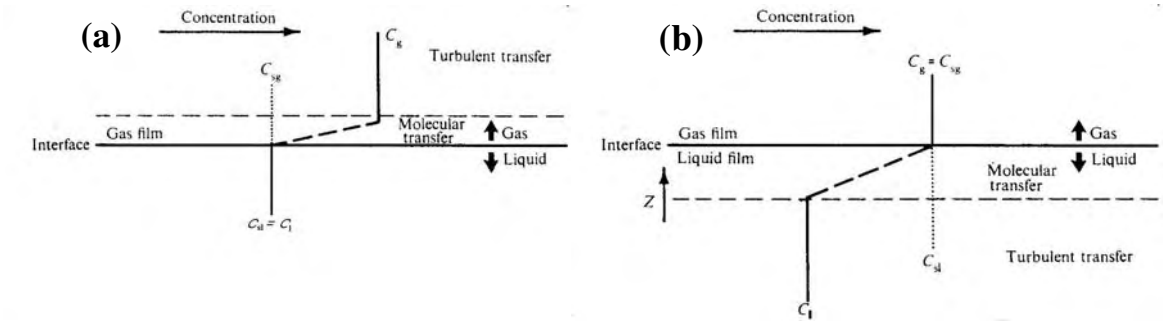

Figure 1.2 Adapted thin film model for (a) NH_3, and (b) DMS (figures adapted from Liss and Slater, 1974).

Using information from the previous paragraph, modified versions of the thin-film model (Figure 1.2) and different equations for calculating DMS and NH_3 fluxes between the ocean and atmosphere (Equation 1.7 and Equation 1.8) can be produced:

$$F = k_L\left[(DMS)_s - \frac{1}{H_{DMS}(DMS)_g}\right]$$

Equation 1.7

$$F = k_G\left[\left(H_{NH_3}.[NH_3]_s\right) - (NH_3)_g\right]$$

Equation 1.8

Note that k_L and k_G still represent the transfer velocity (k) whilst indicating whether the flux is controlled on the liquid or gas side of the interface. These equations are based upon physical theory and do not provide the full story regarding all the differences in the behaviour of these gases. Chemical or biological processes cause changes in atmospheric and oceanic concentrations that directly influence the rate and possibly direction of gas exchange, particularly in the case of NH_3.

For both the DMS and the NH_3 flux calculations, wind speed should be normalised to 10 m above sea level (U_{10}) using a bulk formula (see Hood et al., 2001):

$$U_{ref} = U_{meas}\left[1 - \frac{C_d^{0.5}}{k}\ln\frac{Z_{ref}}{Z_{meas}}\right]^{-1}$$

Equation 1.9

where U_{ref} and U_{meas} are the wind speed for the reference height (Z_{ref}) and the measurement height (Z_{meas}) respectively. k is the von Karman constant (0.4) and the drag coefficient (C_d) is assumed to be 1.1×10^{-3}. This formula is a simplification of reality as it assumes neutral stratification of the atmosphere, and the value for C_d assumes temperature and humidity conditions considered representative of the open ocean (Smith, 1988). However, the error created when calculating gas fluxes is minimal and this assumption can therefore be made with confidence (Hood et al., 2001).

1.1.1 DMS Flux and Wind Speed

Over the years, a number of relationships between wind speed and air-sea gas exchange have been presented in terms of a Schmidt number (*Sc*) of 600 (i.e. CO_2 in freshwater at 20ºC). *Sc* is defined as the ratio of kinetic viscosity to molecular diffusivity. The wind speed-gas exchange velocity relationships can applied to DMS sea-air exchange using the equations below (Liss and Merlivat, 1986) to account for the different *Sc* value for DMS:

$$k_{DMS} = k_{600} . \left(\frac{Sc_{DMS}}{600} \right)^{-\left(\frac{2}{3}\right)} \qquad \text{for } U_{10} \leq 3.6$$

Equation 1.10

$$k_{DMS} = k_{600} . \left(\frac{Sc_{DMS}}{600} \right)^{-\left(\frac{1}{2}\right)} \qquad \text{for } U_{10} > 3.6$$

Equation 1.11

where k_{600} represents the transfer velocity for a gas with $Sc = 600$; and U_{10} is wind speed at 10 metres above sea level in m sec^{-1}. The temperature dependence of Sc_{DMS} can be calculated using the following formula (Saltzman et al., 1993):

$$Sc_{DMS} = 2674.0 - 147.12t + 3.726t^2 - 0.038t^3$$

Equation 1.12

where: t = temperature in ºC.

The original wind speed versus k_L (or k_{600}) relationship was based upon studies in a wind-wave tank, which were then scaled up to a lake with intermediate winds before comparison with oceanic measurements (Liss and Merlivat, 1986). At around the same time, another relationship was devised using a radon-deficient method and assumed no gas transfer until a wind speed of 3 m sec^{-1} at 20 m height (Smethie et al., 1985). This relationship was subsequently modified to incorporate measurements using the global bomb-^{14}C inventory (Tans et al., 1990). Variations in wind speed and direction were then recognised as potentially influential during gas exchange, and a quadratic dependence was suggested (Wanninkhof, 1992). More recent work using an eddy correlation technique has acknowledged the influence of surfactants at low wind speeds and bubble-enhanced transfer at high wind speeds, producing a cubic relationship (Wanninkhof and McGillis, 1999). Numerous dual tracer experiments have attempted to quantify sea-air gas exchange using SF_6 and the more volatile ^3He (e.g. Watson et al., 1991). In particular, a dual tracer

study was carried out in the North Sea, which also used a non-volatile bacterial spore to account for tracer dispersion and dilution (Nightingale et al., 2000b).

All of the above relationships can potentially be used to estimate the water-phase controlled exchange velocity (k_L) of CO_2, and hence DMS. There are significant differences between all the relationships mentioned, particularly at higher wind speeds, which is likely explained by variations in study location (e.g. biological activity) and environmental situation (e.g. surfactants, bubble bursting, rain, etc.); most of these relationships are displayed in Figure 1.3. For all DMS flux calculations made during this project (see Section 4.3.1), the formulation from Nightingale et al. (2000b) was used:

$$k = 0.222\ (U_{10})^2 + 0.333\ U_{10}$$

Equation 1.13

where U_{10} is the wind speed in m sec^{-1} at a standard reference height (10 m above sea level).

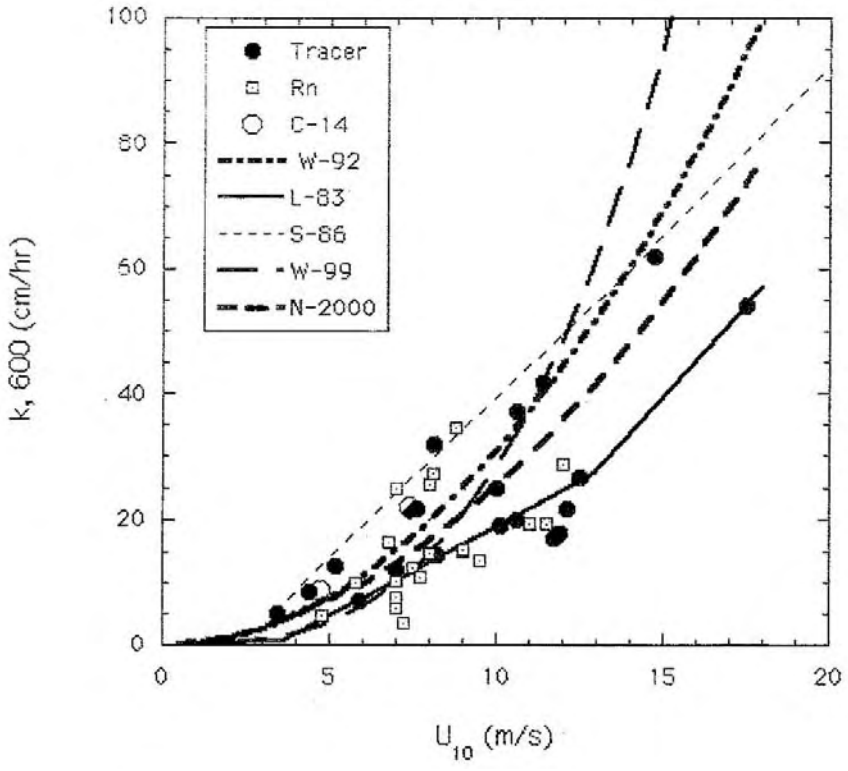

Figure 1.3 Summary of gas exchange results in the ocean and empirical relationships derived, in part, from the data shown. All data have been normalised to $Sc = 600$. The empirical relationships are those of Liss and Merlivat (1986), **L-83**; Wanninkhof (1992), **W-92**; Smethie et al. (1985), **S-86**; Wanninkhof and McGillis (1999), **W-99**; and Nightingale et al. (2000b), **N-2000**. Closed circles (tracer) represent dual-tracer results; open squares (Rn) represent results using the radon-deficient method; open circle (C-14) represents the global estimate based on bomb-radiocarbon (figure taken from Donelan and Wanninkhof, 2002).

As mentioned earlier, there are factors other than wind speed that influence the k_L of DMS. When the ocean surface becomes turbulent enough, it changes in nature and this can dramatically influence the rate of gas exchange between the atmosphere and ocean. Probably the biggest factors are the thresholds at which waves begin to break and the resultant bubbles. The Liss and Merlivat (1986) relationship attempts to deal with this by defining wind speeds at which the k_L versus wind speed relationship alters (3.6 m sec^{-1} and 13 m sec^{-1}); subsequent relationships (Smethie et al., 1985; Wanninkhof, 1992; Wanninkhof and McGillis, 1999; Nightingale et al., 2000b) also acknowledge this influence but without critical wind speed thresholds for capillary waves and breaking waves/bubble formation.

Recent eddy-correlation measurements made with an atmospheric pressure ionization mass spectrometer (APIMS) have facilitated detailed and high frequency study of DMS fluxes (Huebert et al., 2004). Using this data as part of the National Oceanic and Atmospheric Administration (NOAA) Coupled Ocean Atmosphere Response Experiment (COARE) gas flux parameterisation has demonstrated the importance of gas solubility in bubble-mediated transfer (Blomquist et al., 2006). DMS has a higher solubility than CO_2 and the result is a flatter transfer velocity curve as wind speed increases; a power-fit was applied to observed eddy correlation measurements (Blomquist et al., 2006):

$$k_{DMS} = (U_{10})^{1.3}$$

Equation 1.14

The development of technology that enables accurate and frequent measurements of DMS fluxes promises significant improvements in current understanding of air-sea gas exchange.

Raindrops impact upon air-water gas exchange – they contribute to near-surface turbulence and entrain bubbles, which can account for up to 20% of gas exchange during rainfall at low wind speeds (Ho et al., 2000). Areas with low wind speed and high rainfall rate (e.g. wetlands) are most likely to have their gas exchange rates influenced by rainfall (Ho, 1997). Little is known about rainfall induced gas transfer in the open ocean; at low wind speeds, the difference in density between rainwater (fresh) and saltwater may lead to stratification of the water column, reducing gas exchange (Ho, 1997). However, if the wind speed is higher or the raindrop size is larger, then the likelihood of this stratification

being dispersed increases (Ho et al., 2000). Furthermore, the potential disruption of any surfactant layer by raindrops should be considered (Ho, 1997).

It is important to be aware that the gas exchange rate of DMS can be particularly influenced within the 'thin film' of surface waters. Any changes within this microlayer, which is at most tens of microns thick, can significantly alter the diffusivity rate and hence the rate of gas exchange (Hunter, 1997). Biological action could potentially change the chemistry within this layer and therefore alter the reactions that take place with chemical species diffusing across the interface (Hardy, 1997). Recent work has identified that bacteria within the microlayer (the bacterioneuston) are considerably less diverse than communities in pelagic water samples, but suggests they are genetically distinct (Franklin et al., 2005). Other experiments found that adding methanotrophs to the microlayer in a tank setup had a significant influence on the exchange of methane across the air-sea interface (Upstill-Goddard et al., 2003).

The production of surfactants through biological action results in a more viscous surface layer, which can hinder diffusion across the liquid-gas boundary (altering k_L) and reduces the influence of near-surface turbulence (Goldman et al., 1988). However, this effect was not observed in the natural environment during the development of an open ocean algal bloom (Nightingale et al., 2000a). The significant influence of parameters which do not scale with wind speed was acknowledged by Nightingale et al. (2000b) when they evaluated a number of air-sea gas exchange dual tracer experiments.

1.1.2 NH_3 Flux and Wind Speed

Equation 1.8 uses the concentration of NH_3 in both air and liquid in order to calculate the gas flux across the interface. However, NH_3 exists in seawater as part of the following equilibrium:

$$NH_{3(aq)} + H^{+}_{(aq)} \leftrightarrow NH_4{}^{+}_{(aq)}$$

Equation 1.15

Approximately 10% of this nitrogen is in the NH_3 form in seawater when pH = 8.2, temperature = 25°C (Quinn et al., 1996). When seawater is analysed for NH_4^+ using conventional analytical techniques, what is typically measured is the sum of NH_3 plus NH_4^+ so the result is referred to as $\mathbf{NH_X}$. In order to calculate the NH_3 concentration in water, the NH_X value must be corrected using the following formula:

$$NH_{3(aq)} = \frac{K_a.[NH_X]}{K_a + [H^+]}$$

Equation 1.16

where K_a = acid dissociation equilibrium constant of NH_4^+.
K_a has been shown to vary with both temperature and salinity (Khoo et al., 1977; Johansson and Wedborg, 1980). Numerous air-sea gas exchange studies of NH_3 (e.g. Gibb et al., 1999a; McKee, 2001; Johnson, 2004) have used *Equation 1.17* to correct for temperature and salinity variations (from Khoo et al., 1977):

$$pK_a = pK_w + (0.1552 - 0.0003142.t).I_f$$

Equation 1.17

where: pK_w = the thermodynamic dissociation constant of ammonium ion in pure water; t = temperature (°C); and I_f = formal ionic strength of the solution. However, this formulation is incorrect as it does not accurately reproduce the measurements presented within the paper or equivalent measurements presented elsewhere (e.g. Hales and Drewes, 1979; Johansson and Wedborg, 1980).

The most appropriate correction for the effect of temperature and salinity on pK_a uses the following equation (Johansson and Wedborg, 1980):

$$pK_a = -0.467 + (0.00113.S) + \left(\frac{2887.9}{T}\right)$$

Equation 1.18

where: $pK_a = -\log_{10}K_a$; T = temperature in °K; and S = Salinity. Using *Equation 1.16* and *Equation 1.18*, the NH_3 concentration in seawater can be calculated.

The other requirement for *Equation 1.8* is the exchange velocity of NH_3 (k_G). Due to its similarity in molecular shape, weight, size, polarity and hydrogen bonding, the NH_3 molecule is assumed to have a comparable k_G to water (Liss and Slater, 1974). The authors quote the exchange velocity for water as 3000 cm hr^{-1} (or 8.3 x 10^{-3} m sec^{-1}), and this value has been used for many studies (e.g. Quinn et al., 1996). However, for simultaneous atmosphere-ocean flux studies, an empirically derived k_G would improve the accuracy of the flux calculation (Quinn et al., 1988). A linear wind-dependent version of the air-phase controlled exchange velocity now exists (Duce et al., 1991):

$$\mathrm{k_G} = \frac{\mathrm{U_{10}}}{\left[770 + 45(\mathrm{MW})^{\frac{1}{3}}\right]}$$

Equation 1.19

where U_{10} = wind velocity in m s^{-1}; MW is the molar weight of NH_3 (17 g mol^{-1}); and k_G is the exchange velocity in cm sec^{-1}. This relationship is a representation of the atmospheric resistance in both the diffusive layer and the turbulent layer, both of which scale with wind speed and wind stress at the ocean surface (Duce et al., 1991). The inverse of *Equation 1.19* (see also Figure 1.4) is equal to the atmospheric resistance (r_a) and has been shown to compare well with experimental data at an approximate wind speed of 10 m sec^{-1} (Liss and Slater, 1974).

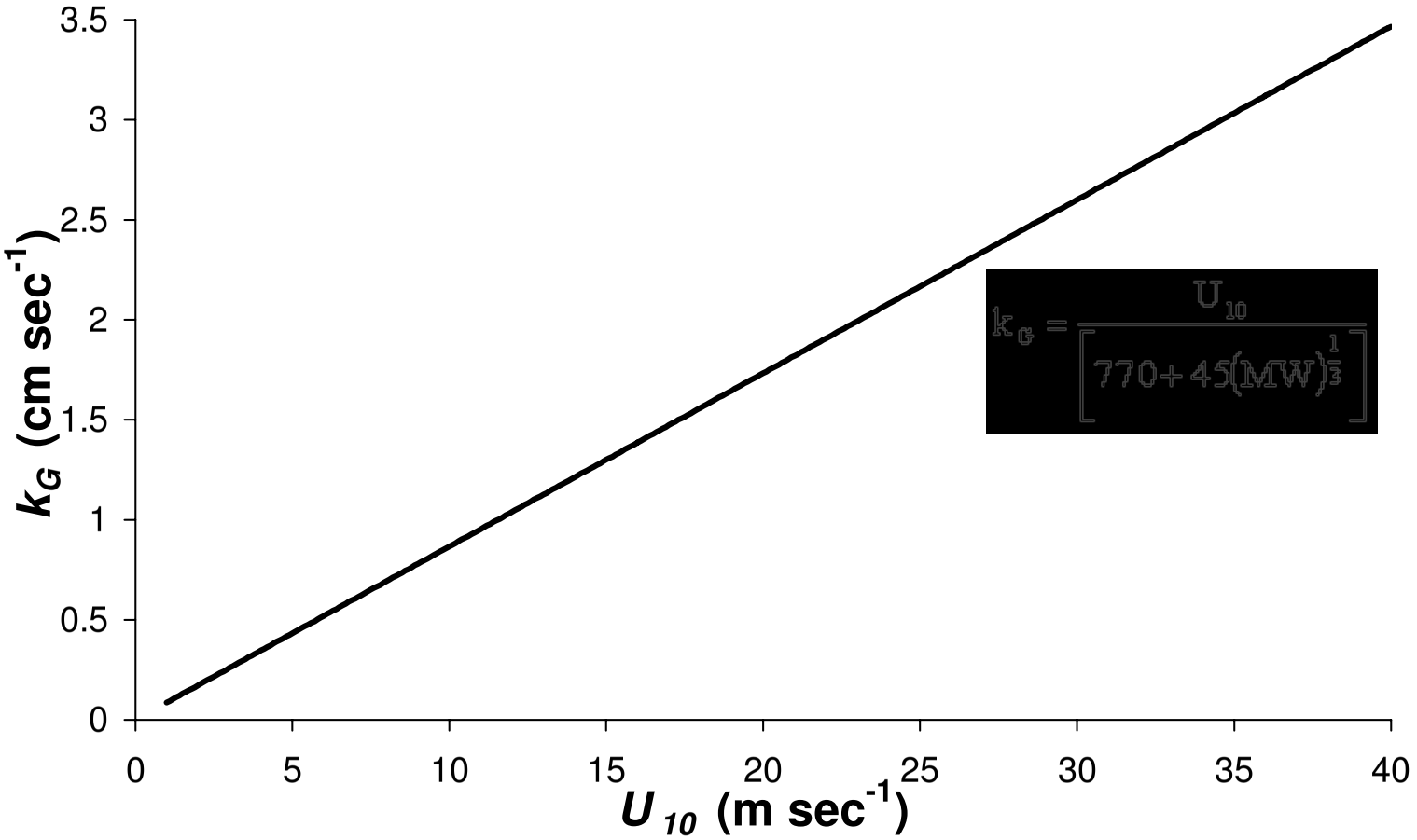

Figure 1.4 Relationship of exchange velocity for NH_3 (k_G) with wind speed (U_{10}). Data plotted using *Equation 1.19*.

1.2 The Reduced Sulphur Cycle

As has been explained, the concentration of DMS in the surface ocean relative to its concentration in the air essentially drives its flux into the atmosphere. As Figure 1.5 clearly illustrates, oceanic concentrations are variable on a spatial (but also temporal) scale; this information (Figure 1.5) is also useful to put into context the data collected for this thesis work. An understanding of the processes controlling seawater concentrations is therefore particularly important in order to quantify and predict such a flux. The following sections attempt to explain current understanding of the biological processes and chemical reactions involved in both the lower atmosphere and surface ocean cycles of reduced sulphur.

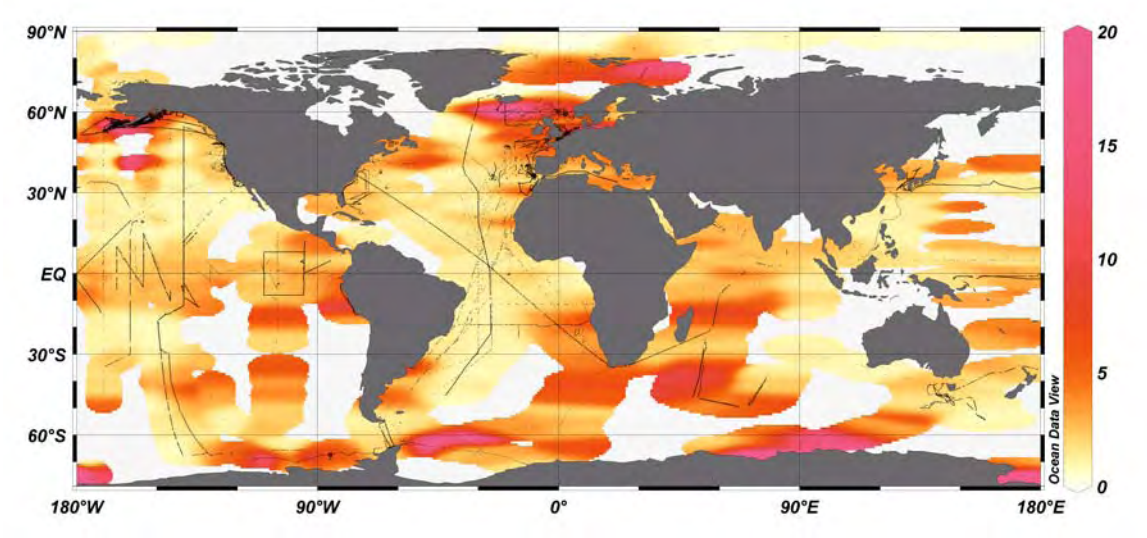

Figure 1.5 Global surface DMS concentrations capped at 20 nM to aid readability; maximum concentrations measured exceed 300 nM. Source = global DMS database http://saga.pmel.noaa.gov/dms/ (Kettle et al., 1999; Kettle and Andreae, 2000). Plot produced using *Ocean Data View* (http://odv.awi-bremerhaven.de/home.html).

1.2.1 Surface Ocean

Whilst atmospheric DMS is considered a direct result of biological activity in the surface ocean, there are multiple pathways by which it can be produced. It is accepted that the main precursor to DMS is β-dimethylsulphoniopropionate ($(CH_3)_2S^+CH_2CH_2COO^-$) or DMSP, which constitutes the major fraction of organic sulphur in many living marine particles (Simo, 2001). DMSP is synthesised by various types of phytoplankton and is a major cell constituent, although the relative rates of production can vary significantly. This leads to three major questions:

- Why is DMSP (and thus DMS) produced?
- What processes lead to DMSP breakdown (see Figure 1.6) and the resultant formation of DMS and acrylic acid?
- What are the loss processes for DMSP and DMS?

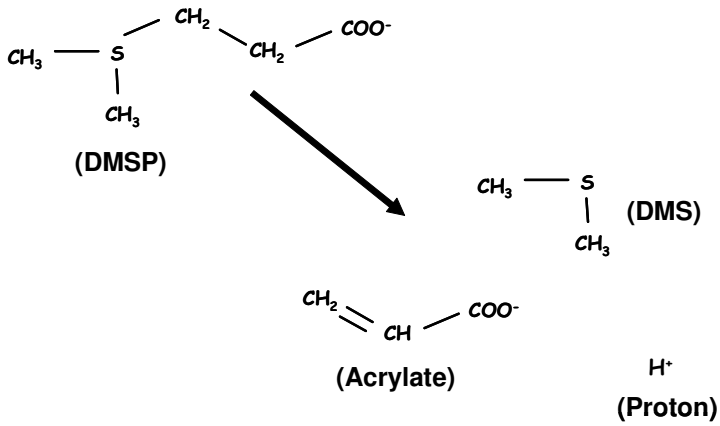

Figure 1.6 The chemical breakdown of a molecule of DMSP and the resulting products – DMS, acrylate and a proton.

Why is DMSP (and thus DMS) produced?

There are a variety of theories concerning why DMSP is produced. One suggestion is that DMSP might act as a methyl donor in metabolic reactions (Simo, 2001). Due to its apparent abundance in phytoplankton, initial suggestions were that DMSP might be a compatible solute used to for osmotic adjustment without interfering with cell function and to protect cell proteins and other cell components from high and low (i.e. freezing) temperatures (Stefels, 2000). Subsequently, a number of links between DMSP production and nitrogen availability have been suggested (concerning osmoregulation and/or excess energy within the cell). These will be addressed in more detail in Section 1.4.

It has been suggested that the production of DMSP and its oxidation products help phytoplankton cells combat oxidative stress resulting from the production of harmful levels of oxidative radicals (Sunda et al., 2002). When taken together, DMSP and its breakdown/oxidation products (DMS, acrylate, dimethylsulphoxide, and methane sulphinic acid) comprise an effective cascade mechanism that protects against harmful oxidative radicals, with DMS in particular more reactive (with hydroxyl radials) than other well-recognised anti-oxidants such as ascorbate and glutathione. Although DMSP is fundamental for this anti-oxidant system, the rate constants for the reaction of DMS and acrylate with hydroxyl radicals (OH•) are 1–2 orders of magnitude greater than for DMSP (Sunda et al., 2002). Furthermore, intracellular DMSP concentrations have been shown to increase under conditions of oxidative stress (e.g. UV radiation, iron limitation, CO_2 limitation) in laboratory cultures of the diatom *Thalassiosira pseudonana* and the coccolithophore *Emiliania huxleyi* (Sunda et al., 2002). In contrast, however, a laboratory study published a month earlier, found no apparent change in the synthesis of DMSP by *Emiliania huxleyi* under UV levels comparable to natural solar conditions (van Rijssel and Buma, 2002).

There is a clear attractiveness to the anti-oxidant theory (Sunda et al., 2002) because of an apparent link with the CLAW hypothesis. DMSP production to protect against oxidative stressors such as solar ultraviolet radiation would facilitate DMS ventilation into the atmosphere, reducing the exposure of the surface ocean to UV radiation. However, as is evident from the variety of suggested DMSP production mechanisms, all theories concerning why DMSP is produced need to be rigorously tested.

A final theory for DMSP production relates to processes involved in actively converting DMSP to DMS and acrylic acid. DMS production is elevated when grazing takes place and it has been suggested that a chemical defence mechanism is operating that protects certain phytoplankton species from herbivores (Wolfe et al., 1997; Steinke et al., 2002c). This shall be discussed further within the section concerning DMSP breakdown and DMS/acrylic acid formation (see below).

What processes lead to DMSP breakdown and the resultant formation of DMS and acrylic acid?

The best way to introduce our current understanding of this complex set of ecological interactions is to use a schematic (Figure 1.7). From this, one can quickly ascertain why attempts to simply correlate DMS with other water column parameters on a large spatial or temporal scale have proven dissatisfactory. DMSP breakdown mainly occurs extracellularly. Whilst some intracellular DMSP is exuded naturally and is therefore related to phytoplankton taxa, biomass and productivity, there are other processes that cause DMSP release from cells (e.g. viral lysis, grazing, algal senescence). In addition, not all dissolved DMSP is converted to DMS (Kiene and Linn, 2000), as discussed at the end of this section. As a result of the alternative consumption pathways and release mechanisms, DMS production is only indirectly related to DMSP measurements or other proxies such as chlorophyll *a* or phytoplankton biomass.

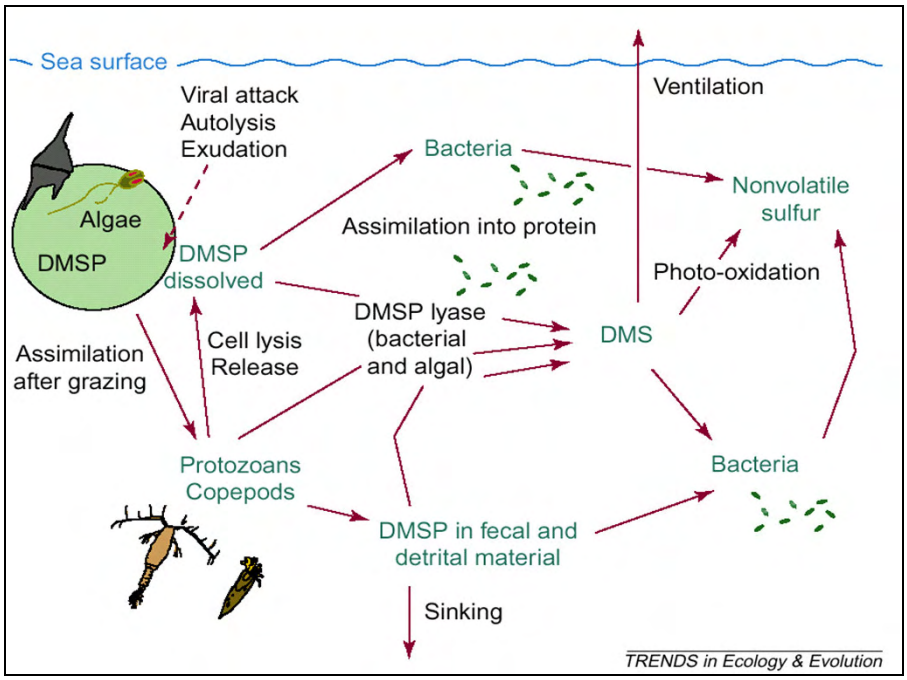

Figure 1.7 The fate of phytoplanktonic DMSP in seawater (figure taken from Simo, 2001).

There are three known mechanisms that cause cell lysis and the release of DMSP into the water column:

- autolysis, where a phytoplankton cell senesces at the end of its life (Malin et al., 1994);
- lytic viral infection, where viruses invade the host, reproduce and then compromise the cell membrane to release the viral progeny (Malin et al., 1998)
- grazing (covered in more detail below).

After DMSP is released into the water column it can be converted to DMS by algal and bacterial DMSP-lyase enzymes. A study by Wolfe et al. (2002) observed physiological DMS production by some algae after shifts in the light regime. When *Emiliania huxleyi* cells in the exponential phase were transferred to the dark the cultures accumulated DMS, but upon transfer back into the light, DMS accumulation ceased within 24 hrs. The authors are, however, unsure whether this was due to DMSP cleavage increasing as a result of dark stress, or a reduction in DMS destruction via oxygen radical scavenging in the dark (Wolfe et al., 2002).

Various phytoplankton species are thought to compartmentalise the DMSP-lyase enzyme away from their intracellular DMSP store. Alternatively, it has been suggested that enzyme activation may only proceed in the presence of a co-factor. Different taxa and even different strains of the same species can be described as high- or low-lyase activity (Steinke et al., 1998; Steinke et al., 2002a). Laboratory studies have shown that algal DMSP-lyase activity (DLA) may be involved in an activated chemical defence reaction of *Emiliania huxleyi* cells against grazing (Wolfe et al., 1997). This species shows strain-specific DLA and grazing experiments with the heterotrophic dinoflagellate *Oxyrrhis marina* indicated that strains with high DLA are consistently grazed at lower rates. This defence mechanism has also been observed in macroalgae during grazing by the sea urchin *Strongylocentrotus droebachiensis* (Van Alstyne and Houser, 2003). In addition to this, certain bacteria contain the DMSP lyase enzyme(s) and can be found free in solution, attached to particles or in the guts and vacuoles of grazers (Simo, 2001). A discussion of DMSP-lyase activity measurements (this study and previous studies) in the natural environment can be found in Chapter 5, Section 5.1.

DMSP is thought to support between 1 and 13% of the bacterial carbon demand in surface ocean waters (Kiene et al., 2000), making it an important growth substrate as well as a significant source of sulphur for marine bacterioplankton. The sulphur demand of bacteria might therefore influence the conversion rate of DMSP to DMS (i.e. high sulphur demand = low conversion from DMSP to DMS due to high sulphur assimilation). Although there is debate concerning the intricacies of the 'DMSP availability hypothesis' (Kiene et al., 2000; Simo, 2001), the basic principle remains the same – DMS production in surface waters is reliant upon both bacterial productivity (and sulphur demand) and the rate of DMSP release from phytoplankton cells.

Grazing by zooplankton is another influence upon DMS concentration in the water column. Several laboratory studies have shown that zooplankton (from micro to macro in size) grazing enhances dissolved DMSP (DMSPd) and DMS production (Dacey and Wakeham, 1986; Malin et al., 1994; Wolfe and Steinke, 1996). Upon ingestion by zooplankton, some DMSPd in the gut of the grazer is converted to DMS via algal and bacterial DMSP-lyase isozymes (Simo, 2001). Ingestion of particulate DMSP (DMSPp) by microzooplankton has been observed in the natural environment (Archer et al., 2003) and the authors considered this process to account for the majority of DMS production within a *Phaeocystis* spp. bloom. It is also worth noting that any DMSP not utilised by bacteria within the zooplankton gut will almost certainly be used as a source of sulphur once excreted, although this may occur below the euphotic zone (another loss mechanism for the surface ocean sulphur cycle).

It is thought that *Emiliania huxleyi* cells are disrupted during microzooplankton grazing, mixing the compartmentalised DMSPp and DMSP-lyase to produce DMS (Wolfe and Steinke, 1996). This process has been suggested as a form of chemical defence against zooplankton grazing (Wolfe et al., 1997); acrylate was suggested as the chemical deterrent due to its antibacterial action (Sieburth, 1960). Based on incubation experiments in the Adriatic Sea, Slezak et al. (1994) concluded that acrylic acid concentrations in natural waters are too low to inhibit bacterioplankton growth. However, the authors' conclusions were focussed on bacteria and considered ambient bulk concentrations so did not address the potential for intracellular acrylic acid build up, which would likely occur either within a microzooplankton digestive vacuole or within the phycosphere (the concentration gradient surrounding the cell).

In laboratory experiments using *Emiliania huxleyi* and a number of different protozoan herbivores, the products of DMSP breakdown were not acutely toxic but did deter grazing (Wolfe et al., 1997). Cells did not need to be fully ingested and lysed to deter a predator, suggesting that the grazers pick up chemosensory cues to select or reject their prey (Wolfe et al., 1997). The authors suggest that the production of DMS and acrylate gradients during prey handling might deter predation without producing detectable changes in bulk DMS concentrations. More recent work concurs: neither DMSP nor the products of its breakdown are thought to be direct deterrents of grazing but they may act as signals for the presence of potentially harmful (toxic) algal cells (Strom et al., 2003b). Another related

piece of work suggested that other 'don't eat me' cues might be found on the cell surface of high DMSP-lyase activity strains of *E. huxleyi* as ingestion did not have to occur for such a cue to be picked up by the grazer (Strom et al., 2003a). Further work is obviously required to determine what type of cues these might be and whether they vary between phytoplankton species. It has recently been suggested that DMS acts as an infochemical for copepods and may facilitate grazing by carnivores (Steinke et al., 2006b). Hence, DMS could play a role in mediating aquatic tritrophic interactions between, for example, small phytoplankton, microzooplankton and mesozooplankton (Steinke et al., 2002c).

Finally, it should be noted that there are significant DMSP consumption pathways involving demethylation and demethiolation that do not lead to DMS production (Figure 1.8). DMSP is a thermodynamically favourable source of sulphur compared to sulphate (Kiene et al., 2000) and DMSP-derived sulphur has already been shown to be readily assimilated by *Protobacteria* (Kiene et al., 1999) and *Synechococcus* (Malmstrom et al., 2005).

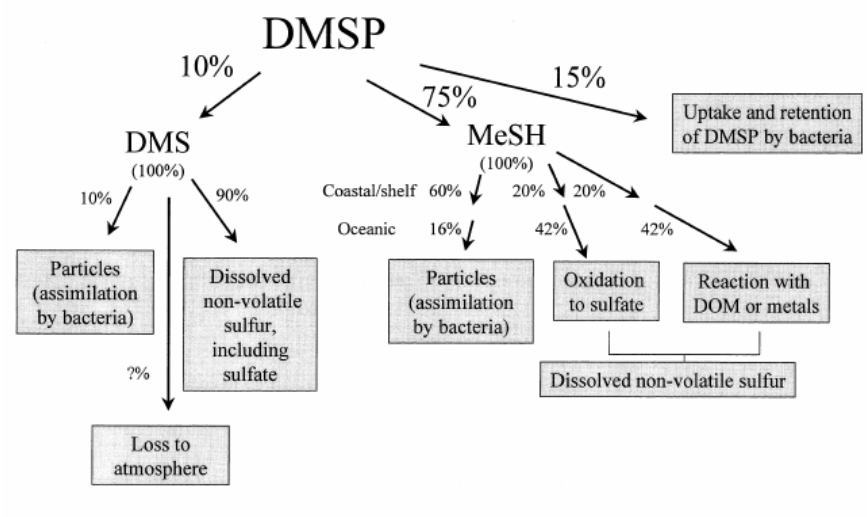

Figure 1.8 Generalised view of the paths and fate of sulphur from dissolved DMSP and its degradation products DMS and methanethiol (MeSH) in seawater based upon average ^{35}S-DMSPd partitioning data collected during 7 oceanic and 13 coastal-shelf whole water samples (figure taken from Kiene and Linn, 2000).

What are the loss processes for DMS?

The dominant processes leading to DMS loss from surface waters are as follows:

- ocean-atmosphere flux
- bacterial consumption
- photolysis, both abiotic and bacterially mediated

Ventilation of DMS from the surface ocean is the loss route of interest due to its climatic significance in the atmosphere, but is considered a relatively small flux in comparison to other routes of DMS destruction – potentially only 10% of oceanic DMS production reaches the atmosphere (Malin et al., 1992). The alternative loss mechanisms need to be accounted for because they are variable even over short timescales and changes in such processes directly affect the surface ocean DMS pool available for emission to the atmosphere. Incubation experiments from the North Sea (Slezak et al., 2001) and the equatorial Pacific (Kieber et al., 1996) suggest that biological consumption of DMS constitutes a relatively minor proportion of DMS loss relative to photochemical loss in the upper few metres of the ocean. It should be noted, however, that the ultraviolet (UV) radiation (wavelength approximately 100-400 nm) also suppresses any bacterial activity during such incubation experiments. In reality, the euphotic zone of the ocean is much deeper and organisms at depth are therefore far better protected from UV rays. The fact that UV radiation can significantly inhibit much of the biological activity due to its negative impact upon DNA should be considered for all studies of biologically-mediated, DMS-related processes in the surface ocean.

The abiotic reaction of DMS in the presence of UV radiation forms dimethylsulphoxide or DMSO, CH_3SOCH_3, (Brimblecombe and Shooter, 1986). DMSO is not the only product of DMS photooxidation – other minor products include dimethylsulphone, $DMSO_2$, and methane sulphinic acid, MSNA (Hatton, 2002). *In situ* light wavelengths and the amount of DOC present influences the relative proportions of different DMS photooxidation products (Hatton et al., 2005). The significance of DMS photooxidation in the surface ocean has been investigated by a number of authors (e.g. Kieber et al., 1996; Brugger et al., 1998; Slezak et al., 2001; Hatton, 2002). DMSO has its own cycle in the surface ocean, which can impact upon the DMS cycle; this is covered in more detail in the proceeding paragraphs.

Briefly, the key points of DMS photolysis are that UV-A and UV-B radiation may remove DMS via different photolysis pathways (Hatton, 2002) and are primarily dependent on irradiance levels, although Dissolved Organic Carbon (DOC) also has a critical influence. The influence of DOC is twofold:

1) Certain DOC compounds such as humic acid act as photosensitisers and their presence influences the photooxidation reaction kinetics (Brimblecombe and Shooter, 1986). Another approach has been to consider the relationship between Chromophoric Dissolved Organic Matter (CDOM) quality (degree of bleaching) and DMS photolysis, as used by Toole et al. (2003) in Sargasso Sea waters.
2) The concentration of DOC in the water column affects the light-absorptive properties of surface waters, altering the depth to which UV rays can penetrate and therefore limiting photooxidation of DMS (Brugger et al., 1998).

DMSO

The concentration of DMSO in surface waters is usually similar to that of DMS (Hatton et al., 1996; Hatton et al., 1999). DMSO is significant to the surface ocean DMS flux as it can act as either a source or sink, influencing how much DMS is available for release into the atmosphere. It was originally thought that DMSO acted primarily as a sink due to oxidation of DMS either via photochemistry (Brimblecombe and Shooter, 1986) or via bacterial processes (Zinder and Brock, 1978), but other laboratory evidence suggests that certain bacteria can reduce DMSO back to DMS (Zeyer et al., 1987). This latter discovery, when combined with other evidence that certain algae synthesize DMSO (Simo et al., 1998; Lee et al., 1999), indicates another potentially significant source of DMS to the surface ocean. DMSO production by algae is generally accepted, but there is ongoing debate as to its use within algal cells. Suggestions include an intracellular electrolyte modifier or a cryoprotectant (Lee and de Mora, 1999), although this has been questioned as Arctic ice-algae were found to contain levels of particulate DMSO that would be unlikely to significantly depress the freezing point of their intracellular fluids (Lee et al., 2001). Another proposal for the role of DMSO in algae is part of the oxidant-defence theory (see earlier in Section 1.1.1).

Regardless of the mechanism or the cause of DMSO production by algae, DMSO is certainly significant in the marine sulphur cycle as it has recently been estimated that there is a wider range of algal species that can produce DMSO than there is for DMSP (Lee et

al., 1999). In addition, DMSO is exceptionally permeable through cell membranes, causing cells to naturally 'leak' DMSO into seawater (Lee and de Mora, 1999). Considering these facts, there is little wonder that bacteria utilise this pool. Recent work has shown that there are certain strains of the *Roseobacter* group of bacteria that are able to aerobically oxidise DMS to DMSO and vice versa (Gonzalez et al., 1999). A chemical reduction pathway from DMSO to DMS no doubt exists but it is far more likely that the biological pathway is dominant (Hatton et al., 2005).

In summary, the oceanic cycling of DMS and related compounds is complex with many biotic and abiotic processes contributing to the overall control of ambient concentrations. As has been mentioned throughout the above discussion, the compounds discussed, in particular DMS, DMSP and DMSO, represent only a small part of the reduced sulphur cycle in the surface ocean, as highlighted in Figure 1.9.

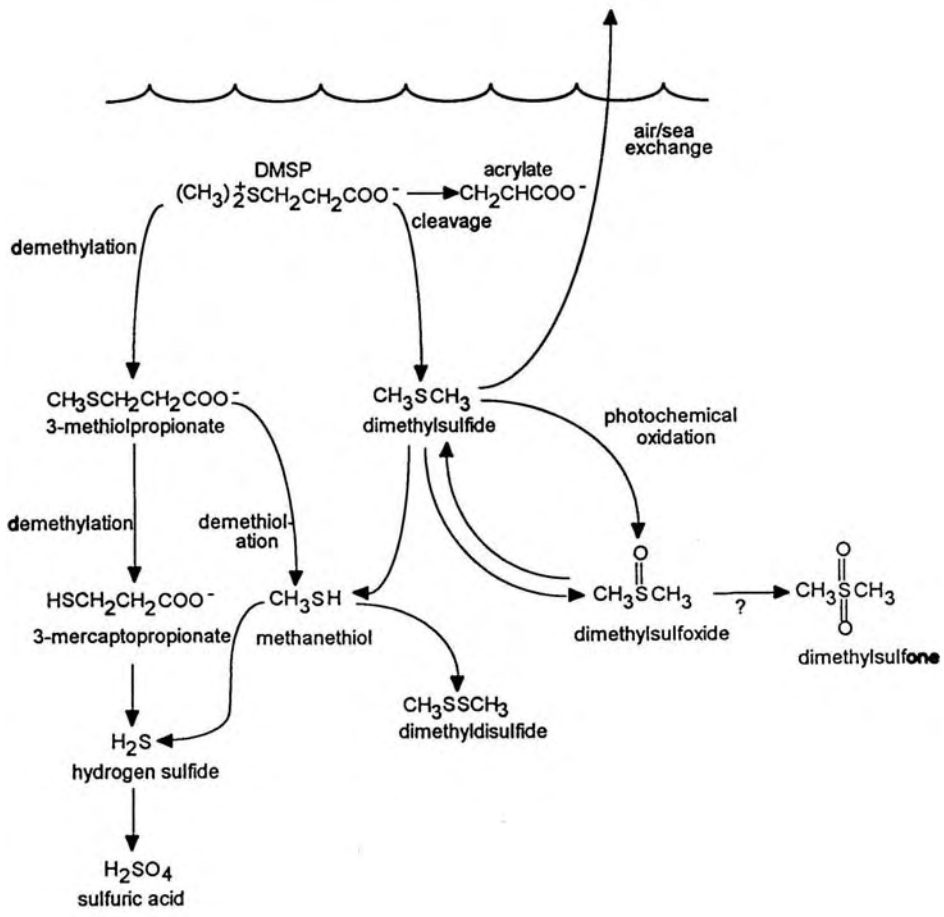

Figure 1.9 Pathways for reduced sulphur cycling in the surface ocean, including the non-sulphurous metabolite of DMSP breakdown, acrylate.

1.2.2 Lower Atmosphere

DMS in ambient air is typically found at concentrations of the order of parts per trillion, ppt (Ayers and Gillett, 2000). The atmospheric concentration is dependent upon biological production in the underlying surface waters and the rate of sea-air gas exchange, which is primarily driven by wind speed (see Section 1.1.1). Evidence of these processes controlling atmospheric concentrations can be found in the literature (e.g. Ayers et al., 1995).

On a slightly longer timescale, oxidation processes are a significant influence. Atmospheric DMS is oxidised through reaction with readily-available radicals in the atmosphere (Figure 1.10); the major products of these reactions are methane sulphonate, MSA, sulphur dioxide, SO_2, and non sea-salt sulphate, $nssSO_4^{2-}$ (Ayers and Gillett, 2000). Other products include DMSO and $DMSO_2$. Two radicals in particular are generally accepted to control the initial oxidation of DMS (Figure 1.10) – during the day the hydroxyl radical ($OH\bullet$) is dominant, while nitrate radicals ($NO_3\bullet$) prevail at night (Atkinson et al., 1984). In the unpolluted marine atmosphere, the daytime reaction of DMS and $OH\bullet$ is the dominant process and controls atmospheric DMS concentration at the global scale, while $NO_3\bullet$ is important as it prevents atmospheric DMS build up during the night (Koga and Tanaka, 1993).

There are two major reaction pathways – *abstraction* and *addition*. $OH\bullet$ and/or $NO_3\bullet$ radicals *abstract* a hydrogen atom, leading to the eventual formation of SO_2 and/or H_2SO_4, or the $OH\bullet$ radical and DMS can react via an *addition* pathway, which predominantly produces MSA (Figure 1.10). For the $OH\bullet$ radical, the relative yields of the two pathways vary depending on temperature, with the *addition* pathway dominant below 270°K (-3°C) and the *abstraction* pathway dominant above 300°K (27°C) (Hynes et al., 1986). The $NO_3\bullet$ radical reaction occurs only via the *abstraction* pathway and is dependent upon the ambient NO_X concentration (Yin et al., 1990a; Yin et al., 1990b). How these radicals interact and compete under varying temperature conditions in the lower atmosphere has a major impact upon the relative strength of each DMS oxidation pathway and the resulting ratio of the products (particularly MSA and SO_2/H_2SO_4). More recently, the influence of the bromine oxide radical $BrO\bullet$has been highlighted (von Glasow and Crutzen, 2004), in particular because it is only involved in the *addition* pathway of DMS oxidation.

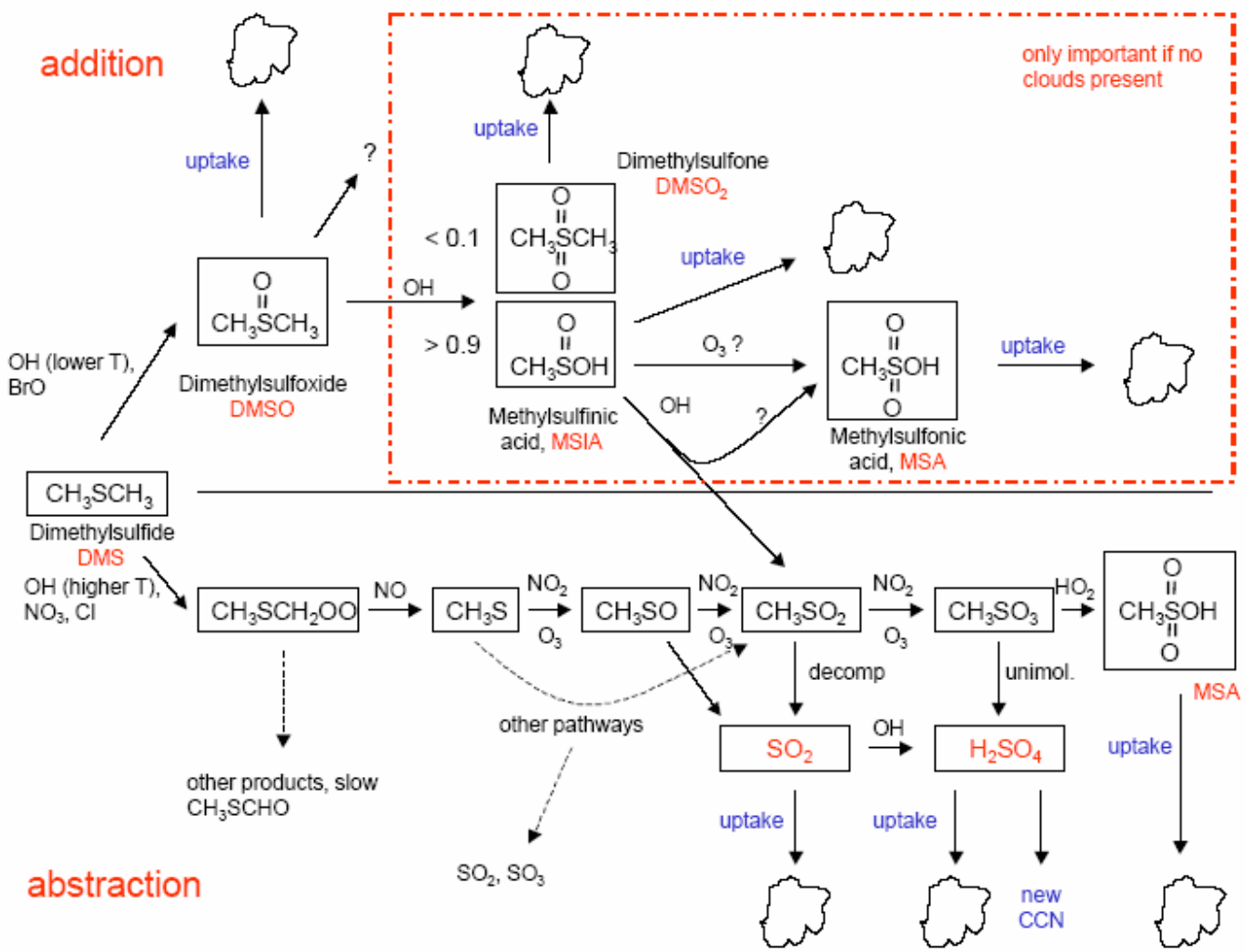

Figure 1.10 Atmospheric, gaseous oxidation reaction pathways of DMS (figure taken from von Glasow and Crutzen, 2004).

A variety of DMS oxidation products as well as DMS itself can be taken up onto existing CCN (Figure 1.11), while only a proportion of the H_2SO_4 produced results in new CCN (Figure 1.10). Aqueous oxidation, or oxidation after uptake onto CCN, can take place to form either MSA or H_2SO_4, but neither of these contributes to new CCN formation (Figure 1.11).

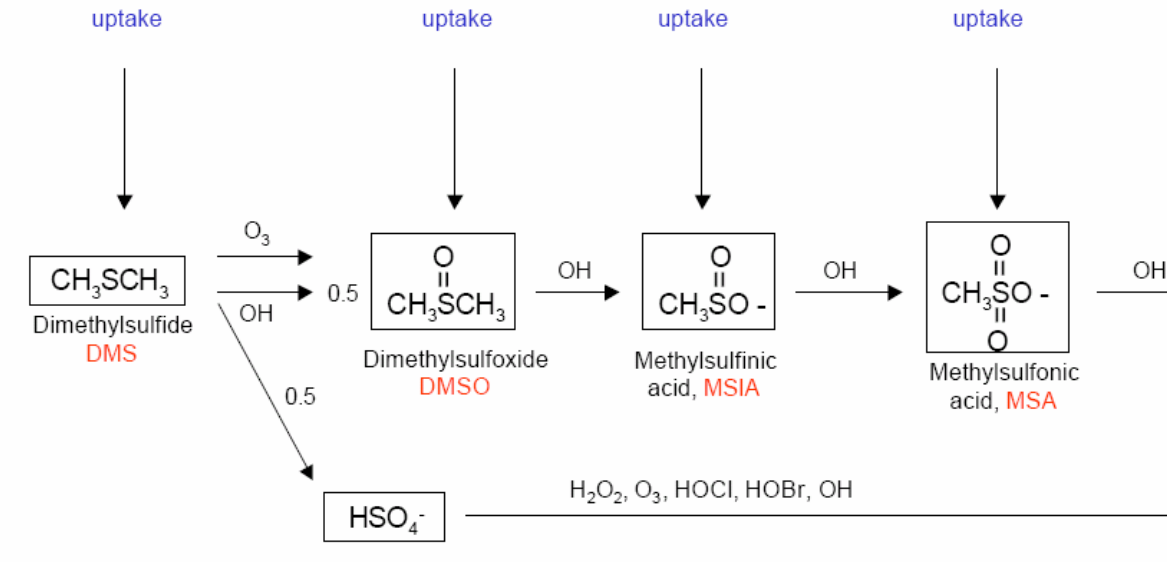

Figure 1.11 Atmospheric, aqueous oxidation reaction pathways of DMS (figure taken from von Glasow and Crutzen, 2004).

Understanding the relative production of SO_2/MSA from DMS oxidation is particularly important when attempting to interpret long-term atmospheric records, e.g. in ice cores (Saigne and Legrand, 1987; Legrand et al., 1988; Legrand et al., 1991; Whung et al., 1994). Other sources of sulphur to the atmosphere such as volcanic emissions and human activity also lead to the formation of SO_2 and sulphate aerosol. MSA, on the other hand, is only produced via DMS oxidation and is therefore a good indicator of DMS emissions. A clear seasonal trend can be seen at certain remote sites where DMS from a marine source predominates, e.g. Amsterdam Island (Sciare et al., 2000) and Antarctica (Savoie et al., 1993). Antarctic ice cores covering the past 160,000 years demonstrate increased concentrations of MSA and sulphate during the last ice age (Saigne and Legrand, 1987; Legrand et al., 1988; Legrand et al., 1991). It is not clear whether this is as a result of increased biological production, possibly as a result of changes in iron supply from the deserts to the oceans (Jickells et al., 2005), a change in trophic interactions favouring DMS production, or just changes in atmospheric circulation and snow deposition patterns. In fact, recent data from the European Project for Ice Coring in Antarctica (EPICA) suggests

that, over the past eight glacial cycles (740,000 years), the nssSO_4^{2-} flux has not changed substantially despite significant changes in climate (Wolff et al., 2006).

As there are three major sources of sulphate to the atmosphere, one challenge has been to identify the relative amounts contributed by sea-salt, anthropogenic and marine biogenic sources. This has been achieved using stable sulphur isotopes (i.e. $\delta^{34}S$), as anthropogenic $\delta^{34}S$ has a distinctly different signature, 0-5‰, compared to biogenic or sea-salt sources, +20‰ (McArdle and Liss, 1995). Distinguishing between marine biogenic and sea-salt sources is more difficult with stable isotopes as little fractionation occurs, but this can be achieved by calculating the % sea-salt (using sodium and chloride as conservative tracers). Using this information, a triangular plot of % sea-salt versus $\delta^{34}S$ can be made, with the three corners representing the major sources of sulphate. This approach has been used on size fractionated aerosol measurements and results suggest that biogenic sulphate mainly contributes to atmospheric aerosol by condensing onto existing particles (Wadleigh, 2004), while the majority of sub-micron sulphate aerosol result from anthropogenic emissions via either long-range transport of particles/SO_2 or from emissions due to shipping (Patris et al., 2000). In addition, this approach enabled Wadleigh (2004) to identify a substantial biogenic sulphate signature that was, rather unexpectedly, not associated with an increase in MSA.

There is a possibility that the oxidation of SO_2 might result in large isotopic fractionation, and it would therefore be important to quantify this effect. There are two oxidation pathways: homogeneous nucleation in the gas phase; and heterogeneous nucleation in the aqueous phase on the surface of aerosol or within cloud droplets. The kinetic process of homogeneous nucleation favours the lighter isotope while heterogeneous nucleation appears to fractionate in favour of the heavier isotope (Tanaka et al., 1994) so these pathways may effectively cancel each other out (McArdle et al., 1998). It has been postulated that precipitation samples might contain a greater proportion of heterogeneously oxidised SO_2 due to greater in and below cloud scavenging. However, a comparison of aerosol and precipitation $\delta^{34}S$ from Wales and Mace Head, Eire, did not find any consistent differences (McArdle et al., 1998).

1.2.3 Climatic Relevance of DMS: the CLAW Hypothesis

Since 1987, a significant amount of scientific endeavour concerning the reduced sulphur cycle in both the lower atmosphere and surface ocean has resulted due to the suggestion that DMS may impact upon global climate. In 1987, the landmark CLAW hypothesis was published, which tied together the following pieces of information (Charlson et al., 1987):

- A large number of phytoplankton species indirectly produce DMS which escapes into the atmosphere and is oxidised to MSA and $nssSO_4^{2-}$ aerosols.
- $nssSO_4^{2-}$ aerosol is found everywhere in the marine atmospheric boundary layer.
- Aerosol particles that act as cloud-condensation nuclei (CCN) in the marine atmosphere are mainly these $nssSO_4^{2-}$ particles.

Based on this information, a feedback loop (Figure 1.12) was proposed in which phytoplankton could self-regulate their environment through the production of DMS, making it more favourable for growth. The biggest uncertainty in this theory is the effect of cloud albedo on DMS production; in order for a regulation of climate to occur, the effect would have to be positive (Charlson et al., 1987). Assuming this was the case, the authors demonstrated that this effect over the oceans could be significant on a global scale.

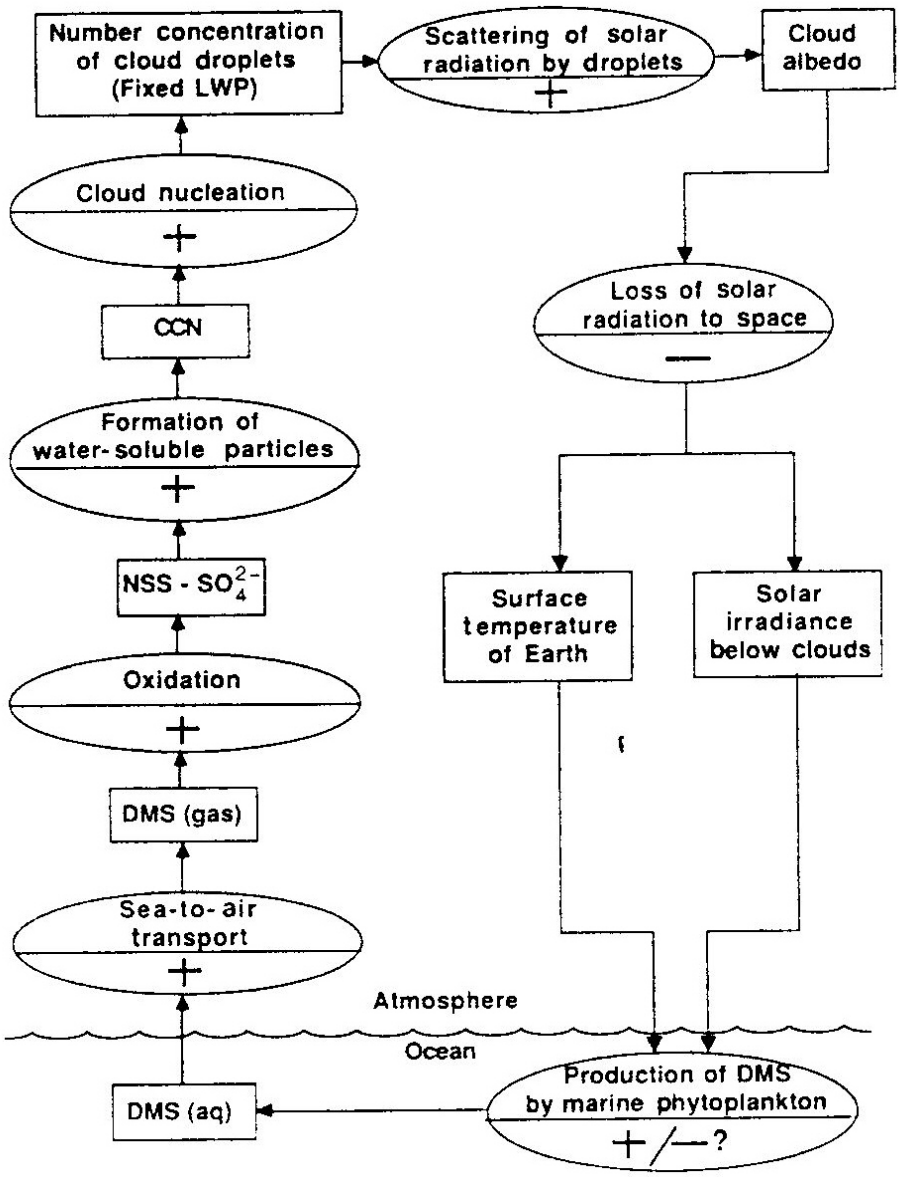

Figure 1.12 Conceptual diagram of the potential climatic feedback loop, later termed the CLAW hypothesis (figure taken from Charlson et al., 1987).

Since this landmark paper, scientists have discovered the system to be far more complex – for example, a lot more is now known about the synthesis of DMSP by phytoplankton. In addition, the timescales of the various processes involved are known to be different, introducing another level of complexity to the feedback loop. As a result, more questions have been posed than have been answered, whilst the biggest questions of all – 'Are the changes in our climate intimately related to DMS production?' and 'How is biological DMS production affected by changing climate?' – are far from being resolved.

1.3 The Reduced Nitrogen Cycle

As with the sulphur cycle, the concentration of NH_3 in surface seawater is a major determinant of its flux. However, in contrast to the sulphur cycle, the concentrations on both sides of the interface are as important as each other, affecting whether the flux is into or out of the ocean. As with other gases, the magnitude of flux is dependent upon wind speed (see Section 1.1.2). The following sections detail current understanding of the processes controlling concentrations of ammonia (NH_3) and its protonated form, ammonium (NH_4^+), in both the surface ocean and the lower atmosphere.

1.3.1 Surface Ocean

The global oceanic nitrogen cycle

In order to understand the reduced nitrogen cycle in the surface ocean, it is essential to put it in the context of the global oceanic nitrogen budget (Figure 1.13). The term *nitrogen* is used here to encompass many nitrogen-containing species and does not just refer to N_2, which is relatively inert in chemical terms. Although the flux estimates are now likely to be out-of-date (e.g. increased anthropogenic activity leading to increased atmospheric and riverine inputs to the ocean), this is a useful summary of the major nitrogen fluxes that interact within the global oceanic nitrogen cycle. The salient point from this diagram is that the individual inputs to and outputs from the euphotic zone are orders of magnitude less than internal cycling within surface waters, which is largely driven by biological activities. The source fluxes of 'new' nitrogen (i.e. nitrogen that is not recycled within the euphotic zone) are important in terms of ocean productivity as a change in these will directly impact upon 'new' production, which among other things directly influences the rate of carbon export to the deep ocean (assuming steady state between the deep ocean and the surface waters). The diffusion of nitrogen across the thermocline into the euphotic zone is a dominant source of new nitrogen yet remains a poorly constrained term. A more recent approach has been to use tritium (^3H) and its radioactive decay product (^3He) to estimate the diffusive flux across the thermocline (Jenkins, 1998).

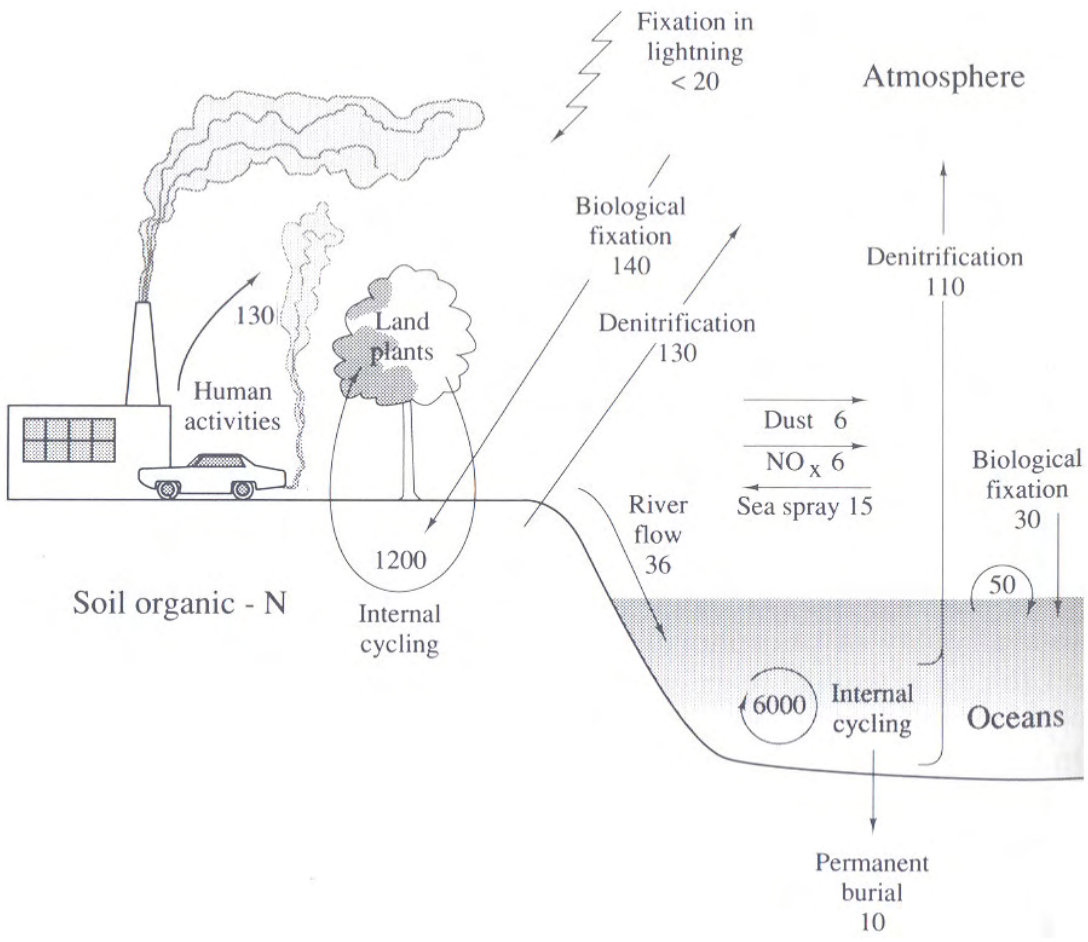

Figure 1.13 The global nitrogen cycle; pools and annual flux in 10^{12} g N (figure taken from Schlesinger, 1991).

Other than NH_4^+ and NH_3, the nitrogen cycle is dominated by nitrate (NO_3^-), as this is thermodynamically stable. Other dominant species are nitrite (NO_2^-), nitrous oxide (N_2O), gaseous nitrogen (N_2), and organic nitrogen (ON). Organic nitrogen can be classified as particulate or dissolved (PON and DON respectively) and this distinction is typically operationally defined by the pore size of the filter used (0.7 µm GF/F is typically used). The nitrogen pools in the surface of the open ocean are dominated by DON (>80%), while PON, NH_4^+, and NO_3^-+NO_2^- represent approximately equal proportions of the remainder (Berman and Bronk, 2003). An important form of DON is urea, $CO(NH_2)_2$, which is commonly exuded by zooplankton. Most of the aqueous inorganic chemical species represent oxidation states of nitrogen ranging from oxidised (NO_3^-, oxidation state +5) to reduced (NH_4^+, oxidation state -3), but an umbrella term is often applied – Dissolved Inorganic Nitrogen (DIN). The methylamines (monomethylamine, MMA; dimethylamine, DMA; and trimethylamine, TMA) also contain nitrogen and are widely distributed in the

marine environment, but at much lower concentrations (up to 2 orders of magnitude lower than ammonium, Gibb et al., 1999b), and are therefore not addressed here.

Figure 1.13 clearly shows the relative significance of 'new' nitrogen to the euphotic zone; if a steady state assumption is made for the surface ocean, new nitrogen inputs will be balanced by export, which is dominated by particulate organic export to the deep ocean. Eppley and Peterson (1979) first identified that the quantification of new production, or uptake of new nitrogen, was important as it would provide an indication of the export rate to the deep ocean. The authors suggested a now well-recognised formula, the *f*-ratio, which is the ratio of new to total (new + regenerated) production.

Measurements of the relative uptake of new versus regenerated nitrogen were first made and defined by Dugdale and Goering (1967) using ^{15}N-labelled compounds in the northwest Atlantic and northeast Pacific oceans. The authors suggested that NH_4^+ uptake (ρNH_4^+) should represent regenerated production as this dominates the regenerated nitrogen pool, while NO_3^- uptake and N_2 fixation rates (ρNO_3^- and ρN_2) should represent new production as these dominate the new nitrogen pools in the deep ocean and the atmosphere respectively. The authors acknowledged that less dominant forms of regenerated (e.g. urea) and new nitrogen (e.g. atmospheric deposition) are omitted. That is not to say, however, that these minor forms are insignificant and this simplification should be considered when interpreting the *f*-ratio. In addition, it should be noted that the *f*-ratio does not typically include N_2 fixation rates.

Biological processes

At this point it is probably worth noting that there is a distinct difference between nutrient *uptake*, nutrient *assimilation* and nutrient *incorporation* by phytoplankton. *Uptake* describes the removal of nutrients from the environment and physical transport into the phytoplankton's cell; *assimilation* describes the use of nutrients by phytoplankton to form small organic molecules and amino acids; and *incorporation* describes the combination of nitrogen-containing molecules to form proteins (Berges, 1997). During periods of nutrient sufficiency, nutrients can be taken up and stored in preparation for periods of nutrient deficiency; this has been termed 'luxury consumption'. This is relevant because, when a phytoplankton cell dies, the cellular membrane breaks (lyses) and releases the intracellular NH_4^+ store that has not yet been assimilated or incorporated into amino acids or proteins.

It has long been established that phytoplankton utilise NH_4^+, urea and NO_3^- as a nitrogen source in that order of preference (Wheeler and Kokkinakis, 1990). It is thought that this physiological preference is derived from an energetic advantage – NH_4^+ is the easiest to assimilate as it is the most reduced nitrogen form available and this is the form used within phytoplankton cells. The less energy a cell expends to get nitrogen into a form appropriate for cell function the better (Wheeler and Kokkinakis, 1990). However, as demonstrated by Rees et al. (2002), the relative concentrations of these chemical species also affect their uptake rates in the natural environment; in this case, the authors demonstrated that elevated urea uptake in the North Sea was driven by higher urea concentrations. Rees et al. (2006) found that, along an Atlantic transect, NO_3^- uptake (ρNO_3^-) was significantly correlated with NO_3^- and chlorophyll concentrations. In contrast, NH_4^+ uptake (ρNH_4^+) was less dependent on NH_4^+ concentration and showed no correlation with other measured environmental variables. As might be expected, the productive Benguela upwelling system off the coast of Africa showed significantly higher ρNO_3^- and ρNH_4^+ relative to oligotrophic areas of the Atlantic (Rees et al., 2006).

Further to the information above, there exists a complex interaction between NH_4^+ and NO_3^- such that the presence or absence of NH_4^+ can influence the uptake rate of NO_3^-. Generally, high NH_4^+ levels will reduce NO_3^- uptake, especially in the presence of low light levels – debate continues as to whether this is due to preferential uptake of NH_4^+, an inhibition of NO_3^- uptake, or both (Dortch, 1990). In addition to this, and of more significance to the NH_4^+ pool, there are reports that the presence of NO_3^- might inhibit NH_4^+ uptake (see Dortch, 1990).

If NO_3^- is taken up by phytoplankton, it must be converted to NH_4^+ as part of the assimilation process via nitrate reductase (NR) enzymes, which reduce NO_3^- to NO_2^- and then to NH_4^+. Numerous NR enzymes exist, with three forms recognised as specific to eukaryotic algae and higher plants (Berges, 1997). Greater variability in NR activity between different species and environmental conditions exists than can be discussed here, although irradiance has been identified as a critical factor (Berges, 1997). For example, one study demonstrated that NR activity in the diatom *Thalassiosira pseudonana* varied over a diel irradiance cycle, but also declined in response to nitrate exhaustion and/or the presence of NH_4^+ (Berges et al., 1995).

During phytoplankton grazing, zooplankton play an important role in the conversion of PON to DON (e.g. Fasham et al., 1990). In addition, mesozooplankton are known to directly excrete NH_4^+, which provides a source of regenerated nitrogen to the phytoplankton community; for example, a study in 2001 used incubation experiments to show that, through direct NH_4^+ excretion, copepods play a significant role in the food web of waters around South Georgia (Atkinson and Whitehouse, 2001). Zooplankton also produce nitrogen-rich faecal pellets that agglomerate and sink. These faecal pellets, or detritus, represent a major bacterial nitrogen source (PON and DON), often within or just below the chlorophyll maximum.

The heterotrophic bacterial decomposition (or remineralisation) of organic nitrogen back into its inorganic form is termed *ammonification* and represents a significant pathway of NH_4^+ regeneration. However, bacteria can also assimilate NH_4^+ rather than produce it (Rodrigues, 1998, and references therein), making the situation more complex. It has been hypothesised that the carbon to nitrogen (C:N) ratio of organic matter drives whether bacteria assimilate or produce NH_4^+ (e.g. Kirchman, 1994). Organic matter with a high C:N ratio (probably in a low nitrogen environment) may drive bacteria to assimilate at least a proportion of their nitrogen demand as inorganic NH_4^+. Conversely, organic matter with a low C:N ratio is likely to be used as an energy source and the process of ammonification dominates (Kirchman, 1994). However, this 'either/or' theory is challenged by observations of natural bacterial assemblages where simultaneous uptake and remineralisation has been observed (Tupas and Koike, 1991). It is likely that both occur at the same time, but to varying degrees depending on the environmental conditions.

The regeneration of inorganic nutrients by heterotrophic bacteria is part of the 'classic' marine food web, while the bacterial assimilation of nutrients is part of the 'microbial loop', as first suggested by Azam et al. (1983). In brief, the microbial loop involves the assimilation of nutrients by bacteria, which are then grazed by heterotrophic flagellates. The nutrients are then transferred up the food chain through microzooplankton and other higher organisms (see Figure 1.14). This process efficiently recycles nutrients and energy within the euphotic zone, sustaining production in the surface oceans (Azam et al., 1983). As a result of the microbial loop, bacterial uptake of NH_4^+ has been shown to influence the biological community. In an experiment conducted in Long Island Sound, size-fractionated uptake rates were affected by varying NH_4^+ concentrations such that bacteria

out-competed phytoplankton NH_4^+ uptake at lower NH_4^+ concentrations (Suttle et al., 1990).

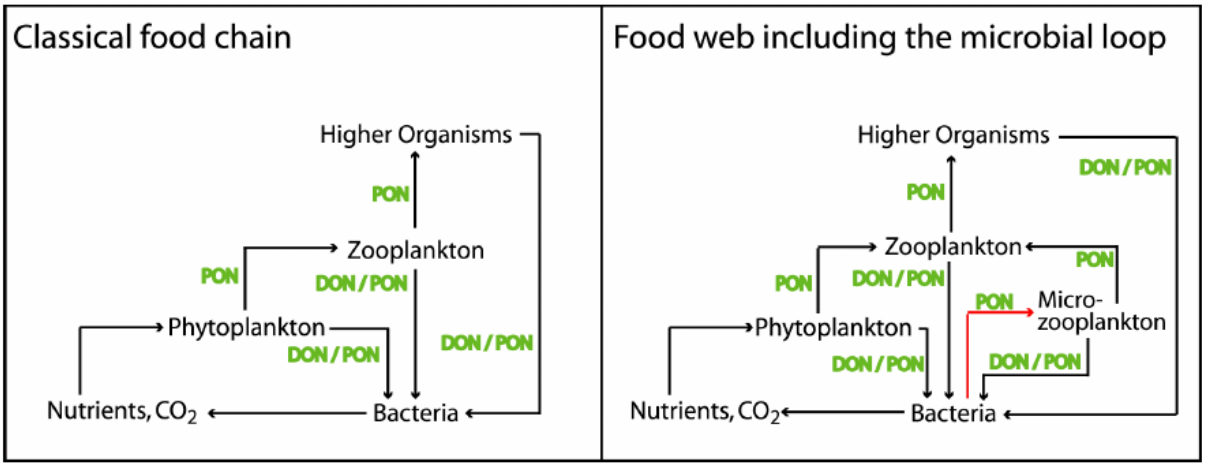

Figure 1.14 Schematic representation of the differences in organic nitrogen pathways between classical and contempory views of the marine food web. The PON pathway from bacteria to micro-zooplankton represents the important part of the microbial loop as it is the base of nutrient supply back up the food chain (figure taken from Johnson, 2004).

Chemoautotrophic bacteria mediate the processes of *nitrification* and *denitrification*, whereby they harness the energy from the oxidation and reduction processes of NO_3^- respectively. Nitrification occurs ubiquitously in the open ocean, whereas denitrification is limited to areas where oxygen is limited such as some sub-euphotic zone waters and sediments (Libes, 1992). The recent discovery of 'anammox' bacteria, which take NH_3 and NO_2^- and oxidise them to N_2, has revolutionised current understanding of the marine nitrogen cycle (Pilcher, 2005). In the anoxic waters of the Black Sea and the Golfo Dulce, Costa Rica, the *anammox* reaction has been shown to be responsible for the removal of NH_4^+ and subsequent production of gaseous N_2 (Dalsgaard et al., 2003; Kuypers et al., 2003). Using ^{15}N-labelled compounds, the conversion rate of NH_3 and NO_2^- to N_2 has been measured, and these results suggest that this process may well be significant to the global oceans, removing up to 15% of the global oceanic nitrogen store (Dalsgaard et al., 2003).

By far the largest potential source of nitrogen to the oceans is the atmosphere, which contains approximately 78% nitrogen, predominantly in the elemental form, $N_{2(g)}$. However, in the marine environment N_2 is only accessible to the diazotrophs (or nitrogen-fixers), which are also called cyanobacteria. A globally significant diazotroph is

Trichodesmium, which is a colonial cyanobacterium ubiquitous throughout the oligotrophic subtropical and tropical oceans (Capone et al., 1997). In the context of NH_4^+, nitrogen-fixers are important as they represent an indirect source of NH_4^+ to the marine environment, although they undoubtedly influence other nutrient (especially carbon) fluxes in the surface ocean as well.

The photoammonification of organic matter was first demonstrated by Bushaw et al. (1996) and is primarily an abiotic process. However, the authors demonstrated that the release of ammonium from humic substances under sunlight and particularly ultra violet light also stimulated further bacterial degradation of organic matter, likely because bacterial nitrogen limitation was relieved. Undoubtedly this process has an impact on the nitrogen cycle when conditions are suitable, but it is likely that this process is only significant in coastal waters where dissolved organic matter concentrations are high from river runoff (Johnson, 2004).

The marine NH_4^+ cycle in the open ocean

Johnson (2004) focussed on the nitrogen cycle from the perspective of NH_4^+ and NH_3, and his thesis contains a useful detailed schematic of the processes described above (Figure 1.15). Certain compartments and processes were omitted or simplified to avoid overcomplicating the diagram, but the key aspects are present (Johnson, 2004). In particular, nitrite (NO_2^-) was omitted and the processes of nitrification and denitrification are only represented from NH_4^+ to NO_3^- and vice versa. Urea was also omitted from the diagram as its processes are very likely to be the same as those for NH_4^+ (except for air-sea gas exchange). Finally, the anammox reaction was not included, presumably because it only dominates in anoxic waters.

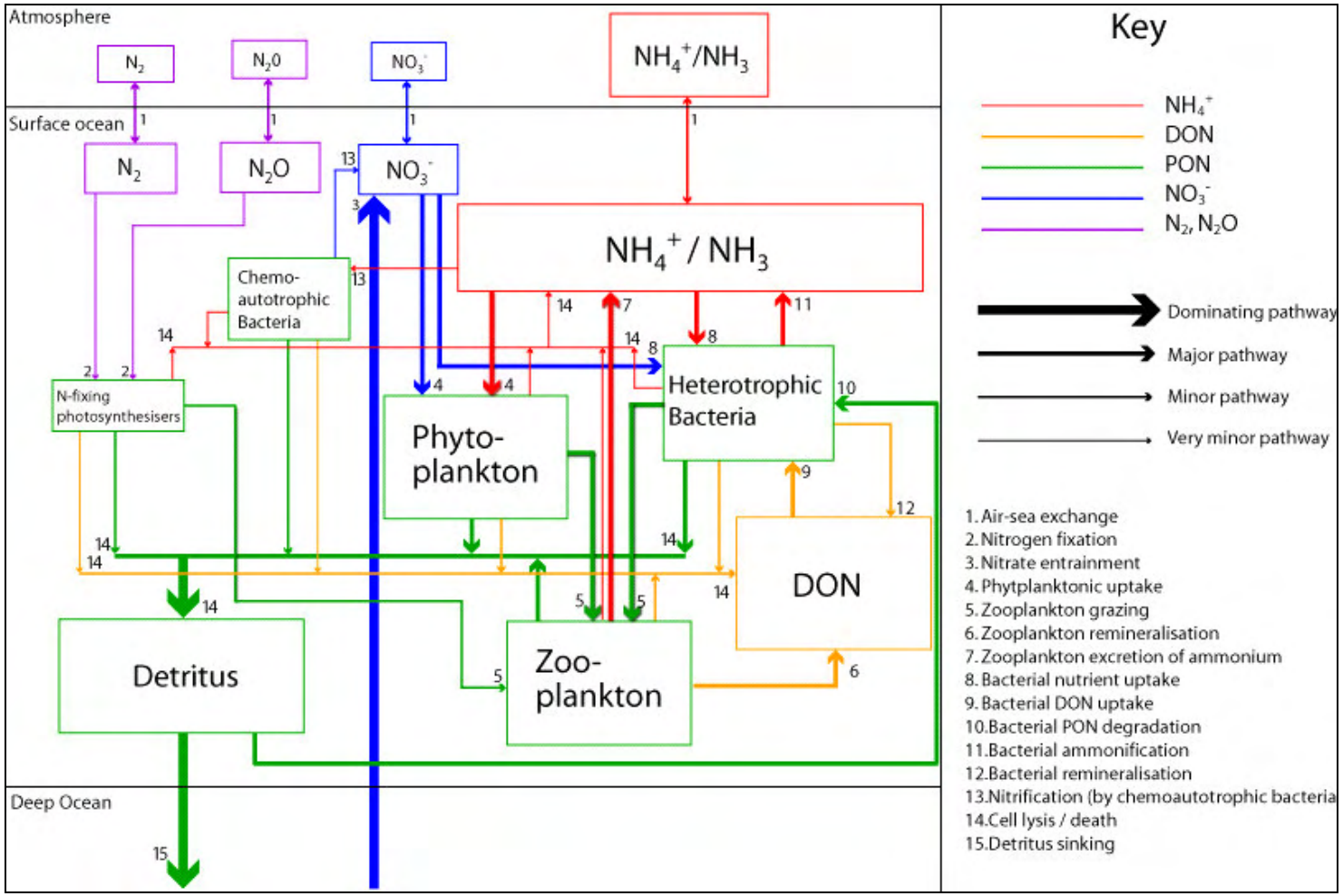

Figure 1.15 A detailed diagram of the marine NH_4^+ cycle in the open ocean, with emphasis on the processes directly and indirectly affecting the cycling of ammonium (figure taken from Johnson, 2004)**.**

Vertical NH_4^+ distributions in the open ocean

The vertical distribution of NH_4^+ in the open ocean does not show a typical 'nutrient profile' such as that seen for NO_3^- (i.e. low at the surface and elevated at depth). The NH_4^+ distribution pattern is dictated by the numerous processes affecting the production/removal of NH_4^+ (see Figure 1.15) and the distribution and density of phytoplankton, zooplankton and bacteria throughout the water column (see previous paragraphs). For example, measurement profiles from the Sargasso Sea and the Gulf Stream demonstrated an NH_4^+ maximum within the seasonal thermocline, and it was suggested that this was linked to a decoupling between NH_4^+ production and uptake processes (Brzezinski, 1988).

1.3.2 Lower Atmosphere

For air masses that have travelled over heavily polluted continental areas, their atmospheric $NH_{3(g)}$ concentrations are largely driven by anthropogenic activities. A natural background level of $NH_{3(g)}$ exists, controlled by emissions from vegetation and soils, but this has been significantly enhanced by other emissions, primarily as a result of intensive farming practises (Galloway et al., 1995). It is estimated that the turnover time for $NH_{3(g)}$ in the atmosphere is about 2 days, so after several days away from the continent all land-sourced $NH_{3(g)}$ should have been removed into aerosol or deposited, and any remaining ought to be of marine origin (Quinn et al., 1987). Maritime air masses display a natural $NH_{3(g)}$ signal that is far lower than that from the continents. For example, measurements of Southern Ocean air that had been away from the influence of land for thousands of kilometres had a mean $NH_{3(g)}$ concentration of 0.06 $\mu g\ m^{-3}$ and a sample standard deviation of 0.03 $\mu g\ m^{-3}$ (Ayers and Gras, 1980). The concept that the oceans might, in certain areas, be a net source of $NH_{3(g)}$ to the atmosphere was first put forward in the 1970s (Georgii and Gravenhorst, 1977) but lacked reliable data until more recently (Johnson, 2004). This development was primarily achieved through new methodology reducing detection limits and an improved sampling coverage of appropriate sites; the first of such data was collected by Quinn et al. (1988). Jickells et al. (2003) have presented fresh evidence that isotopic data might be a viable method for distinguishing between a clean marine source (isotopically light) and a source which has been influenced by anthropogenic emissions (isotopically heavy).

However, in order to calculate whether the remote oceans are a natural source of $NH_{3(g)}$ to the atmosphere, we must first understand more about the various atmospheric processes affecting its gaseous concentration. NH_3 exists in a number of different phase states within the atmosphere; there are four major phases – gaseous, particulate, cloudwater and rainwater, each phase with a different calculated residence time (Figure 1.16).

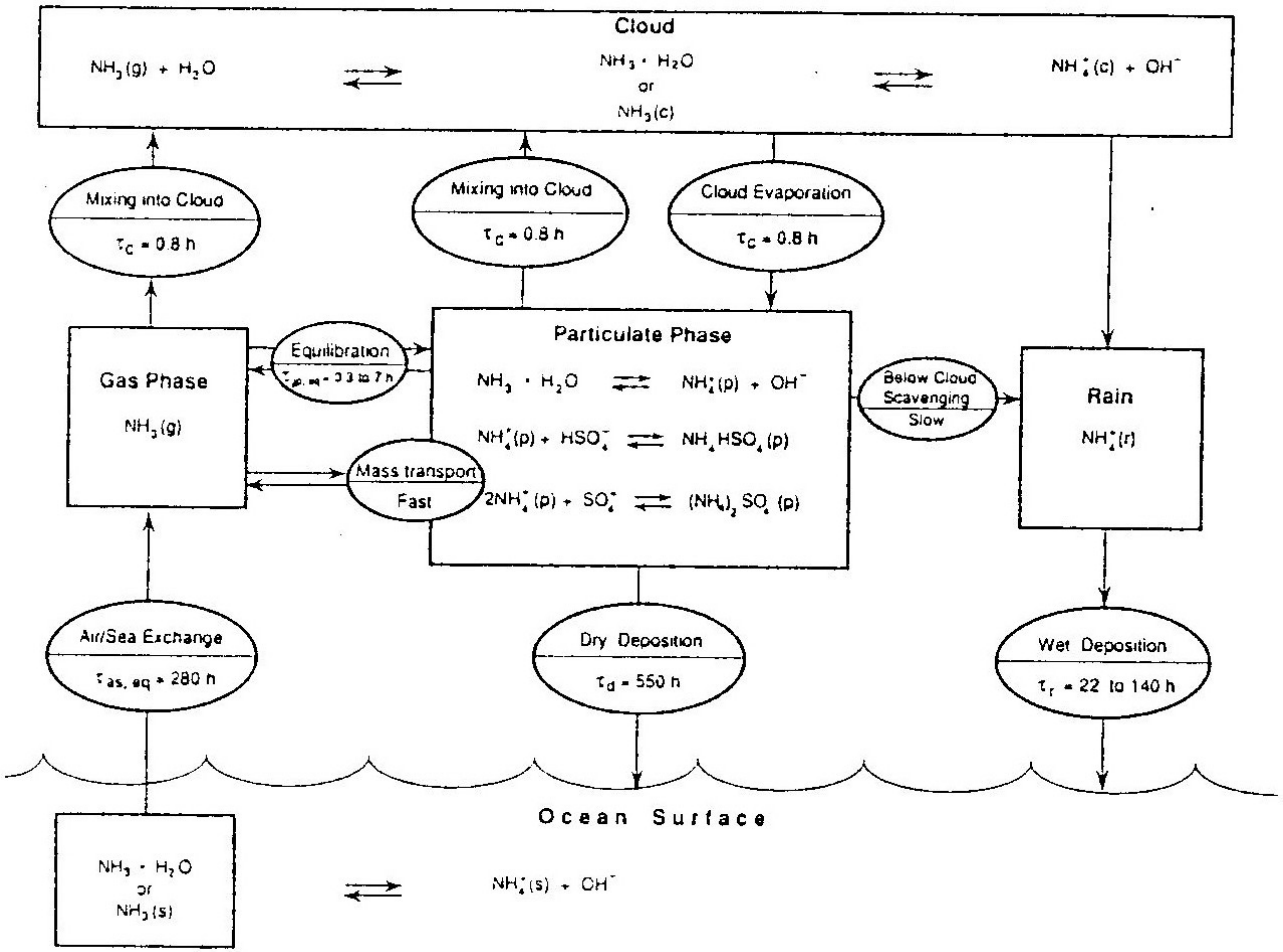

Figure 1.16 Physical and chemical processes of the marine atmospheric ammonia cycle (figure taken from Quinn et al., 1992). Each phase is represented as a box and each process as an oval. Residence times (τ) are calculated in Quinn et al. (1992).

The gas phase plays a central role in the environment as it interacts with all of the other phases. The particulate phase ($NH_4^+{}_{(p)}$) is initially formed when $NH_{3(g)}$ reacts with an acidic aerosol. This may be the most important single neutralisation process in the atmosphere (Harrison and Kitto, 1992). The most common acidic aerosol is sulphuric acid (H_2SO_4) and the reaction forms either NH_4HSO_4, $(NH_4)_2SO_4$ or letovicite ($(NH_4)_3H(SO_4)_2$). However, $NH_{3(g)}$ can also react with hydrochloric acid and nitric acid to form other, more volatile and therefore less stable aerosols, NH_4Cl and NH_4NO_3 (Jickells et al., 2003). The concentration of $NH_4^+{}_{(p)}$ is dependent on the $NH_{3(g)}$ concentration, the $NH_4^+{}_{(P)}/nssSO_4^{2-}{}_{(p)}$ ratio, the relative humidity (RH) and temperature (Quinn et al., 1987). As particulate ammonium ($NH_4^+{}_{(p)}$) is exceptionally deliquescent, the partitioning between aqueous particles and the gas phase is dependent on the disassociation constant of water (K_W), Henry's Law constant (H_C) and the liquid water content of the aerosol. All of these parameters are dependent on temperature and so partitioning between these phases can also be expected to be affected by temperature (Quinn et al., 1987).

Cloudwater ammonium ($NH_4^+{}_{(c)}$) formation operates via at least two mechanisms. The first is essentially the end-member of $NH_4^+{}_{(p)}$ deliquescence and cloud condensation nuclei (CCN) formation. The second mechanism is more direct and involves the attraction of water to a sulphate CCN, and $NH_{3(g)}$ subsequently dissolving into the cloudwater (Quinn et al., 1987). The high solubility of NH_3 means that there is unlikely to be much $NH_{3(g)}$ partitioning out of cloud droplets. Outside of clouds, $NH_{3(g)}$ and $NH_4^+{}_{(p)}$ will partition between the solid and gaseous phases, with the exact ratio depending upon the composition of the particulate aerosol considered. The ultimate fate of both $NH_{3(g)}$ and $NH_4^+{}_{(p)}$ in the atmosphere is deposition, both wet and dry (Quinn et al., 1987; Warneck, 1988).

Equilibrium equations can be formulated for all of the aforementioned phase partitions, but it is important to consider whether the system is actually at equilibrium. Determining the rate of reaction is an important step in order to calculate whether the system might have reached equilibrium or not. An example of this is a study where the aerosol acid neutralisation rate was determined through interpretations of horizontal gradients in acidity (Harrison and Kitto, 1992). The authors found that the rate constant values reduced as the aerosol became more neutralised, concurring with previous laboratory studies (Harrison and Kitto, 1992, and references therein). Quinn et al. (1992) used modelled results based upon such rate constants and compared them with measurements from two areas of the Pacific Ocean in 1987 and 1988. Although there are various errors associated with the

methods and model, the results indicate that the atmospheric system is not always in equilibrium, and that both physical and chemical processes affect the ability of the system to attain equilibrium (Quinn et al., 1992). If this is the case, it makes understanding these processes an even more complex problem.

In order to fully examine the reduced nitrogen cycle in the lower atmosphere, the flux of wet deposition to the sea surface must be considered. The concentration of rainwater ammonium ($NH_4^+{}_{(r)}$) is likely to be a function of the cloudwater ammonium ($NH_4^+{}_{(c)}$) and the rain's efficiency of $NH_{3(g)}$ removal from the atmosphere. A number of datasets demonstrate that, within a factor of two, these assumptions hold (Quinn et al., 1987 and references therein). However, certain measurements indicate that $NH_4^+{}_{(r)}$ / $NH_{3(g)}$ is not actually in Henry's law equilibrium (Ayers et al., 1984). A possible explanation for this is that the solubility of $NH_{3(g)}$ is so high that, under normal cloud conditions, it will reside predominantly in the liquid phase (Brimblecombe, 1984).

The input of nitrogen to the world oceans via atmospheric deposition is relatively insignificant compared to other sources of nitrogen (e.g. deep water upwelling), but it is still important on a regional scale. In oligotrophic regions, episodic nitrogen deposition events have been shown to significantly contribute towards 'new' production (Owens et al., 1992). Another form of nitrogen deposition to the ocean encouraging new production is the sea salt displacement reaction:

$$HNO_{3(g)} + NaCl_{(s)} \rightarrow NaNO_{3(s)} + HCl_{(g)}$$

Equation 1.20

This reaction enhances nitrogen deposition (dry) as the resultant nitrogen aerosol is larger and more prone to gravitational settling (Spokes et al., 2000). It's important to note that this last example is significant in the marine/lower atmosphere nitrogen cycle, but is less related to the cycling of NH_3.

1.4 Interaction of the Cycles

There are some similarities between the reduced nitrogen and sulphur cycles in the surface ocean. An obvious yet significant link between the two cycles is that a phytoplankton cell requires nitrogen to grow, which will ultimately determine the amount of DMSP synthesis (and therefore DMS production) that can occur. Both DMSP and NH_4^+ are released upon cell lysis, while zooplankton grazing can lead to the production of DMS and NH_4^+, although through separate pathways (see Sections 1.1.1 & 1.3.1). However, there are many different processes in the surface ocean that affect NH_4^+ and DMS concentrations in substantially different ways. DMS production depends on phytoplankton speciation and their intracellular content of DMSP, the growth rate of DMSP-producers, and the rate of enzymatic cleavage of DMSP. NH_4^+ concentrations are determined by the bacterial decomposition of organic matter and uptake by phytoplankton and these are in turn determined by the relative availability of NH_4^+, carbon, NO_3^-, and light.

Aside from the similarities, differences and indirect links between the cycles mentioned above, certain evidence has suggested a direct link between the nitrogen and sulphur cycles. Both DMSP and its structural analogue, glycine betaine (GBT, $(CH_3)_2NCH_2CH_2COO^-$), are thought to be effective compatible solutes within phytoplankton cells. It has been suggested that the relative production of DMSP and GBT might be linked on an evolutionary timescale (Simo, 2001). In the open ocean, diatoms thrive in nitrogen replete environments and produce relatively little DMSP, while small coccolithophorids and dinoflagellates are typical of environments with lower nitrogen availability and could have evolved to produce more DMSP. However, there is a significant exception to this theoretical rule - *Phaeocystis* spp. thrives under nitrogen replete conditions, whilst at the same time exhibiting high intracellular DMSP concentrations (Simo, 2001).

Another suggested driver of DMSP synthesis is that it acts as part of an overflow mechanism for excess energy and reduced sulphur when the cell has a high light source but nitrogen is limiting (Stefels, 2000). DMSP is synthesised from methionine ($CH_3S(CH_2)_2CH(NH_2)COOH$) and this process liberates nitrogen for reuse within the cell in alternative amino acid forms; this is particularly important when ambient nitrogen is limiting. In addition, it is hypothesised that this mechanism keeps both methionine and its precursor cysteine at low concentrations, preventing the onset of negative feedback

mechanisms that would inhibit nitrogen (as NH_3) liberation (Stefels, 2000). The cell would therefore be able to utilise an internal nitrogen source despite limiting ambient concentrations, thus sustaining other cellular processes (such as carbon uptake) at an optimum rate. Some fieldwork results have corroborated the concept that phytoplankton might preferentially synthesise DMSP when nitrogen is limiting (Turner et al., 1988). However, more recent evidence from phytoplankton culture work also exists in opposition to this theory (Keller et al., 1999). It is worth noting at this stage that there are numerous compounds that can act as compatible solutes and this complicates the picture somewhat.

The controls on the air-sea flux of NH_3 and DMS are in complete opposition (i.e. NH_3 = gas phase; DMS = liquid phase). The DMS flux is always out of the ocean due to the low atmospheric concentrations, while the NH_3 flux is bi-directional. Any link between the cycles is unlikely to be directly driven by the sea-air flux. In the lower atmosphere, the link between the nitrogen and sulphur cycles is simpler, stronger and highly evident as the interaction of the two elements is a key part of cloud formation, especially in regions away from continental influence. $NH_{3(g)}$ can either dissolve directly into cloud water or, more importantly, can react with acidic sulphate aerosol to form particulate ammonium sulphate. The presence of ammonium in sulphate aerosol has actually been shown to enhance particle nucleation in the marine boundary layer (Coffman and Hegg, 1995), making effective CCN. An increase in the number of sulphate aerosols in the atmosphere enhances the scavenging of $NH_{3(g)}$ and therefore the nitrogen deposition back into the ocean (Liss and Galloway, 1993).

One study exists where simultaneous atmospheric, oceanic and flux measurements were made in the Pacific Ocean for sulphur and nitrogen (Quinn et al., 1990). The results are interesting as the fluxes of both compounds were out of the ocean and of the same order of magnitude, and a relationship within the atmospheric data was apparent (Figure 1.17). No relationship, however, was observed between the concentrations of DMS and NH_3 in the water column. Air mass back-trajectories provide an insight into their history. The numbers plotted on Figure 1.17 represent three different air masses. Air mass **1** displayed some continental influence; air mass **2** had passed over an active Hawaiian volcano and had therefore probably acquired more sulphate aerosol; air mass **3** was the closest in composition to unpolluted marine air (Quinn et al., 1990). As can be seen, nearly all of the air mass **3** samples plot between the 2:1 and 1:1 ratio lines, which represent $(NH_4)_2SO_4$ and NH_4HSO_4 respectively. This phenomenon has also been observed during the AMT

campaign (see Chapter 6 for details) and, as the ocean is the likely input source, a possible linkage between the cycles of reduced nitrogen and sulphur is implied.

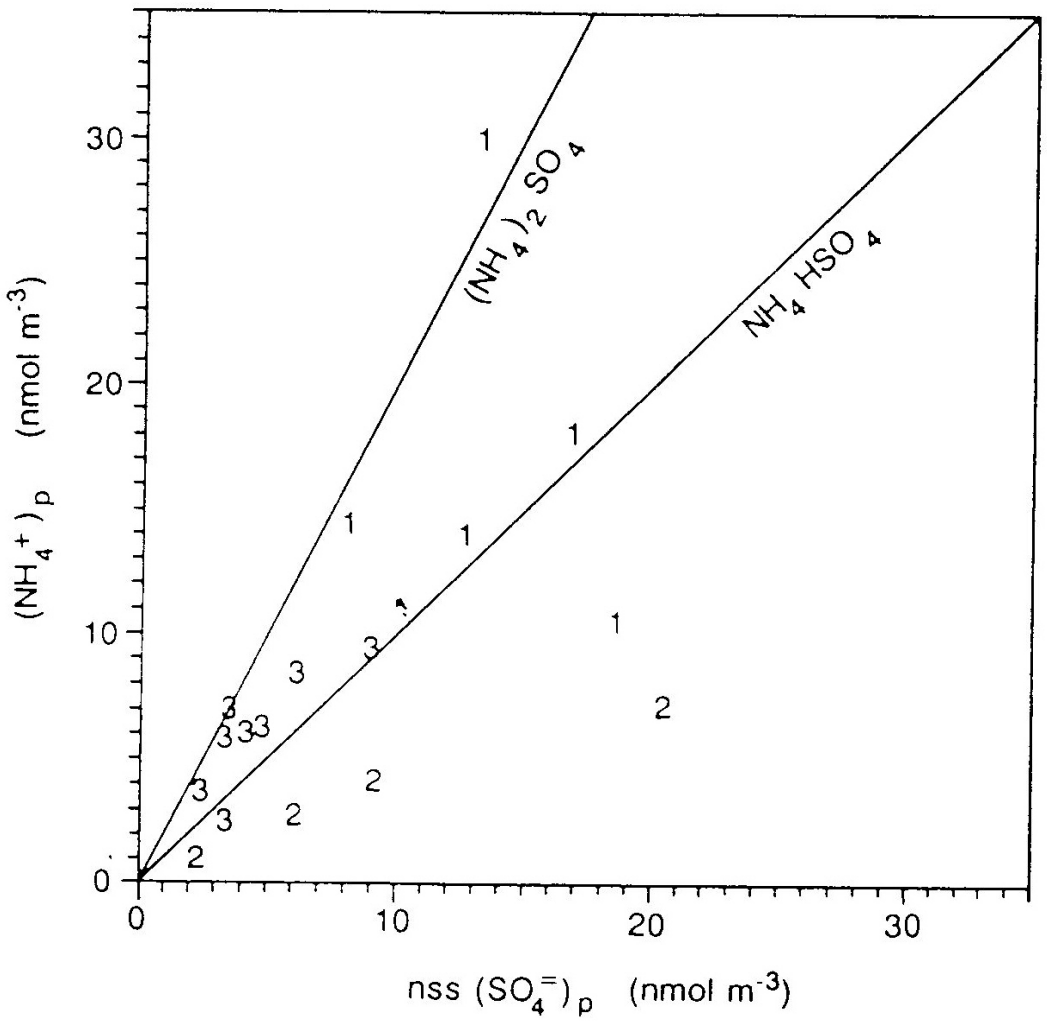

Figure 1.17 Particulate nss$(SO_4^{2-})_p$ versus $(NH_4^+)_p$ for air masses over the Pacific Ocean during April and May, 1988, along 170°W from 50°N to 11°S. Data points are labelled **1**, **2** and **3** corresponding to different sample groups. The lines represent a 2:1 ratio ($(NH_4)_2SO_4$) and a 1:1 ratio (NH_4HSO_4 composition) (figure taken from Quinn et al., 1990).

Taking this concept further, the air-sea fluxes might be expected to corroborate the atmospheric story. Whilst there is little correlation (Quinn et al., 1990), the fluxes are of the same order of magnitude and are both OUT of the ocean. It should be noted that the availability of $NH_{3(g)}$ for reaction (immediate) is quite different to that of DMS as DMS must first be oxidised (taking hours to days). In addition, atmospheric NH_3 data collection occurred throughout a minimum 12 hours period, which would likely obscure any intricacies in the $NH_{3(g)}$ flux signal (Quinn et al., 1990). In contrast, DMS flux calculations

are usually based on discrete measurements and often display significant variability over a relatively small spatial or temporal scale (e.g. Ayers and Gillett, 2000). The differences in reaction rate and sample collection methodology for DMS and NH_3 could impact upon flux calculations, making it difficult to directly compare them.

An atmospheric time series from a remote marine Antarctic site (Mawson station) corroborates the results of Quinn et al. (1990), demonstrating a consistent pattern in the seasonal cycles (over 5 years) of aerosol MSA, $nssSO_4^{2-}$ and NH_4^+ concentrations (Savoie et al., 1993). All element concentrations peak in the austral summer at levels more than an order of magnitude greater than in winter. The timing of these cycles matches that of atmospheric dimethylsulphide as measured by Ayers et al. (1991) and it is therefore highly likely that the aerosol $nssSO_4^{2-}$ has a biological source. Savoie et al. (1993) were unsure as to the origin of the NH_4^+, but suggest an ultimate connection with oceanic biological processes due to the coherence of the seasonal cycle of atmospheric NH_4^+ with MSA and $nssSO_4^{2-}$.

As has been described, the sulphur cycle is very complex and understanding how it fits into the CLAW hypothesis is no minor task. Probably the biggest challenge is whether a change in radiation budget would positively or negatively influence DMS production. However, understanding how the reduced nitrogen cycle fits into this feedback loop is arguably as important. If there is a link between the cycles, then any number of changes in the water column or in the various flux parameters could considerably alter the atmospheric dynamics and hence radiative properties of the remote marine atmosphere. In addition to this, even small differences can have a significant influence on the pH and nitrogen content of natural rainwater, which would have significant implications to marine and terrestrial ecosystems (Charlson and Rodhe, 1982). Finally, when this is all put in the context of the current predictions for climate change and its various implications, a greater comprehension of both of the nitrogen and sulphur cycles is essential.

1.5 The AMT Programme and Thesis Objectives

The Atlantic Meridional Transect (AMT) programme has traditionally utilised the annual passage of the British Antarctic Survey (BAS) research ship, the James Clark Ross (JCR), between the UK and the Falkland Islands (northward in May/June and southward in Sep/Oct). The programme can be divided into two distinct phases of activity in terms of DMS data collection – the first between 1995 and 2000 and the second between 2002 and 2006. In Phase One the project was relatively small; the JCR was utilised as a 'ship of opportunity' and her route was relatively direct, passing close to the African coastline in the northern hemisphere. The second phase of activity was a broader scientific programme with objectives requiring passage into the northern and southern gyres and a much wider range of parameters were measured. DMS(P) data collected during Phase One (AMT-5 and -9) was provided by Conor McKee and the data from Phase Two (AMT-12, -13 and -14) was collected as part of this PhD project. The location of each surface sample point and the routes taken during each cruise are plotted in Figure 1.18.

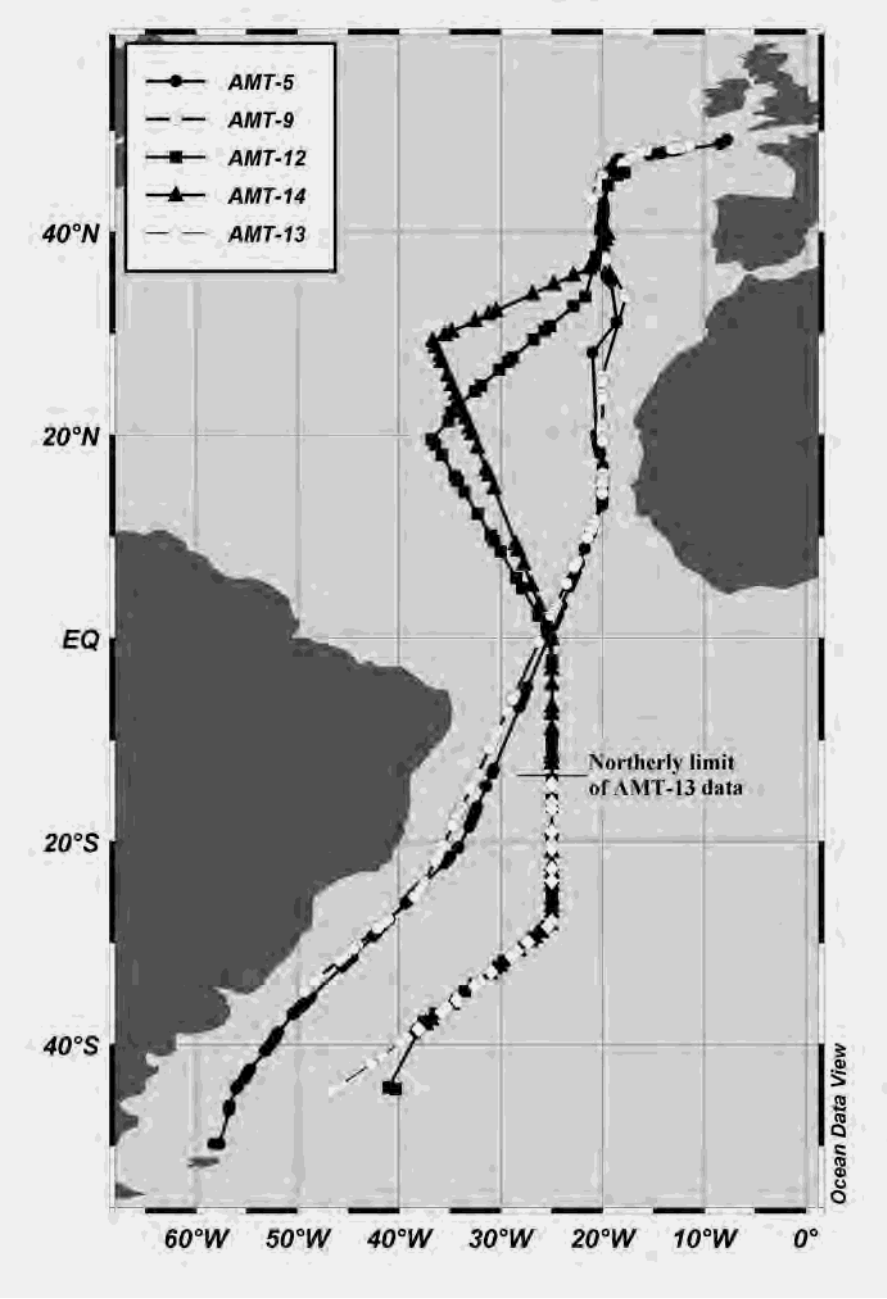

Figure 1.18 Cruise tracks for five Atlantic Meridional Transect cruises (southbound in September, northbound in May) – AMT-5 (Sep. 1997), AMT-9 (Sep. 1999), AMT-12 (May 2003), AMT-13 (Sep. 2003) and AMT-14 (May 2004). Plot produced using *Ocean Data View* (http://odv.awi-bremerhaven.de/home.html).

During the AMT cruises, in addition to DMS(P) measurements, a variety of ancillary biological data was collected from surface waters. In the lower atmosphere, aerosol composition and gaseous NH_3 data were collected during Phase Two of the AMT programme. The intention of this project was to investigate the reduced sulphur and nitrogen cycles in the surface ocean and lower atmosphere and substantiate how they are linked in the remote environment. This work would primarily use the extensive dataset

collected during AMT and investigate the relationships between DMS(P) concentrations and other biological data in the hope that this might reveal the reasons behind the ambient concentrations measured. Further, where gaseous NH_3 data were collected, gas fluxes for both NH_3 and DMS would be calculated and their direction and magnitude compared. Using atmospheric aerosol data, the ratio of particulate sub-micron NH_4^+ to $nssSO_4^{2-}$ would be investigated to see if it corroborated the data of Quinn et al. (1990).

As with most oceanographic and sea-based research, many aspects of the AMT cruises went very well but inevitably, instrumentation problems hampered data collection. Sampling strategy had to be changed in order to accommodate these problems and my data-interpretation intentions also changed. The proceeding chapters should therefore be described as a development of my originally intended data synthesis. Chapter 2 details the data collection methods used throughout the AMT programme. Chapter 3 investigates DMS(P) concentrations and their statistical relationships with concurrent biological measurements in surface waters. Chapter 4 concentrates solely on the upper 10 metres, comparing surface DMS measurements with those that would be predicted using five published predictive algorithms for global surface DMS concentrations. During AMT-14, extra measurements were made of DMSP-lyase activity (DLA) and these novel results are discussed in Chapter 5. Finally, Chapter 6 explores the atmospheric data collected during the AMT programme along with NH_3 flux measurements. This chapter also includes a discussion of the global distribution of the NH_4^+:$nssSO_4^{2-}$ ratio. Chapter 7 attempts to draw together the conclusions of the preceding chapters before identifying areas that the scientific community should address and discussing how future work should progress.

2 Methods

2.1 Seawater Sampling

Samples were either collected from CTD casts at pre-dawn (approx. 0300hrs local time) and mid-morning (approx. 1100hrs local time), or via the ship's non-toxic seawater supply (approx. 1600hrs local time). Samples from the non-toxic seawater supply were only used for flux calculations (see Chapter 4, Figure 4.1) and not for any other type of data synthesis. The CTD system used was a *Sea-Bird 9/11 plus* fitted with a sampling rosette of 20 litre Niskin bottles. Whilst removing samples from the Niskin bottles, every effort was made to minimise degassing. Water samples were transferred using a length of polyvinylchloride (PVC) tubing into 750 ml amber glass bottles fitted with gas-tight stoppers. Prior to analysis, samples were stored in these amber bottles at ambient sea surface temperature for a maximum of three hours.

2.2 Sampling and quantification of DMS and DMSP

All DMS analyses were carried out using purge and trap (see Turner et al., 1990). Before purging each sample of DMS, the seawater was gently filtered through 25 mm glass-fibre filters (GF/F, Whatman Ltd., Kent, UK; nominal retention size 0.7 µm) to isolate particulate DMSP (DMSPp). During AMT-5, -9 and -12, 20 ml of sample was filtered and the filters were stored in crimp-sealed vials with 10 M sodium hydroxide (NaOH) to hydrolyse DMSPp into DMS for analysis by purge and trap the next day. During AMT-13 and AMT-14 a slightly different approach was taken and a larger volume (50 ml) of seawater was filtered. These filters were placed in sealed 4 ml vials with 3 ml of 500 mM NaOH. Samples were equilibrated at a constant temperature (30ºC) for DMS analysis by headspace the following day (see method described below). 5 ml sub-samples of purged filtrate were transferred to 20 ml vials with excess NaOH (1 ml of 10 M NaOH) to cleave dissolved DMSP (DMSPd) to DMS. These were then filled with distilled water to eliminate any headspace, sealed and stored until the next day for analysis by purge and trap.

Purge and trap analysis for DMS involved bubbling an inert gas (oxygen-free nitrogen, purge time = 15 min for a 20 ml sample, 20 min for a 50 ml sample; flow rate = 60 ml min^{-1}) through the sample to strip it of volatile gases. These gases were then dried

before passing through a trap, which consisted of a 30 cm section of chromatographic material (Tenax-TA, Scientific Instrument Services Inc., New Jersey, USA) enclosed in a 50 cm length of 1/8th inch (approximately 3.2 mm) diameter Teflon tubing. The trap was cooled to approximately 0°C in a salt-ice-water dewar to trap and concentrate DMS, before being desorbed and flushed into the gas chromatograph by heating with boiling water. The original purge and trap method was described by Turner et al. (1990) but, unlike the method described above, this involved trapping the DMS cryogenically at – 150°C before injection into the GC (see Figure 2.1).

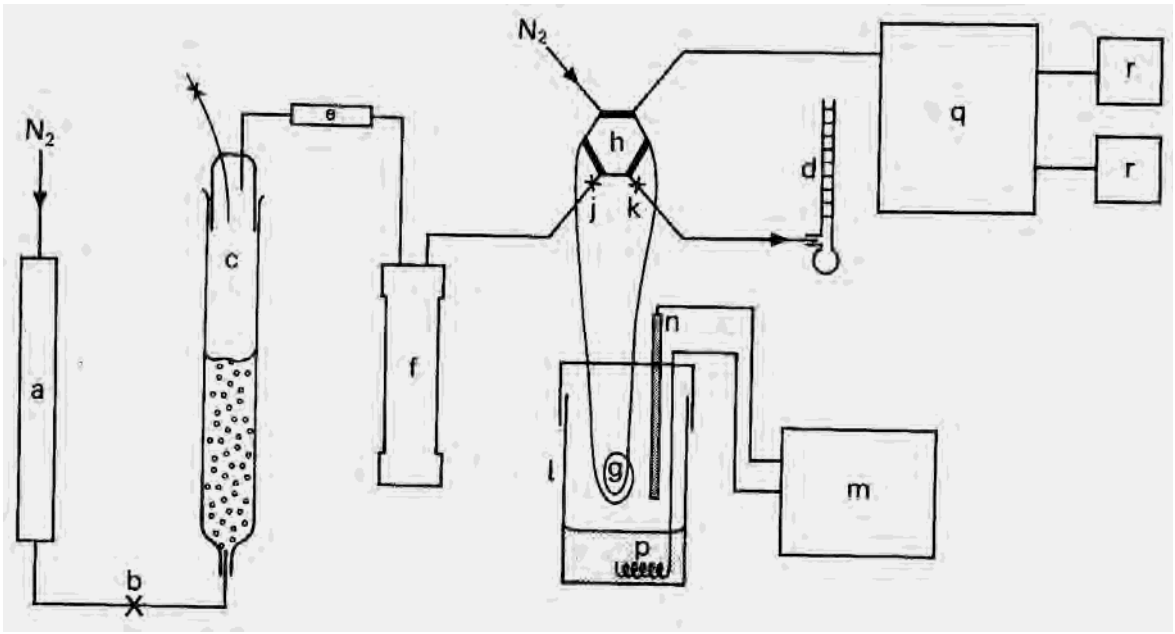

Figure 2.1 Schematic of original purge and trap system (figure taken from Turner et al., 1990). (a) gas scrubber; (b) needle valve; (c) purge chamber; (d) flow meter; (e) water trap; (f) nafion drier; (g) cold trap; (h) six-port valve; (j,k) two-port valves; (l) dewar; (m) temperature controller; (n) temperature probe; (p) 47-Ω resistor; (q) GC with FPD; (r) integrators. It should be noted that the method used in this work used a dewar filled with a salt-ice-water mixture to cool a trap filled with adsorbant material (Tenax-TA) and as a result, parts (m), (n) and (p) were not necessary. In addition, modern GCs are now connected to a computer and software package, which act as a more sophisticated equivalent of an integrator (r).

Headspace analysis for DMS involved piercing the PTFE septum and removing 250 µl of gas from the headspace for direct injection onto the GC column. The in-vial detection limit for this headspace method is approximately 25 nM. This method required an increase in the volume of sample filtered; this was tested and shown to not significantly impact upon measured DMSPp concentrations (Figure 2.2).

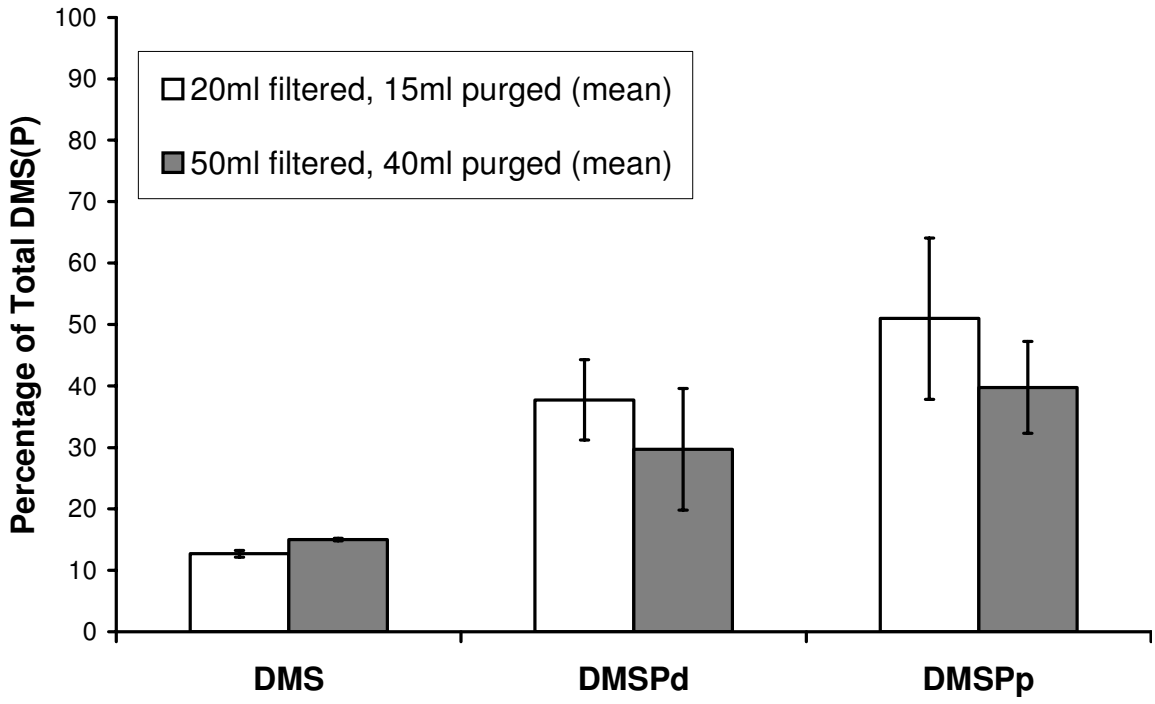

Figure 2.2 Mean of triplicate measurements of the same sample using the 20 ml or the 50 ml filtration methods; error bars represent 1 standard deviation about the mean. Although the 50 ml filtration method did appear to produce lower DMSPp concentrations than the 20 ml filtration method, they were not significantly lower and did not result in elevated DMSPd concentrations. Data presented as percentage of total DMS(P) to aid comparability between methods.

All samples were quantified using a gas chromatograph (GC 2010; Shimadzu, Milton Keynes, UK) equipped with a 30 m x 0.53 mm CP-Sil 5CB column (Varian Inc., Oxford, UK) and a flame photometric detector (FPD). The calibration of the system was checked daily using standards prepared by hydrolysing a solution of commercial DMSP (Centre for Analysis, Spectroscopy and Synthesis (CASS), University of Groningen Laboratories, The Netherlands) with excess concentrated NaOH (10 M for purge and trap, or 500 mM for headspace). The analytical error of these procedures was 5%, 20% and 20% relative standard deviation for DMS (0.7 nM), DMSPd (2.0 nM) and DMSPp (2.7 nM), respectively.

2.3 Sampling and quantification of DMSP-lyase activity

The sampling and analysis protocol used for *in vitro* DMSP-lyase activity (DLA) was an adaptation of the methods described by Steinke et al. (2000) and Harada et al. (2004). Briefly, immediately after collection approximately 1 litre of seawater sample was filtered using low vacuum (< 20 Pa pressure) onto 25 mm glass-fibre filters (Whatman GF/F). Filtration volumes were adjusted to complete filtering within 30 min and filters were not allowed to run dry. The filters were immediately folded in half and placed in a cryovial in a −80°C freezer. All samples were analysed 5 months after their return to the onshore laboratory. Due to the sampling logistics of the campaign it was not possible to directly test for the loss of activity in the AMT samples. Previous measurements have shown that the process of freezing and storage leads to a loss of ~35 % activity (Steinke et al., 2002b). Assuming that this is true for these samples, it will not affect the outcome of this study as the relative changes in DLA are more important than the absolute numbers for the assessment presented in Chapter 5. However, the values presented are likely to be an underestimate of the true *in vitro* DLA *in situ*.

In the laboratory, the frozen filters were placed into 4 ml glass vials containing 3 ml of 0.2 µm sterile-filtered buffer solution (200 mmol L^{-1} TRIS buffer prepared in 500 mmol L^{-1} NaCl solution, pH adjusted to 8.0 with HCl) to permeabilise the cells. Vials were incubated at 30°C, and 50 µl of 1.2 mol L^{-1} DMSP solution added (final concentration = 20 mmol L^{-1}). Following addition of substrate DMSP, at least four 8 µl headspace measurements for DMS were made every 10 min using an autosampler system (AOC 20i+s; Shimadzu, Milton Keynes, UK). Resulting DMS concentrations were used to calculate the DMS production rate and this rate is considered representative of *in vitro* DLA. Blank samples (buffer solution + blank filter + 50 µl DMSP solution) were run in parallel to correct for abiotic DMS release.

2.4 Wind Speed Measurements

The anemometer was positioned with 0 degrees at the ship's bow (approximately 21 m above sea level) and average data recorded every minute. The wind speed data were corrected for ship's direction and speed and then normalised to the standard height used in flux calculations (i.e. 10 m above sea level) using a bulk formula (see Section 1.1 for more detail).

2.5 Ancillary Data Measurements (relevant to Chapters 3, 4 and 5)

High pressure liquid chromatography (HPLC) pigment samples were filtered and the filters kept frozen (−80°C) prior to analysis in the laboratory once on shore; for methods see Poulton et al. (2006). In Chapter 5, three samples had no HPLC pigment information available so additional data from acetone-extracted and fluorometrically-analysed chlorophyll *a* samples was used (for methods see Holm-Hansen et al., 1965).

Nitrate concentrations were determined on board the research ship within 3 hours of collection (see Woodward and Rees, 2001). Discrete F_v/F_m measurements were made on board ship using a fast repetition rate fluorometer as per the method of Moore et al. (2006) and phytoplankton carbon fixation rates were ascertained using radiolabelled ^{14}C-uptake incubations (see Poulton et al., 2006, for further details). Prokaryotes were counted using flow cytometry and two groups of picophytoplankton (*Prochlorococcus* spp. and *Synechococcus* spp.) were identified using their characteristic autofluorescence (see Heywood et al., 2006).

Ancillary data was collected and analysed by: Alex Poulton, Sarah Root, Anna Hickman, Sandy Thomalla (pigment samples); Malcolm Woodward, Katie Chamberlain and Andy Harvey (nutrient samples); Alex Poulton and Mark Stinchcombe (^{14}C-uptake samples); Young-Nam Kim (F_v/F_m samples); Bernhard Fuchs, Glen Tarran, Jane Heywood and Mike Zubkov (picophytoplankton and bacterial samples). All of the above kindly made their data available for interpretation.

3 Linking DMS(P) measurements from the AMT programme with biological parameters

3.1 Introduction

The sub-tropical oligotrophic gyres are low-production environments, with correspondingly low chlorophyll *a* concentrations at the surface (typically < 0.1 µg m^{-3}). DMS produced in these areas vents into a relatively pristine atmosphere (i.e. away from anthropogenic impacts), so the impact of any change in flux is likely to have an impact upon albedo. In addition, these regions cover a considerable percentage (approximately 40%) of the earth's surface (McClain et al., 2004). With respect to DMS and DMSP (hereafter referred to as DMS(P)), these areas are under-sampled and poorly understood (Kettle et al., 1999), a fact that is underlined by the results in Chapter 4. A rough calculation assuming a constant surface concentration (1 nM) and wind speed (10 m sec^{-1}) in the oligotrophic subtropical gyres indicates that they provide at least 1% of the estimated global DMS flux to the atmosphere. Any measurements made in such areas can only help to improve our understanding of the role DMS(P) plays in climate and the sulphur cycle.

The AMT cruises have enabled a significant DMS(P) dataset to be collected, with particular focus on the oligotrophic gyres in the North and South Atlantic. In addition to the reduced sulphur measurements, a wealth of concurrent biological data was collected, providing an opportunity to statistically investigate any links between the biological community and ambient DMS(P) concentrations. To provide some context, the dominant global online database (http://saga.pmel.noaa.gov/dms/) currently contains over 31,000 data points for DMS, with less than 20% of these coupled with measurements of chlorophyll *a*. It is reasonable to expect that fewer still of these have been made in conjunction with measurements of accessory pigments, community primary production rates, or heterotrophic bacterial density.

The AMT database contains over 300 DMS(P) data points and, with the ancillary biological data collected, is a significant dataset from under-sampled regions in the Atlantic ocean. Little ancillary data of relevance is available for AMT-9, so the cruises of interest for this chapter are AMT-5 (Phase One) and AMT-12, -13 and -14 (Phase Two), and their routes are plotted in Figure 3.1. During Phase One of the programme,

concentrations of accessory pigments were collected while the scope for Phase Two was broadened to include, amongst a number of additional parameters, community primary production rates and heterotrophic bacterial density, hereafter referred to as 'production' and 'bacteria' respectively. For a more detailed overview of the AMT programme, please see Robinson et al. (2006). Due to a scarcity of measurements, we have little understanding of whether the reduced sulphur cycle demonstrates any seasonality in the South Atlantic Gyre (SATL) region. The AMT data provide an opportunity to investigate this as AMT cruises 12-14 followed exactly the same track in the SATL, but in opposing seasons (AMT-12 and -14 were during the southern hemisphere's autumn, and AMT-13 was in the spring).

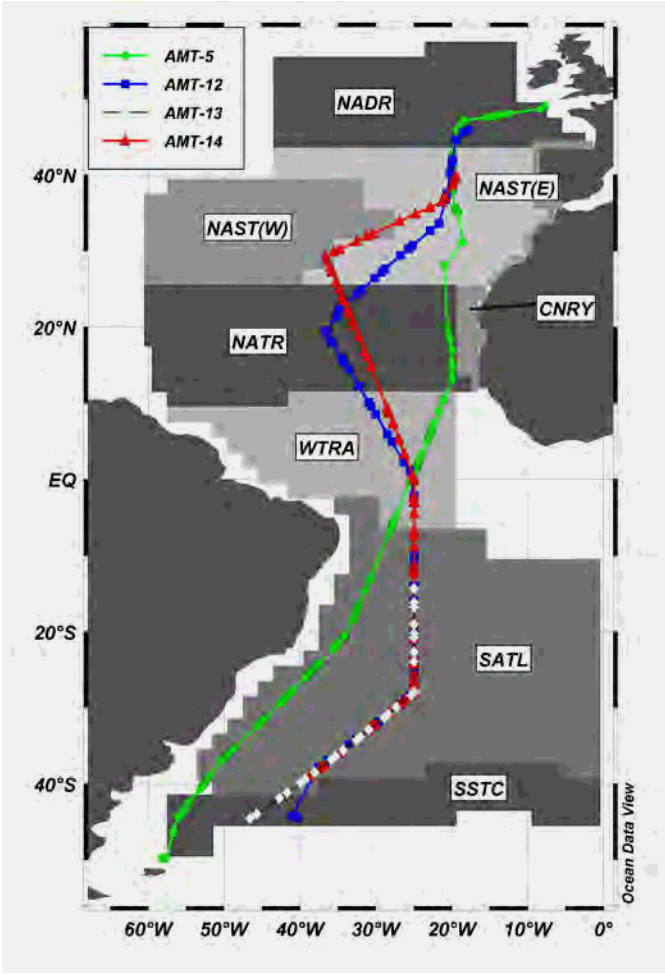

Figure 3.1 Cruise tracks for four Atlantic Meridional Transect cruises (southbound in September, northbound in May) – AMT-5 (Sep. 1997), AMT-12 (May 2003), AMT-13 (Sep. 2003) and AMT-14 (May 2004). The provinces defined by Longhurst (1995) are shown to provide spatial reference: North Atlantic Drift (NADR); North Atlantic Subtropical Gyre-East (NAST(E)); North Atlantic Subtropical Gyre-West (NAST(W)); Canary Current Coastal (CNRY); North Atlantic Tropical Gyre (NATR); Western Tropical Atlantic (WTRA); South Atlantic Subtropical Gyre (SATL); and South Subtropical Convergence (SSTC). Plot produced using *Ocean Data View* (http://odv.awi-bremerhaven.de/home.html).

Throughout this chapter, the acronyms of biogeochemical provinces, as delineated by Longhurst (1995), will frequently be referenced in place of their full titles. In addition, chemotaxonomic pigment markers will be referred to using abbreviations. It is therefore useful to include tables for ease-of-reference (see Table 3.1 and Table 3.2).

Table 3.1 Full biogeochemical province names and their acronyms, as from Longhurst (1995). Figure 3.1 displays the province locations and boundaries; for a full description of delineation methodology, see Longhurst (1995).

Acronym	Full Province Name
CNRY	Canary Current Coastal
NADR	North Atlantic Drift
NAST(E)	North Atlantic Subtropical Gyre - East
NAST(W)	North Atlantic Subtropical Gyre - West
NATR	North Atlantic Tropical Gyre
SATL	South Atlantic Subtropical Gyre
SSTC	South Subtropical Convergence
WTRA	Western Tropical Atlantic

Table 3.2 Pigment abbreviations, their full names and chemotaxonomic algal class and likely role: **S** = major photosynthetic pigment; *(s)* = minor or variably occurring photosynthetic pigment; **P** = major photoprotectant pigment; and *(p)* = minor or variably occurring photoprotectant pigment (after Mantoura et al., 1997; and Gibb et al., 2000). Note that **Chl *b***, **Diatox**, **Diadino** and **Car** were not included in any correlation analysis but will be for any forthcoming publication. **But+Hex** is included as this combination of pigments has been used previously in the DMS research field (Belviso et al., 2001); see Section 3.3.1 for details.

Abbreviation	***Full Pigment Name (or description)***	***Algal Class***								
		Cyanobacteria	*Prochlorophytes*	*Diatoms*	*Prymnesiophytes*	*Chlorophytes*	*Prasinophytes*	*Dinoflagellates*	*Chrysophytes*	*Cryptophytes*
Chl *c*$_3$	Chlorophyll *c*$_3$				**S**				**S**	
Chl *c*$_2$	Chlorophyll *c*$_2$			**S**	**S**			**S**	**S**	**S**
Perid	Peridinin							**S**		
But	19'– Butanoyloxyfucoxanthin				*(s)*				**S**	
Hex	19'– Hexanoyloxyfucoxanthin				**S**					
Fucox	Fucoxanthin			**S**	*(s)*				*(s)*	
Violax	Violaxanthin					**S**	**S**			
Chl *b*	Chlorophyll *b*					**S**	**S**			
DV Chl *a*	Divinyl Chlorophyll *a*		**S**							
Chl *a*	Chlorophyll *a*	**S**		**S**	**S**	**S**	**S**	**S**	**S**	**S**
TChl *a*	An *indicator* of biomass (Sum of **DV Chl *a*** and **Chl *a*)**	See separate DV Chl *a* and Chl *a* pigment affiliations.								
But+Hex	Sum of **But** and **Hex**	See separate But and Hex pigment affiliations.								
Allox	Alloxanthin									**P**
Zeax	Zeaxanthin	**P**	**P**			*(p)*			*(p)*	
Diadino	Diadinoxanthin			**P**	**P**			**P**	**P**	
Diatox	Diatoxanthin			*(p)*	*(p)*			*(p)*		
β-Car	β-Carotene	*(p)*	*(p)*			*(p)*	*(p)*			

3.2 Statistical Procedures

The following section details the procedures and approaches used to statistically examine DMS(P) and ancillary measurements made during the AMT campaign. An understanding of statistical tests, how they should be used and the meaning of their results is of key importance if the results are to have any interpretable value. At this point is should be noted that, if any pigment samples were found to be below the detection limit of the instrument, i.e. 0.002 mg m^{-3} (Poulton et al., 2006), the value used was not zero as this would skew any correlations. Instead, these samples were given a value that was half of the detection limit. This is one of a number of approaches used for samples below the limit of detection. Regardless, the method used is unlikely to have had a large impact upon correlation results as only a small percentage of measurements (0.3 – 6.0%) were below the limit of detection.

3.2.1 Correlations

The simplest approach to identifying a potential relationship between two variables is to correlate them. Two types of correlation can be carried out, depending on the frequency distribution of the data. The usual correlation performed is a Pearson's correlation, and this assumes that the data for both variables are normally distributed (i.e. they show equal variance either side of the mean and therefore have bell-shaped distribution curves). If either variable demonstrates a non-normal distribution, then the correlation procedure should account for this lack of normality; in this case, Spearman's Rank correlation is commonly used and ranks the data lowest to highest value before assessing the degree of correlation between the ranked data. The Pearson's and Spearman's Rank correlation procedures both produce:

1) correlation coefficients (r, Pearson's, or ρ, Spearman's) between -1 and +1, which indicate the level of association between two variables and whether that association has a positive or negative slope (i.e. the closer the value is to -1 or +1, the stronger the negative or positive association). The definition of a 'strong' correlation is relative (Cohen, 1988), and thus varies depending upon the subject matter. For this study, a relatively low correlation coefficient criterion was used (see later) due to the inherent variability of the natural environment and relatively poor current understanding of the reduced sulphur cycle in surface waters.

2) a significance or confidence level (α). When performing a correlation analysis, the null hypothesis (H_0) tested is that there is no correlation between the two variables. The α value indicates the error in rejecting H_0 and is typically < 5% (or α<0.05) at the most. However, it was felt necessary to only identify correlations that were highly significant during this study and all data presented in this work therefore has a rigorously small associated error (α<0.0001); i.e. a certainty of 99.99% or greater that H_0 should be rejected. A rejection of H_0 indicates that the alternative hypothesis (H_1) should be accepted.

If a Spearman's Rank correlation test was used with normally distributed variables, the correlation coefficient (ρ) would be similar to, but not exactly the same as, the Pearson's correlation coefficient (r) for the same data. In this work, prior to all correlation analyses, the 'one-sample Kolmogorov-Smirnov test' was used to identify whether the frequency distribution of data was significantly different from a normal distribution. A large number of variables were found to have distributions that were skewed towards zero so it was decided to consistently use Spearman's Rank so that results could be compared. With such a large dataset, a lot of the correlations were significant (i.e. α<0.0001), despite demonstrating weak associations between variables (i.e. ρ values closer to 0 than +/- 1). In order to reduce the number of results and then interpret them, the following criterion was used:

Only correlation coefficient (ρ) values greater than +0.5 or less than -0.5 can be considered strong enough to be worthy of interpretation.

Based on the previous paragraphs, the term *significant correlation* hereafter refers to associations that satisfy the following criteria: α<0.0001 and ρ greater than +0.5 or less than -0.5. In other words, a strong correlation (positive or negative) with high confidence (99.99% or greater) that the null hypothesis (H_0) should be rejected and the alternative hypothesis thus accepted.

3.2.2 Principal Components Analysis (PCA)

In order to run a Principal Components Analysis (PCA), each variable must be normally distributed; if this is not the case, the data should be *transformed* using power, square root or logarithmic functions. Another term for PCA is *Data Reduction* as the process aims to summarise the interrelationships amongst a set of variables in a concise and accurate

manner, thus aiding conceptualisation of large datasets (Gorsuch, 1983). The PCA method finds a linear combination of variables (a component or factor) that accounts for as much variation as possible. It then finds another component that accounts for as much of the remaining variation as possible and is uncorrelated with the first component. This process continues until there are as many components as there are variables. Usually a few factors account for the majority of the variation and these are extracted to represent all the original variables (those extracted are defined as having Eigenvalues >1), thus reducing the number of variables in the data file whilst accounting for the majority of the variation of the entire dataset.

Subsequently, the PCA components or factors can be *rotated* to minimise the number of variables that have high loadings on each component, simplifying interpretation. A *rotation* maintains the overall percentage variance explained by the components, but that variance is now spread more evenly between the factors. The rotated factor scores (calculated by multiplying each case's original score by the component score) can then be used in place of the original data and correlated with other variables. This is preferable to only using the most highly correlated original variables as the score variables account for a large proportion of the variation of all the original variables.

3.2.3 Analysis of Variance (ANOVA)

The two-sample *t-test* is used to test whether two datasets are significantly different from each other by comparing their variances and means. A one-way ANalysis Of VAriance (ANOVA) is an extension of this and can be used to compare the means of more than two datasets whilst accounting for their variance, and a post-hoc test can then be used to statistically (α<0.05) group the results into subsets. A normally distributed dataset is not required to run an ANOVA test, but the data distribution is assumed to be symmetrical so throughout this work *transformed* data was used to be certain that appropriate data was used for each analysis. For the stringent Tukey's Honestly Significant Different (HSD) post-hoc test, variables are assumed to have equal variance (a similar assumption to that used during a *t-test*). In case this assumption was not met, the Games-Howell correction was used to check how representative the Tukey HSD results were, as recommended by Roberts and Russo (1999). In fact, only two of the variables tested produced different results using the Games-Howell test, the pigments Violax and Perid (see Section 3.3.3). In these cases, the Games-Howell result was always adhered to.

3.3 Results and Discussion

Before embarking upon a detailed discussion of statistical results, it is useful to examine the raw DMS(P) data (Table 3.3) along with an appropriate reference parameter (TChl *a*). Software packages such as *Ocean Data View* (*ODV*, http://odv.awi-bremerhaven.de/home.html) are particularly useful for such data, as they can be used to present vertical depth profiles along a horizontal transect, with colour or dark-light shading to represent concentrations. In particular, such packages can be used to interpolate between data points, which if applied with caution can be a useful tool for providing a more interpretable picture. However, an important aspect of these plots is the exact location of the data points, as these provide the reader with a critical view of the extent to which the plot has been interpolated from the original data. The pages below display vertical sections of DMS, DMSPd, DMSPp and TChl *a* along four AMT transects, plotted using *ODV*. All figures range between 45°S and 45°N, extend to 120m depth, and use the same interpolation settings (*VG Gridding*, a weighted mean) for every section to aid comparability (Figure 3.2, Figure 3.3, Figure 3.4, and Figure 3.5 refer to AMT cruises -5, -12, -13, and -14 respectively). Following these figures, the general patterns are briefly summarised and discussed.

Table 3.3 Mean, minimum (min) and maximum (max) DMS, DMSPd and DMSPp concentrations (nM) measured on each AMT cruise, as well as a summary of all cruises.

Cruise	DMS			DMSPd			DMSPp		
	Mean	*Min*	*Max*	*Mean*	*Min*	*Max*	*Mean*	*Min*	*Max*
AMT-5	1.01	0.03	13.4	8.18	0.49	33.9	13.2	0.22	67.2
AMT-9	1.07	0.14	10.9	4.93	0.41	37.4	13.9	0.80	112.9
AMT-12	1.11	0.01	6.7	3.78	0.11	24.7	8.8	0.16	104.0
AMT-13	1.05	0.11	3.4	8.26	0.94	34.3	14.5	0.08	229.7
AMT-14	0.96	0.01	3.1	3.47	0.22	11.3	3.4	0.01	34.9
All Cruises	*1.04*	*0.01*	*13.4*	*5.67*	*0.11*	*37.4*	*10.5*	*0.01*	*229.7*

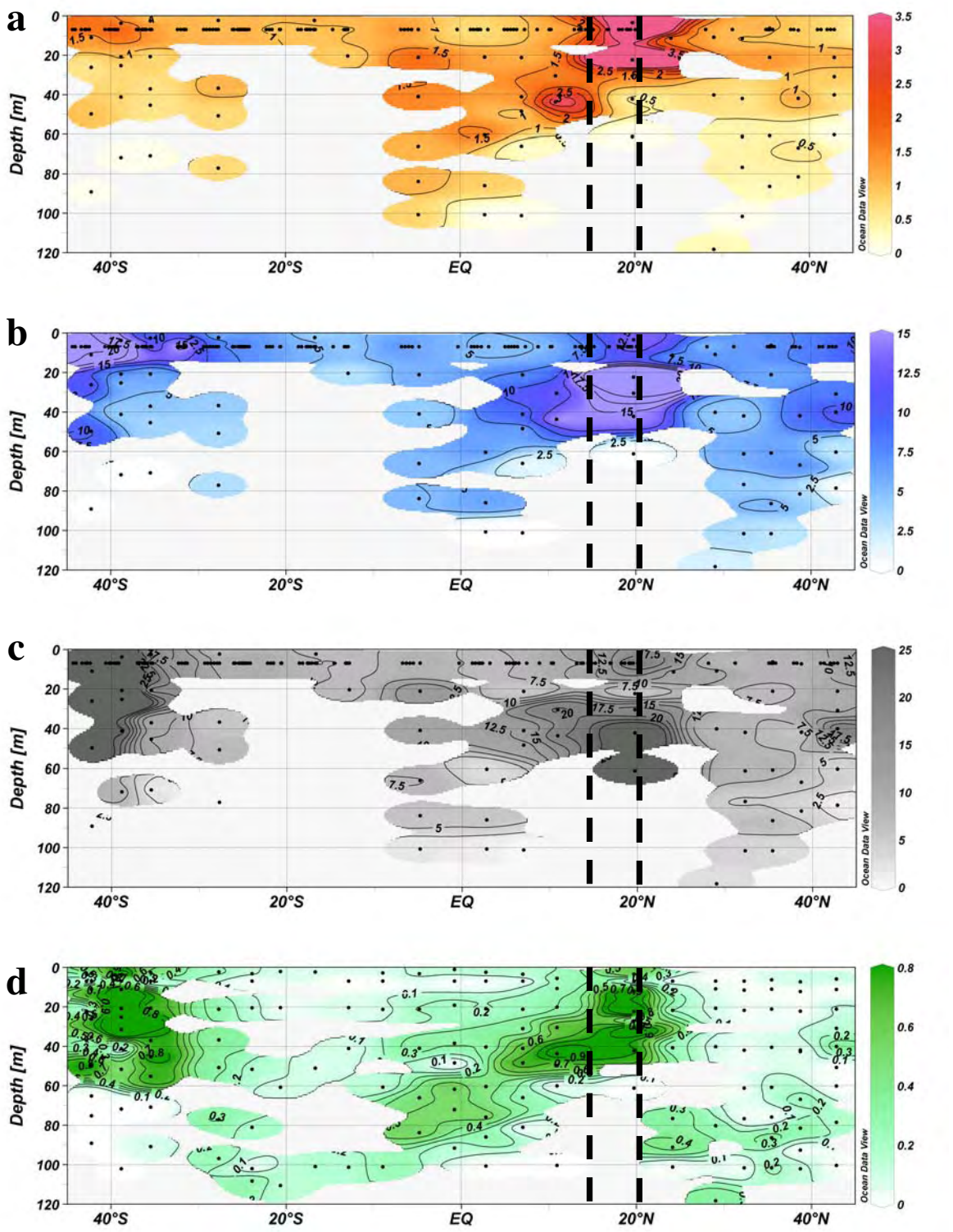

Figure 3.2 Depth contour plots of (a) DMS (red); (b) DMSPd (blue); (c) DMSPp (grey); and (d) TChl *a* (green) along AMT-5 (the green cruise track on Figure 3.1). Sample points are indicated (black dots). Contour lines are set at intervals of 0.5 nM; 2.5 nM; 2.5 nM; and 0.1 µg L^{-1} for DMS, DMSPd, DMSPp and TChl *a* respectively. Scales have been capped at 3.5 nM; 15 nM; 25 nM; and 0.8 µg L^{-1} for readability and thus a small minority of points exceed these values. The Canary Current Upwelling system as defined by Hooker et al. (2000) is marked with dashed lines. Equivalent plots with unlimited scales are included in the appendix (Figure I).

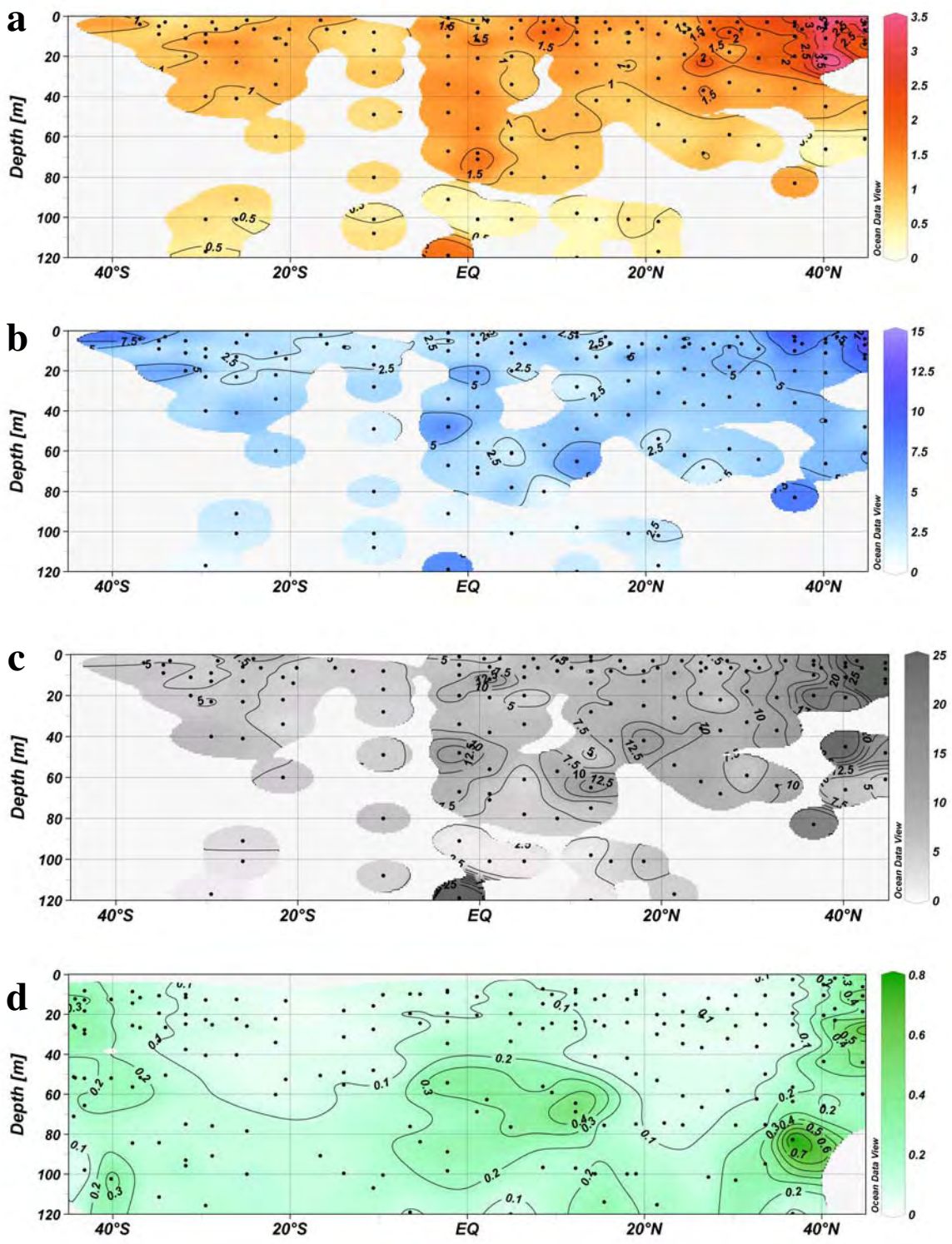

Figure 3.3 Data from AMT-12 (the blue cruise track on Figure 3.1). Otherwise, legend is as for Figure 3.2. Equivalent plots with unlimited scales are included in the appendix (Figure II).

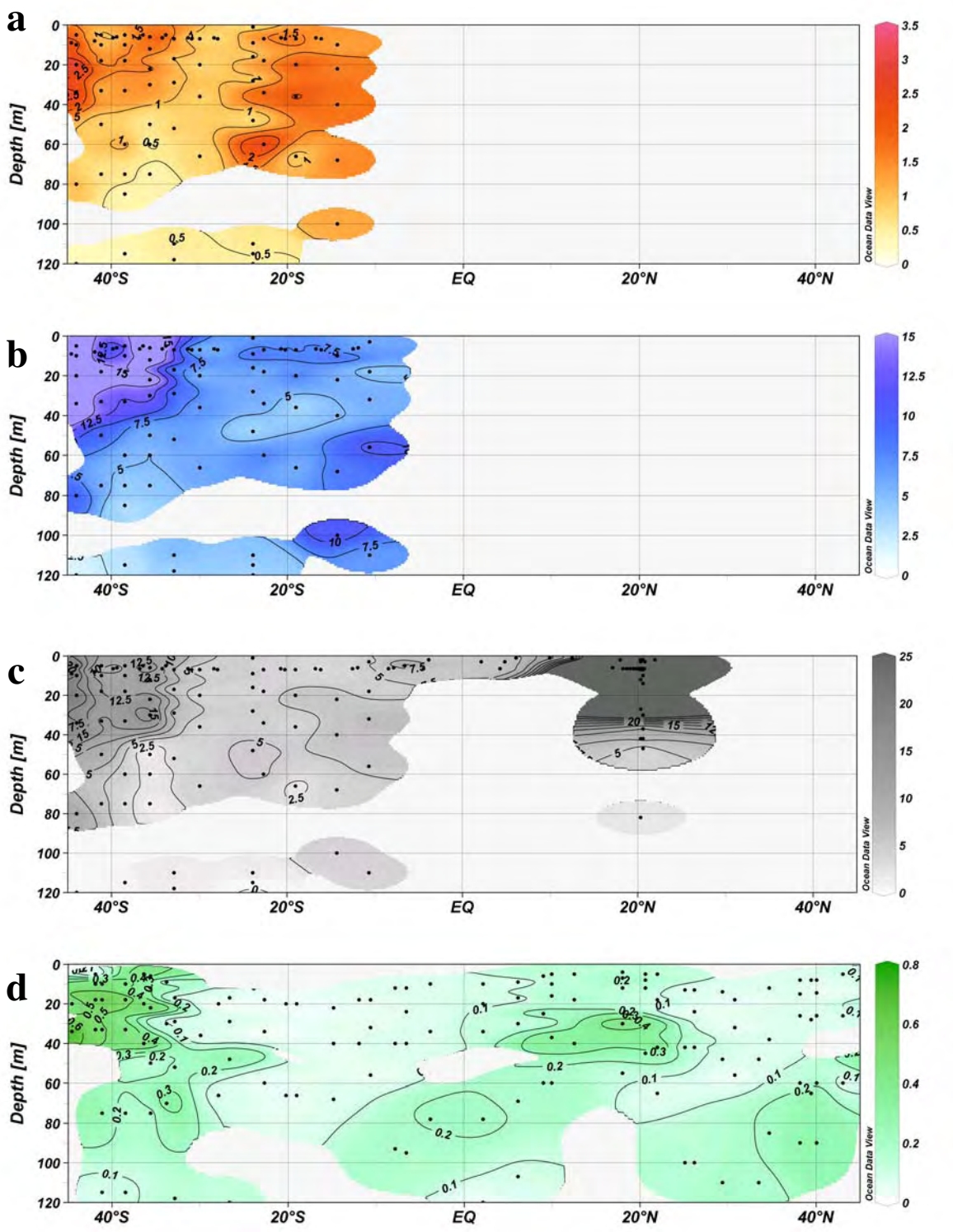

Figure 3.4 Data from AMT-13 (the white cruise track on Figure 3.1). North of 14°S, no DMS and DMSPd data was collected due to equipment malfunction. DMSPp data between the upwelling region (approximately 20°N) and 14°S were collected and stored until the equipment was fixed. Otherwise, legend is as for Figure 3.2. Equivalent plots with unlimited scales are included in the appendix (Figure III).

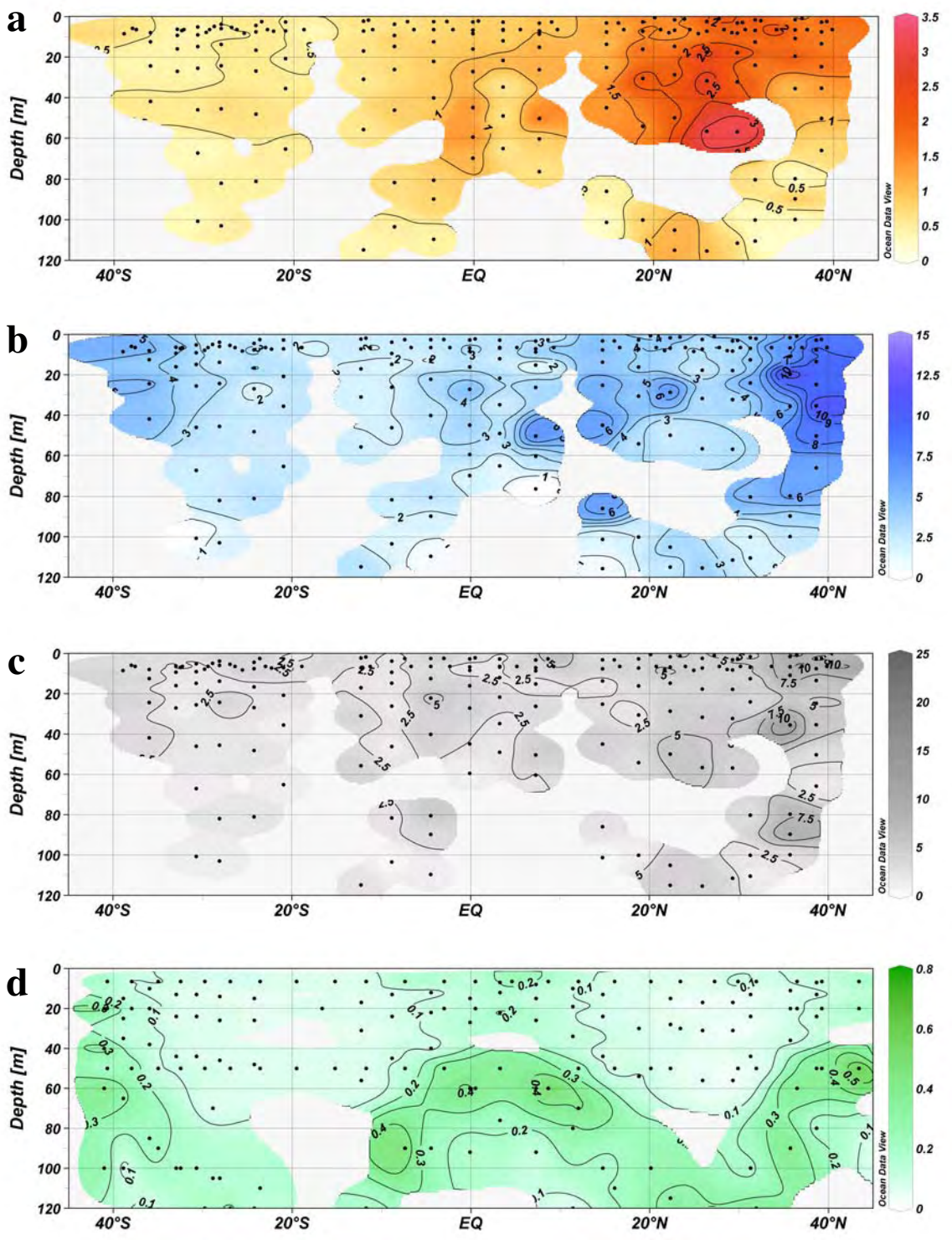

Figure 3.5 Data from AMT-14 (the red cruise track on Figure 3.1). Otherwise legend is as for Figure 3.2. Equivalent plots with unlimited scales are included in the appendix (Figure IV).

When examining the sections, AMT-5 (Figure 3.2) stands out because the waters encountered exhibit higher chlorophyll and DMSPp concentrations. The major difference between AMT-5 and the other cruises was the cruise track (Figure 3.1), because AMT-5 did not progress as deep into the oligotrophic gyres (the same difference applies to AMT-9, Table 3.3). Although the waters encountered were still considered oligotrophic during AMT-5 and -9 (i.e. below ~0.1 mg m^{-3} TChl *a*), they were unlikely to have been as nutrient limited (because they were closer to nutrient-rich ocean margins) compared to those encountered during AMT-12-14, and thus biological production and biomass were higher. Another striking aspect is the influence of the Mauritanian upwelling at approximately 20°N seen during AMT-5 and AMT-13 (Figure 3.2 and Figure 3.4 respectively). This feature is apparent in all four displayed parameters (DMS, DMSPd, DMSPp, and TChl *a*) and is a good example of an oceanographic region where production, biomass and DMS(P) are intimately linked. The higher latitude regions of the AMT transects experience greater seasonality and also demonstrate an equivalent relationship between production/biomass and DMS(P). However, this only occurs during the spring bloom, which takes place at opposing times of the year in each hemisphere; i.e. elevated concentrations in the high latitude northern hemisphere during May/June (AMT-12 and -14), and elevated concentrations in the high latitude southern hemisphere during Sep./Oct. (AMT-5 and -13).

In oligotrophic regions such as the North and South sub-tropical gyres, the chlorophyll maximum (chl max) does not coincide with increased DMS(P) concentrations (AMT-14 is a good example of this, see Figure 3.5). This makes sense when considered in the context of previous results that demonstrate poor global correlation between DMS or DMSP and chlorophyll *a* (e.g. Kettle et al., 1999). Above the chl max in the gyres, there are both inter- and intra-cruise variations in DMS concentration. An extreme example of this occurred during AMT-14 (Figure 3.5) in the surface waters of the North Atlantic sub-tropical gyre – elevated DMS levels were observed that were <u>not</u> associated with changes in DMSP <u>or</u> TChl *a*. This phenomenon is discussed at length in Section 3.3.4.

As can be seen in all cruise sections (and in Table 3.3), DMSP (both particulate and dissolved) concentrations exhibit substantial variation over relatively small spatial scales (vertically and horizontally) as well as inter-cruise differences. This possibly reflects the more direct relationship with biological activity and as a result, creates a 'snap-shot' view of a dynamic system. It also highlights the possibility that the sub-tropical gyres, so often considered to be constant throughout the year, might demonstrate biological variations that

affect DMS(P) concentrations (Section 3.3.3 discusses this in more detail). So far, the results presented and discussed have focussed only upon DMS(P) concentrations and the prime indicator of biological activity, TChl *a*. Equivalent plots could be produced for each accessory pigment, production, and bacteria. However, in order to examine such a large volume of data, produce quantifiable results and come to robust conclusions, statistical tests must be used to investigate the dataset. The results of such analyses are presented and discussed in the following pages (Sections 3.3.1, 3.3.2 and 3.3.3).

3.3.1 Correlations

Previous work

Although phytoplankton are the primary source of DMS to oceanic waters, attempts to correlate DMS with the predominant phytoplankton photosynthetic pigment, chlorophyll *a*, have often proven unsuccessful (e.g. Burgermeister et al., 1990; Kettle et al., 1999); the more direct product of biological activity is DMSP. The ACSOE (Atmospheric Chemistry Studies in the Oceanic Environment) lagrangian time series experiment studied DMSP dynamics within a the North Atlantic eddy core over four days (Simo et al., 2002). The authors suggested that DMSP production might be linearly related to primary production, as on-deck incubations demonstrated a diel variation in both primary production and DMSP production throughout a twenty-four hour period. It should be noted that all DMSP production rates were not measured but inferred from changes in ambient DMSP concentrations and the exponential decrease of total DMSP consumption in dark incubations (Simo et al., 2002). Nevertheless, these results suggest that the rate of DMSP production might be related to the rate of primary production.

Instead of chlorophyll *a*, other research has focussed on the accessory pigments, which provide an indication of the phytoplankton species composition. A number of surveys from Antarctic waters have demonstrated strong correlations between DMSPp and Hex (DiTullio and Smith, 1995; Turner et al., 1995; Trevena et al., 2003), due mainly to the high incidence of *Phaeocystis antarctica* (a known DMSP producer, Keller et al., 1989). Whilst the typical marker pigment for *Phaeocystis* is Fucox, in the iron-limited waters of the Antarctic, Hex and But synthesis is induced in *Phaeocystis* at the expense of Fucox (van Leeuwe and Stefels, 1998).

Another study investigating the relationships between DMS(P) and accessory pigments was based upon a substantial dataset collected from the central Atlantic Ocean, the subtropical northeast Atlantic Ocean, the Ionian Sea, and the Indian sector of the Southern Ocean (Belviso et al., 2001). A significant relationship was identified between DMSPp and But+Hex for DMSPp in the <10 µm size fraction (r^2=0.84, α<0.001, n=189). The authors consider the sum of But+Hex a robust estimator of autotrophic pico- and nano-planktonic biomass and suggest the relationship could be used to predict global nanoplanktonic DMSPp concentrations (Belviso et al., 2001). However, as they acknowledge, there are likely to be problems associated with such a predictive relationship; for example, *Phaeocystis* normally synthesises Fucox rather than But or Hex, unless iron limited (van Leeuwe and Stefels, 1998). When performing correlations in this study, But+Hex was included for comparative purposes. The work of Belviso et al. (2001) has since been adapted in order to create a global predictive algorithm for surface DMS concentrations that uses a community composition index created from accessory pigment ratios (Aumont et al., 2002; Belviso et al., 2004b). These predictive relationships and others are discussed in more detail in Chapter 4.

After AMT-5 data was collected, the DMS(P) measurements were correlated with ancillary pigment data (McKee, 2001). To summarise, little correlation was observed between DMS or DMSPd and Chl *a* or any of the accessory pigments, but stronger correlations were observed between DMSPp and both Hex (r^2=0.698, α<0.001, n=103) and Chl c_3 (r^2=0.693, α<0.001, n=102). These biomarker pigments (Hex in particular) are often found in prymnesiophyte and dinophyte algae (see Table 3.2), which are known to be high DMSPp producers (Keller et al., 1989). In addition, a strong significant correlation was observed with Allox (r^2=0.650, α<0.001, n=87), which is a biomarker for cryptophyta (Table 3.2). Based on lab studies, cryptophyta are thought to be relatively low DMSPp-producing (Keller et al., 1989), although this is not necessarily representative of field conditions. A correlation between variables does not, of course, indicate a direct link. The covariance of Allox with DMSPp may be solely due to cryptophytes increasing when DMSP producers (e.g. Hex) increased. As the current AMT dataset is now significantly bigger than that of McKee (2001), it is of interest to investigate whether the relationships identified by McKee (2001) are maintained when data from the AMT-12-14 cruises are included.

Overall trends

As previously mentioned, accessory pigment data was collected during AMT-5; during Phase Two (AMT-12-14), this data was again collected, along with production and bacteria data. Wherever possible, DMS(P) data was correlated with all of these variables. Data could only be correlated if it had been collected at the same time and from the same depth as the associated measurement. Inevitably this process led to a reduction in the number of correlated points, with different correlations yielding different numbers of points. For example, fewer points can be seen for DMS(P) data correlated with production as production was not measured as frequently due to time and manpower restraints. This underlines the need for a large initial dataset if numerous biological factors are to be investigated simultaneously for possible relationships with DMS(P).

Upon examination of the entire AMT dataset, only a few correlations are evident (Table 3.4). The only pigment to correlate significantly with any of the reduced sulphur compounds was violaxanthin (Violax), part of the recovery (dark) phase of the xanthophyll cycle, which helps protect the cells of some algal species against damage due to excess light energy (Porra et al., 1997). Violax and zeaxanthin (Zeax) constitute the respective dark and light end-products of a xanthophyll cycle and 'quench' damaging free radical activity, particularly that of singlet oxygen ($^1O_2$), and enable the cell to survive high-light conditions with minimal damage (Porra et al., 1997). The association between DMSPp and a photo-protective pigment (Table 3.4) is particularly interesting when considered in the context of the DMSP-lyase activity (DLA) results from AMT-14 (discussed in Chapter 5) and supports the recent anti-oxidant hypothesis of Sunda et al. (2002), detailed in Section 1.1.1.

Table 3.4 Significant[i] correlations, of DMS, DMSPd and DMSPp with phytoplankton pigment concentrations, heterotrophic bacterial density (bacteria) and carbon fixation rates (production) for the entire AMT dataset. ρ = Spearman's Rank Correlation Coefficient; n = number of data points. All correlations are positive unless indicated by a minus sign. See Table 3.1 for an explanation of the acronyms used for ocean provinces and Table 3.2 for the abbreviations used for phytoplankton pigments.

Variable	DMS	DMSPd	DMSPp
Violax			ρ=0.537; n=304 (not significant once AMT-5 removed)
Bacteria			ρ=0.527; n=349
Production	ρ=0.576; n=188		ρ=0.509; n=198

Other significant positive correlations identified for the entire dataset are between DMSPp and both production and bacteria (Table 3.4). In addition, DMS concentrations demonstrate a significant positive correlation with production, despite current understanding that overall food web structure and function can influence DMS (Simo, 2004). A critical aspect of correlations is that they can suggest a direct relationship between two variables when in fact none exists; this can occur when there is covariance of more than two variables, a fact pertinent to these and later results. For the AMT dataset, the correlation between bacteria and production is significant (ρ=0.676; n=141; α<0.0001), indicating substantial covariance. It is not clear how an increase in bacteria could directly contribute to an increase in DMS(P). Current understanding suggests that DMS and DMSPd can be utilised as a carbon and sulphur source by certain bacterial strains (e.g. Gonzalez et al., 1999; Kiene et al., 2000; Zubkov et al., 2001) but this would be expected to drive a negative correlation between DMS(P) and bacteria. Negative correlations with bacteria were not observed within AMT results (even after subdivision of the dataset, see later) and it is difficult to explain how a positive correlation could occur via a direct link. In contrast, production relates to biological activity and is arguably more likely to be positively linked with DMS(P) concentrations. The above information suggests that the link between DMS(P) and bacteria is indirect, occurring because production (known to co-vary with bacteria) correlates significantly with DMSPp.

[i] See Section 3.2.1 for the discussion and definition of a 'significant correlation'.

As all of the relevant variables tested in the AMT dataset are known to vary significantly, it is perhaps unsurprising that not very many of them correlate well with DMS(P) concentrations. In particular, the AMT dataset incorporates a variety of factors that are likely to have considerably affected the variables considered, so these must be addressed in some way. Specifically, the following three factors will have had an impact:

1) Spatial Variation (Horizontal). The AMT dataset covers a number of ocean provinces (see Figure 3.1) that are defined on the basis of global ocean circulation patterns, latitudinal variations in light (and UV), nutrient availability/flux and temperature. These differences can result in radical changes in biological community structure and its growth rate and function.

2) Spatial Variation (Vertical). In oligotrophic waters, the chl max is determined by a balance of essential resources – the upward supply of nutrients versus the downward supply of light (Huisman et al., 2006). These will vary with geographical position and large-scale circulation patterns. In near-surface waters, photo-protection is often necessary against light damage whereas light availability at depth is lower and photosynthetic cells must channel more resources into harvesting the same amount of light. The phytoplankton community in waters experiencing high-light conditions has therefore adapted to its various locations in the water column, i.e. a depth-dependent balance between photosynthetic pigments and photo-protective pigments (Claustre and Marty, 1995, and references therein). The chl max is indicative of the depth distribution of this balance. Further, when the chl max is shallow (i.e. a strong upward flux of nutrients) and/or the ocean is more productive, light cannot penetrate as far down through the water column as phytoplankton cells rapidly attenuate the light.

3) Temporal Variation. The AMT cruises took place in opposing seasons (AMT-5 & -13 in Sep./Oct. and AMT-12 & -14 in May/June) and although the subtropical and tropical provinces encountered along the AMT transects have previously been shown to exhibit relatively constant biomass standing stock year-round (Claustre and Marty, 1995; Gibb et al., 2000), some seasonality has been observed in other biological measurements (Claustre and Marty, 1995). Further, the high latitude portions of the AMT transects clearly experience seasonal change.

Due to these three factors, the AMT dataset was sub-divided: (1) by cruise, to account for any seasonality; (2) by biogeochemical province (as defined by Longhurst (1995)), to account for horizontal spatial variations; and (3) surface data (upper 10m) was isolated to exclude depth variations. For (3), the sub-surface data (>10 m) could not be used as it was difficult to divide due to variations in the depth of the chl max; e.g. the chl max in equatorial regions was approx. 50 m compared to in the oligotrophic gyres where it was ≥ 100 m (see also Figure 3.3). The following sections describe the significant correlations identified once the AMT dataset was sub-divided into these three categories.

Trends per cruise

As soon as the AMT dataset was divided by cruise, a number of significant associations between variables could be identified (Table 3.5). It is unsurprising that the particulate form of DMSP (i.e. that associated with cells) consistently demonstrates a greater number of significant correlations with pigment data than either DMSPd or DMS, as it is directly produced by phytoplankton. The number of significant correlations per cruise is highly variable, with none identified for AMT-14 and sixteen identified for AMT-5. It is possible that the high number of correlations for AMT-13 (seventeen) is due to the reduced spatial coverage, and therefore reduced variation, in DMS(P) during that cruise. Although the initial reason for dividing the dataset by cruise was to look at potential seasonality, it also enables a rudimentary analysis of the difference between cruise tracks.

As discussed in Section 3.3, both AMT-5 and AMT-13 passed through the Mauritanian upwelling (Figure 3.1). The upwelling cruises demonstrate a greater number of significant correlations and the influence of productive upwelling waters is likely to have driven these correlations. As described previously, the difference between the AMT-5 cruise track and the tracks of subsequent cruises explains the elevated Chl *a* concentrations observed (Figure 3.2). The difference in cruise track may also explain the stronger correlation between TChl *a* (and Chl *a*) and DMSPp during AMT-5 compared to AMT-13 (Table 3.5). TChl *a* has often been considered an indicator of phytoplankton community biomass and production on a global scale but in contrast, phytoplankton pigmentation in clear, nutrient-poor waters responds to the high light intensities at the surface (photo-inhibition) and low light intensities (light limitation) at depth (Gibb et al., 2000). This may further explain the lack of significant correlations between pigment data and DMS(P) for AMT-12 and -14, as they are a poor representation of phytoplankton biomass or production for such regions.

Table 3.5 Significant[i] correlations of DMS, DMSPd and DMSPp with phytoplankton pigment concentrations, heterotrophic bacterial density (bacteria) and carbon fixation rates (production) during AMT, divided by cruise. ρ = Spearman's Rank Correlation Coefficient; n = number of data points. All correlations are positive unless indicated by a minus sign. See Table 3.1 for an explanation of the acronyms used for ocean provinces and Table 3.2 for the abbreviations used for phytoplankton pigments.

	DMS	**DMSPd**	**DMSPp**
AMT-5		Chl c_2 (ρ=0.587; n=67) Perid (ρ=0.534; n=72) Hex (ρ=0.552; n=67) Violax (ρ=0.520; n=69) Chl *a* (ρ=0.538; n=67) TChl *a* (ρ=0.565; n=72)	Chl c_3 (ρ=0.559; n=69) Chl c_2 (ρ=0.622; n=67) Perid (ρ=0.546; n=70) Hex (ρ=0.567; n=67) But+Hex (ρ=0.524; n=68) Fucox (ρ=0.600; n=70) Violax (ρ=0.712; n=69) Allox (ρ=0.630; n=70) Chl *a* (ρ=0.749; n=65) TChl *a* (ρ=0.675; n=70)
AMT-12	Bacteria (ρ=0.501; n=96) Production (ρ=0.651; n=63)	Production (ρ=0.671; n=54)	Production (ρ=0.728; n=61)
AMT-13	Bacteria (ρ=0.694; n=67) Production (ρ=0.711; n=40)	Perid (ρ=0.584; n=48) Fucox (ρ=0.547; n=48) Violax (ρ=0.594; n=48) Chl *a* (ρ=0.545; n=47) TChl *a* (ρ=0.554; n=47) Bacteria (ρ=0.779; n=75) Production (ρ=0.681; n=45)	Perid (ρ=0.635; n=57) Fucox (ρ=0.580; n=57) Violax (ρ=0.607; n=57) Zeax (ρ=0.552; n=57) Chl *a* (ρ=0.536; n=56) TChl *a* (ρ=0.573; n=56) Bacteria (ρ=0.824; n=87) Production (ρ=0.870; n=52)
AMT-14			

[i] See Section 3.2.1 for the discussion and definition of a 'significant correlation'.

Significant correlations were observed between all three reduced sulphur species and both bacteria and production for AMT-12 and AMT-13 (Table 3.5). As discussed earlier, the correlations of DMS(P) with bacteria may well be an indirect association due to covariance of bacteria and production. It is particularly interesting that the relatively strong relationships with production and bacteria during AMT-12 are not present at all within the AMT-14 dataset. As both cruises occurred at the same time of year and followed similar cruise tracks, there is no obvious explanation for this difference. These observations, coupled with the distinct inter-cruise variability in the number of correlations with pigments, suggest that, when looking for seasonality in the AMT dataset, the focus should be on a smaller spatial scale, concentrating only on a single ocean province. The province most appropriate for such a study is the SATL as AMT-12, -13 and -14 followed exactly the same transect in the southern hemisphere (see Section 3.3.3 for results and discussion).

At this juncture, the issue of inter-correlation between, and covariance of, variables should be fully addressed. All phytoplankton contain more than one accessory pigment, and thus an algal group is likely to be represented (and therefore correlate with) more than one other pigment. In addition, as nutrient and light availability increase, the production and biomass of the whole phytoplankton community will increase. Whilst the community composition (and thus its pigment composition) may change due to species' competitive abilities in different environments, there is also likely to be a degree of covariance between different pigments. This can be demonstrated using a correlation matrix of the pigment data discussed in both this and subsequent sections (Table 3.6). As can be seen, a lot of the pigment groups co-vary, so a correlation of DMS(P) with one pigment is likely to result in correlations with others. This fact should be borne in mind when interpreting all correlation results.

Table 3.6 Correlation matrix for pigment data (all AMT cruises), illustrating the inter-correlation (Spearman's Rank ρ) between variables. All correlations involved >300 data points. $^{(*)}\alpha<0.0001$. Significant correlations as defined in Section 3.2.1 are highlighted.

	Chl c_3	Chl c_2	Perid	But	Hex	But+Hex	Fucox	Violax	Allox	Zeax	DV Chl *a*	Chl *a*	TChl *a*
Chl c_3		0.829*	0.411*	0.435*	0.498*	0.483*	0.511*	0.342*	0.549*	0.043	0.111*	0.488*	0.441*
Chl c_2			0.336*	0.423*	0.497*	0.480*	0.460*	0.326*	0.550*	0.119	0.246*	0.463*	0.409*
Perid				0.626*	0.704*	0.687*	0.747*	0.617*	0.526*	0.257*	0.250*	0.768*	0.735*
But					0.917*	0.961*	0.809*	0.641*	0.613*	-0.011	0.298	0.820*	0.810*
Hex						0.985*	0.869*	0.713*	0.709*	0.098	0.328	0.881*	0.852*
But+Hex							0.862*	0.708*	0.688*	0.055	0.312	0.878*	0.857*
Fucox								0.727*	0.670*	0.157	0.233*	0.876*	0.878*
Violax									0.515*	0.056	0.011	0.698*	0.740*
Allox										0.166	0.290	0.674*	0.622*
Zeax											0.689	0.220*	0.072*
DV Chl *a*												0.369*	0.196*
Chl *a*													0.945*

Trends per province

Once the AMT dataset was divided into provinces, the number of significant correlations reduced considerably. This is unlikely to be due to the reduction in the number of data points as there is still enough data for potential correlations to be classed as significant. Most likely, the division by province isolated the higher production regions, which were the major driver of correlations between chlorophyll (and/or other associated parameters) and DMS(P) in the dataset as a whole. Bearing this in mind, some interesting patterns emerge from the results (Table 3.7). All of the significant correlations presented relate to lower latitude regions (SATL, NATR, NAST(E)). Of particular interest is that the only pigments to significantly correlate with DMSP (dissolved and particulate) were Violax and Zeax, which are the respective dark and light phases of a photo-protective xanthophyll cycle (Porra et al., 1997). As discussed earlier in this section, the positive associations between DMSP and these pigments in waters that are often light-stressed, supports the concept that the role of DMSP is part of a photo-protective mechanism (Sunda et al., 2002).

Significant positive correlations were also observed between DMS(P) and production and/or bacteria (Table 3.7). As discussed earlier, the covariance of two variables (bacteria and production) could explain most of the association between DMS(P) concentrations and bacteria. As descried in the *Overall trends* and the *Trends per cruise* sections, an association was observed between the phytoplankton community's production and ambient DMS(P) concentrations (Table 3.7). Considering the poor relationship between Chl *a* and DMS(P) in oligotrophic waters, this is of considerable interest. Unlike Chl *a*, carbon fixation represents the activity of the phytoplankton community, and may therefore help to explain the better correlation with DMS(P).

Table 3.7 Significant[i] correlations of DMS, DMSPd and DMSPp with phytoplankton pigment concentrations, heterotrophic bacterial density (bacteria) and carbon fixation rates (production) during AMT, divided by biogeochemical province. ρ = Spearman's Rank Correlation Coefficient; n = number of data points. All correlations are positive unless indicated by a minus sign. See Table 3.1 for an explanation of the acronyms used for ocean provinces and Table 3.2 for the abbreviations used for phytoplankton pigments. Once AMT-5 data was removed, most correlations reduced in strength and were therefore no longer found to be significant (does not include bacteria and production as these variables were not measured during AMT-5); those found no longer to be significant are highlighted. The only correlation that remained significant after AMT-5 data removal (marked by ¿) was Violax vs. DMSPd in the SATL (ρ=0.547, n=98).

	DMS	**DMSPd**	**DMSPp**
SATL	Production (ρ=0.565; n=93)	¿Violax (ρ=0.520; n=117)	Violax (ρ=0.548; n=121) Bacteria (ρ=0.579; n=147) Production (ρ=0.587; n=96)
NATR		Production (ρ=0.673; n=34) Bacteria (ρ=0.607; n=69)	Violax (ρ=0.555; n=47) Bacteria (ρ=0.699; n=72)
NAST(E)		Zeax (ρ=0.549; n=58) Bacteria (ρ=0.759; n=39)	

When discussing results in the *Trends per cruise* section, it was identified that the cruise transect for AMT-5 differed quite radically from the cruise tracks of subsequent AMT cruises (Figure 3.1). As a result, when looking at the *Trends per province*, it was considered important to address the influence AMT-5 may have had upon the correlation results. In Table 3.7, the significant correlations highlighted were found to no longer have as strong an association (i.e. $\rho \geq +0.5$) once AMT-5 data was removed. Importantly, this change does not include the bacteria and production correlations as such data was not collected during AMT-5. Of the pigments that significantly correlated with DMS(P) values, only one correlation remained (and in fact strengthened slightly) after AMT-5 data was removed: DMSPd vs. Violax (ρ=0.547; n=98). None of the significant correlations discussed so far have been particularly strong (i.e. close to +1 or -1), so it is unsurprising that a reduction in the number of data points, particularly those from the higher biomass waters encountered during AMT-5, resulted in a reduction in the strength of association between most variables. However, this also highlights the fact that perceived global correlations used for modelling purposes are not necessarily representative of low production environments (this is discussed in more detail in Chapter 4).

[i] See Section 3.2.1 for the discussion and definition of a 'significant correlation'.

Trends in surface waters

In this section, the AMT dataset has been significantly reduced; initially, the focus is purely on surface waters (upper 10 m), and subsequently, the surface waters are divided by cruise and by province. With a reduced number of data points and a highly rigorous significance criteria (α<0.0001), the number of 'significant correlations' reduced substantially. In effect, a large number of the sub-divided AMT surface data categories were unable to produce meaningful correlations as they contained too few data points. It should therefore be noted that the correlations discussed throughout this section are biased somewhat by the number of data points available. In particular, the production and bacteria versus DMS(P) correlations, sub-divided by province, did not contain enough data points to produce significant correlations. In statistical terms, this is determined using a *power* test, defined as the probability that the decision to accept the null hypothesis (H_0) is incorrect (Cohen, 1988). The non-significant results for this section were tested using the tables of Kraemer and Thiemann (1987), and the majority found to contain too few data points for the correlation analysis to be powerful enough to identify a statistically significant correlation. Therefore the absence of a correlation should not be interpreted as a lack of correlation.

Once depth variations were removed from the AMT dataset, the number of significant correlations with DMSP (dissolved and particulate) increased relative to the overall dataset (compare Table 3.8 with Table 3.4). Any correlations observed between DMS(P) and bacteria/production were not strong enough to meet the criteria defined in Section 3.2.1 (i.e. $\geq +0.5$ or ≤ -0.5). In profile, the production maximum – approximately 0.1 mmol C m^{-3} day^{-1} in the sub-tropical gyres (Poulton et al., 2006) – was consistently identified in sub-surface waters above the chl max, and this may explain the notable absence of any correlations between DMS(P) and production at the surface (< 10 m). Many of the significant correlations were with accessory pigments associated with known DMSP-producers (Hex, But, Perid and Fucox are often associated with prymnesiophytes and dinoflagellates; see Table 3.2). Other significant correlations were with Chl *a* (present in all phytoplankton groups) and Violax (part of a xanthophyll cycle). The latter suggests a link with light stress, as discussed in previous sections.

Of particular interest are the significant correlations between DV Chl *a* and DMS/DMSPd as they are <u>negative</u> (Table 3.8). In itself, this is not counter-intuitive. DV Chl *a* is considered a pigment marker of the Prochlorophytes, and in the oligotrophic gyres covered

by the AMT transects, the dominant phototrophic organism is *Prochlorococcus* spp., both in terms of cells per ml and biomass (Zubkov et al., 2000). *Prochlorococcus* contributes a negligible percentage of the total DMSP (and thus DMS), even in oligotrophic waters (Corn et al., 1995). It is possible that, when *Prochlorococcus* numbers are substantially reduced, an ecological niche exists that can be exploited by other DMSP (and thus DMS) producers.

Table 3.8 Significant[i] correlations of DMS, DMSPd and DMSPp with phytoplankton pigment concentrations, heterotrophic bacterial density (bacteria) and carbon fixation rates (production) for the AMT data from surface waters only. ρ = Spearman's Rank Correlation Coefficient; n = number of data points. All correlations are positive unless indicated by a minus sign. The first row of results refers to the significant correlations in the overall surface data; the second row refers to those remaining after AMT-5 data was removed; the third row refers to those for AMT-5 data only; the fourth row refers to the SATL gyre data only; and the fifth row refers to the SATL gyre data with AMT-5 data removed. See Table 3.1 for an explanation of the acronyms used for ocean provinces and Table 3.2 for the abbreviations used for phytoplankton pigments.

	DMS	**DMSPd**	**DMSPp**
Overall	$^{(-)}$ DV Chl *a* (ρ=-0.551; n=48)	But (ρ=0.705; n=44) Hex (ρ=0.756; n=45) But+Hex (ρ=0.727; n=44) Fucox (ρ=0.606; n=45) Violax (ρ=0.724; n=42) Chl *a* (ρ=0.684; n=44) TChl *a* (ρ=0.584; n=44) $^{(-)}$ DV Chl *a* (ρ=-0.557; n=45)	Peridinin (ρ=0.548; n=52) Hex (ρ=0.608; n=52) But+Hex (ρ=0.583; n=52) Fucox (ρ=0.590; n=52) Violax (ρ=0.715; n=50) Chl *a* (ρ=0.672; n=51) TChl *a* (ρ=0.604; n=51)
Overall (AMT-5 removed)		$^{(-)}$ DV Chl *a* (ρ=-0.651; n=30)	Violax (ρ=0.649; n=38)
AMT-5 only			Allox (ρ=0.869; n=14)
SATL		Hex (ρ=0.820; n=17) But+Hex (ρ=0.814; n=17) Violax (ρ=0.872; n=15) Chl *a* (ρ=0.846; n=17)	Violax (ρ=0.853; n=15)
SATL without AMT-5		But (ρ=0.927; n=11)	

[i] See Section 3.2.1 for the discussion and definition of a 'significant correlation'.

An alternative explanation for the negative correlations between DV Chl *a* and DMS/DMSPd is that *Prochlorococcus* consumes DMSPd. No direct evidence exists of such a phenomena, but *Synechococcus*, another prokaryotic picoplanktonic group, has recently been shown to actively take up and assimilate DMSP as a sulphur source (Malmstrom et al., 2005). Whilst sulphur is exceedingly abundant in seawater in the form of sulphate (approximately 10^7-fold more than DMSP), energy is required to reduce the sulphate before its incorporation into protein. Although Malmstrom et al. (2005) only observed *Synechococcus* to incorporate DMSP and methanethiol, it is possible that DMSP could be utilised as a sulphur source by other autotrophic species (e.g. *Prochlorococcus*). If DMSPd were actively consumed, the dominant source of DMS (i.e. production via enzymatic cleavage of DMSP) may well reduce, leading to a diminishment of the ambient pool.

Once the surface dataset was reduced in size, either by removing AMT-5 data or by sub-dividing by cruise/province, only a few significant correlations remained (Table 3.8). In general, positive associations still exist between DMSP (particulate and dissolved) and Hex, But and Violax. However, little further interpretation can be made as many of the differences between these results and those in previous tables are likely due to the reduction in the number of data points.

Correlation summary

Upon examination of all the correlation results within this section, it is clear that subtly different results can be obtained depending upon how the dataset is subdivided. Whilst unsurprising, this makes summarising 'general' patterns quite difficult as a slightly different message can be gleaned from each table of correlations. In addition, the fact that many of the pigments intercorrelate further hampers the interpretation of results. However, the subdivision of data did help to produce a clearer picture as it allowed tests of whether inter-province or inter-cruise variability was masking unseen relationships within the dataset.

A comparison of the number of significant correlations observed between each variable and any reduced sulphur compound enables an overall comparison between variables for the AMT dataset. It should be noted that bacteria and production would be disadvantaged in this comparison as the relevant measurements were not made during AMT-5. However, the results are interesting as they show that the photo-protective pigment, Violax, significantly correlated more often (thirteen times) than any other variable tested, while carbon fixation rates (production) correlated significantly eleven times. All of the significant Violax correlations were with DMSP, while four of the eleven significant production correlations were with DMS. In comparison the traditional indicator of biomass (TChl *a* or Chl *a*), only correlated significantly seven times. These results suggest that in oligotrophic regions, carbon fixation rates may provide a better indicator of DMS(P) production than biomass. Secondly, the significant positive correlations of DMSP with Violax corroborates the theory that DMSP might be part of a photo-protective strategy (Sunda et al., 2002). These conclusions confirm those already inferred directly from Table 3.4.

3.3.2 Principal Components Analysis (PCA)

Data covariance is a problem that can be circumnavigated to a certain extent using Principal Components Analysis (PCA), which accounts for the variance of the entire dataset and reduces the number of variables to a more manageable number (see Section 3.2.2 for further detail). This statistical method was initially applied to all of the available data, but was not found to be useful as the pigment data grouped as one component (or factor) and the production and bacteria data grouped together as a second component. This did not reduce the number of variables in a manner that was useful for data interpretation, and it was therefore decided to apply PCA to the pigment data only. It should be noted that But+Hex and TChl *a* were not included as they are functions of pigment data already included in this analysis (see Table 3.2).

As Table 3.9 shows, the PCA extracted the maximal variance from each variable (transformed pigment); the minimum fraction extracted was 0.704 for Allox. Three rotated components or factors (F_1, F_2 and F_3) were then used from the PCA to represent >80% of the extracted data (Table 3.10) in further analyses.

Table 3.9 Fraction of variance (where 1 = 100%) extracted from the initial AMT dataset for each transformed pigment (variable). As can be seen, the majority of the variance for each variable was incorporated into the PCA (minimum extraction of approximately 70%).

Variable	Initial	Fraction Extracted
$\log_{10}$(Chl c_3)	1.00	0.843
$\log_{10}$(Chl c_2)	1.00	0.888
$\log_{10}$(Perid)	1.00	0.713
$\log_{10}$(But)	1.00	0.768
$\log_{10}$(Hex)	1.00	0.900
$\log_{10}$(Fucox)	1.00	0.872
$\log_{10}$(Violax)	1.00	0.759
$\log_{10}$(Allox)	1.00	0.704
$(\text{Zeax})^{0.5}$	1.00	0.827
$\log_{10}$(DV Chl *a*)	1.00	0.842
$\log_{10}$(Chl *a*)	1.00	0.898

Table 3.10 Principal components (or factors, *F*) extracted from the entire AMT pigments dataset. In the first set of columns (sums of squared loadings), factors with Eigenvalues >1 (F_1 – F_3, highlighted) were selected as representative of the dataset and used for further analysis; these account for >80% of the variance of the entire AMT pigment dataset. The second set of columns (rotated sums of squared loadings) demonstrates how a *Varimax* rotation apportioned the variance as evenly as possible across the selected factors whilst explaining an equal cumulative % variance.

Component	Sums of Squared Loadings			Rotated Sums of Squared Loadings		
	Initial Eigenvalues	*% of Variance*	*Cumulative % Variance*	*Rotated Eigenvalue*	*% of Variance*	*Cumulative % Variance*
F_1	6.1	55.1	55.1	5.0	45.7	45.7
F_2	1.7	15.2	70.3	2.3	20.6	66.2
F_3	1.3	11.6	81.9	1.7	15.7	81.9
F_4	0.6	5.5	87.4			
F_5	0.4	3.5	90.9			
F_6	0.3	2.7	93.6			
F_7	0.2	1.9	95.5			
F_8	0.2	1.8	97.3			
F_9	0.2	1.4	98.6			
F_{10}	0.1	0.9	99.5			
F_{11}	0.1	0.5	100.0			

The component matrix presented in Table 3.11 provides an indication of the initial variables represented by each PCA factor. Using an understanding of known DMSP-producers and the results from Section 3.3.1, it is possible to predict which factor is likely to best correlate with the DMS(P) data. In particular, F_1 represents But, Hex and Fucox (pigment markers for Prymnesiophytes, Chrysophytes and Dinophytes, known DMSP-producers) and Violax (part of a xanthophyll cycle that correlated well with DMS(P) measurements in Section 3.3.1). As the majority of pigments' variance was accounted for, a strong correlation with DMS(P) might therefore be expected for F_1. In contrast, the relatively ubiquitous Chl c_3 and Chl c_2 represent F_2, while Zeax and DV Chl *a* (both markers for Prochlorophytes, poor DMSP-producers) represent F_3. Components F_2 and/or F_3 would not therefore be expected to correlate particularly well with the DMS(P) data.

Table 3.11 The component matrix enables the user to identify which of the three selected factors explain the majority of the variance of each initial variable (i.e. pigment). As highlighted (light/yellow) in the table: F_1 can be used to represent the majority of the variance of Perid, But, Hex, Fucox, Violax and Chl *a*; F_2 can be used to represent the majority of the variance of Chl c_3 and Chl c_2; and F_3 can be used to represent the majority of the variance of Zeax and DV Chl *a*. Allox was not well represented by any one factor, with only approximately half of the variance accounted for by F_1 and F_2 (highlighted dark/green).

Variable	**Rotated Component (Factor)**		
	F_1	F_2	F_3
$\log_{10}$(Chl c_3)	0.218	0.892	0.000
$\log_{10}$(Chl c_2)	0.258	0.901	0.099
$\log_{10}$(Perid)	0.817	0.080	0.196
$\log_{10}$(But)	0.834	0.260	0.073
$\log_{10}$(Hex)	0.879	0.339	0.113
$\log_{10}$(Fucox)	0.888	0.286	0.033
$\log_{10}$(Violax)	0.861	0.095	-0.094
$\log_{10}$(Allox)	0.624	0.550	0.110
$(\text{Zeax})^{0.5}$	0.101	-0.030	0.903
$\log_{10}$(DV Chl *a*)	0.008	0.140	0.907
$\log_{10}$(Chl *a*)	0.919	0.231	-0.013

Using the definition from Section 3.2.1, there are no 'significant correlations' between PCA factors and DMS(P) data in the correlation matrix (Table 3.12); these results are corroborated by X-Y plots of transformed data (Figure 3.6). One of the stipulations used in Section 3.2.1 to define a 'significant correlation' was that the strength of the correlation had to be $\geq +0.5$ or ≤ -0.5. Secondly, a strict criterion of $\alpha<0.0001$ was used to identify only the highly significant correlations. If these rules are relaxed for the results in Table 3.12, some correlations are evident. The two most notable correlations confirm the theory postulated in the previous paragraph because, of the three PCA factors, F_1 correlates most strongly with the DMSPd and DMSPp measurements (Table 3.12 and Figure 3.6). The strength of these correlations is clearly lower and less significant than with individual pigment concentration data (specifically, Violax; $\rho=0.537$, $\alpha<0.0001$; Table 3.4). This indicates that, once the majority of variance in the AMT pigment dataset has been accounted for, the DMSP concentrations remain largely unexplained by pigment concentrations alone. Based on the results of Section 3.3.1, this is likely due to variations in production not linked to changes in pigment concentration.

Table 3.12 Correlation matrix of reduced sulphur compounds (DMS, DMSPd and DMSPp) versus PCA factors (F_1, F_2 and F_3). ρ = Spearman's Rank Correlation Coefficient; n = number of data points; significant correlations marked $^{(**)}$ $\alpha<0.01$, or $^{(*)}$ $\alpha<0.05$. Letters in brackets refer to the relevant plot in Figure 3.6.

PCA Factor	DMS	DMSPd	DMSPp
F_1	ρ = -0.028; n = 289 (a)	$^{(**)}$ ρ = +0.365; n = 275 (b)	$^{(**)}$ ρ = +0.437; n = 294 (c)
F_2	$^{(*)}$ ρ = -0.133; n = 289 (d)	$^{(*)}$ ρ = +0.125; n = 275 (e)	ρ = +0.077; n = 294 (f)
F_3	ρ = +0.013; n = 289 (g)	ρ = -0.098; n = 275 (h)	ρ = -0.081; n = 294 (i)

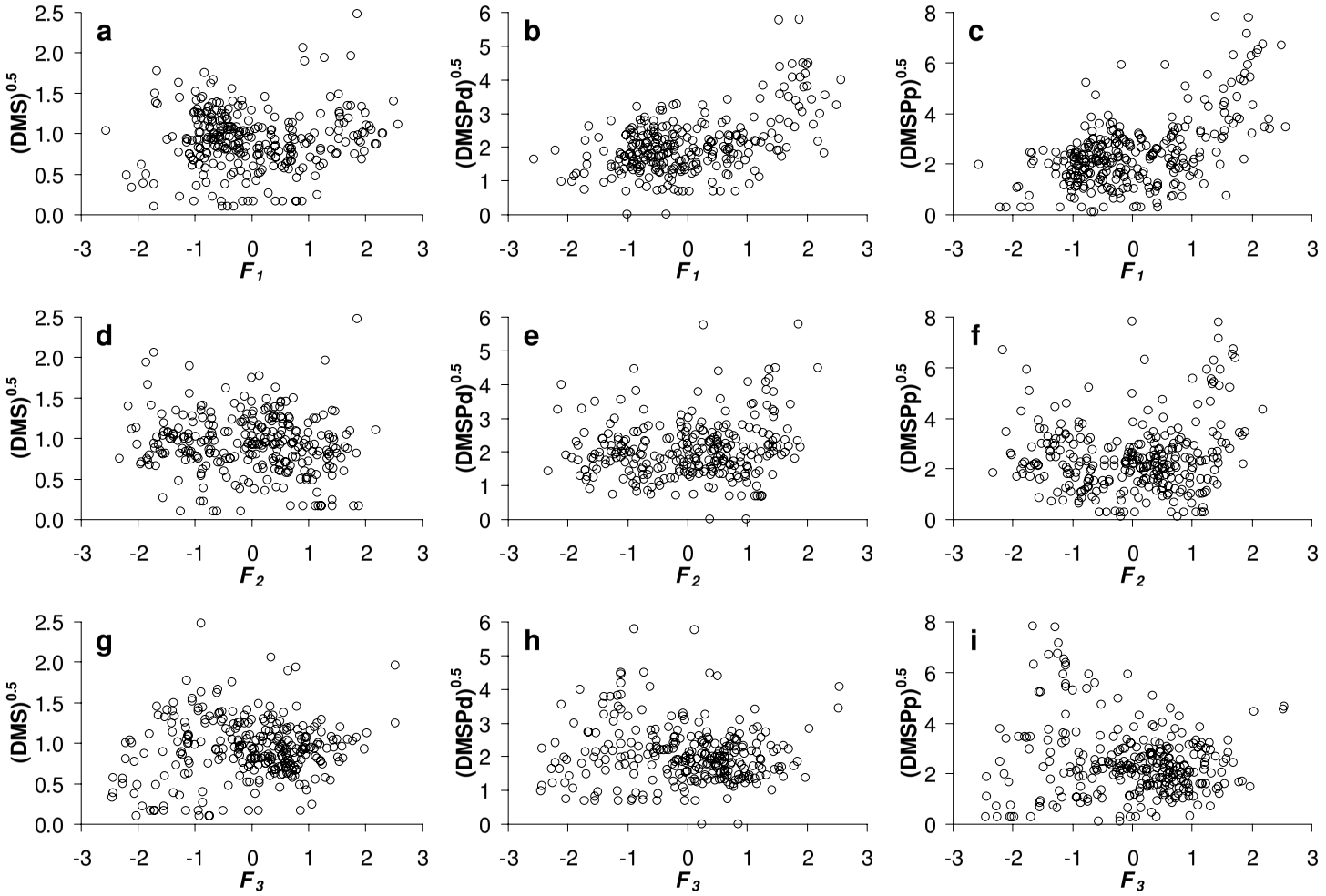

Figure 3.6 Scatter plot matrix of PCA factors: F_1 (plots a, b and c); F_2 (plots d, e and f); and F_3 (plots g, h and i), versus transformed DMS(P) values: $DMS^{0.5}$ (plots a, d and g); $DMSPd^{0.5}$ (plots b, e and h); and $DMSPp^{0.5}$ (plots c, f and i).

As discussed in Section 3.3.1, AMT-5 was different in that the cruise track did not progress as far into the oligotrophic gyres. Correlation results (Section 3.3.1) clearly show that the removal of AMT-5 data has an impact upon the relationships observed within the dataset (both overall and when divided by ocean province). It was therefore logical to run PCA on the AMT dataset with AMT-5 data removed. All variables (pigments) were well-described by this second PCA except Allox (a fraction of only 0.43 was extracted, Table 3.13). The extraction accounted for 78% of the variance (compared to 82% in Table 3.10) and, as with the PCA for the entire dataset, produced three components (abbreviated in this case by *C*) with Eigenvalues >1. The three components represented the same groups of pigments, but in a slightly different order (Table 3.13). C_1 can be used to represent Perid, But, Hex, Fucox, Violax and Chl *a*, but C_2 best represents Zeax and DV Chl *a* while C_3 now best represents Chl c_3 and Chl c_2.

Table 3.13 The component matrix enables the user to identify which of the three selected factors explain the majority of the variance of each initial variable (i.e. pigment). As highlighted (light/yellow) in the table, C_1 can be used to represent the majority of the variance of Perid, But, Hex, Fucox, Violax and Chl *a*; C_2 can be used to represent the majority of the variance of Zeax and DV Chl *a*; and C_3 can be used to represent the majority of the variance of Chl c_3 and Chl c_2. Allox was not well represented by any one factor, but the majority of variance was accounted for by C_1 (highlighted dark/green).

Variable	Rotated Component (Factor)		
	C_1	C_2	C_3
$\log_{10}$(Chl c_3)	0.121	-0.017	0.913
$\log_{10}$(Chl c_2)	0.051	0.151	0.901
$\log_{10}$(Perid)	0.844	0.223	0.088
$\log_{10}$(But)	0.862	0.029	0.093
$\log_{10}$(Hex)	0.912	0.126	0.129
$\log_{10}$(Fucox)	0.919	0.134	0.091
$\log_{10}$(Violax)	0.825	-0.148	-0.120
$\log_{10}$(Allox)	0.553	0.296	0.191
$(\text{Zeax})^{0.5}$	0.183	0.871	0.056
$\log_{10}$(DV Chl *a*)	0.026	0.906	0.062
$\log_{10}$(Chl *a*)	0.946	0.088	0.065

Of course, the result of interest is whether the Spearman's Rank Correlation between components (C_1 - C_3) and DMS(P) values was improved or weakened by the removal of AMT-5 data. Only two correlations were significant at all (in fact both were α<0.01):

C_1 versus DMSPd (ρ=0.241; n=215; α<0.01)

C_1 versus DMSPp (ρ=0.246; n=233; α<0.01)

These correlations are plotted using transformed DMSPd and DMSPp data (Figure 3.7) and, encouragingly, are similar to the first PCA results (Table 3.12). The strengths of the correlations between C_1 and DMSP (dissolved and particulate forms) have reduced considerably and, when comparing Figure 3.7a&b with Figure 3.6b&c, it can be seen that this is likely due to the removal of high DMSP and C_1 data values. In summary, the removal of AMT-5 has shown that a similar (and expected) correlation exists with F_1/C_1, regardless of whether AMT-5 data is included or not (i.e. regardless of how oligotrophic the water is). However, this relationship is not as strong or significant as the individual correlations in Section 3.3.1, indicating other influencing factors.

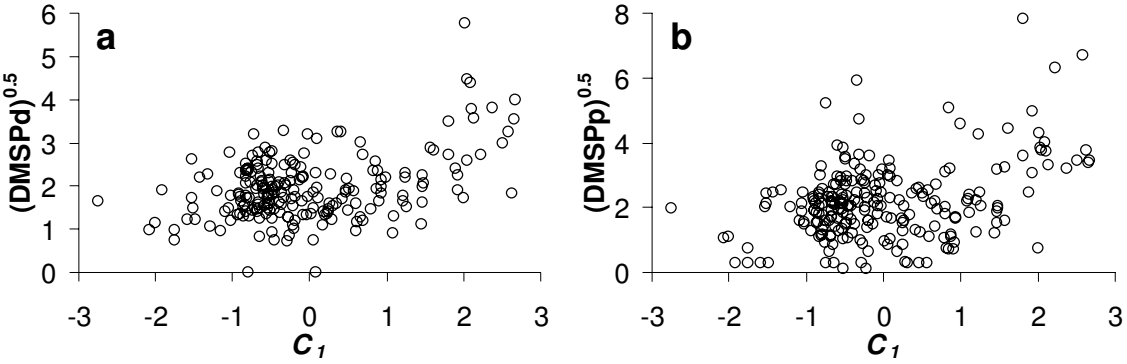

Figure 3.7 Scatter plots of PCA component C_1 (AMT dataset with AMT-5 data removed) versus transformed (a) DMSPd ($DMSPd^{0.5}$) and (b) DMSPp ($DMSPp^{0.5}$).

3.3.3 Seasonality in the South Atlantic gyre?

Previous investigations have discovered that the overall biomass standing stock in oligotrophic environments is relatively unchanged throughout the course of a year (Claustre and Marty, 1995; Gibb et al., 2000). However, observations in the northern tropical Atlantic indicate that, whilst the community structure and standing stock are stable between seasons, water column stratification and production rates vary significantly between spring and autumn (Claustre and Marty, 1995). It is therefore of interest to see if DMS(P) concentrations in oligotrophic regions during the AMT project appear to be influenced by these seasonal changes. In order to assess this, it is important to account for any confounding factors such as spatial variability. The SATL provides a perfect vehicle for such a study as the cruise tracks during AMT-12-14 were identical in this region and represent measurements for two seasons (AMT-12 and AMT-14 in southern hemisphere autumn, AMT-13 in spring). A comparison (i.e. ANOVA) of the results from these cruises may indicate whether the reduced sulphur cycle is affected by seasonality.

DMS(P) data and ancillary biological measurements were investigated using the ANOVA method described in Section 3.2.3. In order to best interpret the results, plots of the means (± standard error of the mean) of each cruise for each variable (Figure 3.8), and a table displaying whether the differences were significant (Table 3.14) are required. DMS, DMSPd and DMSPp display similar patterns, with differences in DMSPd concentrations the most significant (Figure 3.8 and Table 3.14). Interestingly, the southern hemisphere spring (AMT-13) concentrations were higher than those in autumn (AMT-12 and -14) and the only other variable with a significant result and similar pattern was production (Figure 3.8 and Table 3.14). Production has been observed to vary significantly in another oligotrophic system in the North Atlantic despite overall biomass remaining unchanged (Claustre and Marty, 1995), and results from Section 3.3.1 also suggest that production may drive a change in DMS(P) concentrations in such regions.

Table 3.14 Statistical determination of significantly different (α<0.05) cruises in the SATL; AMT-12 and -14 were during the southern hemisphere autumn, AMT-13 during the spring. For optimum interpretation of these results, use this information with the plots in Figure 3.8.

Parameter	**Cruises Sig. Diff? (α<0.05)**
DMS	AMT-14 sig. diff. to AMT-12 and -13
DMSPd	AMT-13 sig. diff. to AMT-12 and -14
DMSPp	AMT-14 sig. diff. to AMT-12 and -13
Production	AMT-13 sig. diff. to AMT-12 and -14
Chl a	Only AMT-13 and AMT-14 sig. diff. to each other
Violax	AMT-14 sig. diff. to AMT-12 and -13
Perid	No Differences
DV Chl a	All Different
Zeax	AMT-14 sig. diff. to AMT-12 and -13
TChl a	No Differences
Chl c3	Only AMT-12 and AMT-14 sig. diff. to each other
Chl c2	AMT-14 sig. diff. to AMT-12 and -13
Allox	AMT-12 sig. diff. to AMT-13 and -14
Bacteria	AMT-12 sig. diff. to AMT-13 and -14
Fucox	No Differences
But	No Differences
Hex	No Differences
But+Hex	No Differences

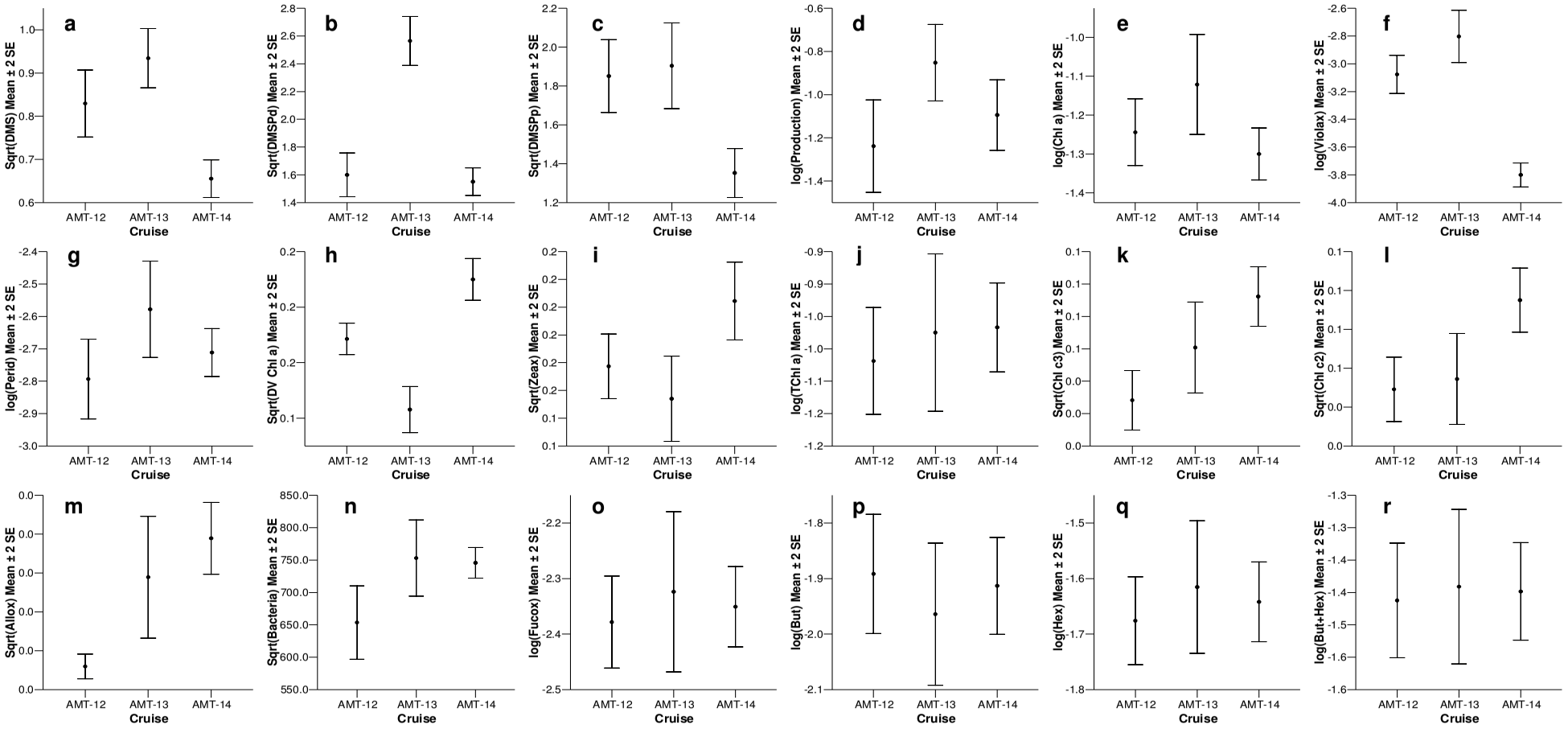

Figure 3.8 Plots of average (mean) ± 2SE (2 Standard Error = error bars) for AMT-12, AMT-13 and AMT-14. Plots represent transformed: (a) DMS; (b) DMSPd; (c) DMSPp; (d) Production; (e) Chl *a*; (f) Violax; (g) Perid; (h) DV Chl *a*; (i) Zeax; (j) TChl *a*; (k) Chl c_3; (l) Chl c_2; (m) Allox; (n) Bacteria; (o) Fucox; (p) But; (q) Hex; and (r) But+Hex.

As well as the seasonal trends in DMS and DMSPp already mentioned, the Chl *a*, Violax and Perid plots show a similar trend, but only certain cruises can be differentiated statistically (Figure 3.8 and Table 3.14). Violax has previously been shown to correlate significantly and positively with DMSP, so it is unsurprising that a similar trend in mean concentration is observed. Chl *a* and Perid change in a similar manner to the reduced sulphur compounds, suggesting that the change in community production drives a change in speciation. Indeed, the polar opposite of the aforementioned trend is exhibited by DV Chl *a*, i.e. low during the southern hemisphere spring, AMT-13; and high during autumn, AMT-12 and -14 (see Figure 3.8 and Table 3.14). Zeax, another marker for the Prochlorophytes and a photo-protective pigment, demonstrates a similar pattern to DV Chl *a*, although AMT-12 and -13 cannot be distinguished statistically (Figure 3.8 and Table 3.14).

Based on the production and DV Chl *a* results, it would seem that as the productivity of the phytoplankton community increases in spring, the Prochlorophytes (i.e. *Prochlorococcus*) become less prevalent, and the data suggests (not significantly) that Perid-containing phytoplankton (possibly dinoflagellates) may fill that niche. As this change in community structure occurs, the DMS(P) levels are affected, most notably the DMSPd concentrations. TChl *a* results cannot be separated statistically at all (Figure 3.8 and Table 3.14), which corroborates the results of Claustre and Marty (1995), but this is understandable as TChl *a* is a function of DV Chl *a* plus Chl *a* and these pigments demonstrate opposing trends, each effectively nullifying the effect of the other. Ideally, more data should be collected for this region during the southern hemisphere spring to confirm these interpretations.

3.3.4 Unusually high DMS concentrations observed in the NAST during AMT-14

During AMT-14, unusually high concentrations of DMS were encountered between approximately 25°N and 30°N (for relevant region, see Figure 3.9), with sub-surface concentrations of approximately 3 nM (Figure 3.10a). In comparison, the equivalent sub-surface concentration for the same region latitude and region during AMT-12 was 1.1 nM (Figure 3.3). Increased biological production is an obvious candidate for these increased DMS concentrations but this would suggest a proportional increase in DMSP concentrations. No clear pattern is apparent in the dissolved and particulate DMSP concentrations and, if anything, there is a suggestion that DMSPd concentrations may have reduced slightly for the area in question (Figure 3.5). Had DMSP-production and DMSP-lyase activity (DLA) increased (and DMS loss terms remained constant or reduced), an increase in DMS concentrations would be expected. No DMSP production measurements were made during AMT-14, and DLA measurements from chl max and surface waters do not suggest any unexpected levels of activity for the relevant stations (see Chapter 5, Figure 5.2). It was hoped that the ancillary data (biological and physical) might help explain the observed DMS 'hotspot'.

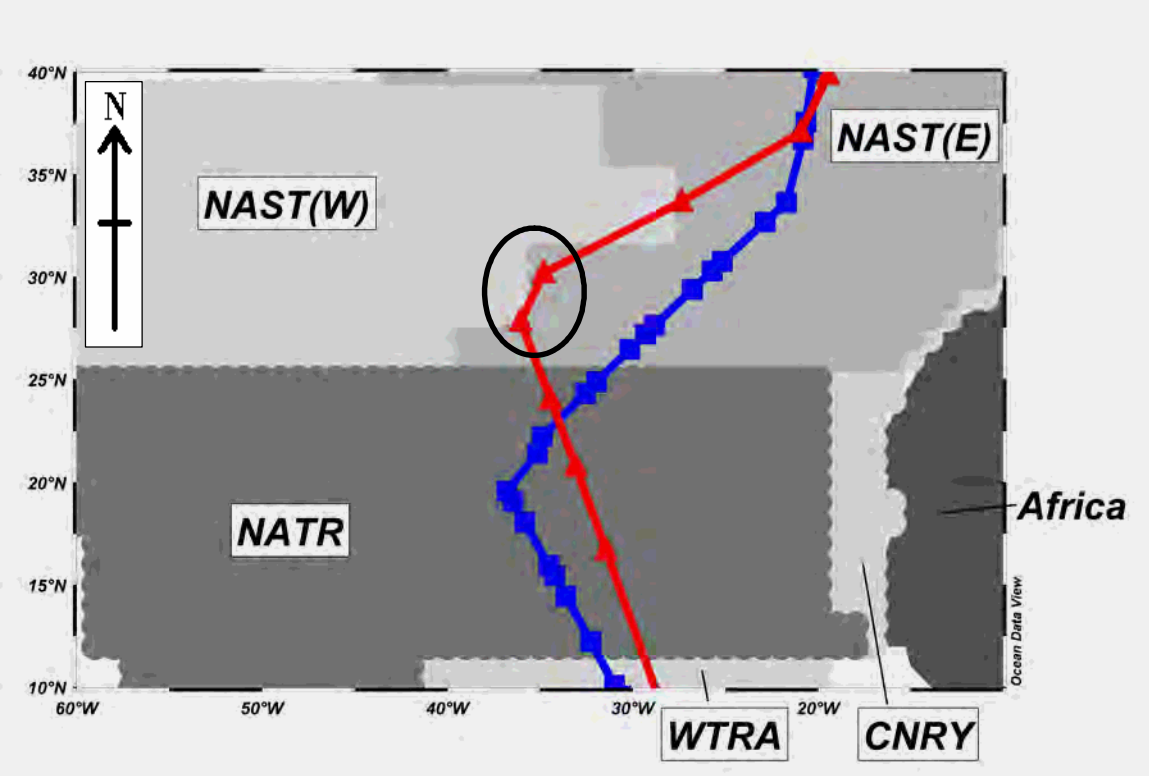

Figure 3.9 Close-up view of northern hemisphere gyre-focussed AMT cruise tracks. Both AMT cruises were northbound and occurred during the northern hemisphere's spring (May/June) in 2003 (AMT-12, squares) and 2004 (AMT-14, triangles). The provinces defined by Longhurst (1995) are shown to provide spatial reference: North Atlantic Sub-Tropical Gyre – East (NAST(E)); North Atlantic Sub-Tropical Gyre – West NAST(W); Canary Current Coastal (CNRY); North Atlantic Tropical Gyre (NATR); and Western Tropical Atlantic (WTRA). The circled region during AMT-14 is the focus of this section (Section 3.3.4). Plot produced using *Ocean Data View* (http://odv.awi-bremerhaven.de/home.html).

Although AMT-14 concentrations were twofold higher than previous AMT measurements from the NAST, the most notable aspect of these waters was reflected by the concurrent biological data. As expected for oligotrophic gyre waters, Chl *a* measurements were typically low (< 0.1 µg L^{-1}, Figure 3.5). However, whilst these regions are typically dominated by *Prochlorococcus* (Zubkov et al., 2000), which use DV Chl *a* instead of Chl *a* for photosynthesis (Wright and Jeffrey, 1997, and references therein), their density dropped sharply as the DMS concentrations increased (Figure 3.10b). A similar drop was observed in heterotrophic bacterial density (Figure 3.10c).

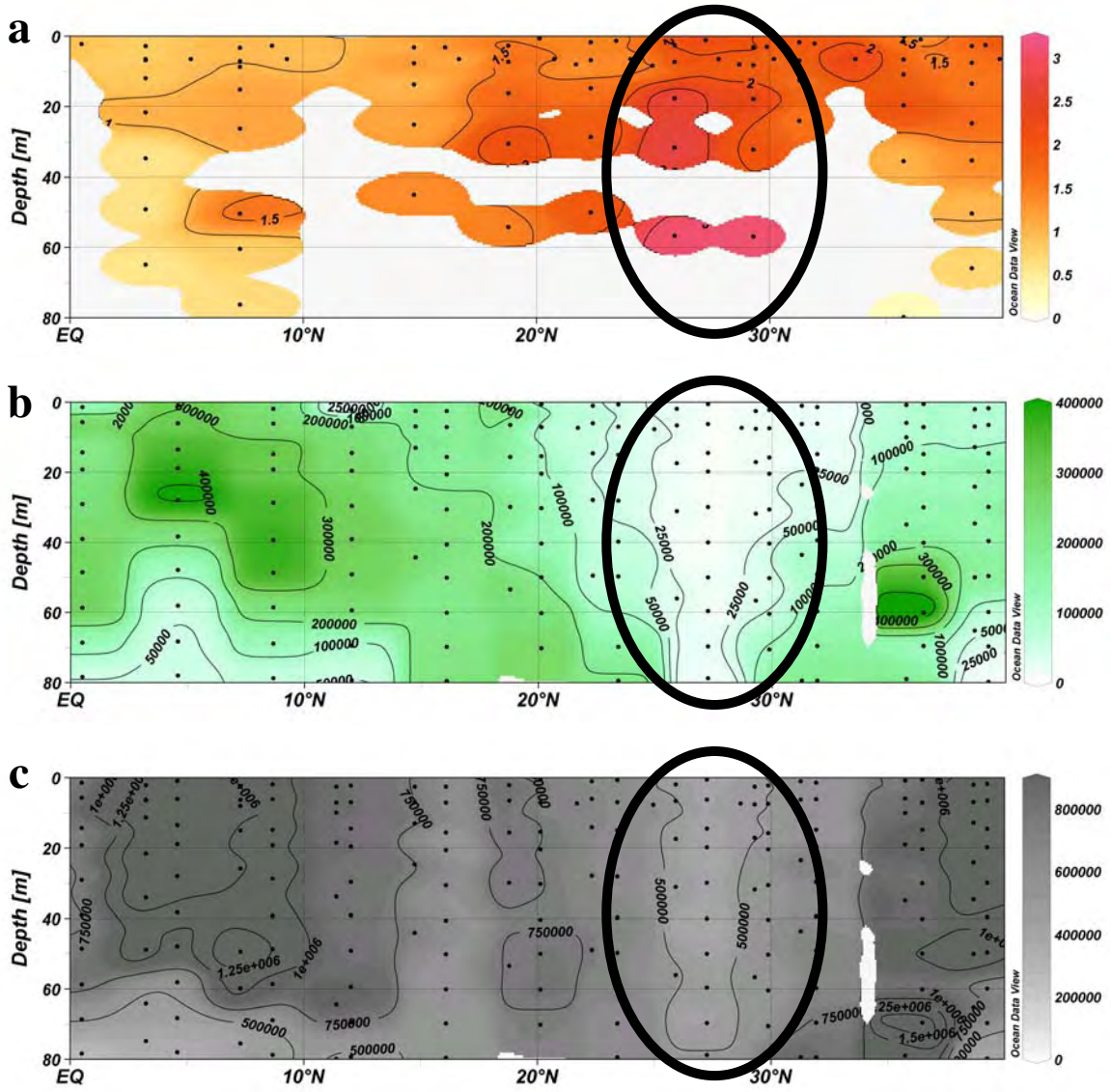

Figure 3.10 Depth contour plots of (a) DMS (red); (b) *Prochlorococcus* density in number ml^{-1} (green); and (c) heterotrophic bacterial density in number ml^{-1} (grey) during the northern section of AMT-14 (the red cruise track on Figure 3.1, equator to 40°N). Sample points are indicated (black dots) and the location of the DMS 'hotspot' circled on each section. Contour lines are set at intervals of 0.5 nM and 250,000 cells ml^{-1} for DMS and heterotrophic bacterial density respectively. For *Prochlorococcus* density, contour lines were set at 100,000 cells ml^{-1} with extra contours for 50,000 and 25,000 cell ml^{-1}. For DMS and heterotrophic bacterial density, scales have been capped respectively at 3.5 nM and 900,000 cells ml^{-1} for readability and thus a small minority of points exceed these values. Equivalent plots for DMS and heterotrophic bacterial density with unlimited scales are included in the appendix (Figure V).

Surface water carbon fixation provides an indication of the overall phytoplankton community activity. During AMT-14, size-fractionated carbon fixation shifted dominance from the small (0.2-2 µm) fraction to the large (>2 µm) fraction within the DMS hotspot (Figure 3.11b), although a similar shift was observed at a similar latitude during AMT-12 (Figure 3.11a). Further to this, total carbon fixation rates reduced between 25°N and 30°N, but no more than would be expected in gyre waters; total carbon fixation during AMT-12 was in fact lower than during AMT-14 (Figure 3.11c).

As discussed in Section 3.3.1, it is conceivable (but unproven) that *Prochlorococcus* assimilates DMSP. The decline in *Prochlorococcus* numbers may therefore have resulted in an increase in DMSP and thus DMS. However, this is unlikely to have been the case as DMSPd concentrations were observed to stay constant or even reduce. In a similar vein, heterotrophic bacteria have been observed to consume DMS (e.g. Gonzalez et al., 1999; Zubkov et al., 2002; Zubkov et al., 2004), and thus a decline in their numbers could be linked to an increase in DMS concentrations. Whilst this remains a possibility, it is unlikely because the rate of DMS consumption in such waters is low and DMS production would have had to continue in the absence of DMS consumption for a significant period of time for concentrations to build up to observed levels (Zubkov, M., *Pers. Comm.*).

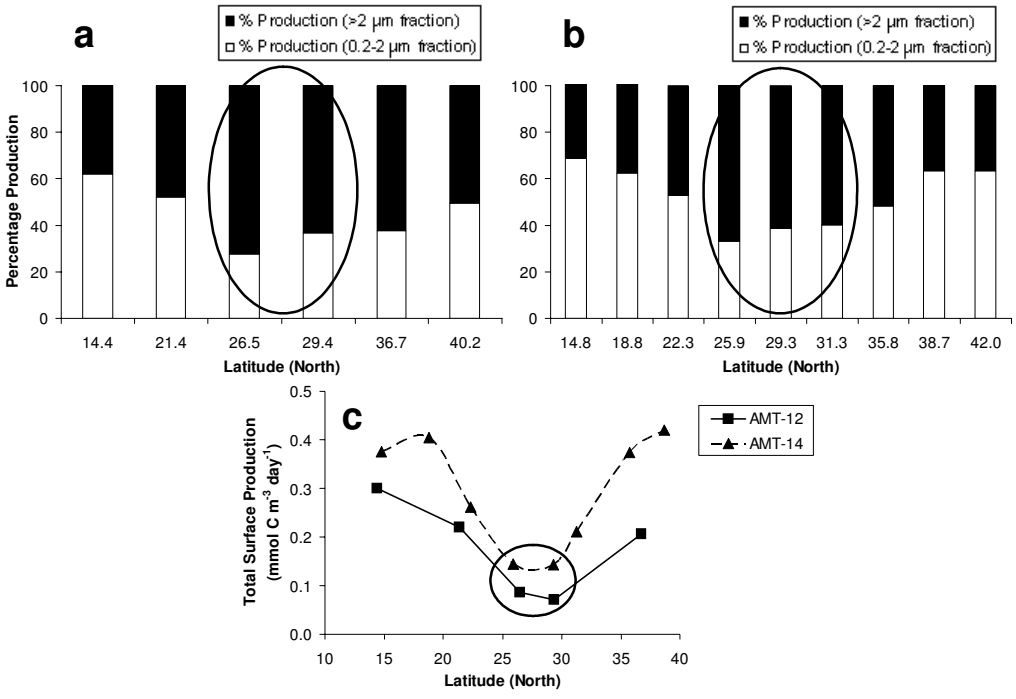

Figure 3.11 Balance of size-fractionated carbon fixation (%) in North Atlantic Sub-Tropical surface waters during (a) AMT-12 and (b) AMT-14. Total carbon fixation (c) is plotted for reference (squares, AMT-12; triangles, AMT-14). The focus of this section (Section 3.3.4) is circled on all plots.

As the biological measurements fail to satisfactorily explain the elevated DMS concentrations, we must consider the physical structure of the water column. The following pages contain AMT-14 CTD profiles from the NAST (Figure 3.12) and for comparison the SATL (Figure 3.13), with each station's DMS depth profile overlain. The DMS hotspot profiles in the NAST are CTDs 67 and 71, and the subsurface DMS maxima can clearly be identified. Of greatest interest are the corresponding density profiles, which suggest that the water column is stratified to the surface (i.e. every parcel of water is less dense than the water directly below it). Certainly this provides an explanation for the reduced biological activity as the phytoplankton and bacterioplankton could easily have become nutrient-limited. Explaining an increase in DMS concentrations with this mechanism is less straightforward. One suggestion might be that the stratified surface layers have physically capped any DMS produced and restricted the sea-air gas flux. However, as is evident in Figure 3.12, CTD profiles outside of the DMS hotspot demonstrate a similar structure. This difference could be explained by the length of time that the water column has been fully stratified, i.e. increase in time capped = increase in DMS concentration. The fact that the SATL profiles (Figure 3.13) look completely different to those in the NAST (i.e. contain a clearly defined mixed layer), suggests this might be a possibility, but we have no way of discerning that this is the driving factor.

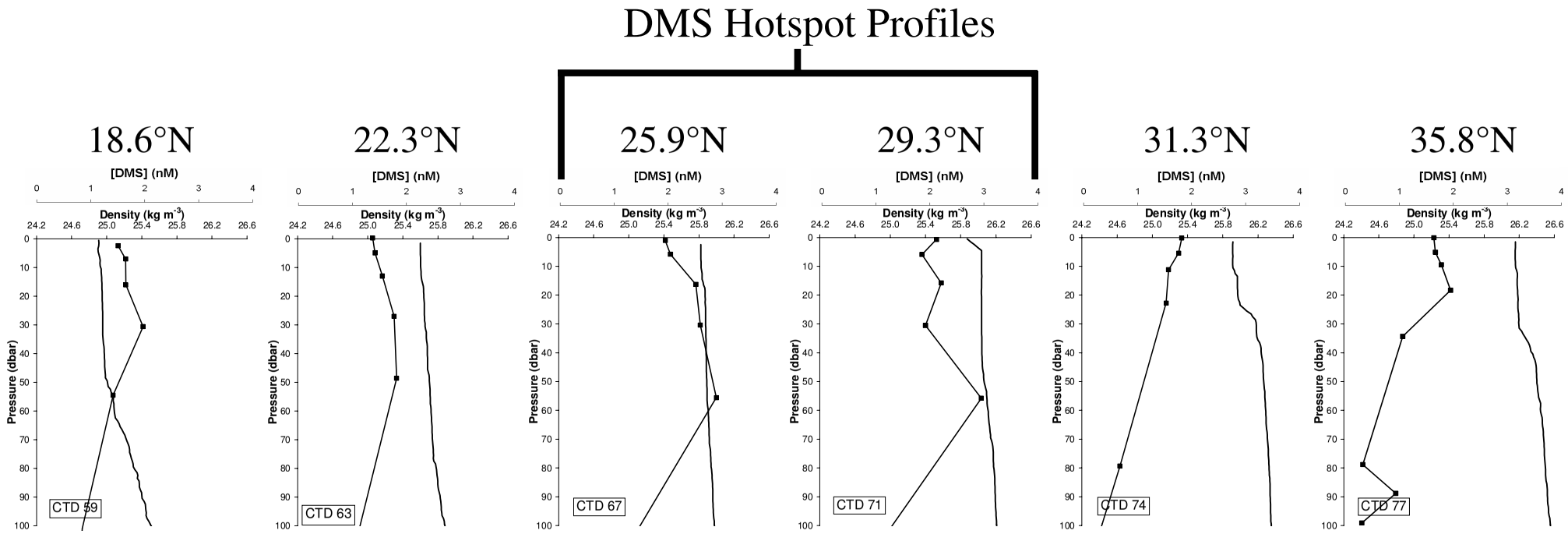

Figure 3.12 Water column structure as defined by density (solid line) and DMS concentration profile (filled squares) for the upper 100 m during the northern section of AMT-14. The relevant CTD casts (CTDs 59 to 77; 16°N – 35°N) are plotted. The specific DMS hotspot profiles are CTDs 67 and 71. All plots have exactly the same scales to aid comparability.

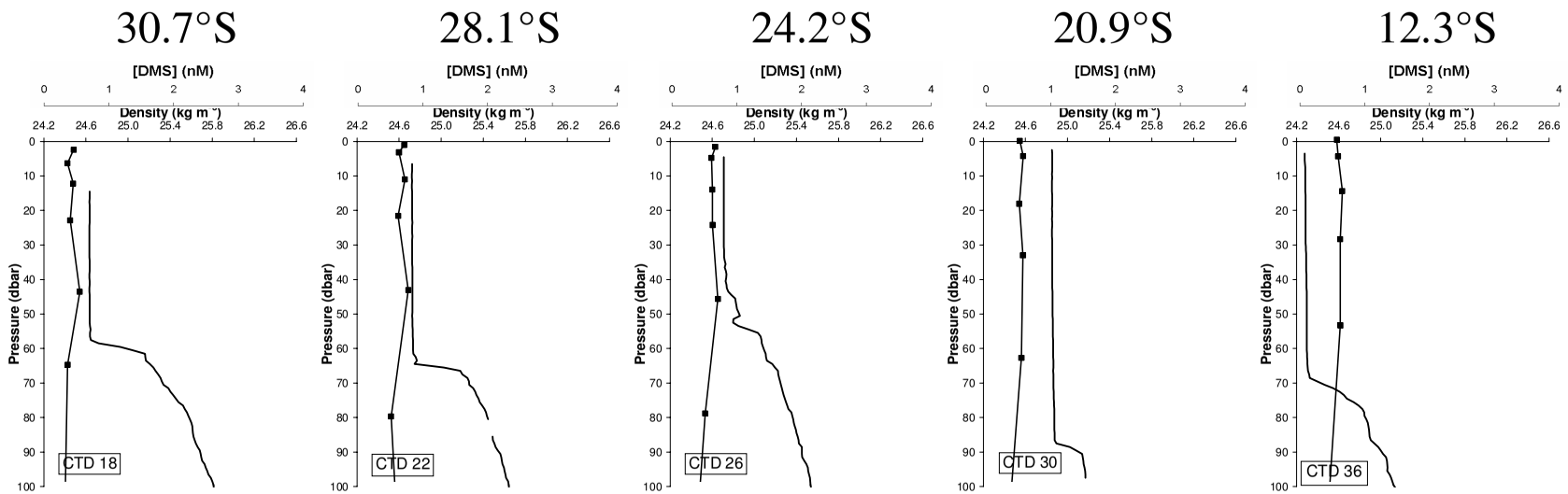

Figure 3.13 Water column structure as defined by density (solid line) and DMS concentration profile (filled squares) for the upper 100 m during the southern section of AMT-14. The relevant CTD casts (CTDs 18 to 36; 33°S – 12°S) are plotted. All plots have exactly the same scales to aid comparability.

A valid question to address is whether a phenomenon similar to the AMT-14 DMS hotspot has ever previously been observed. The most extensive DMS database available can be found online (http://saga.pmel.noaa.gov/dms/), and surface measurements from this plus AMT-12 and -14 data are displayed in Figure 3.14. Despite this extensive collection of DMS measurements and the fact that it covers all seasons, surface concentrations have not previously been observed within the local region. One pertinent point is that no measurements have previously been made as far west as AMT-14, and therefore there is no way of knowing whether or not this is a transient feature. More measurements are essential from this region and further west if we are to identify and characterise the processes driving this DMS hotspot and any other similar phenomena.

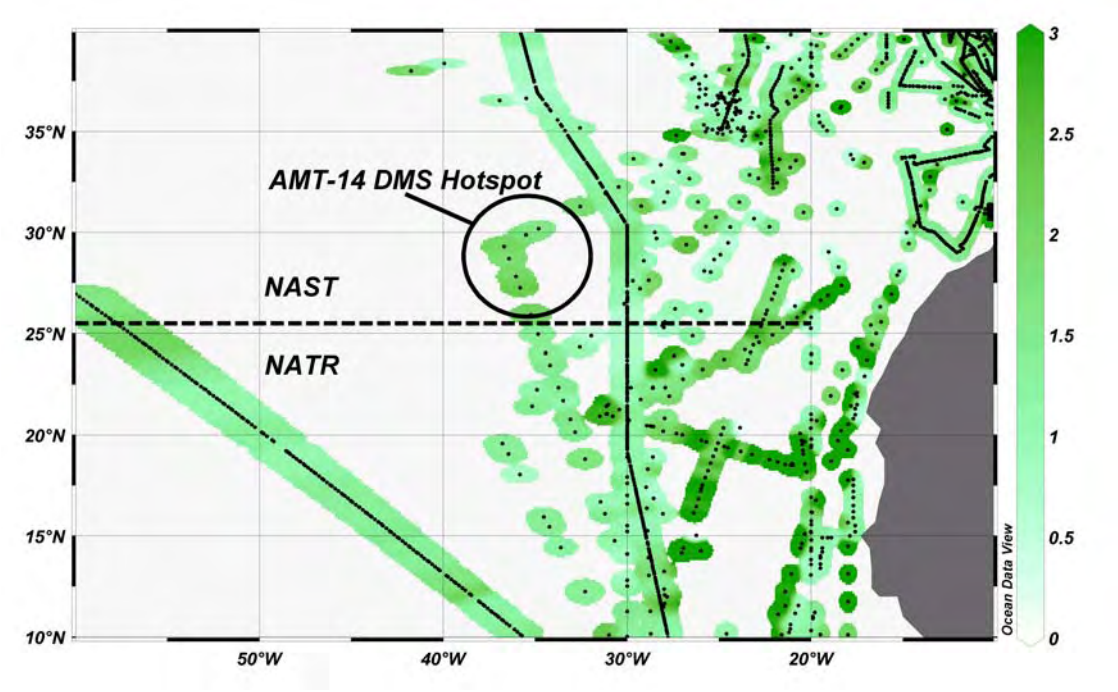

Figure 3.14 Currently available surface DMS concentrations (nM) within the northern hemisphere (10°N – 40°N; 60°W – 10°W), including measurements from the global DMS database (http://saga.pmel.noaa.gov/dms/) and samples from the AMT-12 and -14 cruises. The DMS scale has been capped at 3 nM to distinguish smaller-scale variations. According to Longhurst (1995), the distinction between the North Atlantic Sub-Tropical Gyre (NAST) and the North Atlantic Tropical Region (NATR) lies along 25.5°N (dashed line). The elevated DMS concentrations encountered during AMT-14 are circled.

Beyond the North Atlantic, time series measurements from the oligotrophic Sargasso Sea have identified a regular increase in DMS concentrations during the summer months (Dacey et al., 1998). Unusually, this increase in DMS occurs while DMSP concentrations are observed to reduce, suggesting a similar scenario to the DMS hotspot observed during AMT-14. Subsequent work on the Sargasso Sea dataset has identified significant positive

correlations between DMS concentrations and light, in particular ultraviolet light (Toole and Siegel, 2004), suggesting another link with the anti-oxidant hypothesis of Sunda et al. (2002). Unfortunately no UV measurements were made during AMT-14 and no data exists from the DMS hotspot region in the days preceding the observations, so we are unable to test such a theory.

3.4 Summary

Certain results from this chapter (Figure 3.2; Table 3.4; Table 3.7; and Table 3.8) clearly show that AMT-5 differed significantly from subsequent cruises as the transect did not progress as far into the subtropical gyres (see Figure 3.1). This clearly demonstrates the difference between the definition of oligotrophic, gyre-like conditions using measurements, versus the definition of the North and South oligotrophic gyres as defined by Longhurst (1995). This difference should be borne in mind if extrapolating results from such regions across the entire Longhurst province or if planning future research in these and similar regions of the world's oceans.

In Section 3.3.1, results from previous correlations between DMS(P) and accessory pigments were discussed. In particular, the work of Belviso et al. (2001) and McKee (2001) indicated DMSPp linkages with Hex+But (Belviso et al., 2001), and with Hex and Allox (McKee, 2001). Overall, the AMT results do not corroborate these trends, although when surface data was isolated, significant correlations were observed with But, Hex and But+Hex (Table 3.8). In particular, the correlation between DMSPp and Allox appears to have only occurred during AMT-5 (Table 3.5 and Table 3.8). In the oligotrophic waters of the North and South Atlantic, phytoplankton community carbon fixation rates appear to represent a more accurate indicator of ambient DMS(P) (in particular DMSPp) concentrations than Chl *a* or TChl *a* (Table 3.4, Table 3.5 and Table 3.7). Numerous significant correlations between DMSPp and Violax (Table 3.4, Table 3.5, Table 3.7 and Table 3.8) add statistical weight to the anti-oxidant hypothesis first proposed by Sunda et al. (2002). Combined with the DLA results from Chapter 5, this strongly suggests that the reduced sulphur cycle plays a role in combating oxidative light stress in phytoplankton.

Correlations using the factors or components created using PCA and pigment data corroborate individual correlation results whilst taking into account the majority of variation within the pigment dataset (see Section 3.3.2). However, the correlation coefficients (ρ) are weaker and the significance (α) lower than individual correlations, suggesting that at least one other factor plays a major role (e.g. phytoplankton production). ANOVA results for the SATL indicate that seasonality does exist within the reduced sulphur cycle and relates to differences in carbon fixation (see Section 3.3.3). Further, the results suggest that in spring, carbon fixation increases, subtly changing the community composition and resulting in a change in DMS(P) levels. More data is required to verify

these conclusions. The DMS hotspot encountered during AMT-14 (see Section 3.3.4) is a phenomenon previously unseen in the NAST, although a similar trend has been observed in the Sargasso Sea (see Dacey et al., 1998). The changes in DMS co-occurred with changes in certain biological parameters and the water column's physical structure. This information provides clues as to the cause of such a DMS hotspot, but firm conclusions are limited because measurements were not made as part of a lagrangian study, which would have provided a good context for data interpretation.

4 Comparing AMT data with proposed algorithms for global surface DMS concentrations

4.1 Introduction

During recent years a number of different algorithms have emerged, all of which aim to predict DMS concentrations from various biogeochemical and physical parameters. Anderson et al. (2001) use globally gridded fields of chlorophyll concentration (C), light (J) and a nutrient term based on Michaelis-Menten uptake kinetics (Q) to predict DMS concentrations. Aumont et al. (2002) use a plankton community composition index calculated from ancillary pigment concentrations, and a variation of this was used by Belviso et al. (2004b). Simo & Dachs (2002) built upon a previously proposed relationship between DMS production and the depth of the mixed layer, MLD (Simo and Pedros-Alio, 1999) to create global DMS fields from a parameterisation that combines the depth of the mixed layer and chlorophyll *a* concentrations. Aranami and Tsunogai (2004) used new data from the Pacific to examine the Simo and Dachs (2002) algorithm. They suggest that most of the variations in surface DMS concentration could be explained by a dilution model where the product of DMS concentration and MLD was equal to a constant.

A recent paper (Belviso et al., 2004a) produced an inter-comparison between five different global DMS climatologies (Anderson et al., 2001; Aumont et al., 2002; Simo and Dachs, 2002; Chu et al., 2003; Belviso et al., 2004b), using the Kettle et al. (1999) DMS climatology as reference. The authors concluded that uncertainties in sea-surface DMS concentrations derived from different global climatologies are greater than those associated with the air-sea gas transfer velocity (Belviso et al., 2004a). In addition, certain climatologies showed a better fit with measurements from particular regions, indicating that the various relationships are more (or less) appropriate in different areas (Belviso et al., 2004a).

In this chapter, surface DMS concentration, chlorophyll concentration and DMS flux data is presented for five research cruises during the AMT programme (AMT-5, -9, -12, -13 and -14; see Figure 1.18) and attention is paid to the spatial variability of these parameters. The significant amount of data and the large spatial coverage enabled a comparison of DMS measurements with the following, recently-published algorithms, formulated using

biogeochemical and biogeophysical parameters: Anderson *et* al. (2001); Aumont et al. (2002); Belviso et al. (2004b); Simo & Dachs (2002); and Aranami & Tsunogai (2004), hereafter referred to as **AN01**, **AU02**, **BE04**, **SD02** and **AT04** respectively. Of the five models, **AT04** appears to fit the AMT dataset the best, although some unexplained variation still remains.

A modified version of this chapter has been accepted for publication in Deep-Sea Research II (Bell et al., 2006b).

4.2 Defining Near-Surface Waters

The process of air-sea gas exchange occurs across molecular layers adjacent to the gas-liquid interface (Liss and Slater, 1974), and the flux is consequently determined by oceanic and atmospheric concentrations in close proximity to this interface (see Chapter 1). In practice, however, it is very difficult to sample the seawater microlayer (tens of microns thick at most). It is customary for samples to be collected from the 'near-surface' layer and, for the purposes of this chapter, it is important to establish the depth of this layer. On each CTD cast, every effort was made to fire a Niskin bottle as close to the surface as possible, but sea-surface conditions (wind speed, swell, etc.) sometimes made this difficult or impossible. As a result, the top bottle was deeper for some profiles than for others. However, it should be noted that the poorer the sea-state, the more homogeneous the top few metres of the water are likely to be, which might partially compensate for the increased depth of sampling. In order to encompass all of these variations in depth, and to include samples taken from the ship's non-toxic supply at 6.5 m, it was decided that when analysing the data, the depth considered to be 'surface' (or 'near-surface') would be 10 m or less. This depth is considered to be shallow enough to represent near-surface waters. The majority of surface bottles were in fact much closer to the surface, with 90% of all data points relating to samples taken at a depth of 6.5m or less. Where near-surface data for ancillary parameters was used, the water was consistently from the same depth as that analysed for DMS and DMSP.

4.3 Results and Discussion

The cruise tracks from Phase One (AMT-5 and -9) and Phase Two (AMT-12–14) of the AMT project have both similarities and differences (Figure 1.18). In particular, the transects from Phase Two progress much further into the oligotrophic gyres compared with those from Phase One. All Phase Two cruises followed the same cruise track in the southern hemisphere, but diverged in the northern hemisphere. During the southbound AMT-13, equipment problems meant that no DMS or DMSP data were collected until approximately 14ºS. Both AMT-5 and -9 made similar deviations into the nutrient-rich upwelling waters off the coast of North-West Africa. In addition to the spatial variation, the AMT cruises occurred during opposing seasons: AMT-5, -9 and -13 were during Austral spring, while AMT-12 and -14 were during Austral autumn. These differences are important and their relevance is discussed later.

Here, the dataset is divided into the ocean biogeochemical provinces identified by Longhurst (1995) (Figure 1.18). However, as has been acknowledged by Longhurst (1995), the borders and characteristics of these provinces shift due seasonal changes and longer-term phenomena such as El Niño and the Atlantic Oscillation Index. Also, parameters in spatially distinct areas of a province are unlikely to be consistent due to natural heterogeneity. An example that is pertinent here is the South Atlantic subtropical gyre (SATL), which Longhurst (1995) suggests could potentially be sub-divided into East and West provinces (similar to the North Atlantic subtropical gyres, NAST(E) and NAST(W)). However, Longhurst (1995) did not delineate these two potential zones in the SATL, one under the westerly winds and the other below the trade winds, due to a lack of data. It is essential to highlight these uncertainties when interpreting data that has been divided into biogeochemical provinces.

4.3.1 Surface DMS Concentration and Flux

Flux calculations were made for every surface DMS measurement, using an average wind speed from the previous 10 minute period. Please refer to Section 1.1 (in particular Section 1.1.1) for further details on how DMS fluxes were calculated.

A visual description of the variability of chlorophyll and DMS concentrations, wind speed and resultant sea-to-air flux during AMT is shown in Figure 4.1. It is important to note here that, for the chlorophyll *a* measurements on AMT-9, a fluorometric method was used rather than high-pressure liquid chromatography, and this will have led to differences in the concentrations relative to the other cruises (Mantoura et al., 1997). The Mauritanian upwelling region (approximately 20ºN) sampled during AMT-5 and -9 is evident in the chlorophyll *a* sections and the increased biological activity clearly leads to some elevated DMS concentrations and estimated sea-to-air fluxes (e.g. 13.4 nM DMS and 28.8 µmol m^{-2} day^{-1} flux, AMT-5). In each hemisphere's spring, the high latitude regions display increased biological activity and DMS concentrations on all cruises, although this pattern appears dampened during Phase Two of the project (AMT-12 to -14). The signature of the equatorial upwelling is less clear – elevated chlorophyll *a* concentrations in this region are evident, with varying intensity probably linked to variations in the strength of the upwelling, but this does not always translate to higher DMS concentrations.

Although wind speed clearly has a major influence on the flux of DMS to the atmosphere (see Figure 1.3), abrupt changes in wind speed are not always evident in the flux data. For example, there is little change in the flux at approximately 45°N during AMT-12 despite an increase in DMS concentration (from 1.1 nM to 6.7 nM); this is due to a concurrent drop in wind speed (from 6.0 m sec^{-1} to 3.2 m sec^{-1}). Whether the wind speed and DMS concentration co-vary (e.g. 30°N during AMT-14) or not will clearly have a significant impact on the overall DMS flux.

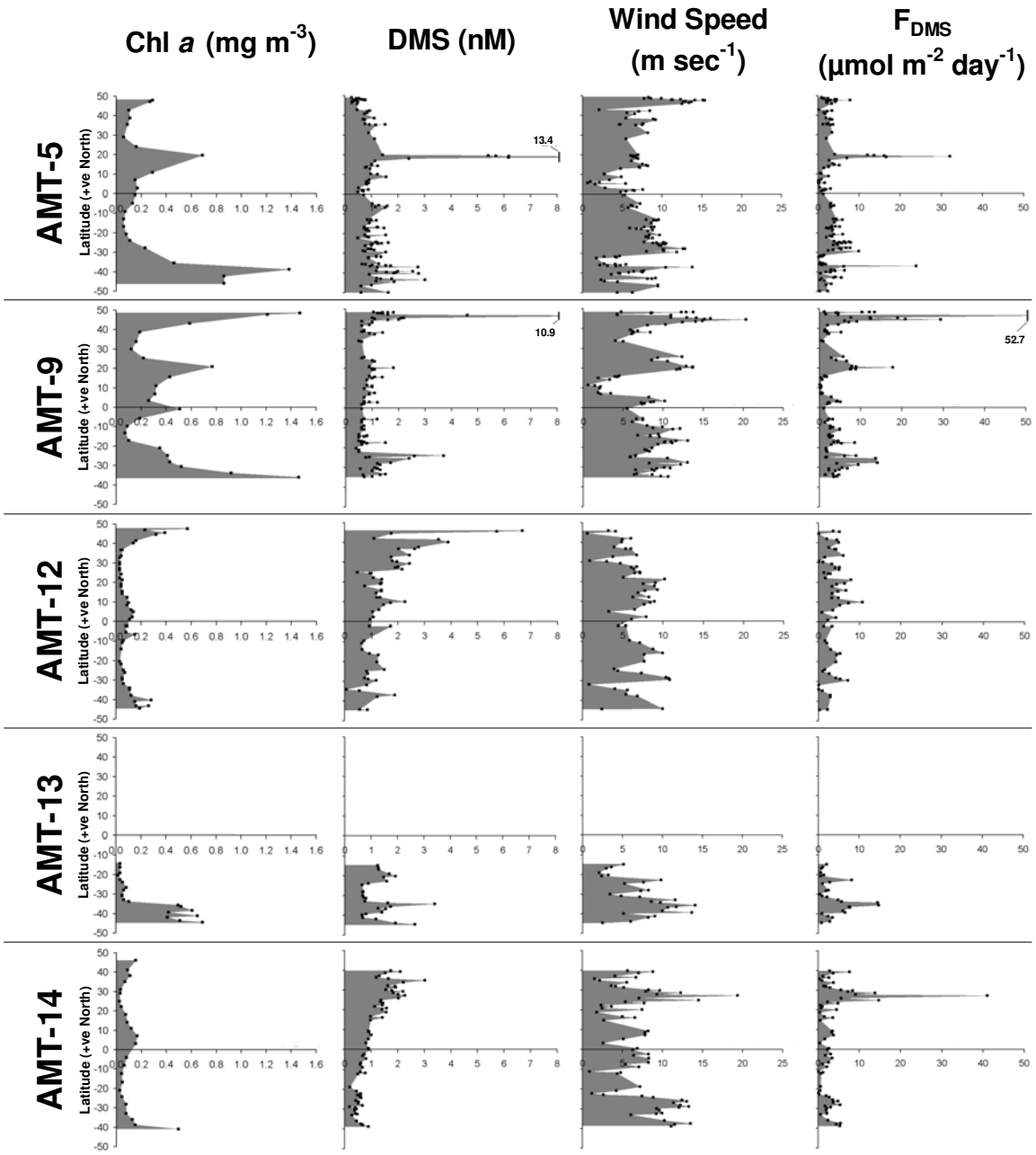

Figure 4.1 Total Chlorophyll *a* concentration (Chl *a*), DMS concentration, wind speed and DMS flux measurements for five Atlantic Meridional Transect (AMT) cruises. To aid comparison between cruises, each parameter is shown using the same scale and any off-scale values are labelled. AMT-9 Chl *a* measurements may be overestimated as they were based on a fluorometric method, whilst the other four cruises used high-pressure liquid chromatography (see Mantoura et al., 1997). The contrast in peak widths observed for Chl *a* (Phase One broader than Phase Two) is likely due to variations in sampling frequency.

Whilst the format used in Figure 4.1 is useful for comparative purposes, it is difficult to draw more specific conclusions. As a second step, the data were sorted by biogeochemical province and basic statistics calculated (Table 4.1). Although all the cruise tracks passed through the same biogeochemical provinces, the chlorophyll *a* plots in Figure 4.1 clearly show that concentrations during Phase One were substantially higher than during Phase Two, particularly in the subtropical gyres. This is most likely due to the difference between the cruise tracks, with Phase Two cruises progressing further into the oligotrophic gyres. As a result, it was decided to only include data from the Phase Two cruises that are more representative of 'gyre conditions'. In addition, of the eight Longhurst provinces sampled during the AMT programme (Figure 3.1), only the four provinces that were regularly sampled are included in Table 4.1.

Table 4.1 Mean, median and range of surface DMS concentration, wind speed and DMS flux measurements per biogeochemical province. Data does not include AMT cruises -5 and -9 as they did not progress as deep into the gyres. Only those provinces sampled regularly are included in the table (i.e. NAST(W), NADR, SSTC and CNRY were excluded). Please see Table 3.1 for full biogeochemical province names and their acronyms, as from Longhurst (1995).

Province	**Surface [DMS] (nM)**			**Wind Speed (m sec^{-1})**			**DMS Flux (µmol m^{-2} day^{-1})**			**No. of**
	Mean	*Median*	*Range*	*Mean*	*Median*	*Range*	*Mean*	*Median*	*Range*	**Samples**
NAST(E)	2.1	1.9	1.1–3.9	5.1	5.3	0.9–8.8	3.2	3.1	0.2–7.6	26
NATR	1.3	1.4	0.5–2.0	6.7	7.1	1.8–14.5	3.7	3.3	0.4–14.7	25
WTRA	1.1	0.9	0.7–2.3	6.6	6.8	2.6–8.9	3.4	3.3	0.4–10.6	19
SATL	0.9	0.7	0.1 – 3.4	7.3	7.4	0.8 – 13.5	2.7	2.1	0.1 – 14.5	68

There is little pattern apparent in the variations of mean and median surface DMS concentration and flux (Table 4.1). The median wind speed from each province, however, is consistently higher than the mean, indicating an infrequent occurrence of high wind speeds. The data clearly shows that DMS flux data from different regions during Phase Two of AMT cannot easily be distinguished from each other (with the exception of the smaller range for NAST(E)). There is a striking contrast between the highly variable discrete DMS concentration, wind speed and flux measurements (Figure 4.1) and the remarkably similar averages and ranges per province (Table 4.1). Whilst generalisations are possible (e.g. an average flux per province), caution should be taken when interpreting such results, as a substantial level of detail is lost in the process.

4.3.2 Predictive Algorithms

The five algorithms tested in this chapter (see summary Table 4.2) were originally developed using a number of different measured or calculated parameters, some of which were taken from global fields derived from satellite data (e.g. surface [NO_3^-] in **AN01**; MLD in **SD02**). Great effort was made to exactly reproduce the various methods, with the exception that in all cases parameters were calculated from measured data rather than satellite-based climatologies. As climatological data is often temporally and spatially smoothed, it is expected that using climatological data rather than measured data would have lead to a poorer fit with the relevant predictive algorithms (i.e. **AN01** and **SD02**). Unfortunately, time limits did not allow the time necessary to fully test this premise.

The following sections describe the algorithms used and their derivations before comparing the collected AMT data with each relationship. In each case, the data is presented in two ways: divided by (a) cruise; and (b) province. It was hoped that this would distinguish between any potential variations due to season (i.e. by cruise) and/or biogeochemical region (i.e. by province). During AMT-9, no nutrient or accessory pigment data was collected and the DMS data from this cruise could therefore only be used in concert with mixed-layer depth values (i.e. only the **SD02** and **AT04** algorithms).

Table 4.2 Algorithms for predicting sea surface DMS concentrations tested using the AMT dataset. The **AU02** and **BE04** algorithms use very similar data (Norwegian fjord data removed for **BE04**). Upon reformulation by Belviso et al. (2004b), **AU02**a became a two-part relationship (**BE04**a(i) & (ii)) while the two part relationship of **AU02**b(i) & (ii) became **BE04**b. For **BE04**, equations a(i) and a(ii), are dependent on a critical value for non-diatom TChl *a* (defined as TChl $a \times [1\text{-}Fp]$). For **AT04**, the authors suggest a constant value of 60 ± 30 µmol m^{-2} based on their data, hence initial comparison with the AMT dataset used constants of 30, 60 and 90 µmol m^{-2}.

Algorithm	*Eqn. I.D.*	*Equation*	*Reference*
AN01	a(i)	$[DMS] = 2.29$ for $log_{10}(CJQ) \leq 1.72$	Anderson et al. (2001)
	a(ii)	$[DMS] = 8.24.[log_{10}(CJQ) - 1.72] + 2.29$ for $log_{10}(CJQ) > 1.72$	
AU02	a	$Total\ DMSPp = (20 \times TChla \times Fp) + \left(13.64 + \frac{0.10769}{(1.0 + 24.97(1 - Fp) \times TChla)^{-2.5}}\right)$	Aumont et al. (2002)
	b(i)	$DMS : DMSPp = 0.015316 + \frac{0.005294}{0.0205 + Fp}$ for $Fp \leq 0.6$	
	b(ii)	$DMS : DMSPp = 0.674Fp - 0.371$ for $Fp > 0.6$	
BE04	a(i)	$Total\ DMSPp = (20 \times \text{TChl } a \times Fp) + 21$ for TChl $a' \leq 0.3$ mg m^{-3}	Belviso et al. (2004b)
	a(ii)	$Total\ DMSPp = (20 \times \text{TChl } a \times Fp) + (356.4 \times \text{TChl } a' - 85.5)$ for TChl $a' > 0.3$ mg m^{-3}	
	b	$DMS:DMSPp = 0.231 - 3.038Fp + 13.0Fp^2 - 38.05Fp^3 + 41.12Fp^4 - 16.32Fp^5$	
SD02	a(i)	$DMS = -Ln(MLD) + 5.7$ for $Chl/MLD < 0.02$	Simo and Dachs (2002)
	a(ii)	$DMS = 55.8(Chl/MLD) + 0.6$ for $Chl/MLD \geq 0.02$	
AT04	a	$DMS \times MLD = Constant$ for $Chl/MLD < 0.02$	Aranami and Tsunogai (2004)

AN01 predicted from chlorophyll, light and nutrients

In 2001, Anderson et al. presented an algorithm predicting surface DMS concentrations (*[DMS]*, nM) from surface chlorophyll concentrations (*C*, mg m^{-3}), mean daily short-wave radiation (*J*, W m^{-2}) and a nutrient limitation term (*Q*, dimensionless), which was able to reproduce geographic patterns broadly similar to the global DMS database (Kettle et al., 1999). The expression was termed a 'broken-stick' regression because it consisted of two parts (see also Table 4.2):

$$[DMS] = 2.29 \qquad \text{for } log_{10}(CJQ) \leq 1.72$$

Equation 4.1

$$[DMS] = 8.24.[log_{10}(CJQ) - 1.72] + 2.29 \qquad \text{for } log_{10}(CJQ) > 1.72$$

Equation 4.2

The term Q is a Michaelis-Menten nutrient limitation factor that has often been used in ecosystem models (Anderson et al., 2001):

$$Q = \frac{N}{(K_N + N)}$$

Equation 4.3

where N = nitrate concentration and K_N = half saturation constant, both measured in mmol N m^{-3}. For the purposes of their study, the authors used 0.5 mmol N m^{-3} for K_N, and it was decided to use the same value to maintain comparability. For some data points, when calculating Q (*Equation 4.3*), the nitrate (N) concentration was below the detection limit (2 nM). In these cases, the detection limit value was used, which may have lead to an overestimation of Q. However, any reduction in Q would only reduce $log_{10}(CJQ)$ (i.e. a shift left along the X axis of Figure 4.2), and would not change any of the overall conclusions.

In order to produce their global maps, Anderson et al. (2001) used global fields for their nutrient and light terms (based on model data) but the basis of this study was to use *in situ* measurements. As a result, the numbers used to calculate each predicted DMS concentration were real-time measurements of the surface chlorophyll concentration, the surface nutrient concentration and an average of the daily solar radiation (300–3000 nm bandwidth). In order to determine the value for the horizontal part of the broken-stick algorithm, Anderson et al. (2001) smoothed the global DMS dataset by averaging successive groups of 23 records, creating 114 data pairs from 2,622 initial cases. This process, along with the inherent differences between real-time measurements and global fields of nitrate and light data, may well have introduced noticeable differences between predicted values (Anderson et al., 2001) and measured values (this study).

When looking at the results (Figure 4.2), it is evident that the **AN01** algorithm does not resolve the variations in DMS concentration observed during the AMT cruises at all well. The majority of points can be considered as low-DMS areas (all the data fall within the flat part of the broken-stick regression), which are readily acknowledged as being poorly resolved by the algorithm (Anderson et al., 2001). Beyond this, the major detail emerging from Figure 4.2 is that the **AN01** relationship over-predicts the DMS concentration for 98 out of 106 data points (92%), often by at least twofold. When looking at the results by cruise (Figure 4.2a), no apparent pattern can be seen. In general the same applies for the

data divided by region (Figure 4.2b), although there are slight differences between provinces. The data from both sides of the North Atlantic subtropical gyre (NAST(E) and NAST(W)), plot consistently closer to the **AN01** line than the South Atlantic subtropical gyre (SATL) results. The SATL province was sampled during both Austral spring and autumn, while few NAST(E) or NAST(W) measurements (from AMT) were made during the northern hemisphere's autumn. As a result, it is difficult to deduce whether or not the observed differences between the gyres are the result of seasonal changes.

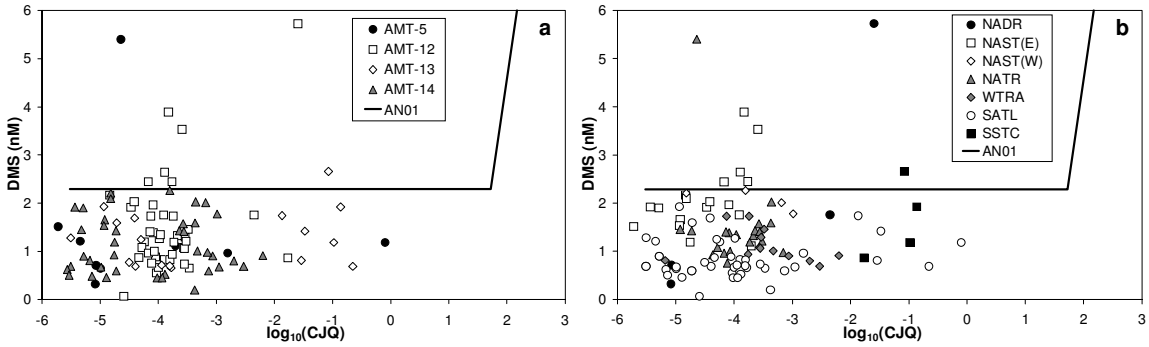

Figure 4.2 Surface DMS concentrations for AMT-5, -12, -13 and -14 plotted against $\log_{10}$(CJQ), calculated from measured values of surface chlorophyll *a* (C), daily radiation (J) and a nutrient term (Q). Panel (a) divides the data by cruise: AMT-5 = filled circle; AMT-12 = open square; AMT-13 = open diamond; AMT-14 = grey triangle. Panel (b) divides the data by biogeochemical province: NADR = filled circle; NAST(E) = open square; NAST(W) = open diamond; NATR = grey triangle; WTRA = grey diamond; SATL = open circle; SSTC = filled square. In both plots, the predictive algorithm proposed by Anderson et al. (2001), **AN01**, is shown as a solid black line.

AU02 / BE04 predicted from a community composition index and chlorophyll

Aumont et al. (2002) and Belviso et al. (2004b) have developed algorithms that predict surface DMS and DMSPp concentrations from chlorophyll *a* and community composition data. The community composition index, *Fp*, is a ratio of depth-integrated (denoted by Σ) pigment biomarkers:

$$Fp = (\Sigma fucoxanthin + \Sigma peridinin) \times (\Sigma fucoxanthin + \Sigma peridinin + \Sigma 19'\text{-}BF + \Sigma 19'\text{-}HF + \Sigma zeaxanthin + \Sigma TChl\ b + \Sigma alloxanthin)^{-1}$$

Equation 4.4

This is effectively the ratio of diatom and dinoflagellate pigments (fucoxanthin and peridinin, respectively) to total pigments (Claustre, 1994). The total depth-integrated pigment concentration represents the main phytoplankton groups in the ocean – fucoxanthin (diatoms), peridinin (dinoflagellates), 19'-butanoyloxyfucoxanthin (19'–BF, chrysophytes), 19'-hexanoyloxyfucoxanthin (19'–HF, prymnesiophytes), zeaxanthin (cyanobacteria), TChl *b* (defined as the sum of Chlorophyll *b* and divinyl-chlorophyll *b*; green flagellates) and alloxanthin (cryptophytes). The *Fp* ratio is effectively an estimator of diatom plus dinoflagellate (i.e. species involved in new production) biomass in a phytoplankton community. A low value is indicative of an oligotrophic environment where the community is dominated by photo-adaptive pigments, while a high value indicates a highly productive community (Claustre, 1994).

The modelling study of Aumont et al. (2002) was based on the concept that DMSPp and total chlorophyll *a* (TChl *a*) could be divided into 'diatom' and 'non-diatom' proportions using the *Fp* ratio:

$$\textit{Non-diatom DMSPp (DMSPp´)} = \textit{Total DMSPp} - (20 \times \textit{TChl a} \times \textit{Fp})$$

Equation 4.5

$$\textit{Non-diatom TChl a (TChl a´)} = \textit{TChl a} \times (1 - \textit{Fp})$$

Equation 4.6

Based on field measurements, the DMSPp-to-TChl *a* ratio for phytoplankton communities dominated by diatoms (and to a lesser extent dinoflagellates) was suggested to be approximately 20 mmol g^{-1} (Aumont et al., 2002), and this was incorporated into *Equation 4.5*. Using data from various projects (ALBATROSS, EUMELI, DYFAMED, PROSOPE and Antares cruises), the authors then derived a relationship between DMSPp´ and TChl *a´* ($r^2 = 0.84$; $n = 189$):

$$DMSPp' = 13.64 + \frac{0.10769}{\left(1.0 + 24.97 TChla'\right)^{-2.5}}$$

Equation 4.7

Using *Equation 4.5*, *Equation 4.6* and *Equation 4.7*, Total DMSPp concentrations in surface waters were then predicted from the following formula (see also Table 4.2):

$$Total\ DMSPp = (20 \times TChla \times Fp) + \left(13.64 + \frac{0.10769}{(1.0 + 24.97(1 - Fp) \times TChla)^{-2.5}}\right)$$

Equation 4.8

Further, the surface DMS concentrations could also be predicted if *Equation 4.8* was used in conjunction with a two-part relationship derived from the same data, which linked the *Fp* ratio to the DMS-to-DMSPp ratio; $r^2 = 0.51$; $n = 125$ (see also Table 4.2):

$$DMS:DMSPp = 0.015316 + \frac{0.005294}{0.0205 + Fp} \qquad \text{for } Fp \leq 0.6$$

Equation 4.9

$$DMS:DMSPp = 0.674Fp - 0371 \qquad \text{for } Fp > 0.6$$

Equation 4.10

For **BE04**, Belviso et al. (2004b) modified *Equation 4.7*, *Equation 4.8*, *Equation 4.9* and *Equation 4.10* to make the algorithms more applicable to a global scale and re-evaluated the lines of best fit (Norwegian fjord data with high *Fp* ratios and exceptionally variable DMS and DMSP concentrations were removed). *Equation 4.7* was changed into a two-part equation (another 'broken-stick' relationship):

$$DMSPp' = 21 \text{ nmol L}^{-1} \qquad \text{for TChl } a' \leq 0.3 \text{ mg m}^{-3}$$

Equation 4.11

$$DMSPp' = 356.4 TChl\ a' - 85.5 \qquad \text{for TChl } a' > 0.3 \text{ mg m}^{-3}$$

Equation 4.12

The reformulation of *Equation 4.8* was then dependent on whether TChl *a´* was less than or greater than 0.3 mg m^{-3} (see also Table 4.2):

$$Total\ DMSPp = (20 \times \text{TChl } a \times Fp) + 21 \qquad \text{for TChl } a' \leq 0.3 \text{ mg m}^{-3}$$

Equation 4.13

$$Total\ DMSPp = (20 \times TChla \times Fp) + (356.4TChla' - 85.5) \quad \text{for TChl } a' > 0.3 \text{ mg m}^{-3}$$

Equation 4.14

After the same dataset modification mentioned earlier, *Equation 4.8* became (see also Table 4.2):

$$DMS:DMSPp = 0.231 - 3.038Fp + 13.0Fp^2 - 38.05Fp^3 + 41.12Fp^4 - 16.32Fp^5$$

Equation 4.15

The data used to create *Equation 4.8*, *Equation 4.9* and *Equation 4.10* (**AU02**) and *Equation 4.13*, *Equation 4.14* and *Equation 4.15* (**BE04**) were from surface waters alone and not depth integrated, including the pigment concentrations used to calculate the *Fp* ratio. When comparing the DMS and DMSPp data collected during AMT with the relationships from **AU02** and **BE04**, all TChl *a* and pigment concentrations used in the equations above were measured surface values.

Before comparing the AMT data with the **AU02** and **BE04** relationships, it is instructive to compare the algorithms themselves. As can be seen in Figure 4.3a&b, there is little difference between the two algorithms for predicted DMSPp´. The **AU02** algorithm is arguably better in principle as it allows for variations in DMSPp´ when TChl *a´* values are low, whereas with **BE04** DMSPp´, a fixed value is given below a TChl *a´* threshold. In both cases, the predicted DMS:DMSPp ratio (Figure 4.3c&d) is also very similar for low *Fp* ratio values, but the relationships deviate significantly above a *Fp* ratio of 0.6. This is not relevant to this study as the waters of interest have much lower *Fp* ratios.

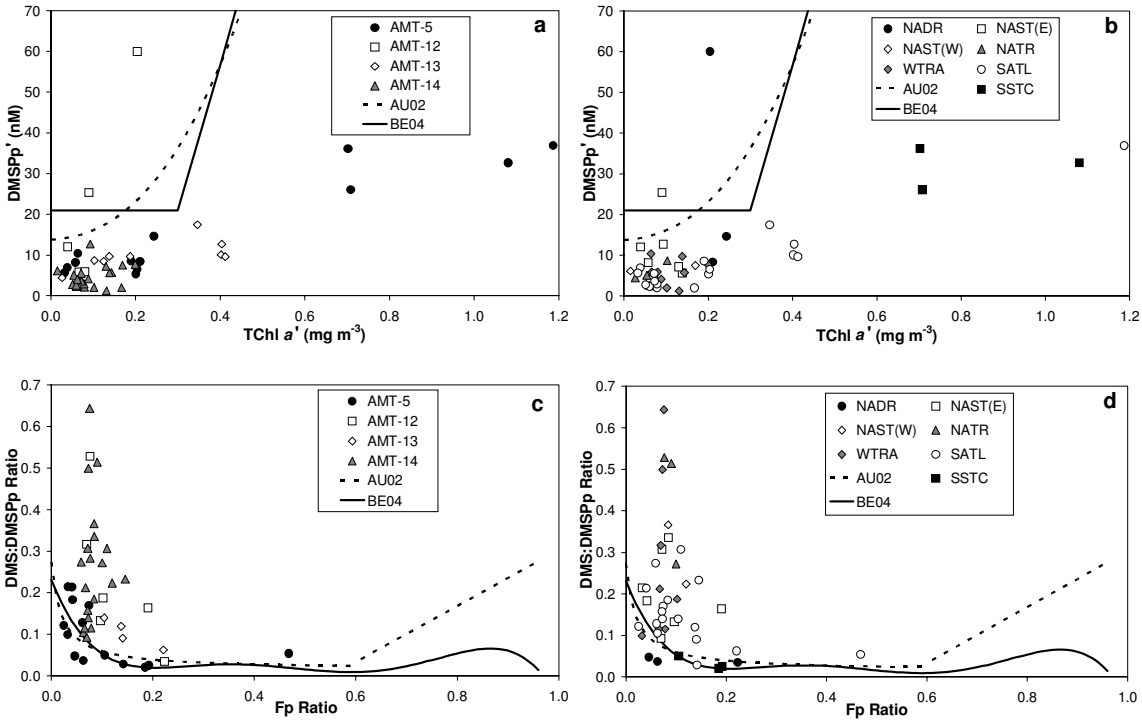

Figure 4.3 Comparison of data with predictive algorithms **AU02**, Aumont et al. (2002), and **BE04**, Belviso et al. (2004b). For all plots, the dashed line represents **AU02** (*Equation 4.8*, *Equation 4.9* and *Equation 4.10*), and the solid line represents **BE04** (*Equation 4.13*, *Equation 4.14* and *Equation 4.15*). For panels (a) and (b), each point is a DMSPp´ concentration, calculated from measured surface DMSPp, the *Fp* ratio and the Total Chlorophyll *a* (TChl *a*) concentration (*Equation 4.5*), plotted against TChl *a´*, calculated from measured surface TChl *a* and the *Fp* ratio (*Equation 4.6*). For panels (c) and (d), the AMT data points are the measured DMS:DMSPp ratios plotted against the measured *Fp* ratios. In plots (a) and (c), the data is divided by cruise: AMT-5 = filled circle; AMT-12 = open square; AMT-13 = open diamond; AMT-14 = grey triangle. In plots (b) and (d), the data is divided by biogeochemical province: NADR = filled circle; NAST(E) = open square; NAST(W) = open diamond; NATR = grey triangle; WTRA = grey diamond; SATL = open circle; SSTC = filled square.

Although the **AU02** and **BE04** relationships are different, the differences are subtle enough that the AMT data can be compared with both at the same time. The **AU02** and **BE04** algorithms tend to over-predict AMT DMSPp´ concentrations in that only 2 of 52 data points (4%) fall above the algorithm lines and they under-predict the DMS:DMSPp ratios with only 4 of 52 data points (8%) falling below the algorithm lines (Figure 4.3a-d). Using the ratio and DMSPp´ results to calculate a predicted DMS concentration will increase the overall error but, due to the combination of under- and over-prediction, the algorithms' inaccuracies will tend to cancel each other out. For the upper two panels, dividing the DMSPp´ data by cruise (Figure 4.3a) or by province (Figure 4.3b) provides no real clues to the data's distribution. However, for the SSTC (South Subtropical Convergence) values collected during AMT-5, the implication is that the non-diatom and non-dinoflagellate

phytoplankton present contained much less DMSPp than might be expected based on the **AU02** and **BE04** algorithms. The DMS:DMSPp ratio plots, divided in the same manner (Figure 4.3c&d), are interesting since the data collected during AMT-5 is in good agreement with the algorithm lines. This cruise did not progress as far into the oligotrophic gyres and, when the data is broken down by province, it can be seen that a number of these points are from higher latitude waters (i.e. NADR, North Atlantic Drift, and SSTC). It is likely that the location of data used to create and/or test these algorithms will have influenced the formulae proposed by Aumont et al. (2002) and Belviso et al. (2004b).

The data used to create both **AU02** and **BE04** are from a variety of locations (see Aumont et al., 2002; Belviso et al., 2004b), including remote oligotrophic regions. In these studies separate attempts were made, using different datasets with a large geographical coverage, to independently verify the algorithms proposed. The level of success was mixed, with model performance varying depending on the region in question. It is therefore not surprising that in certain biogeochemical provinces, the DMS:DMSP ratios and DMSP concentrations from AMT were more accurately predicted than in others.

SD02 & AT04 relationships predicted using the MLD

The relationships described in this section link surface DMS concentrations with the MLD (Simo and Dachs, 2002; Aranami and Tsunogai, 2004). The principle behind them is that a shallow mixed layer favours DMSP producers such as coccolithophores and dinoflagellates whilst increased UV has a negative impact upon bacteria, reducing DMS consumption (Simo and Pedros-Alio, 1999). The first algorithm to be proposed (**SD02**) used DMS data from the global database (Kettle et al., 1999) and climatological MLD values. More recent work (**AT04**) used measurements of surface DMS concentrations and the MLD from the North Pacific.

For **SD02**, DMS data points from the Kettle database with concurrent chlorophyll *a* (Chl) measurements were filtered to remove any pairs with DMS > 100 nM and/or Chl > 15 mg m^{-3} (leaving 2385 pairs) and a climatological MLD applied. The data pairs were grouped, either by cruise-origin or by latitudinal band and average values obtained (Simo and Dachs, 2002). From the resultant 43 points, the authors produced the following algorithms (see also Table 4.2):

$$DMS = -Ln(MLD) + 5.7 \quad \text{for } Chl/MLD < 0.02$$

Equation 4.16

$$DMS = 55.8(Chl/MLD) + 0.6 \quad \text{for } Chl/MLD \geq 0.02$$

Equation 4.17

AT04 compared their surface DMS concentrations with measured MLD values. The authors found that DMS concentrations were higher in shallower MLD, and lower in deeper MLD than the **SD02** algorithm (Aranami and Tsunogai, 2004). Based on their data, they suggested that surface DMS concentrations could be explained via a simple dilution model (see also Table 4.2):

$$DMS \times MLD = constant \quad \text{for } Chl/MLD < 0.02$$

Equation 4.18

From their dataset, the authors suggested a constant value of 60 ± 30 µmol m^{-2}. When comparing the AMT dataset with **AT04**, the following constants were therefore used: 30, 60 and 90 µmol m^{-2}.

MLD determination

A number of different methods are available to calculate the MLD, with critical thresholds for salinity, temperature or density often arbitrarily decided (Montegut et al., 2004). To determine their MLD values, Simo and Dachs (2002) used the Samuels & Cox monthly global climatologies and applied a well-known and often-used criterion: a density difference of 0.125 kg m^{-3} from the surface (Levitus, 1982). The work of Aranami and Tsunogai (2004) does not specify a MLD determination method.

The depth of the surface mixed layer varies depending on the timescale involved and this determines how the MLD should be considered and calculated (Montegut et al., 2004). Above the main thermocline, the surface ocean can be divided into two major parts (Brainerd and Gregg, 1995):

- water that is currently *mixing*; and
- water that is *mixed* but has not been in contact with the atmosphere for a certain time period (between a few days and a week).

When considering how to determine the MLD, the timescale of interest for DMS concentrations is in line with biological processes, which can change over relatively short timescales (days). The criterion used should therefore avoid picking up the diurnal cycle, but should ideally pick out the *mixing* layer rather than the *mixed* layer.

The method employed by Simo and Dachs (2002) often picks up the *mixed* layer rather than the *mixing* layer, so a finer criterion would be preferable (Simo, R., *Pers. Comm.*). A more recent approach uses a temperature difference of 0.2°C and a reference depth of 10 m (to avoid diurnal near-surface heating) and is far more successful at picking up the *mixing* layer (Montegut et al., 2004). To accommodate differences in MLD methodology, the MLD for this study was initially determined using two methods. The first used a 0.125 kg m^{-3} density difference (hereafter referred to as MLD_D) and enabled comparison of the AMT data with the proposed **SD02** relationship. The second method used a temperature difference of 0.2°C (Montegut et al., 2004) to examine whether the *mixing* layer (hereafter referred to as MLD_T) provided a better fit than the *mixed* layer. As can be seen in Figure 4.4, for 71 out of 117 cases (61%) both methods agreed on the MLD within 5 metres. For the majority of those cases that did not agree, MLD_D was greater than MLD_T, indicating that the MLD_T method tended to pick up more recent changes (i.e. the *mixing* layer) whereas the MLD_D method only identified the longer-term and therefore less appropriate *mixed* layer. Based on the theoretical approach outlined above, and considering the good agreement with many MLD_D values (Figure 4.4), the depth of the mixed layer presented in Figure 4.5a-c is MLD_T.

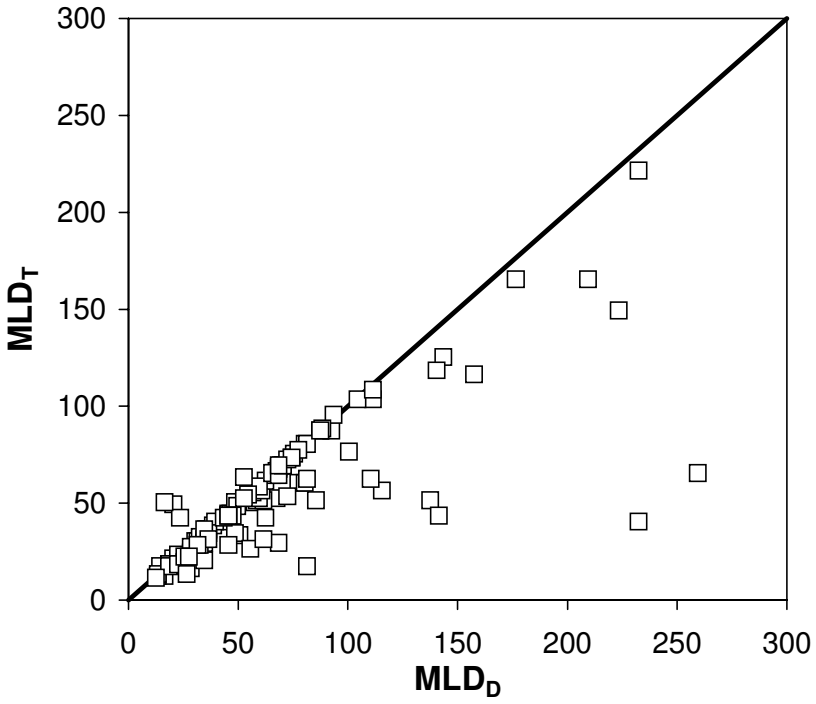

Figure 4.4 A comparison of the two methods used in this study (AMT-5, -9, -12, -13 and -14) to define the depth of the mixed layer (MLD): MLD_D uses a density difference of 0.125 kg m^{-3} from the surface; MLD_T uses a temperature difference of 0.2ºC from a reference depth of 10 m (see text). Good agreement between the methods can be seen for 61% of the dataset, but for most of the cases where there is disagreement, the density-based method (MLD_D) predicts a deeper MLD, corroborating theory.

*Comparing AMT data with **SD02 / AT04***

When a relationship between surface DMS concentrations and the depth of the mixed layer was suggested (Simo and Dachs, 2002), the authors acknowledged that any link was a shortcut for prediction before full mechanistic understanding had been achieved. The relationship gives an indication of how the physical processes (sunlight, heat flux, wind speed, ocean mixing) were interacting with those processes producing and consuming DMS. However, the later work of Aranami and Tsunogai (2004) suggests that the relationship may be due simply to the effect of dilution. It is important to consider the differences between the original studies in MLD determination – for **SD02** a climatological value was applied, while **AT04** used measured data. For this study, the only parameters required for the comparisons with **SD02** and **AT04** were the depth of the mixed (or mixing) layer and the surface chlorophyll concentration, so every surface DMS and chlorophyll measurement with a concurrent depth profile could be used (i.e. data from all AMT cruises). Of the 119 data points, only 3 were equal to or greater than the *Chl/MLD*

critical threshold of 0.02 (see *Equation 4.16* and *Equation 4.17*). It would be difficult to draw any conclusions from such a small number of points so they are not considered as part of this study, and the focus is instead on the relationships proposed for *Chl/MLD* < 0.02.

Overall, the **SD02** algorithm overestimates the surface DMS concentration in 99 of the 116 points (approx. 85%) (Figure 4.5a). Indeed, a similar comparison using independent data from oligotrophic waters midway between the Azores and the Portuguese coast found a similar pattern for MLDs less than 100 m (Belviso et al., 2004a). If MLD_D is used rather than MLD_T, a similar lack of agreement between the algorithm and the AMT data is observed, although the tendency to predict a deeper mixed layer reduces the number of points that are overestimated (3% fewer points are overestimated; data not shown).

When the AMT data is divided by cruise (Figure 4.5a), there is no observable pattern. If we ignore the **SD02** algorithm line and divide the data by province, there is an indication that the data may be clustering (Figure 4.5b). Although this initially appears interesting, the possibility that seasonal processes are driving the clustering cannot be ruled out. For the South Atlantic subtropical gyre (SATL), the data points with MLD > 100 m are almost all from AMT-13, which was in the Austral autumn whilst AMT cruises -12 and -14 were in Austral spring. Upon detailed examination of profiles from all of these cruises, it is apparent that the depth of mixing during AMT-13 was not as easy to define as on the other cruises, which goes some way towards explaining the variations observed. Very little of the AMT dataset represents the northern subtropical gyre (NAST) during that hemisphere's autumn, when a similar variation in MLD definition might be expected. In summary, the clustering observed might be less clear if both seasons were accounted for in both hemispheres.

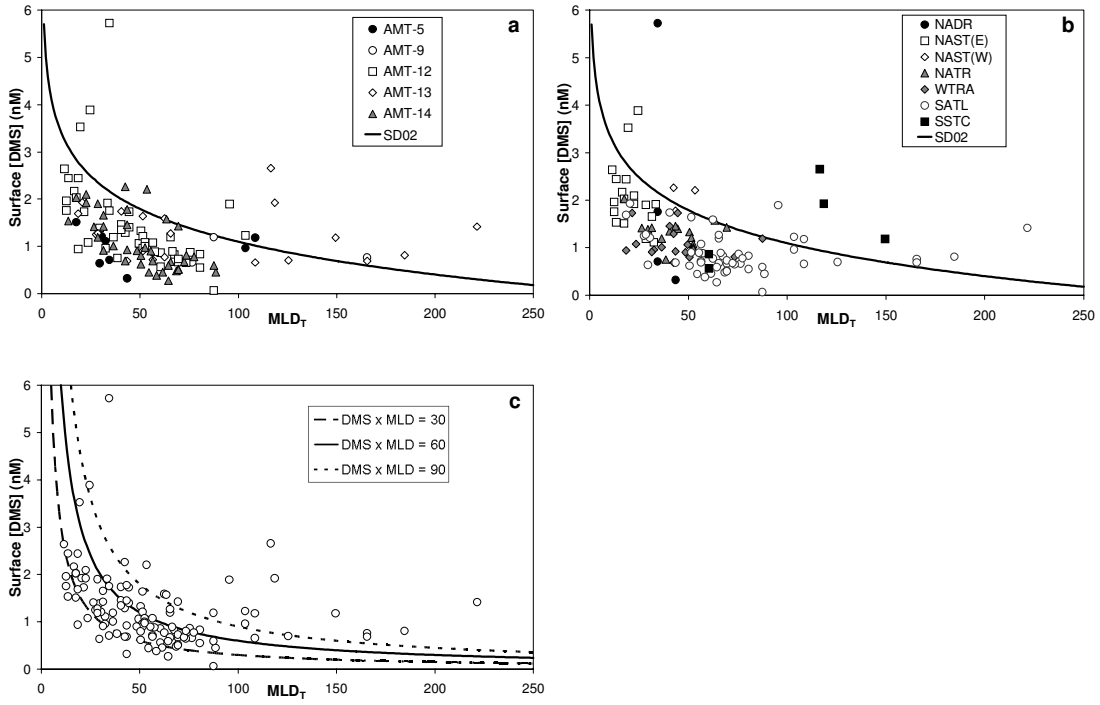

Figure 4.5 Measured surface DMS concentrations for AMT-5, -9, -12, -13 and -14 plotted against the mixed layer depth (MLD_T), calculated from profile data using a temperature difference of 0.2°C relative to a reference depth of 10 m (see text). Panel (a) divides the AMT data by cruise: AMT-5 = filled circle; AMT-12 = open square; AMT-13 = open diamond; AMT-14 = grey triangle. The solid line represents the predictive algorithm of Simo and Dachs (2002). Panel (b) divides the data by biogeochemical province: NADR = filled circle; NAST(E) = open square; NAST(W) = open diamond; NATR = grey triangle; WTRA = grey diamond; SATL = open circle; SSTC = filled square. Panel (c) displays all the AMT data and compares it with the dilution model proposed by Aranami and Tsunogai (2004): $DMS \times MLD = constant$, where the suggested values were 30, 60 and 90 µmol m^{-2}.

The AMT data fits best-to the **AT04** algorithm (Figure 4.5c) and this can be shown by comparing plots of observed DMS concentrations against residual values (predicted minus observed DMS concentrations) for each algorithm (Figure 4.6a&b). Obtaining the modulus of these residuals meant they could be compared quantitatively, as the median value for each algorithm could then be calculated. The median modulus was used instead of the mean as the **AU02** and **BE04** algorithms produced a number of extremely high values, which skewed their mean values considerably. The lower the median modulus residual, the better the fit was considered to be between the observed data and the predicted concentration. The data of Aranami and Tsunogai (2004) indicated a constant of 60 ± 30 µmol m^{-2} for their algorithm, but a large proportion of the AMT data actually sits between the constant lines of 30 and 60 µmol m^{-2} (51 out of 117 points, 44%). The **AT04** constant was optimised to the AMT data by finding the lowest median modulus residual, and then used the predicted data from this optimised constant (40 µmol m^{-2}) to compare with the

other algorithms. As expected, the optimised **AT04** algorithm produced the lowest (best) median modulus residual (0.32 nM) while the other algorithms ranked in the following order: **AU02** (0.64 nM); **SD02** (0.76 nM); **BE04** (0.96 nM); and **AN01** (1.21 nM).

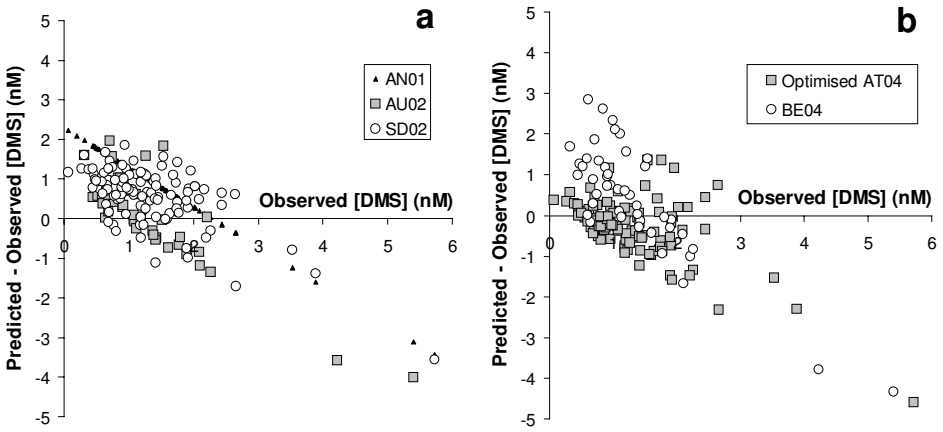

Figure 4.6 Measured DMS concentrations plotted against residual DMS concentrations (predicted minus observed) for all five algorithms, separated into two plots for clarity. Panel (a) displays **AN01** (small filled triangles), **AU02** (grey squares), and **SD02** (open circles). Panel (b) displays **BE04** (open circles) and the optimised **AT04** line, DMS × MLD = 40 µmol m^{-2} (grey squares). Panel (a) excludes 4 data points for **AU02** where the algorithm significantly over-predicts DMS concentrations (residual values not shown are 6.1, 6.7, 24.8 and 26.5 nM). Panel (b) excludes 2 data points for **BE04** where the algorithm significantly over-predicts DMS concentrations (residual values not shown are 8.8 and 13.0 nM). These exclusions were necessary to ensure the scales are appropriate so that the remaining data is both readable and comparable.

While the AMT data fits the **AT04** dilution model reasonably well, the scatter suggests that using the optimised constant of 40 µmol m^{-2} would add little to current understanding. The data do appear to be related in some way to the depth of the mixed layer, but this has been acknowledged as an indirect approach to predicting surface DMS concentrations. A basic premise of both the **SD02** and **AT04** algorithms is that the physics exerts a control on the biology. The fit of the AMT dataset with the **AT04** model corroborates this theory, but the scatter indicates that other processes are at work. Whether or not these processes are physical, chemical or biological is unclear. Based on the results of this study, the **AT04** dilution model is the best predictor of surface DMS concentrations for the oligotrophic waters sampled during the AMT programme. However, a degree of error must be accepted if the algorithm is to be incorporated into a global model.

4.4 Summary

The AMT dataset provides new insights on the accuracy of recent predictive algorithms in remote, oligotrophic waters. Fluxes from these areas can be highly variable, influenced by both high wind speeds and elevated DMS concentrations. Comparison of this new dataset with recent predictive algorithms demonstrates a general weakness (and often overestimation) when predicting DMS concentrations for such waters, a point recently made by Belviso et al. (2004a). Statistically, the data best fits a dilution model based upon the depth of the mixed layer (Aranami and Tsunogai, 2004), but still demonstrates considerable scatter (Figure 4.5c). More studies of the reduced sulphur cycle in oligotrophic waters are required in order to produce models that better-predict surface DMS concentrations and improve understanding of why surface DMS concentrations should scale with MLD. Considering the vast regions of the world's oceans that are oligotrophic – approximately 40% of the earth's surface area (McClain et al., 2004), and the potential impact of DMS to the relatively pristine overlying atmosphere, these areas deserve significant further attention.

5 Spatial variability in DMSP-lyase activity during AMT-14

5.1 Introduction

DMSP is chemically stable in seawater with a half-life of ~8 years at 10°C (Dacey and Blough, 1987). Consequently, DMS production from DMSP is thought to be dependent on DMSP-lyase activity (DLA). The DMSP-lyase enzymes that catalyse this reaction have been found in a wide range of marine organisms including phytoplankton (Stefels and van Boekel, 1993; Steinke et al., 1998; Niki et al., 2000), fungi (Bacic and Yoch, 1998), bacteria (de Souza and Yoch, 1995; Gonzalez et al., 1999) and macroalgae (Van Alstyne and Houser, 2003).

The role of DLA in the ecophysiology of marine organisms is uncertain but several functions for this process have been described, including the production of chemosensory attractant and deterrent compounds (Steinke et al., 2002c, and references therein). It has also been suggested that algal DLA is part of an activated chemical defence reaction during grazing (Wolfe et al., 1997). Finally, evidence suggests that DLA is central to an anti-oxidative stress mechanism involving DMSP, DMS, acrylate, DMSO and methane sulphinic acid (Sunda et al., 2002). All of the above possibilities are discussed in more detail in Section 1.1.1.

During an *Emiliania huxleyi* bloom study in the North Atlantic in 1998, Steinke et al. (2002a) demonstrated that the coccolithophore contribution to DLA was approximately 26%, with the remaining activity attributed to particles larger than 10 µm. This information, combined with a significant correlation with peridinin ($r^2 = 0.88$, $p < 0.02$), a chemotaxonomic marker for dinophytes, linked DLA with phototrophic dinoflagellates found in the surface waters. Further analysis of the same data set revealed a significant relationship with the photo-protective pigment diadinoxanthin ($r^2 = 0.96$, $p < 0.01$), with highest concentrations at the surface. Fieldwork conducted a year later in the North Sea (Steinke et al., 2002b) also produced a significant relationship with diadinoxanthin ($r^2 = 0.63$, $p < 0.01$). More recently, research on the oligotrophic waters of the Sargasso Sea demonstrated similar results, with DLA (normalised to chlorophyll *a*) highest at the surface and closely following the depth profile of diadinoxanthin (Harada et al., 2004). These

studies provide further evidence for the role of DLA in producing anti-oxidants under conditions of photo-oxidative stress.

The AMT-14 cruise in May 2004 provided the opportunity to focus on DLA and related sulphur compounds in the southern and northern gyres (Figure 5.1). These central gyres are characterised by high light intensities and low nutrient concentrations – conditions that have the potential to induce oxidative stress in phytoplankton in the euphotic zone. We hypothesised that DLA would increase in these areas and predicted that samples taken close to the surface would demonstrate high DLA relative to those at lower light levels in the chlorophyll maximum (chl max).

A modified version of this chapter has been submitted to Aquatic Sciences and is currently under review (Bell et al., 2006a).

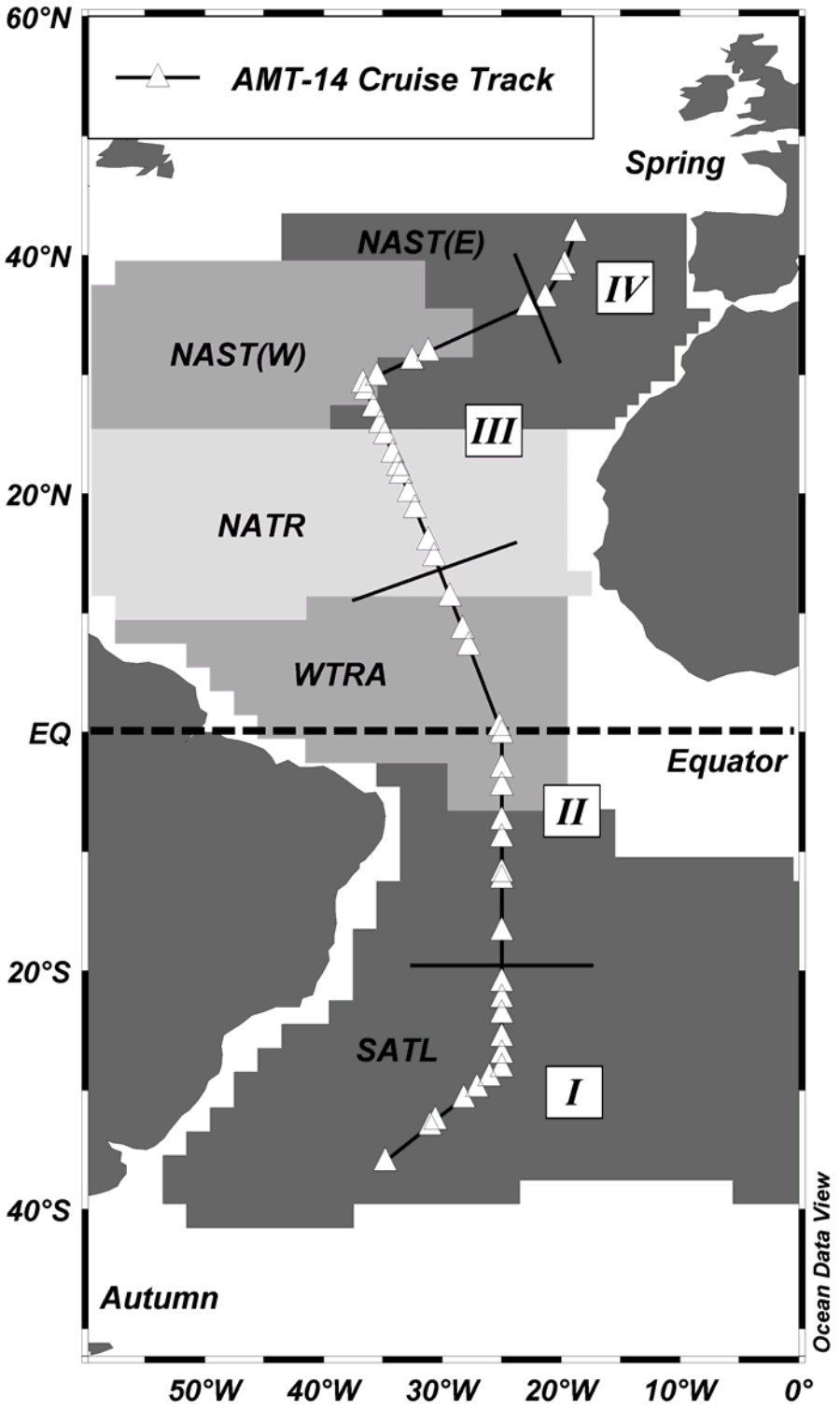

Figure 5.1 Cruise track and sample locations for AMT-14 cruise northbound from the Falkland Islands to the UK (May 2004). Samples were divided into four geographical sections (I-IV) as part of the data analysis (see text). The provinces defined by Longhurst (1995) are shown to provide spatial reference: North Atlantic Subtropical Gyre-East (NAST(E)); North Atlantic Subtropical Gyre-West (NAST(W)); North Atlantic Tropical Gyre (NATR); Western Tropical Atlantic (WTRA); and South Atlantic Subtropical Gyre (SATL). In addition, the season for each hemisphere is indicated. Plot produced using the freely-available *Ocean Data View* (http://odv.awi-bremerhaven.de/home.html).

5.2 Waters Sampled for DMSP-Lyase Activity (DLA)

Samples from the surface and chlorophyll maximum (chl max) were collected at pre-dawn (approx. 0300 hrs local time) and late-morning (approx. 1100 hrs local time). For surface samples, Niskin bottles were closed as near as possible to the ocean's surface. The depth varied depending on the sea-state; the mean surface bottle depth was 3.1 m and the range was 0.5 – 8.0 m (n = 44). In the regions sampled, the chl max was considered representative of low-light conditions as it was located either on or close to the 1% light level. The mean chl max depth was 105.3 m (n = 44) while the depth range was greater than for the surface bottles (47 – 150 m) because of the shallower chl max in equatorial upwelling waters.

5.3 Results and Discussion

Field measurements of DLA have been made previously in a number of locations and significant variations in activity have been observed in the North Atlantic, 0.1 – 142.3 nmol L^{-1} h^{-1} (Steinke et al., 2002a); the North Sea, 4.0 – 207.0 nmol L^{-1} h^{-1} (Steinke et al., 2002b); and the oligotrophic Sargasso Sea, 60 – 300 nmol L^{-1} h^{-1} (approximated data from figure 3 in Harada et al., 2004). The AMT-14 cruise track passed through predominantly oligotrophic waters and DLA was lower, covering a range from 0 (no activity detected) to 58.6 nmol L^{-1} h^{-1}. Samples were taken for DMS, DMSP and DLA in the southern gyre, equatorial upwelling and northern gyre, from 35°S to 40°N (Figure 5.1). *In vitro* DLA in the chl max (Figure 5.2a) was consistently low throughout the cruise (0 to 8.7 nmol L^{-1} h^{-1}; mean = 2.1 nmol L^{-1} h^{-1}). In comparison, the surface DLA showed relatively high variability and ranged from 0 to 58.6 nmol L^{-1} h^{-1} (Figure 5.2a). These variations in surface DLA, and their spatial distribution over a more geographically extensive transect than previously studied, are the focus of this chapter.

The AMT-14 transect can be divided into sections I to IV based on the ratio of DLA to total chlorophyll *a* (DLA:TChl *a*; Figure 5.2c), where TChl *a* (Figure 5.2b) represents the sum of chlorophyll *a* and divinyl chlorophyll *a* for HPLC, or Chl *a* for fluorometric measurements. Sections I and III show elevated surface DLA:TChl *a* (approximately > 100 nmol L^{-1} h^{-1} μg^{-1} TChl *a* while in sections II and IV surface DLA:TChl *a* is generally low (approximately < 100 nmol L^{-1} h^{-1} μg^{-1} TChl *a*; Figure 5.2c). Sections I and III are thus considered 'high' surface DLA while sections II and IV are considered 'low' surface DLA. It is important to note that the majority of DLA:TChl *a* variability is driven by changes in DLA rather than changes in TChl *a*.

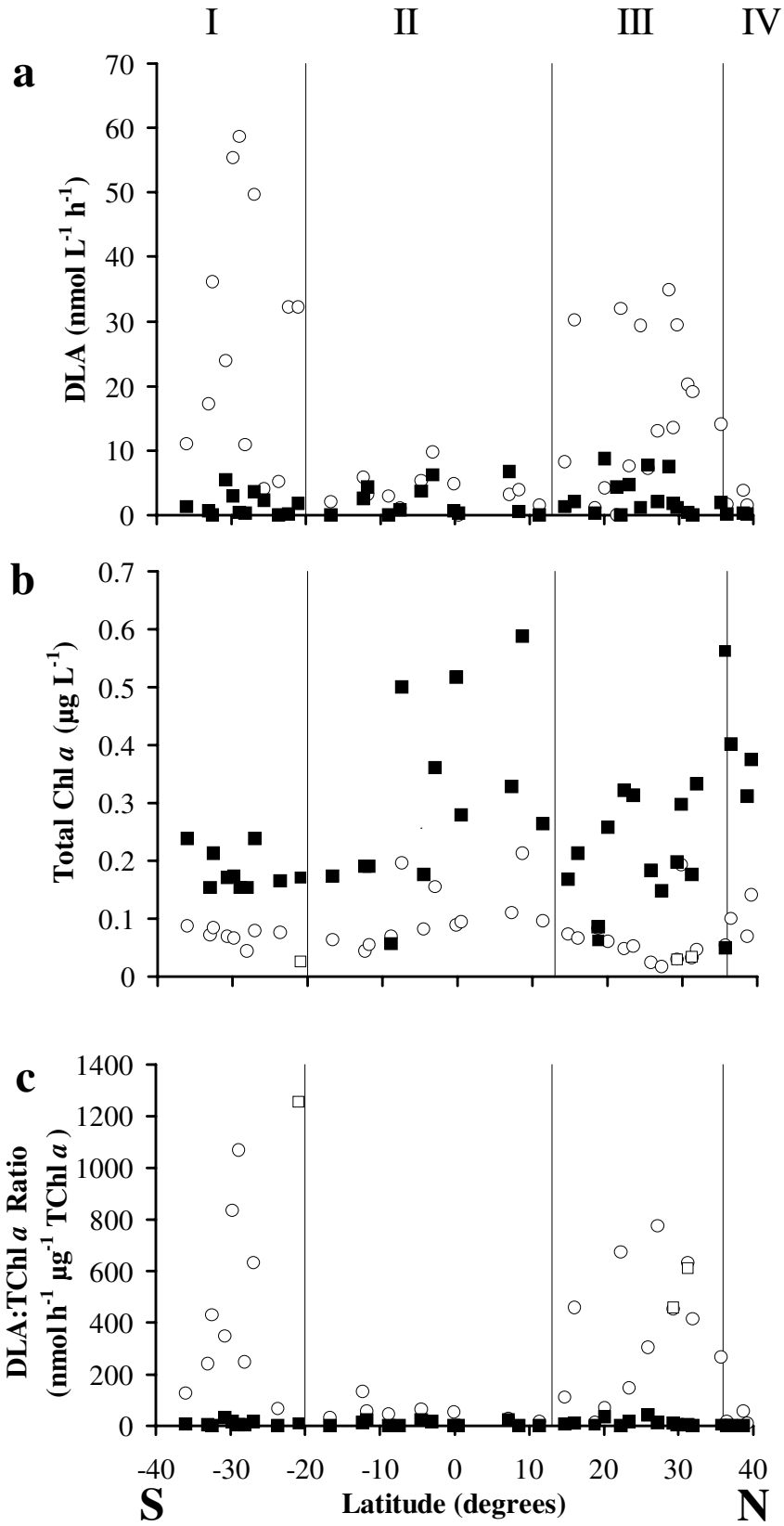

Figure 5.2 Latitudinal distribution of data for (a) DLA (nmol L^{-1}); (b) Total Chl *a* (µg L^{-1}); and (c) DLA:TChl *a* (nmol h^{-1} μg^{-1} TChl *a*). Open circles (HPLC chlorophyll) and squares (acetone-extracted chlorophyll) denote surface samples and samples from the chlorophyll maximum are represented by filled squares. In this and subsequent figures sections I to IV (see text) are labelled along the top of the figure and indicated by solid vertical lines.

The well-recognised Longhurst classification of the world oceans in terms of biogeochemical regions (Longhurst, 1995) describes the northern limit of the South Atlantic sub-tropical gyre (SATL) to be approximately 7°S. However, the distinction between section I (high DLA) and section II (low DLA) in the southern hemisphere is observed at approximately 20°S. In contrast, the region of elevated DLA in the northern hemisphere (section III; 13°N to 36°N) fits reasonably well with two of the Longhurst (1995) provinces – the North Atlantic sub-tropical gyre (NAST; 12°N to 25°N) and North Atlantic tropical region (NATR; 26°N to 43°N).

Given that the regions of elevated DLA did not show a complete fit to established biogeochemical provinces, the data set was explored for any relationships with ancillary data. In particular, parameters were investigated that relate directly to DLA (i.e. DMS and DMSP concentrations) and those that may be indirectly related (e.g. nutrient concentrations, ^{14}C-fixation rates, accessory pigment concentrations, light intensity). It is important to recognise that these samples were analysed for *in vitro* DLA rather than *in vivo* DLA. However, new information on the substrate kinetics of *in vitro* and *in vivo* DLA during a mesocosm experiment suggest that *in vitro* data are similar to *in vivo* activities in some natural populations (Steinke et al., *Submitted*). It is instructive to make comparisons with ambient DMS and DMSP concentrations in the water column. As would be expected, surface DMS concentrations vary throughout the AMT-14 transect, but the pattern observed in DLA:TChl *a* for sections I/III and sections II/IV is not repeated in the surface DMS concentrations (Figure 5.3a). This is of no particular surprise as biological turnover, sea-air gas flux, and photo-oxidation have been shown to be dominant but variable loss terms for DMS in oligotrophic surface waters (Kieber et al., 1996).

On the basis of laboratory studies with phytoplankton cultures, it has been suggested that oxidative stress produces a protective response leading to elevated DMS and DMSPp production (Sunda et al., 2002). Ambient DMS concentrations increased as the transect progresses northwards and this is most likely due to the onset of spring in the northern hemisphere (Figure 5.3a). Surface DMSPd (Figure 5.3b) and DMSPp (Figure 5.3c) concentrations follow the same general pattern as DMS, although there is greater variability in the DMSPp concentrations. None of the DMS, DMSPd or DMSPp concentrations demonstrate the more distinct pattern observed for DLA. This is highlighted when DLA is normalised to DMSPp (Figure 5.3d) because sections I and III

can still be clearly distinguished. It is worth noting at this stage that ambient concentrations of DMS or DMSP may not correlate well with DLA because additional factors influence their turnover time (e.g. sea-air flux; biological production and consumption processes).

Harada et al. (2004) use their DLA and DMSPp values to calculate a potential turnover time (*Equation 5.1*) for the DMSPp pool, presenting a 5 min turnover time on average for their oligotrophic Sargasso Sea samples. Equivalent turnover times for this study range between 1 and 211 min, with an average of 13 min for sections I/III and 23 min for sections II/IV. If total DMSP (i.e. DMSPd + DMSPp) is used in the calculations, the average turnover time for DMSP increases to 24 min for sections I/III and 41 min for sections II/IV. Such calculations are hypothetical as they assume that *in vitro* values are representative of *in vivo* values and that all DMSP is freely mixed with all available DMSP-lyase enzymes. In addition, the calculation assumes that true DMSP-lyase enzyme activity is always operating at near saturation levels. This is unlikely given that recent estimates using Michaelis-Menten type enzyme kinetic data suggest longer turnover times during a mesocosm experiment, from 310 d at the beginning to 1 d at the end (Steinke et al, *Submitted*).

$$Turnover\ Time = \frac{[DMSPp]}{DLA}$$

Equation 5.1

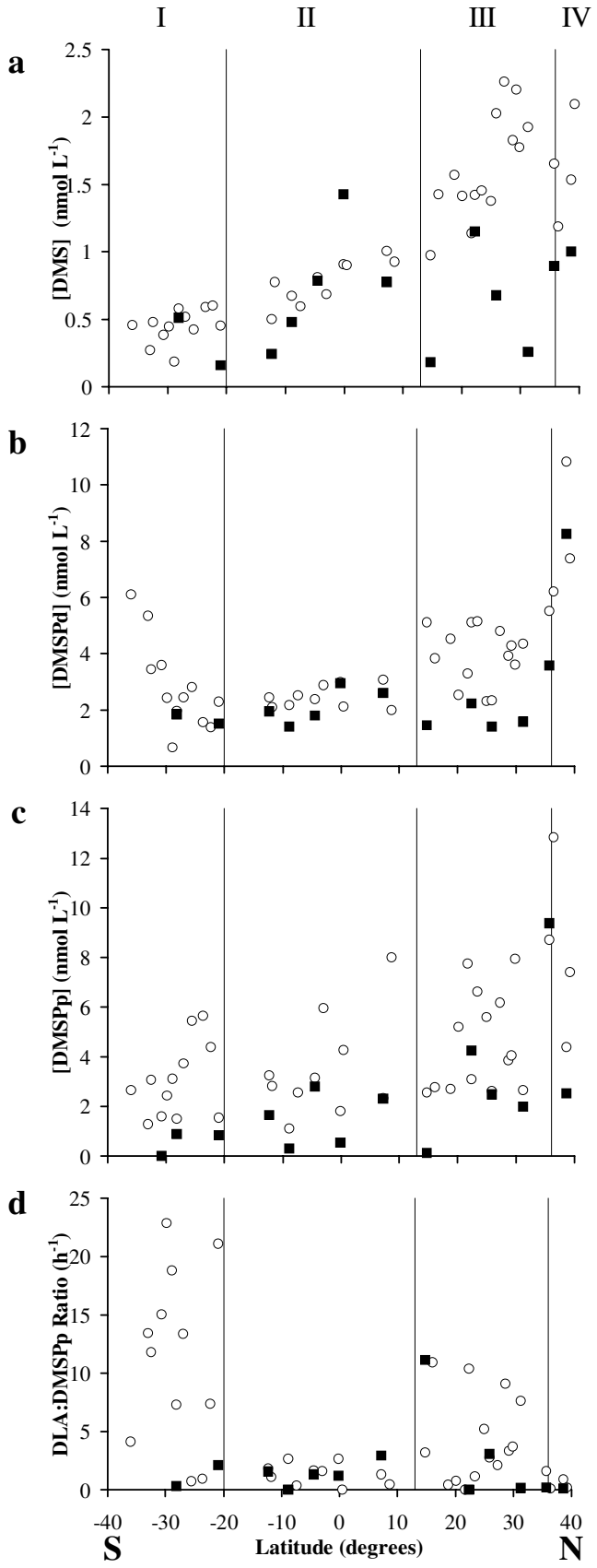

Figure 5.3 Latitudinal distribution of data for (a) DMS (nmol L^{-1}), (b) DMSPd (nmol L^{-1}), (c) DMSPp (nmol L^{-1}) and (d) DLA:DMSPp ratio (h^{-1}). Open circles denote surface samples and samples from the chlorophyll maximum are represented by filled squares.

Plotting DLA:TChl *a* against phytoplankton carbon fixation provides an insight into the DLA:TChl *a* data that is not immediately obvious when it is plotted against latitude (Figure 5.4). The horizontal and vertical lines on this plot represent the mean values for each axis. While DLA:TChl *a* shows variability at most ^{14}C-fixation rates, it is notable that only two above-average DLA:TChl *a* samples (i.e. > 131.7 nmol L^{-1} h^{-1} μg^{-1} TChl *a*) were observed at carbon fixation rates greater than 0.28 mmol C m^{-3} d^{-1}. This finding suggests that in regions of higher carbon fixation (i.e. higher production), DLA:TChl *a* is unlikely to be high because conditions are more amenable for phytoplankton growth (i.e. nutrient-sufficient, appropriate light levels, etc.). This is in agreement with the proposed role of DLA in a DMSP-based anti-oxidant cascade (Sunda et al., 2002).

Nutrient limitation is one of a number of possible causes of oxidative stress in phytoplankton cells in oligotrophic surface waters. The ambient nutrient concentrations (nitrate, NO_3^-, Figure 5.5a) clearly demonstrate that cells at the surface are, as expected, nutrient limited relative to those at the chl max. However, the depth of the nitracline (defined as the depth of the 1 µmol L^{-1} NO_3^- isopleth, Figure 5.5a) provides a better indication of nutrient availability as a deep nitracline indicates a low nutrient supply to the surface. In the northern hemisphere, the deepening of the nitracline clearly coincides with section III where DLA:TChl *a* increases (Figure 5.5d), while in the southern hemisphere the elevated DLA:TChl *a* values were also measured when the nitracline was deep (section I). In section II, the equatorial region exhibits low DLA and a correspondingly shallow nitracline (i.e. greater nutrient supply). However, South of approximately 5°S in section II, the nitracline deepens while surface DLA stays low. With the exception of this region, most of the higher DLA values appear to be associated with a low nutrient supply.

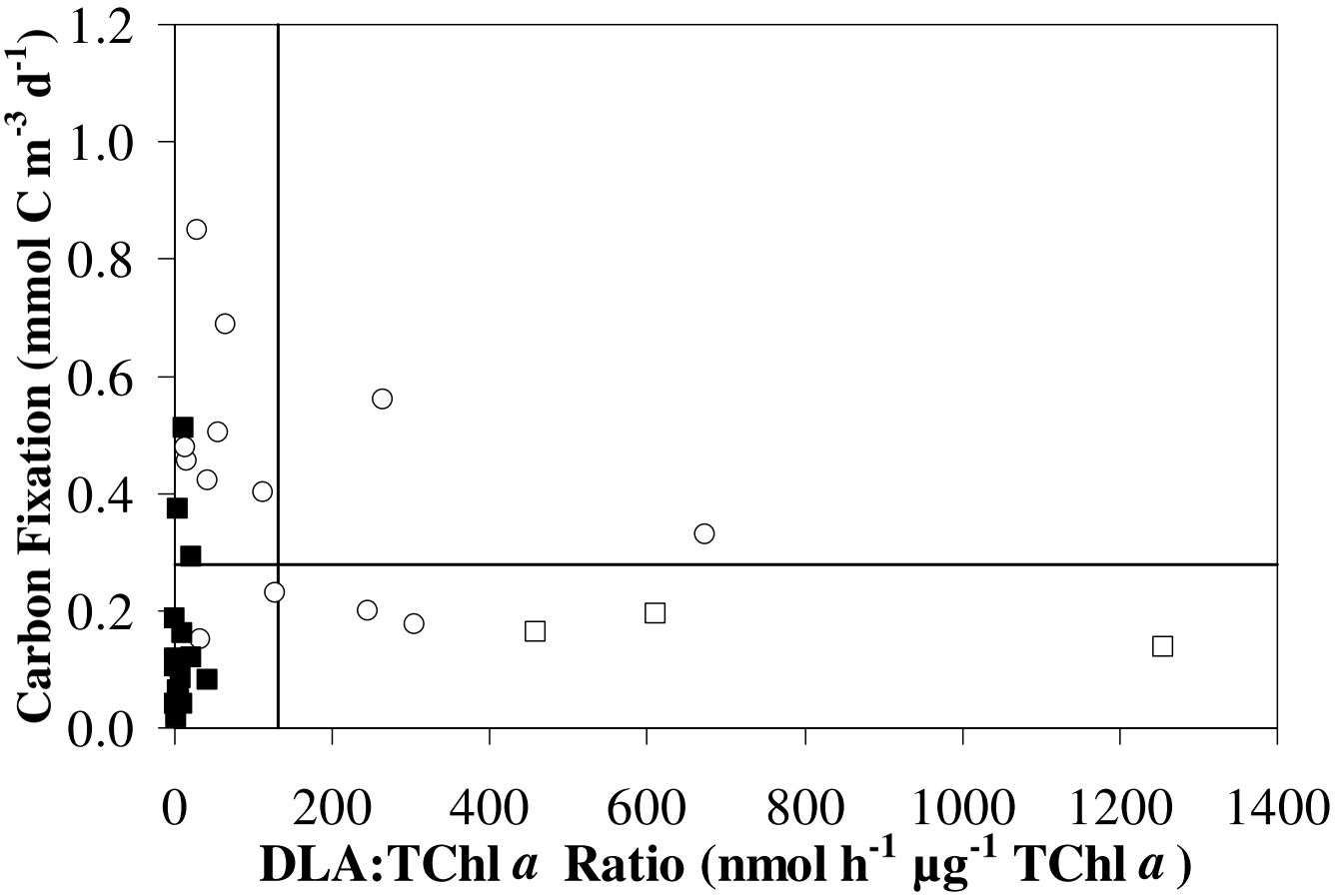

Figure 5.4 Plot of phytoplankton carbon fixation (mmol C m^{-3} d^{-1}) versus DLA:TChl *a* ratio (nmol h^{-1} μg^{-1} TChl *a*). Open circles denote surface samples and samples from the chlorophyll maximum are represented by filled squares. The mean concentrations for carbon fixation (0.28 mmol C m^{-3} d^{-1}) and DLA (131.7 nmol h^{-1} μg^{-1} TChl *a*) are plotted as solid lines on the vertical and horizontal axes.

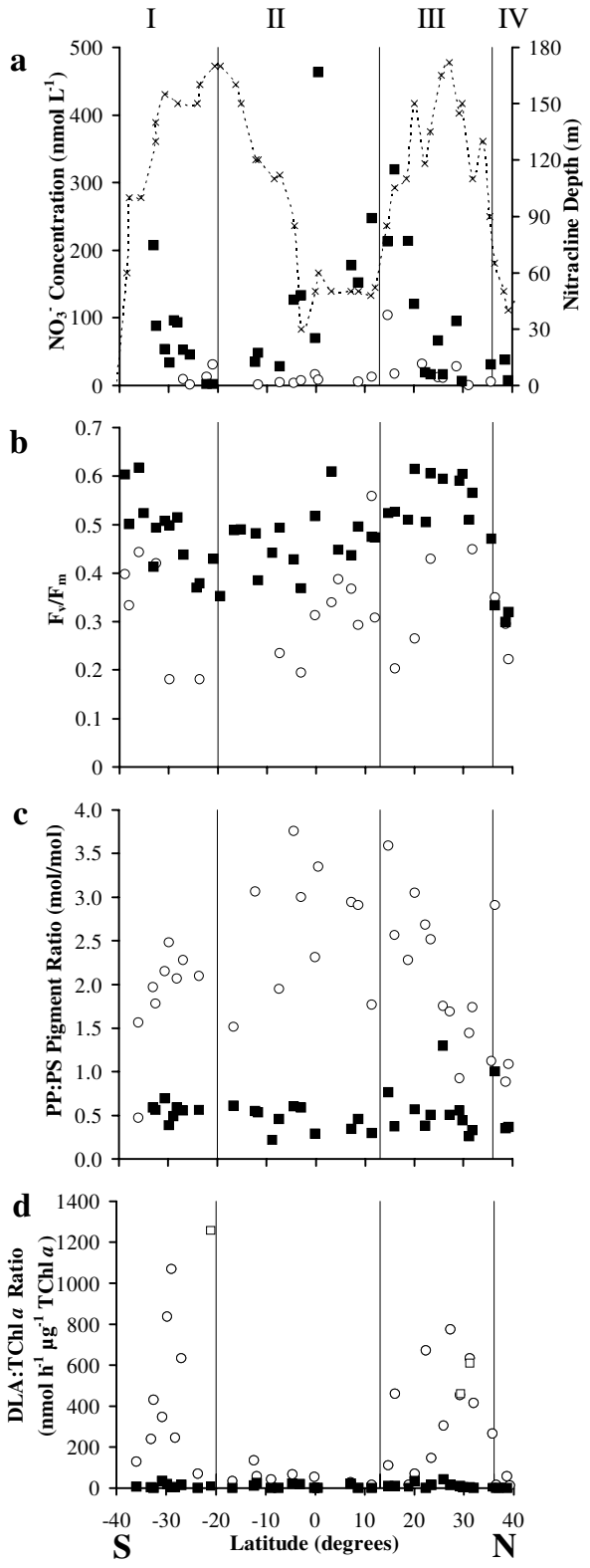

Figure 5.5 Latitudinal distribution of (a) nitrate concentration, NO_3^- (nmol L^{-1}), and depth of nitracline (defined as depth of 1 µmol L^{-1} NO_3^- isopleth); (b) F_v/F_m; (c) photoprotective pigment (PP) to photosynthetic pigment (PS) ratio (mol/mol), and (d) DLA:TChl *a* (nmol h^{-1} μg^{-1} TChl *a*). For ease of comparability, (d) shows the same data as figure 2c. Open circles (HPLC chlorophyll) and squares (acetone-extracted chlorophyll) denote surface samples and samples from the chlorophyll maximum are represented by filled squares. Dashed line in (a) represents nitracline depth (m). See text for definitions of PP:PS and F_v/F_m.

Fast repetition rate fluorometry facilitates the calculation of the F_v (variable fluorescence) to F_m (maximum fluorescence) ratio, which represents photochemical efficiency and has often been used as a general indicator of photosynthetic health for natural phytoplankton assemblages and cultures (Falkowski and Raven, 1997). Throughout AMT-14, F_v/F_m values were lower in surface waters relative to chl max values (Figure 5.5b). This could be due to light stress (Falkowski and Raven, 1997), nutrient limitation (Parkhill et al., 2001), taxonomic variability (Moore et al., 2006) or a combination of all three. Although the data suggests that cells at the surface are potentially in a more stressful environment, the surface values do not demonstrate obvious co-variation with DLA.

If DLA increases due to light stress then variations in photo-protective pigment concentrations might also be expected to co-vary with DLA values. Indeed, previous studies from a range of environments have found significant relationships between DLA and accessory pigment concentrations (Steinke et al., 2002a; 2002b; Harada et al., 2004). Whilst different phytoplankton groups dominate in different ocean regions and seas, these studies have all described a significant correlation between DLA and the commonly occurring photo-protective pigment, diadinoxanthin. This pigment is part of the diadinoxanthin-diatoxanthin xanthophyll cycle, a photo-protective mechanism found in major phytoplankton groups, including diatoms, dinoflagellates and haptophytes (Porra et al., 1997). However, our data demonstrates no such correlation between DLA and diadinoxanthin or any other xanthophyll cycle pigment.

The phytoplankton community was classified using an approach similar to that used by Gibb et al. (2000), which identifies the relative investment in photo-protective (PP) versus photosynthetic (PS) pigments. This index divides the molar concentrations of the major PP accessory pigments (diadinoxanthin, zeaxanthin and alloxanthin) by the major PS accessory pigments (peridinin, 19′-butanoyloxyfucoxanthin, fucoxanthin, 19′-hexanoyloxyfucoxanthin and prasinoxanthin) along the AMT cruise track. The PP:PS ratio is consistently higher at the surface relative to the chl max (Figure 5.5c), i.e. a greater relative investment in PP pigments in surface waters. The PP:PS ratio correlates significantly and positively with DLA (*Spearman's* $\rho = 0.53$, $p < 0.01$, $n = 68$) but the correlation is not exceptionally strong because, as with F_v/F_m, the pattern of the surface data does not follow that of surface DLA. Photo-protective pigment production is designed to help the cell in redistributing energy, protecting photosystem II from over

excitation in high light conditions whilst maintaining photosynthetic rates (Falkowski and Raven, 1997). In contrast, it has been suggested that DLA is part of a process designed to protect the cell against excess harmful oxidative radicals formed due to numerous stressors, not just elevated light (Sunda et al., 2002). It therefore should not be expected that photo-protective pigments display exactly the same patterns as DLA, because other factors such as nutrient limitation (e.g. by nitrogen or iron) and intracellular CO_2 shortage contribute to the potential for oxidative stress and may also influence DLA.

The starting hypothesis for this chapter was that DLA would increase with factors that cause oxidative stress. Therefore, if DLA is related to the level of oxidative stress experienced, it might vary with the length of light exposure to the water column over recent hours. The late-morning CTD data was investigated for the surface light history of the local region (total irradiance received) over the past 2–4 hrs, but this revealed no clear pattern (data not shown). However, it is interesting that the high surface DLA samples (i.e. sections I and III) from the late-morning CTD had higher activity than those surface samples from the pre-dawn cast, with the exception of two days in section III (Table 5.1). Whilst these samples were spatially distinct and therefore only represent a pseudo time-series, the regions covered by sections I and III are large oligotrophic gyres and the biological, chemical and physical conditions can be expected to remain relatively constant over the distance travelled between the pre-dawn and late-morning casts. These results are in agreement with other results from somewhat similar waters, which suggest a link between the reduced sulphur cycle and light exposure (Toole and Siegel, 2004). Elevated DMS concentrations are observed every summer in the Sargasso Sea and demonstrate a strong, significant correlation with photosynthetically active radiation and UV.

Table 5.1 Surface DLA values from pre-dawn (PD) and late-morning (LM) CTD casts. Each PD and LM sample pair was selected from the same day and was from the same section. The final column represents the difference between LM and PD. Sections I and III demonstrate elevated DLA in the LM cast relative to the same day's PD cast, with the exception of two days in section III (20 May '04 and 23 May '04).

Section	Date	Pre-Dawn DLA (PD) (nmol L^{-1} h^{-1})	Late-Morning DLA (LM) (nmol L^{-1} h^{-1})	LM – PD
I	05 May '04	17.2	36.1	18.9
I	06 May '04	23.9	55.3	31.4
I	07 May '04	10.8	49.7	38.9
II	11 May '04	5.9	3.2	−2.7
II	12 May '04	2.9	1.0	−2.0
II	13 May '04	5.3	9.7	4.4
II	14 May '04	4.8	0.0	−4.8
II	16 May '04	3.1	3.9	0.8
III	18 May '04	8.2	30.2	22.0
III	19 May '04	1.2	4.2	3.0
III	20 May '04	32.0	7.6	−24.4
III	21 May '04	7.2	13.0	5.7
III	22 May '04	13.5	29.5	15.9
III	23 May '04	20.2	19.1	−1.1
IV	26 May '04	3.8	1.6	−2.3

With the methods used here (see Methods; Section 2.3), the water-column DLA measured is nominally representative of the size fraction greater than 0.7 µm. As a result, the data are unlikely to include DLA for all unattached bacteria, although some may have been retained as filtration proceeded. An experiment in 1999 in the St. Lawrence estuary found that free-living bacteria and free enzymes accounted for only a small (< 10%) proportion of the overall DMS production, corroborating previous findings (Scarratt et al., 2000, and references therein). These samples were collected in more oligotrophic waters and the DLA could relate to a combination of phytoplankton DLA, particle-attached bacterial DLA and the activity of some unattached bacteria that may have been retained on the filter. An inherent problem with the methods currently used to determine DLA is that there is a possibility that variable proportions of free-living and particle-attached bacteria contribute to observed variations in surface DLA.

5.4 Summary

The novel data set presented here was collected over a wide geographic range covering the oligotrophic northern and southern gyres of the Atlantic. Considerable variability in surface DLA was observed, but these variations did not relate particularly well with observed DMS and DMSP concentrations. Oxidative stress is less likely for phytoplankton cells in nutrient-replete, high productivity waters and elevated DLA:TChl *a* was not observed when the nitracline was shallow or when carbon fixation rates were greater than 0.28 mmol C m^{-3} d^{-1}. However, surface waters with low ^{14}C-fixation and a deep nitracline did not always display elevated DLA. At the surface, F_v/F_m values were lower and the PP:PS accessory pigment ratio was higher, which may be due to generally more stressful conditions at the surface. However, neither of these parameters correlate well with surface DLA. Comparison between pre-dawn and late-morning CTD casts suggests that the DLA response to changes in light conditions is relatively rapid, although no correlation could be found between recent light history and DLA. The relationship between oxidative stress and DLA in open ocean waters deserves further attention in order to fully understand what causes the variations in surface DLA observed during this study; this is essential to improve understanding of how DLA may influence ambient DMS concentrations and the subsequent ocean-atmosphere flux of this climate-cooling trace gas.

6 Atmospheric gaseous and aerosol nitrogen and sulphur measurements

6.1 Introduction

Having addressed the reduced sulphur cycle in the surface ocean in chapters 3-5, this chapter focuses on the atmosphere and discusses relevant results from the AMT programme. The oxidation of atmospheric DMS to sulphate (SO_4^{2-}) and the subsequent role of SO_4^{2-} aerosol in the formation of cloud condensation nuclei (CCN) are core components of the CLAW hypothesis (Charlson et al., 1987). Atmospheric ammonia (NH_3) reacts readily with sulphate aerosol, facilitating new particle nucleation (Coffman and Hegg, 1995). For these reasons the atmospheric data collected during AMT is of interest. After a methods section (Section 6.2), Section 6.3 focuses on atmospheric concentrations of the products of DMS oxidation, methane sulphonic acid (MSA) and non-sea-salt sulphate ($nssSO_4^{2-}$). The subsequent section (Section 6.4) concentrates on reduced nitrogen, i.e. gaseous ammonia ($NH_{3(g)}$) and its flux to and from the ocean. The final section (Section 6.5) combines results relating to both the nitrogen and sulphur cycles, and discusses them in the context of current theory. In particular, *in situ* DMS and $NH_{3(g)}$ fluxes are compared and remote marine atmospheric aerosol ammonium to non-sea-salt sulphate ratios (NH_4^+:$nssSO_4^{2-}$) are discussed using AMT and other data from the literature.

Due to instrumentation problems, oceanic NH_4^+ and atmospheric $NH_{3(g)}$ samples were only collected concurrently during AMT-14 and thus flux calculations for NH_3 could be made for this cruise alone. In addition, atmospheric MSA concentrations were only measured during AMT-14. As a result, the first two result sections (6.3 and 6.4), discuss data collected during AMT-14 in May 2004 (for cruise track, see Figure 1.18 in Section 1.5, Chapter 1). Initially, Section 6.5 discusses NH_3 and DMS fluxes and is thus also solely focussed on data collected during AMT-14. However, once the focus shifts onto the NH_4^+:$nssSO_4^{2-}$ ratio in aerosol, data from AMT-12, -13 and -14 is discussed. Finally, relevant results are presented from an extensive literature search.

6.2 Atmospheric methodologies

The following sections provide some detail on the collection and analysis methods for the chemical species discussed in this chapter.

6.2.1 Concentration of chemical species in aerosol

All AMT atmospheric aerosol samples were collected and analysed by Alex Baker, Tim Jickells and Karabi Biswas, who kindly made their data available for interpretation here. All aerosol samples were collected on Whatman 41 filters using a high-volume (1 m^3 min^{-1}) cascade impactor (Figure 6.1), set up to separate samples into coarse (>1 µm diameter) and fine (<1 µm diameter) particles, which broadly represent two different aerosol formation routes (Raes et al., 2000). The coarse mode aerosol is formed predominantly by physical processes (e.g. spray from the ocean or dust resuspended from the continents), while gas-to-particle conversion forms fine mode aerosol (e.g. $SO_{2(g)}$ conversion to sulphate aerosol).

The cascade impactor was set up to collect these samples using three stages. Two stages and filters were placed nearest to the air intake of the impactor. The first initiated the flow-field of air, which aids separation of fine and coarse mode particles (see Figure 6.1), and the second collected the majority of particles >1 µm in size. These two filters were extracted together and represent the coarse mode aerosol sample. A third filter (Whatman 41 cellulose, with ~0.1 µm pore size) was placed beneath the slotted filters and the extract from this represented the fine mode aerosol sample. Samples were generally changed once a day and sampled an average air volume of ~1400 m^3 with a flow of ~0.5 m^3 sec^{-1}.

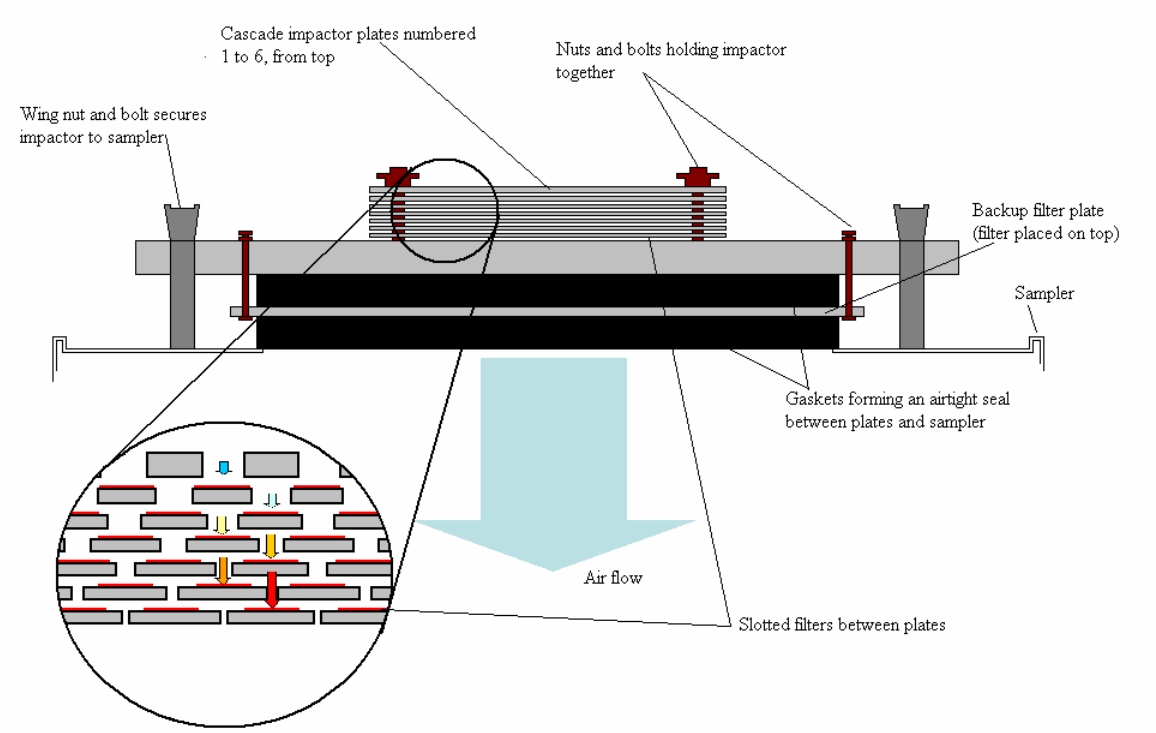

Figure 6.1 Diagrammatic representation of how a cascade impactor is set up and operated. Although 6 impactor stages were available, only 3 stages were used (see text). Diagram courtesy of Tim Lesworth.

It is possible that the Whatman 41 filters also collected gas phase nitric acid (HNO_3) and ammonia (NH_3). However, nitrate is found predominantly in the coarse mode due to the reaction of HNO_3 with sea salt aerosol, thus suppressing any fine mode deposition of HNO_3 (Pryor and Sorensen, 2002).

Throughout this chapter, the term 'major ion' refers to the dominant chemical species found in the aerosol. In terms of the extraction and analysis described here, the following major ions and chemical species were all analysed using ion chromatography after extraction into milliQ water:
Ammonium (NH_4^+), Sulphate (SO_4^{2-}), Nitrate (NO_3^-), Chloride (Cl^-), Sodium (Na^+), Calcium (Ca^{2+}), Potassium (K^+) and Methane Sulphonic Acid (MSA).

6.2.2 Atmospheric gaseous NH_3 concentrations

Atmospheric gaseous NH_3 was collected using a system commonly known as a 'filter pack'. Two filter packs were used in parallel to account for any variability, with a third pack deployed as a blank, which was disconnected from the vacuum pump; the filters from the blank filter pack were used to blank correct the data. The filter pack systems were positioned at the fore (front) of the monkey island (top deck) and sampling only ever occurred when the net wind direction (i.e. wind direction corrected for ship's motion) was from forward of the ship's funnel. Filter pack setup was as shown in Figure 6.2:

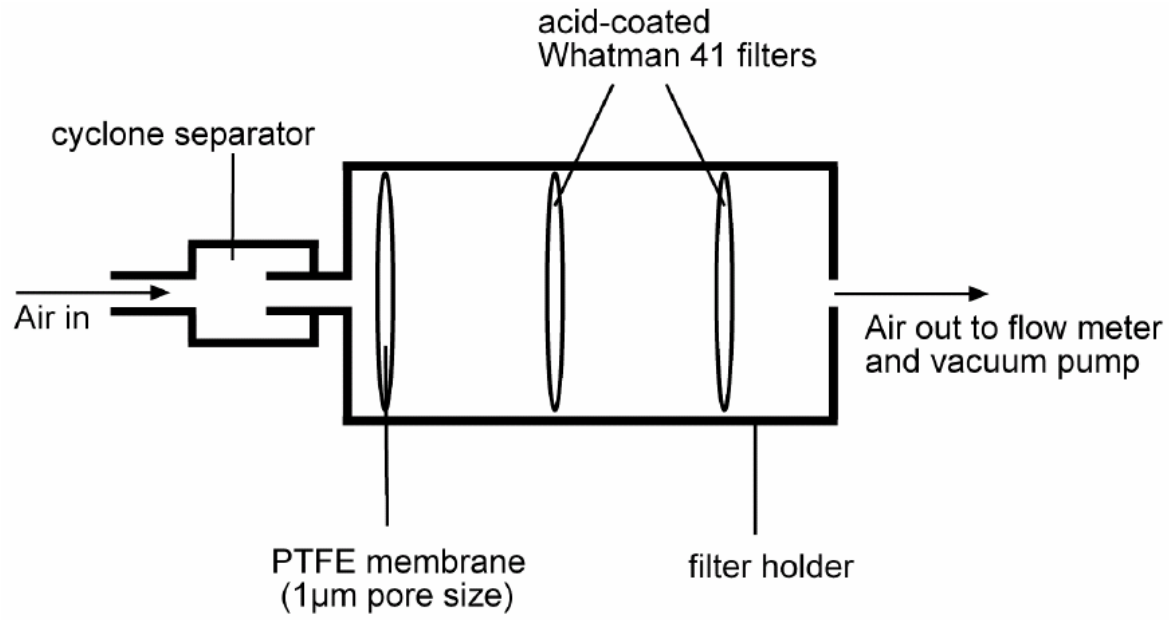

Figure 6.2 Schematic diagram of a filter pack system (figure taken from Johnson, 2004). Whatman 41 filters were coated with oxalic acid.

Air is sucked through the filter pack using a vacuum pump set at a flow rate between 5 and 100 dm^3 min^{-1} (Johnson, 2004). The cyclone separator spins the air to remove the larger particles (approximately > 0.9 µm in diameter) and this prevents the PTFE filter from clogging with sea salt particles. In order to collect solely gaseous NH_3, aerosol particles must first be removed using a PTFE pre-filter. As air passes through the acid-coated (oxalic acid) filters, the gaseous NH_3 is stripped out and held on the filter. The principle behind having more than one filter is that some NH_3 may pass through the first filter and be 'mopped up' by the second. In addition, it has been observed that the vacuum pump is actually strong enough to suck acid off the filters (T. Lesworth, *Pers. Comm.*) so it is essential that oxalic acid is retained from the first filter at least.

Quinn et al. (1990) report that at room temperature and 75% relative humidity, oxalic acid-coated filters had a collection efficiency for $NH_{3(g)}$ of 103±30%. Despite this, a number of potential problems have been identified with the filter pack method. The first noteworthy criticism is that the method does not account for volatilisation of aerosol particles (specifically NH_4NO_3 and NH_4Cl) on the PTFE pre-filter. These volatilised gases may then pass through the PTFE filter and be trapped on the acid-coated filters. Secondly, if the aerosol trapped on the PTFE filter is acidic, this may lead to gaseous NH_3 reacting with aerosol before it reaches the acid-coated filters. Following an in-depth discussion of the pros and cons of different methods, Johnson (2004) concludes that although more expensive methods are available, with due care and attention the filter packs are still a viable option for sampling atmospheric gaseous NH_3.

For the majority of samples on AMT-14, the filter packs were run to collect an integrated sample over approximately one day. A flow meter was placed between the filter pack and the vacuum pump, and this was used to record the volume of air that had passed through each filter pack. Taking great care not to contaminate the filters, the filter packs were changed in a glove box (pumped with NH_3-free air) and each filter placed in a pre-labelled 50 ml corning tube which was frozen until analysis back in the laboratory. It is very easy to cause contamination throughout the collection and analysis of NH_3 as human skin is a significant source of contamination (Johnson, 2004). Thus, a strict cleaning protocol was observed throughout the sampling and analysis procedures. Prior to use, all glassware was soaked in 5% Decon for 24 hrs, rinsed with milliQ water and then soaked in milliQ for 24 hrs. Hands and forearms were washed thoroughly, dried and latex gloves put on before handling anything involved in either sampling or analysis.

Gaseous NH_3 was analysed as aqueous NH_4^+ using the spectrophotometric method of Holmes et al. (1999). MilliQ water was added to the corning tube to create an aqueous 'sample' and this was then analysed. Analysis involved adding 1 ml of 'Working Reagent' to a 25 ml sample (or standard), which produces a linear calibration range up to 2.5 µM. Working Reagent is a mix of the following:

- **Disodium tetraborate solution** (80 g in 2 litres MilliQ water)
- **OPA (ortho-pthaldealdehyde) solution** (4 g in 100 ml ethanol). OPA is light sensitive and hence the solution should be stored in the dark.
- **Sodium sulphite solution** (1 g in 125 ml MilliQ water) to prevent the OPA solution from reacting with any amino acids and other amines.

Working Reagent (2 litres of disodium tetraborate buffer, 10 ml sodium sulphite and 100 ml of OPA) was then added to the samples/standards (1 ml added to 25 ml of sample/standard produces a linear response up to 2.5 µm), which were incubated in the dark to allow the fluorescent reaction to develop. As shown in Figure 6.3, the samples/standards needed to be incubated for at least 3 hrs for the reaction to fully develop. After full development of fluorescence, it plateaus for approximately 20 hours before gradually decaying over a number of days (Figure 6.3). To account for variation in the fluorescence over time, the Working Reagent was added to the standards at the same time as the samples and they were both then analysed at the same time. Analysis was carried out on a Jasco FP-740 spectrofluorometer, which was set to measure the light emission at a wavelength of 420 nm after excitation of a sample at a wavelength of 380 nm. All samples were blank corrected using Working Reagent + MilliQ water.

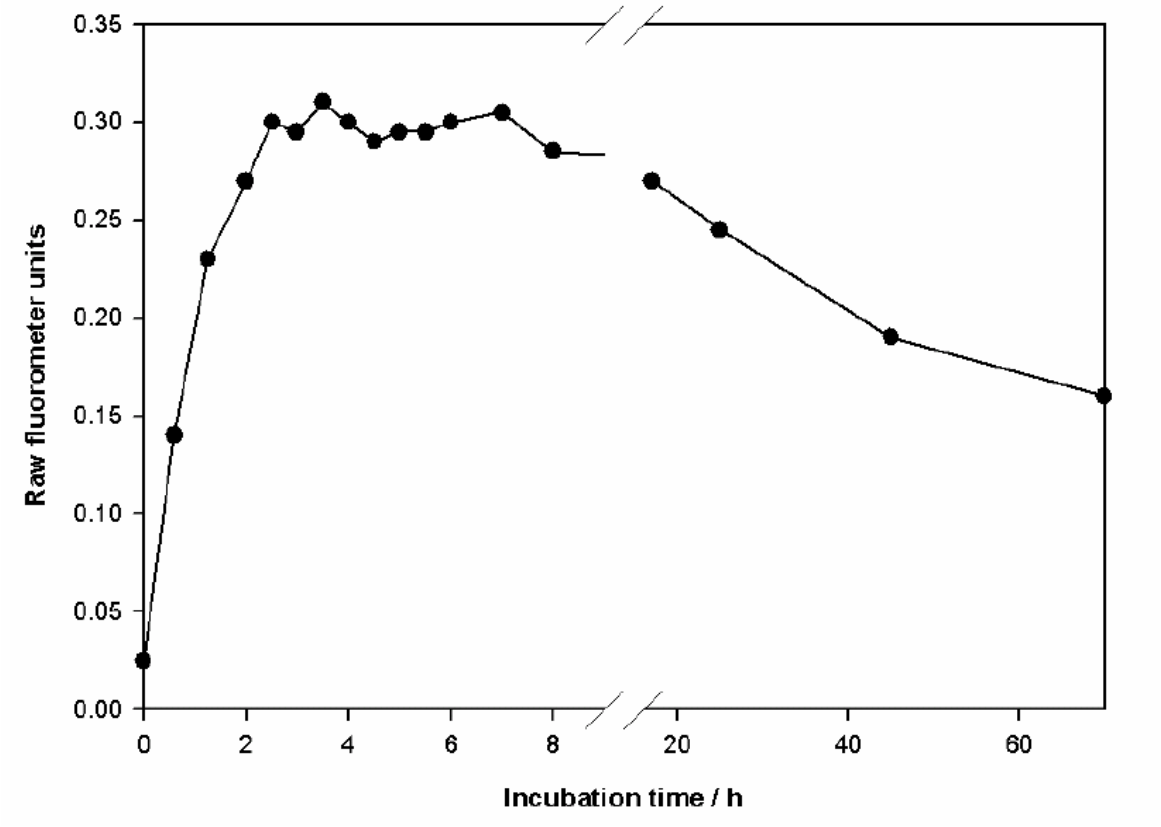

Figure 6.3 The fluorescence development-plateau-decay cycle of the OPA method (figure taken from Holmes et al., 1999).

Having calculated the amount of NH_3 that had been trapped on each filter, the atmospheric concentration could be calculated using the total volume of air that had passed through the filter pack. In addition to blank-correcting the filter pack samples, the blank filter packs were used to indicate the uncertainty for each sample. Two standard deviations about the mean of the NH_3 on the blank filters from every AMT blank filter pack provided an estimate of the uncertainty associated with each filter pack. However, to produce an idea of the uncertainty in nmol m^{-3}, this was then divided by the average volume of air to pass through all the filter packs during AMT-14. This value (±3.66 nmol m^{-3}) could then be used as an indication of the uncertainty for each filter pack. When the mean atmospheric concentration for each sample was calculated from the two sample filter packs, the propagated uncertainty was ±2.59 nmol m^{-3}.

6.2.3 Sea-salt correction of marine aerosol composition

Throughout this chapter, reference will be made to non-sea-salt ions (i.e. nssSO_4^{2-}, nssK^+, nssCl^-, nssCa^{2+}). Essentially, these are the concentrations of ions in the aerosol after the correction for sea salt influences. To calculate this, the ratio of the respective ion (*X*) to sodium (Na^+) in seawater is used. Na^+ is used as it is abundant in seawater, is not concentrated or diluted during the production of sea spray, and is thought to be relatively inert during atmospheric processing. In order to calculate the sea salt component of an ion in aerosol, the following equation was used:

$$[X]_{SW} = [Na^+] \times \left(\frac{[X]}{[Na^+]} \right)_{SW}$$

Equation 6.1

where the subscript *SW* represents 'in seawater'. This assumes that all sodium (Na^+) in the atmosphere is from the ocean and that the ratio of *X* to Na^+ in the sea salt aerosol formed is the same as in the ocean. The ratios for SO_4^{2-}, K^+, Cl^- and Ca^{2+} (to Na^+) in seawater are 6.026×10^{-2}, 2.180×10^{-2}, 1.16453 and 2.180×10^{-2} respectively (Stumm and Morgan, 1981). To calculate the non-sea-salt fraction, the sea-salt fraction is then taken from the total value.

6.2.4 Air mass source classification and back trajectories

In order to help identify air mass source, 5-day air mass back trajectories were determined for each sample using the NOAA Hysplit model FNL version (Draxler and Rolph, 2003). The model was set to allow vertical motion to be modelled and each back trajectory was run from 00:00 hrs each day from the latitude and longitude noted at the beginning of each sampling period. The AMT air masses were classified into seven categories: *North Atlantic, Remote*; *North Atlantic, European*; *Saharan*; *South Atlantic, South East*; *African Biomass Burning*; *South Atlantic, Remote*; and *South Atlantic, South Pacific*. Back trajectories were run for heights of 15 m and 1000 m above mean sea level, although the only trajectories presented in Figure 6.12, Figure 6.13 and Figure 6.14 were those from 15 m. The 15 m trajectory indicates where the air mass itself has travelled over the last 5 days, while the 1000 m trajectory attempts to account for the gravitational settling out of dust particles from the upper atmosphere. Both the *Saharan* and *African Biomass Burning* categories were therefore identified using the 1000 m back trajectory rather than the 15 m back trajectory. Air masses that had spent the majority of the five days over the ocean were classified as remote and were then sub-divided by the wind direction; these four air masses were: *North Atlantic, Remote*; *South Atlantic, South East*; *South Atlantic, Remote*; and *South Atlantic, South Pacific*.

In addition to the back trajectories, a number of chemical 'clues' helped to confirm the source location of the air masses. Air masses influenced by biomass burning (*African Biomass Burning*) show elevated $nssK^+$ (Cachier et al., 1995); air masses influenced by anthropogenic activity (*North Atlantic, European*) demonstrate high NO_3^- and NH_4^+ concentrations; and high $nssCa^{2+}$ concentrations (> 5 nmol m^{-3}) are an indicator of dust. Finally, visual clues are also helpful as dust influenced samples are often tinged a reddish-brown and blacker samples are indicative of combustion sources from either pollution or biomass burning.

6.3 Atmospheric sulphur

The dominant reaction products of atmospheric DMS oxidation are MSA and $nss SO_4^{2-}$. Before the atmospheric results from AMT-14 are discussed, it is worth considering certain background information. As discussed in Section 1.2.2, the relative proportion of MSA and $nss SO_4^{2-}$ produced by DMS oxidation varies with temperature (Hynes et al., 1986) and has therefore been observed to vary with latitude (e.g. Bates et al., 1992a; Leck et al., 2002a). It was first shown that the rate of hydroxyl radical ($OH^{\bullet}$) addition increased with reducing temperature (Hynes et al., 1986), resulting in an increased MSA:$nss SO_4^{2-}$ ratio in the atmosphere. However, it has subsequently been identified that the decomposition of the methylsulphonyl radical ($CH_3SO_2^{\bullet}$) and the methylsulphinylperoxyl radical ($CH_3SO_3^{\bullet}$) to sulphuric acid and ultimately SO_4^{2-} (see Figure 1.10) are other aspects of the DMS atmospheric oxidation scheme that are strongly temperature dependent (Yin et al., 1990a). Should these radicals not decompose, they will be oxidised to MSA instead, increasing the MSA:$nss SO_4^{2-}$ ratio; the influence of this has been demonstrated in modelling studies (Ayers et al., 1996; Koga and Tanaka, 1999).

Further to the effect of temperature, the relative abundances of atmospheric oxidants also impact upon the MSA:$nss SO_4^{2-}$ ratio. In contrast to $OH^{\bullet}$, which demonstrates relatively stable atmospheric concentrations, the concentration of the nitrate radical ($NO_3^{\bullet}$) shows considerable temporal variability because it is rapidly photolysed. As a result, DMS oxidation by $NO_3^{\bullet}$ is an efficient nighttime loss term and dominates at higher latitudes during the dark winter months (Koga and Tanaka, 1996); this reaction has been shown to favour the production of MSA (Yin et al., 1990b). Recent results from a comparison of modelled and measured global MSA:$nss SO_4^{2-}$ ratios suggest that the distribution of the DMS-derived MSA:$nss SO_4^{2-}$ ratio cannot be explained by marine biological activity (i.e. DMS production) and temperature alone, and suggests that photochemistry indeed plays a role (Gondwe et al., 2004). The authors' suggested explanation is that light not only impacts upon $NO_3^{\bullet}$ photolysis, but that the photochemical production of $OH^{\bullet}$ should not be neglected (Gondwe et al., 2004).

More recent work has demonstrated the importance of halogen chemistry for DMS oxidation pathways, with bromine oxide (BrO) playing a particularly important role (von Glasow and Crutzen, 2004). The authors showed that the inclusion of halogens in a one-dimensional model led to increased importance of the addition pathway in DMS oxidation

and thus reduced the potential impact on cloud albedo (von Glasow and Crutzen, 2004). An extensive and detailed summary of DMS oxidation in the atmosphere has been recently published (Barnes et al., 2006) and concludes that more multiphase model studies such as conducted by von Glasow and Crutzen (2004) are needed to improve prediction of atmospheric MSA:nssSO_4^{2-} ratios. Finally, physical mechanisms should not be neglected as wet and dry deposition processes have been shown to remove MSA preferentially to nssSO_4^{2-} (see Gondwe et al., 2004 and references therein).

Clearly many of the parameters discussed in the paragraphs above were not or could not be measured as part of the AMT campaign, but it is instructive to consider them when interpreting the results. Figure 6.4 presents the MSA concentrations measured along the AMT-14 transect, with the secondary axis showing the calculated DMS flux (see Section 1.1.1 for methodology). As is clear, the degree of co-variation between the DMS flux and MSA concentration is relatively poor. This is unsurprising for four reasons:

(1) The oxidation of DMS to MSA is not immediate, taking upwards of a day to oxidise in the remote atmosphere, during which time the air mass will have moved considerable distance over the ocean.
(2) The DMS flux calculation uses the average wind speed from the previous 10 minutes and is thus an 'instantaneous' measure and not comparable to atmospheric oxidation products that have formed over a longer timescale.
(3) The proportion of MSA produced per mole of DMS changes with temperature and is therefore likely to change with latitude.
(4) Atmospheric concentrations are dependent on the mixed layer depth of the marine boundary layer; increasing mixed layer depth dilutes the concentration.

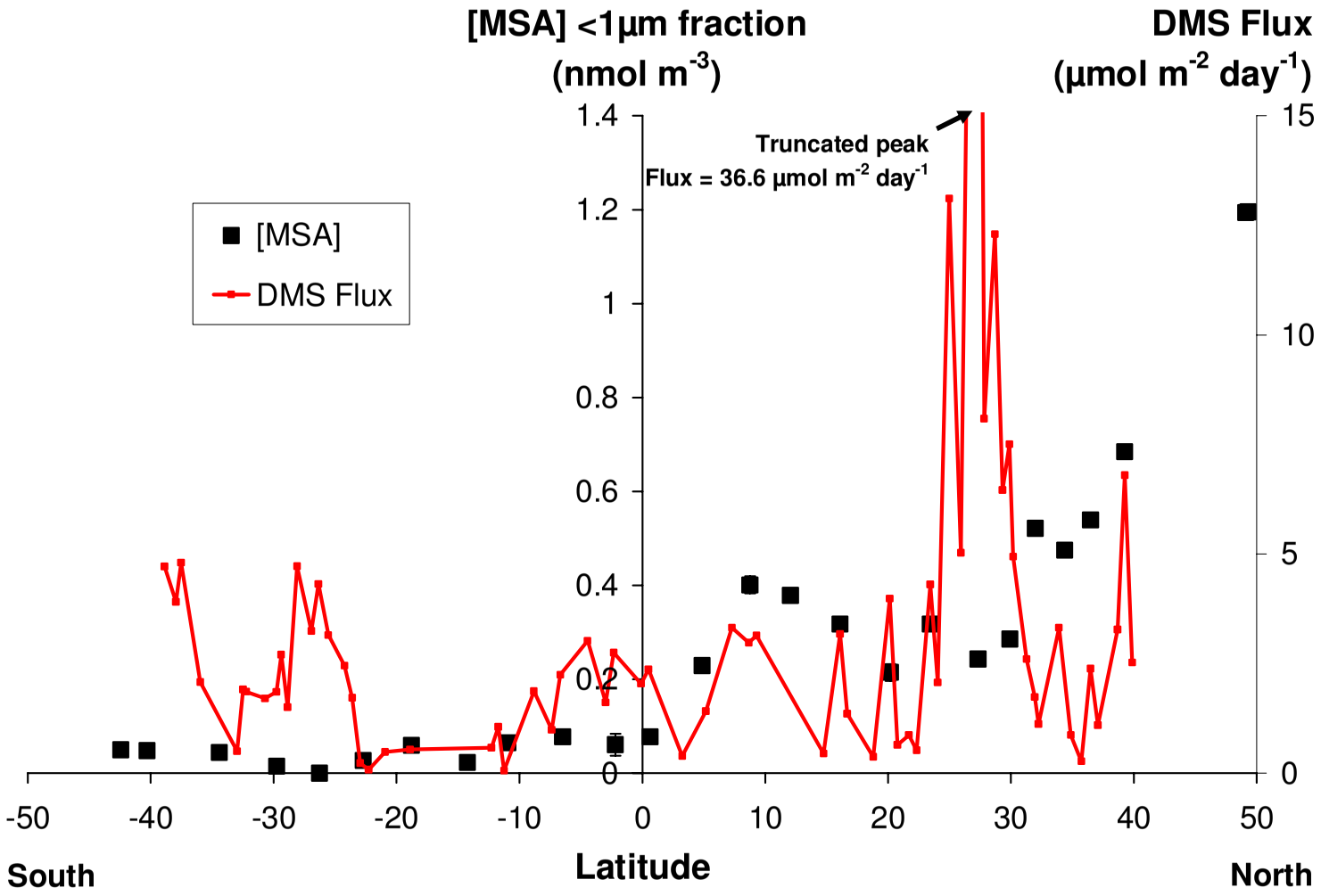

Figure 6.4 Latitudinal distribution of fine fraction (<1 µm) atmospheric MSA concentration (filled squares) and DMS flux (red dots and line) along the AMT-14 transect. Error bars on MSA concentrations represent one standard deviation, but these are so small as to only be seen on one point close to the equator.

When surface seawater DMS concentrations are plotted against atmospheric MSA concentrations, a similar trend with latitude can be seen for both variables (Figure 6.5). Although numerous factors are involved in dictating atmospheric MSA concentrations, the source strength of DMS will certainly play a role. Whilst DMS measurements were immediate and only represent current conditions, it is reasonable to assume that oceanic DMS concentrations in these areas do not vary substantially over the temporal and spatial scales involved. As a result, deviations in MSA concentrations away from the seawater DMS trend are more likely driven by changes in atmospheric processing due to temperature, oxidative radicals, wet and dry deposition, mixing, etc.

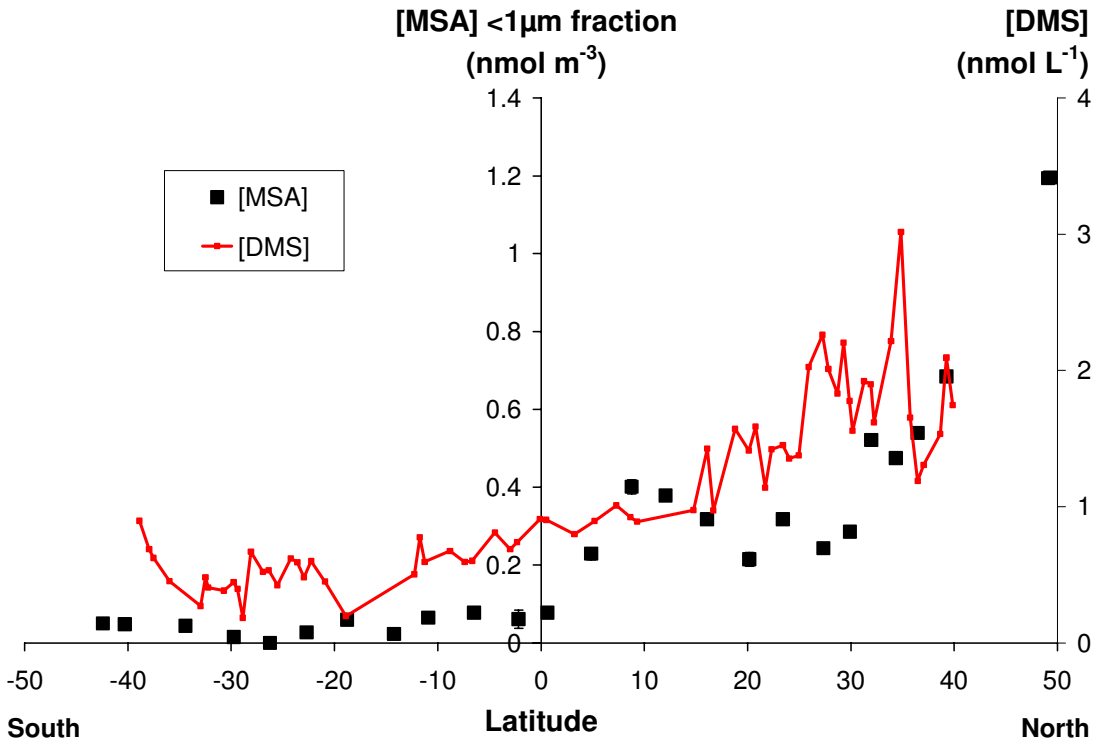

Figure 6.5 Latitudinal distribution of fine fraction (<1 µm) atmospheric MSA concentration (filled squares) and seawater surface DMS concentration (red dots and line) along the AMT-14 transect. Error bars on MSA concentrations represent one standard deviation, but these are so small as to only be seen on one point close to the equator.

Much of the atmospheric processing of DMS produces differing MSA:nssSO_4^{2-} ratios, so it is instructive to consider this ratio in the context of surface seawater DMS concentrations (Figure 6.6). Whilst MSA is exclusively produced by the oxidation of DMS, it is unlikely that all measured nssSO_4^{2-} has a biological source. This is discussed in more detail in the proceeding paragraph using data presented in Figure 6.7. In the high latitude southern hemisphere, it is less likely that the air masses sampled were significantly influenced by anthropogenic sources of nssSO_4^{2-}. The elevated MSA:nssSO_4^{2-} ratios measured in this region are most likely driven by the reduced atmospheric temperatures driving the MSA-SO_4^{2-} branching ratio towards MSA production (i.e. increasing the ratio).

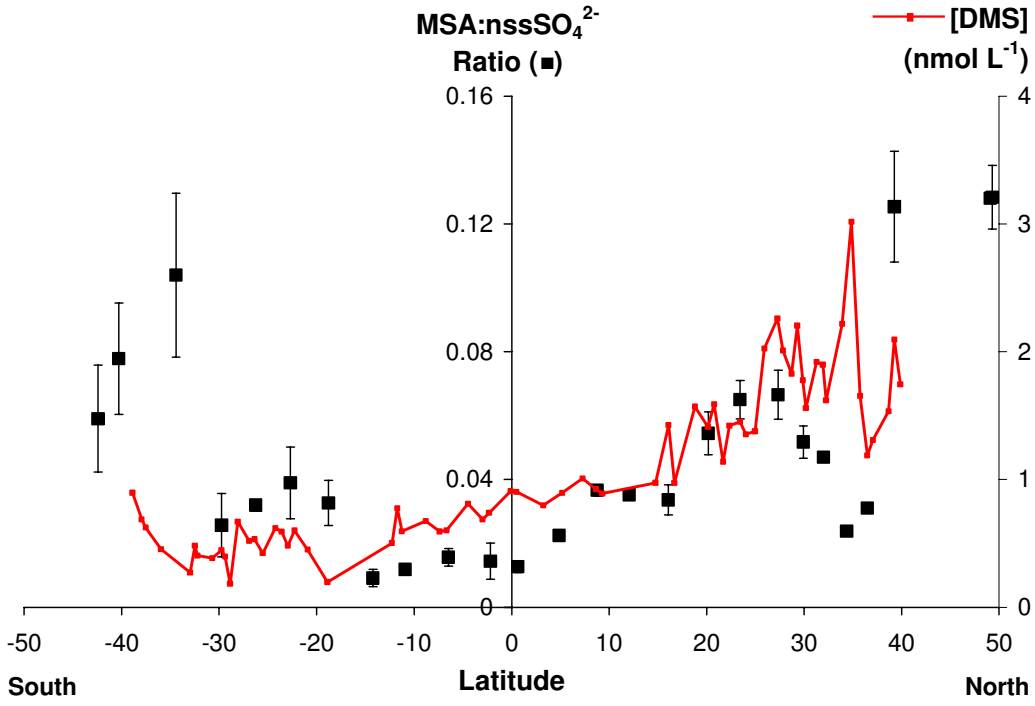

Figure 6.6 Latitudinal distribution of fine fraction (<1 µm) atmospheric MSA:nssSO_4^{2-} ratio (filled squares) and seawater surface DMS concentration (red dots and line) along the AMT-14 transect. Error bars on MSA:nssSO_4^{2-} ratios represent one standard error.

The MSA:nssSO_4^{2-} ratio data plotted in Figure 6.6 has again been plotted against latitude in Figure 6.7, but without distinguishing between the northern and southern hemispheres. The AMT-14 data clearly shows a latitudinal dependence – the ratio increases as latitude increases (i.e. temperature reduces). Once samples identified as having been influenced by Saharan dust or European pollution (Section 6.2.4) are removed, the slope of the regression line increases. This clearly shows how terrestrial or anthropogenic sources of sulphate can disrupt remote marine atmospheric chemistry and alter composition ratios, a point worth considering later in the discussion of NH_4^+:nssSO_4^{2-} ratios (Section 6.5.2).

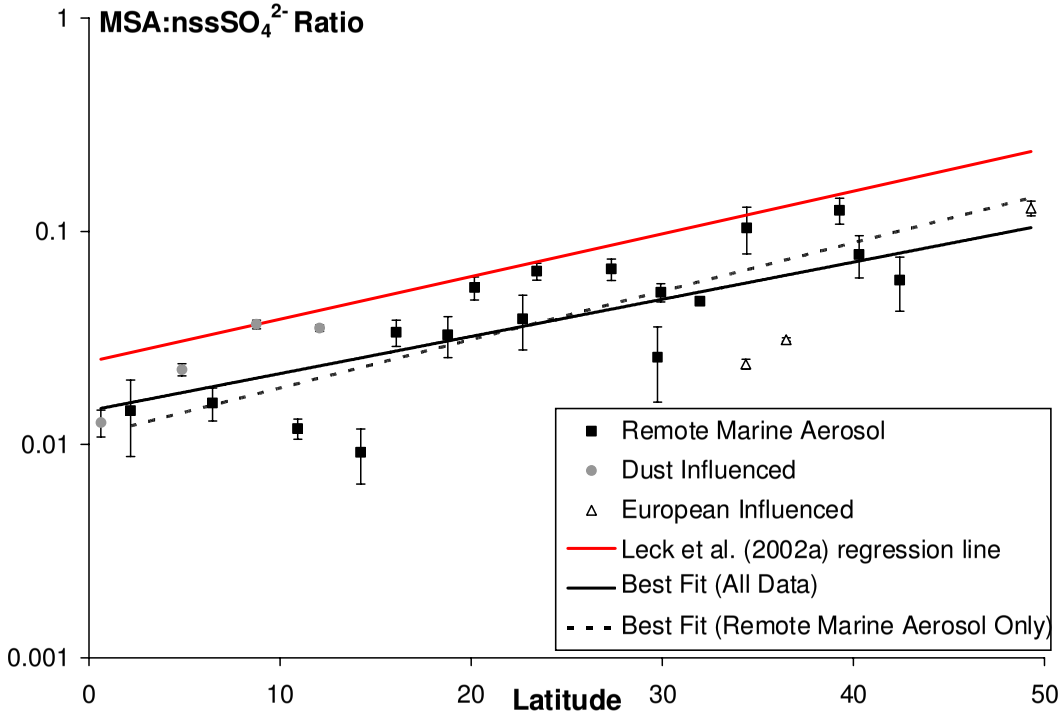

Figure 6.7 MSA:nssSO_4^{2-} ratio (note log scale) in the fine (<1 µm) fraction, plotted against latitude (North and South). Samples influenced by Saharan dust (grey filled circles) or influenced by European pollution (open triangles) are distinguished from remote marine samples (filled squares). Error bars on MSA:nssSO_4^{2-} ratios represent one standard error. Best fit regression lines are shown for all AMT-14 data (solid black line; $y=0.0144e^{0.0401x}$, $r^2=0.570$) and for AMT-14 data after removal of Saharan and European samples (dashed line; $y=0.0109e^{0.0523x}$, $r^2=0.661$). The published equation for the Leck et al. (2002a) regression line was $(MSA:nssSO_4^{2-})^{\%}=2.443e^{(-0.02.LAT)}$, $r^2=0.837$. Leck et al. (2002a) plotted their line with both hemispheres separated (South as negative) so in order to plot the line on Figure 6.7, -0.02 had to be changed to +0.02. After this change and a conversion from %MSA to MSA fraction, the regression line in the plot above (solid red line) now follows $y=0.02433e^{(0.02x)}$.

Also plotted on Figure 6.7 is the regression line from Leck et al. (2002a), which plots above the AMT regression lines, although this is possibly due to a difference in how the best fit lines were produced. In contrast to Figure 6.7, Leck et al. (2002a) plot their line using data (remote marine only) from both hemispheres, but plot South as negative when they draw their regression line. Figure 6.7 clearly demonstrates the temperature dependence of the MSA:nssSO_4^{2-} ratio, but the relationship is not perfect and the same is true for the data of Leck et al. (2002a). It is likely that other factors will have influenced branching ratio of MSA-SO_4^{2-} (e.g. photochemical production/destruction of $OH^{\bullet}/NO_3^{\bullet}$ radicals; halogen chemistry, especially that of BrO; deposition history (wet and dry) of the air mass).

6.4 Atmospheric ammonia

Ammonia (NH_3) is the primary basic gas in the atmosphere (Seinfeld and Pandis, 1998) and reacts with available acids either on the surface of pre-existing aqueous phase aerosol, or as part of new particle formation. In the aqueous phase (i.e. as ammonium, NH_4^+), it has also been shown to influence the pH of natural rainwater, neutralising some of the acidity contributed by the dissociation of acidic gases such as CO_2 and SO_2 (Charlson and Rodhe, 1982). Ultimately, both aerosol and rainwater are deposited back to the earth's surface and, whether deposited to the ocean or to the land, the nitrogen deposited is a key nutrient for most biological systems (e.g. Schlesinger, 1991; Owens et al., 1992).

Much of Chapter 1, which details the air-sea flux and the cycling of NH_3 within the lower atmosphere (Sections 1.1.2 and 1.3.2 respectively), covers background information relevant to this section's results. In summary, the key influences upon the strength and direction of the NH_3 flux are the relative balance of atmospheric and oceanic concentrations, although ocean temperature also plays a significant role (Johnson, 2004). This is best illustrated using Figure 6.8, which demonstrates the equilibrium (Henry's law) lines for various ocean and atmosphere NH_3/NH_X concentrations at a variety of temperatures. Certain simultaneous field measurements in the atmosphere/ocean have also suggested that the ocean may be a source of NH_3 to the atmosphere (Quinn et al., 1988; Gibb et al., 1999a). Nitrogen stable isotope measurements of aerosol NH_4^+ provide further evidence, indicating that the ocean is a source of NH_3 and contributes isotopically lighter nitrogen (as NH_3) to the atmosphere (Jickells et al., 2003).

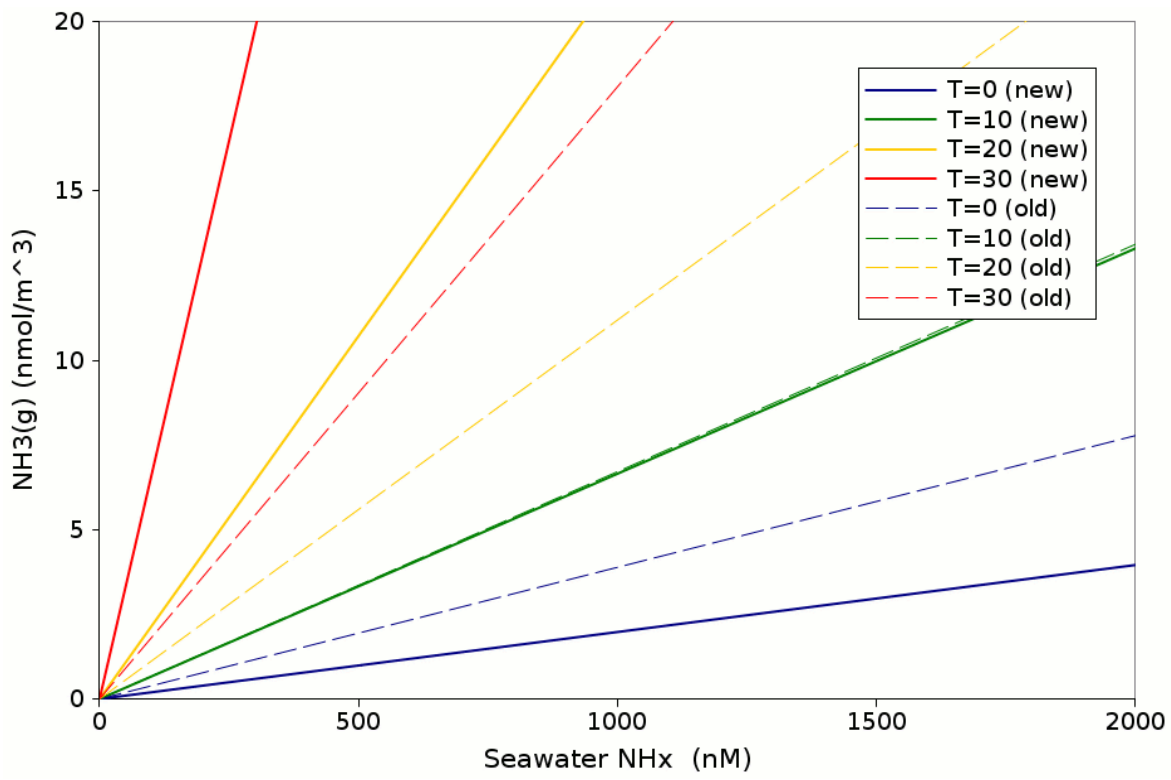

Figure 6.8 Henry's Law (H_C) equilibrium between atmosphere and ocean over a range in ocean temperatures. At each relevant temperature, above the line represents a flux INTO the ocean, while below the line represents a flux OUT of the ocean. *Old* (dashed lines) refers to H_C using the incorrect pKa formulation from Khoo et al. (1977) while *New* (solid lines) refers to H_C calculated using the correct pKa formulation (Johansson and Wedborg, 1980). Note $NH_X = NH_3 + NH_4^+$. Figure courtesy of Martin Johnson (*Pers. Comm.*).

High resolution (i.e. every 10 min) atmospheric NH_3 measurements have recently been published from the Aerosols99 cruise in the Atlantic (Norman and Leck, 2005). Over a three-day period in the temperate South Atlantic, the atmospheric NH_3 measurements exhibited diel variation, unrelated to changes in boundary layer height, and the authors suggest this may be due to variations in oceanic source strength. Unfortunately concurrent oceanic measurements were not made and thus no fluxes are presented. However, typical atmospheric NH_3 concentrations in the South Atlantic and Indian Oceans were low (typical range = 1.1 and 3.2 nmol m^{-3}), which would likely facilitate an ocean to atmosphere flux (Norman and Leck, 2005). In contrast, the cold, high-latitude waters sampled by Johnson (2004) in the northern North Sea and northeast Atlantic in December 2001, led to a consistent flux into the ocean, despite atmospheric NH_3 levels similar to those observed by Norman and Leck (2005).

Figure 6.9a shows the air-sea flux of NH_3 during AMT-14 and, for this plot and all subsequent plots, a positive flux is OUT of the ocean into the atmosphere, and a negative flux is INTO the ocean from the atmosphere. Unfortunately no oceanic pH measurements (required for the flux calculation, see Section 1.1.2 for details) were made on the AMT-14 transect and thus it was necessary to approximate pH in order to calculate the NH_3 flux. Two values were used so that the impact of a potential yet realistic change in pH on the flux calculation could be identified (Figure 6.9a). For many high latitude regions, an equivalent change in pH would not have a significant impact upon the direction of the NH_3 flux. However, as can be seen in the sub-tropical and tropical waters sampled, a change of 0.2 pH units significantly impacts upon the NH_3 flux, often changing its direction (Figure 6.9a). In order to discuss the NH_3 flux results further, we must examine the detail behind the flux calculation, in particular the influence of the atmospheric and oceanic concentrations (Figure 6.9b&c respectively) and seawater temperature (Figure 6.9d).

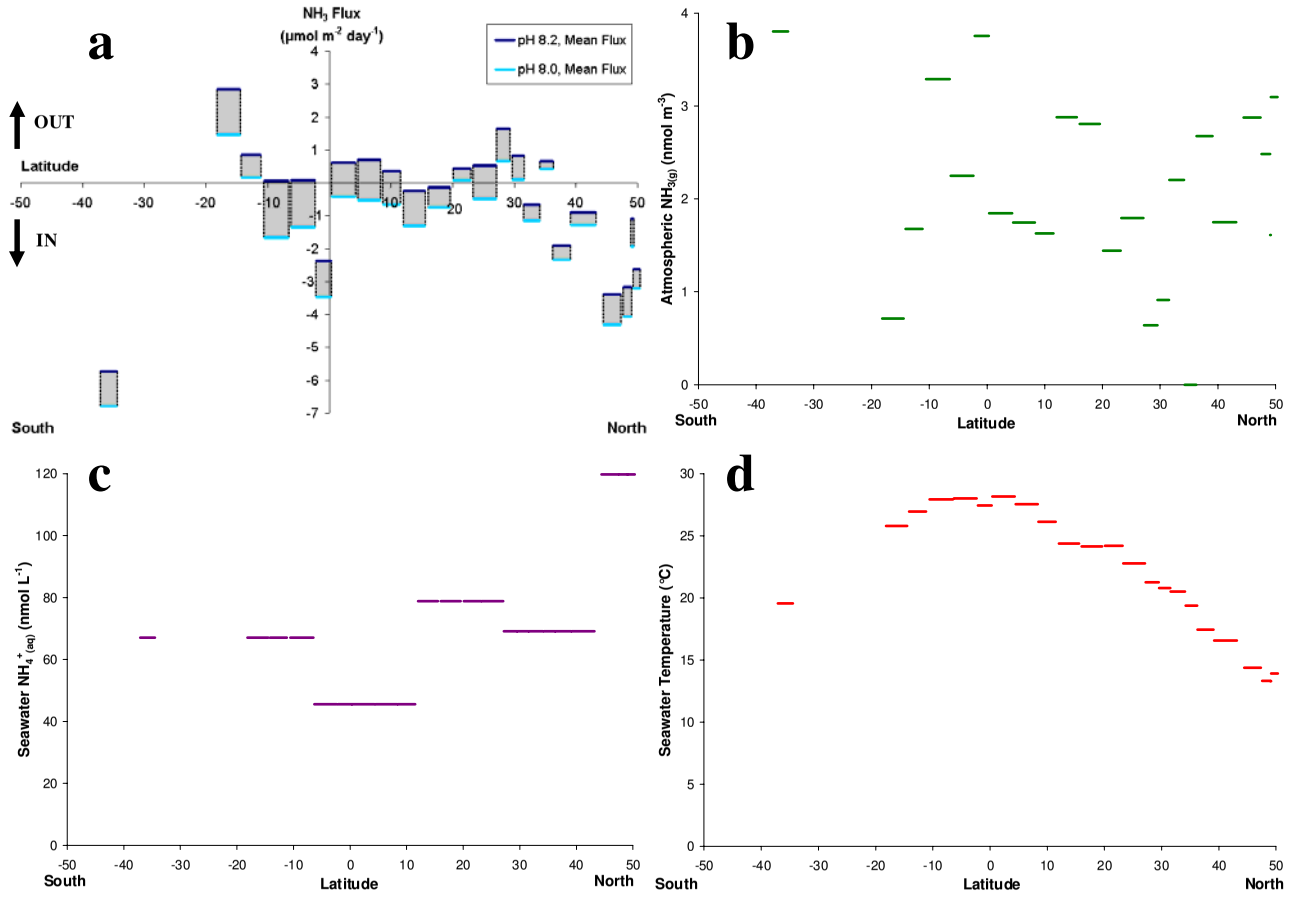

Figure 6.9 NH_3 flux (a; blue lines); mean atmospheric $NH_{3(g)}$ from two blank-corrected filter packs (b; green lines); seawater $NH_4^+{}_{(aq)}$ (c; purple lines); and seawater temperature (d; red lines), along the AMT-14 transect. A negative flux represents a flux into the ocean and vice versa. As no oceanic pH measurements were made throughout the cruise, it was necessary to approximate the pH; two appropriate pH values were used in (a) for comparative purposes, pH 8 (light blue) and pH 8.2 (dark blue). The data in plots (b), (c) and (d) represent the values used for the flux calculation.

When examining Figure 6.9b, the most striking point is the relative consistency of the atmospheric NH_3 concentrations, ranging between < 1 and 4 nmol m^{-3}. Encouragingly, these measurements are the same order of magnitude as those recently published for similar parts of the Atlantic (Norman and Leck, 2005). As expected, average seawater NH_4^+ concentrations were consistently low (< 100 nM) for the majority of the cruise. Perhaps the salient point to take from this plot is the effect of temperature on the NH_3 flux. There are parts of the AMT-14 transect that, in terms of atmospheric and oceanic concentrations, are very similar yet their fluxes are in opposing directions; e.g. 12°S versus 40°N. This difference is caused by temperature; a flux out of the ocean in warm, 27°C, waters and vice versa for colder, 17°C, waters (Figure 6.9a&d).

A final point is the range of potential fluxes that can be achieved with data from this study. For the majority of environmental conditions encountered and regions sampled, the NH_3 flux is finely poised and could potentially be into or out of the ocean (Figure 6.10). Limits of concentration for atmospheric and oceanic concentrations were used to calculate maximum and minimum fluxes (plus intermediates). The atmospheric upper and lower limits were calculated using the error of each sample (calculated using two standard deviations of the average blank filter) to set minimum and maximum atmospheric concentrations. The oceanic limits were identified as the minimum and maximum surface concentrations measured throughout the sampling period (defined by the duration of each atmospheric sample collection; see Section 6.2.2). The extreme fluxes (*Min. Air, Max. Ocean* and *Max. Air, Min. Ocean*) are unlikely to be representative but define the 'flux bracket' for each sampling period. The intermediate combinations provide an indication of the more likely direction and magnitude of each calculated flux.

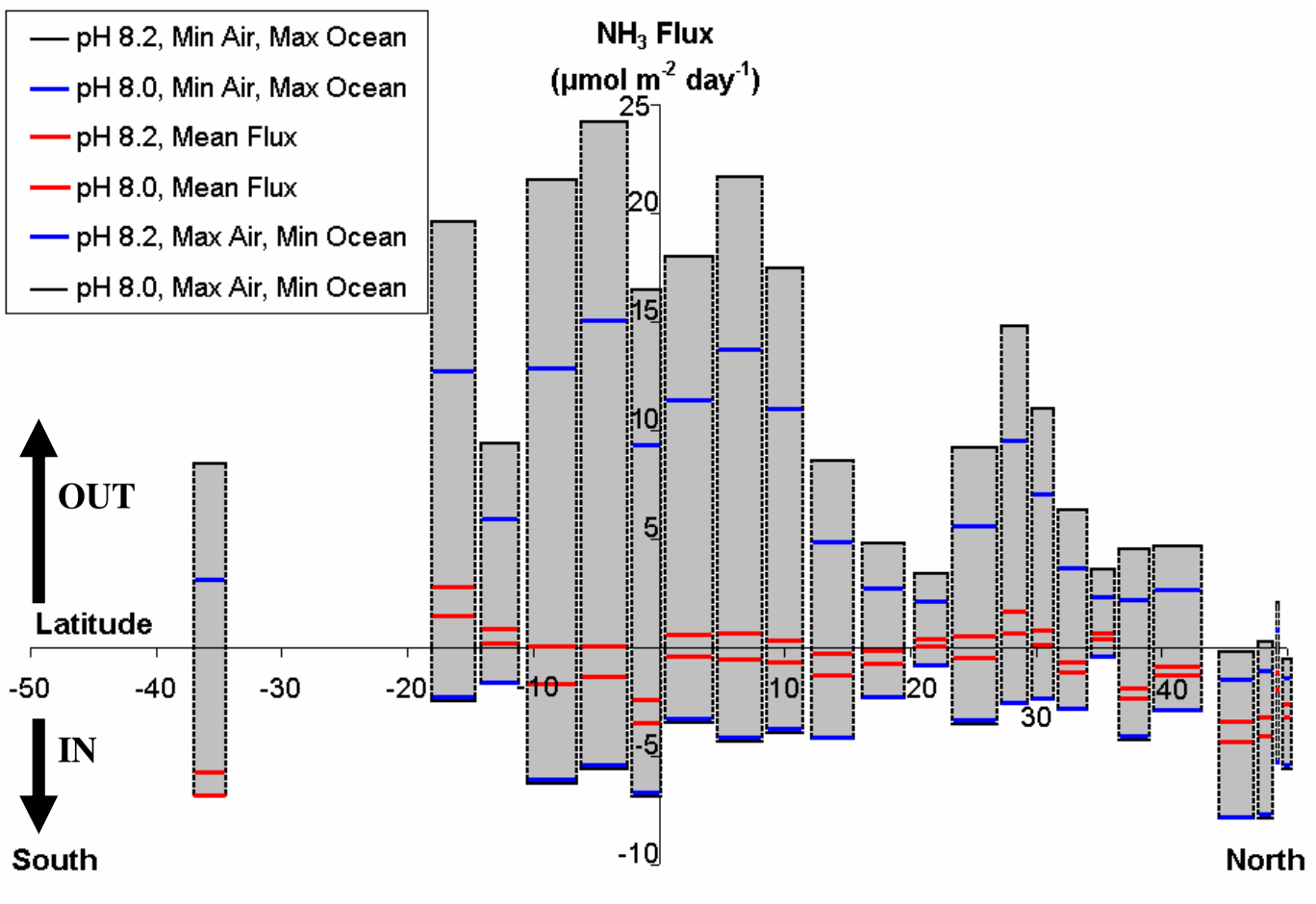

Figure 6.10 The range of possible NH_3 fluxes along the AMT-14 transect; a negative flux represents a flux into the ocean and vice versa. Thick red lines represent the mean fluxes, with thinner lines used as the combination of oceanic and atmospheric concentrations become more extreme (black more extreme than blue). Please note that some of the fluxes into the ocean overlay on top of each other and thus cannot be seen.

The main point from Figure 6.10 is that, even with one set of analysis, the potential range in flux (and even direction) is relatively substantial due to the methods used. Whilst quick to perform, the existing method of analysis for ocean concentrations is often difficult to operate at very low levels. In addition, ambient nitrogen (especially NH_4^+) in surface waters has a high turnover rate and thus measured concentrations can change significantly over very short timescales. This contrasts strikingly with the method of atmospheric NH_3 analysis, which can require up to 36 hrs per sample. By far the biggest source of analytical error for atmospheric sampling is the variation in blank filter concentration, and this introduces large uncertainties in any measurements made in low-concentration atmospheric NH_3 regions. As such, the ocean-atmosphere NH_3 flux along the AMT-14 transect ranges from -6.8 to +24.2 μmol m^{-2} day^{-1} and its direction and magnitude are difficult to quantify with confidence.

6.5 A linkage between atmospheric nitrogen and sulphur cycles?

The atmospheric aerosol composition data collected by Covert (1988) and in particular Quinn et al. (1990) has lead to the suggestion that the reduced nitrogen and sulphur cycles in remote marine environments might be linked between the ocean and atmosphere (Quinn et al., 1990; Liss and Galloway, 1993). The data of Quinn et al. (1990) demonstrate a NH_4^+:$nssSO_4^{2-}$ aerosol composition ratio consistently close to one, a partially neutralised sulphate aerosol (ammonium bisulphate, NH_4HSO_4). The authors suggested this might be due to a link between the factors controlling the production and flux of biogenically mediated NH_3 and $nssSO_4^{2-}$ (in this case, DMS-derived SO_4^{2-}). However, no correlations between seawater DMS and NH_3 concentrations and fluxes were observed, although the fluxes were in the same direction and of the same order of magnitude (Quinn et al., 1990). Liss and Galloway (1993) took the concept of a linkage between the cycles a step further, suggesting that marine micro-organisms might switch from glycine betaine (GBT, an osmolyte and the nitrogen analogue of DMSP) to DMSP during periods of nitrogen limitation and that this might explain the atmospheric coupling.

Since the initial study of Quinn et al. (1990), a comprehensive survey in remote regions of oceanic NH_3 and DMS concentrations, their fluxes and the atmospheric composition of marine aerosol has not been carried out. Numerous studies have measured the atmospheric composition of remote marine aerosol; these are summarised later in this section and are therefore not discussed in any detail here. The AMT programme represented an opportunity to make relevant sulphur and nitrogen measurements in the remote marine environment, and an examination of these results is now presented. Statistical analysis was performed on the oceanic reduced sulphur and nitrogen data collected during AMT cruises -12, -13 and -14. Spearman's Rank correlation analysis showed very weak but statistically significant correlations of NH_4^+ with DMSPd (Spearman's $\rho = 0.25$, $\alpha < 0.01$; $n = 116$) and DMSPp (Spearman's $\rho = 0.39$, $\alpha < 0.001$; $n = 129$) in the surface (mixed layer) of the ocean. No significant correlation was observed between oceanic DMS and NH_4^+. These results indicate that there is little direct correlation between the reduced sulphur and nitrogen cycles in the surface ocean for the remote regions studied.

As stated in Section 6.1, technical difficulties with equipment for measuring both atmospheric NH_3 and oceanic NH_4^+ meant that NH_3 fluxes could only be calculated for AMT-14. Figure 6.11 presents a visual comparison of the DMS and NH_3 fluxes from AMT-14; as in previous sections a positive flux is out of the ocean and vice versa. At high latitudes, the NH_3 flux, as discussed in Section 6.4, is always likely to be into the ocean due to low seawater temperatures. In contrast, the concentration gradient for DMS is always such that the flux will be out of the ocean. Any linkage between the fluxes is therefore only really likely in warmer low latitude waters. It is difficult to identify any consistent trends in the NH_3 and DMS fluxes, even when focussing upon the lower latitude regions (Figure 6.11).

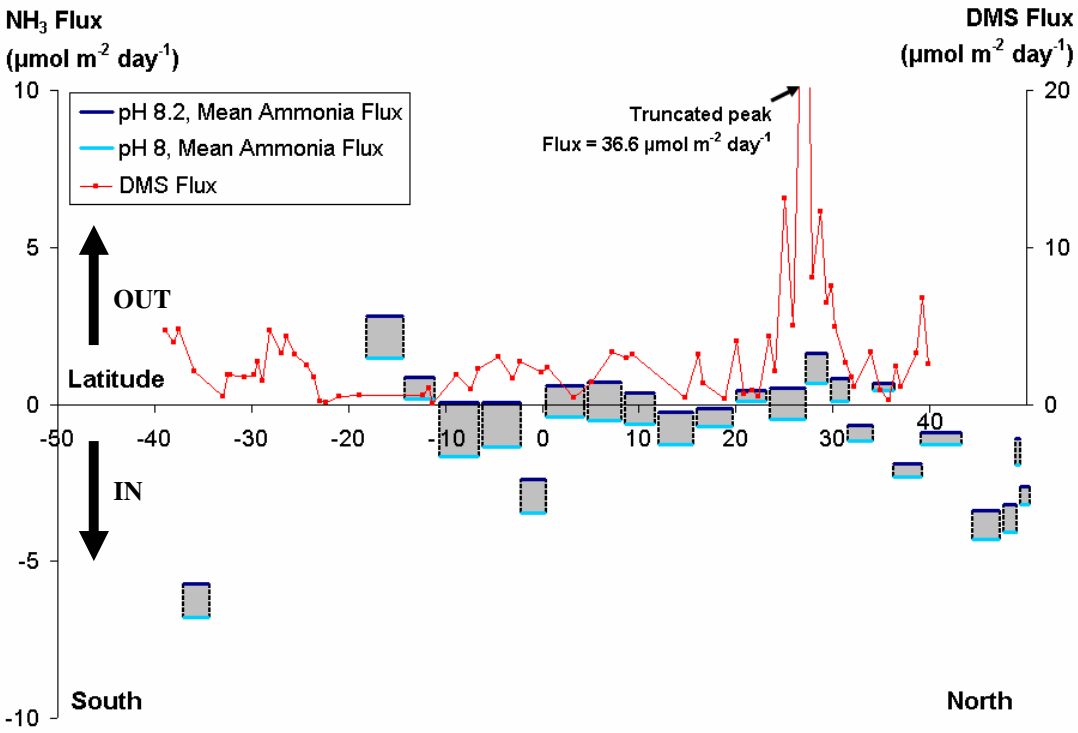

Figure 6.11 The fluxes of NH_3 (blue lines) and DMS (red line and dots) along the AMT-14 transect; a negative flux represents a flux into the ocean and vice versa. Two NH_3 fluxes are presented representing different assumed pH values (see Section 6.4 for detail).

No consistent linkages in atmospheric gaseous concentrations or fluxes could be seen for NH_3 and DMS, so the next step is to analyse the atmospheric aerosol data collected during AMT. On the proceeding three pages, fine mode (<1 µm diameter) aerosol NH_4^+ and $nssSO_4^{2-}$ concentrations and air mass back trajectories for samples collected during AMT-12, -13 and -14 are presented (Figure 6.12, Figure 6.13 and Figure 6.14, respectively). Fine mode aerosol data is presented as the majority of gas-to-particle conversion is generally considered to produce sub-micron particles. However, it should be noted that this concept has been contested (O'Dowd et al., 1997b; Cainey and Harvey, 2002) because low vapour pressure gases such as SO_2 readily condense onto pre-existing aerosol surfaces and it is suggested that their size distribution may therefore be dominated by coarse mode particles (> 1 µm diameter). All three cruises are presented in the same manner, with part (a) of each plot displaying 5-day air-mass back trajectories colour-coded as per the dominant influence on the air mass composition (as defined in Section 6.2.4). Part (b) of each plot displays, in the same manner as Quinn et al. (1990), the measured NH_4^+ and $nssSO_4^{2-}$ concentrations in aerosol and uses the same colour coding as part (a).

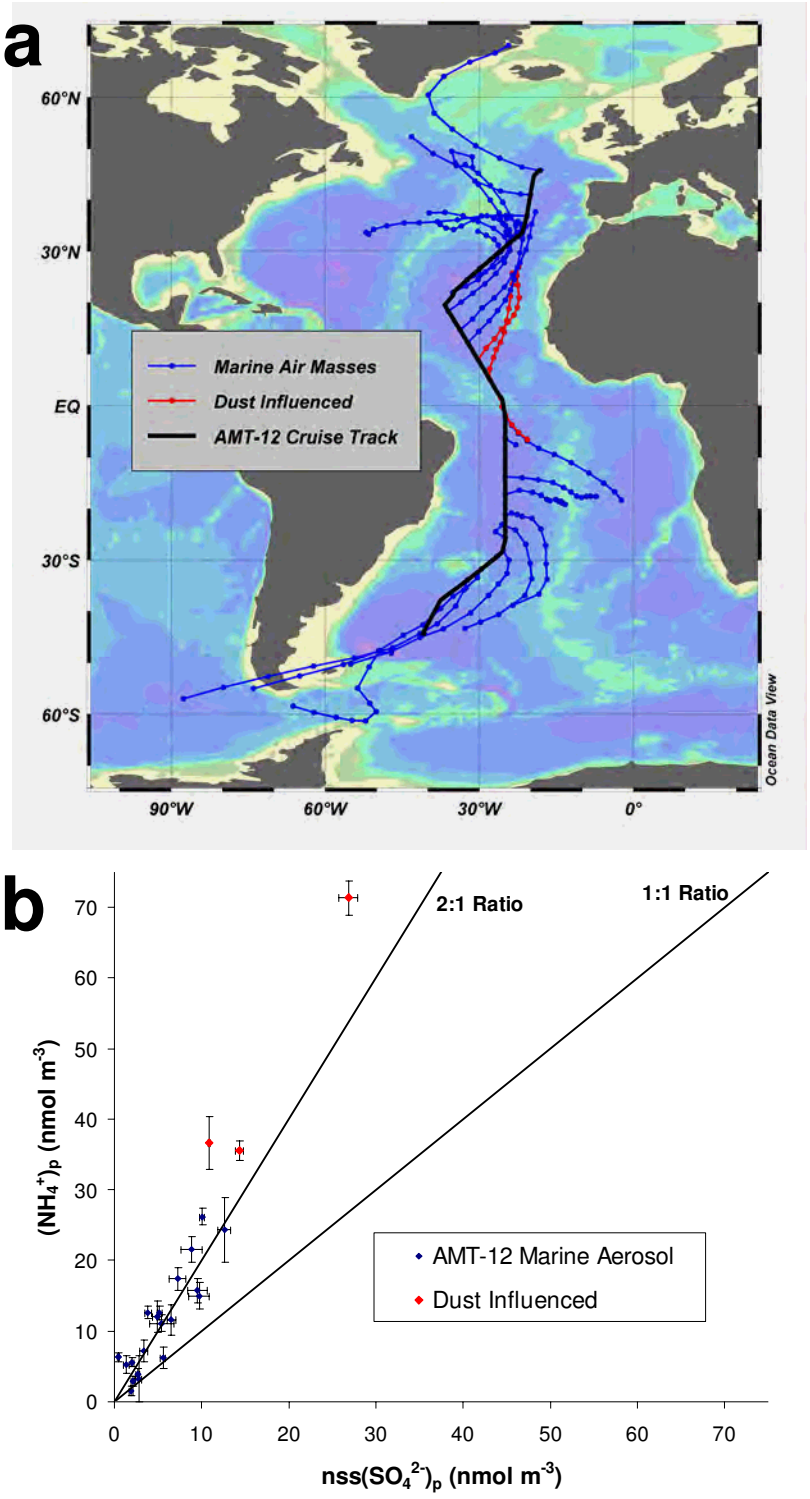

Figure 6.12 Part (a) displays 5-day air mass back trajectories at 15 m above mean sea level for AMT-12 samples, each dot representing half a day. Samples are colour-coded depending on whether they were deemed 'Marine' (blue) or Saharan 'Dust' influenced (red) using criterion defined in Section 6.2.4. Part (b) displays the concentration of particulate $nssSO_4^{2-}$ vs. NH_4^+ in each (<1 µm) sample, colour-coded as in (a). Error bars represent one standard deviation. Solid lines are the aerosol composition lines for $(NH_4)_2SO_4$ (2:1) and NH_4HSO_4 (1:1).

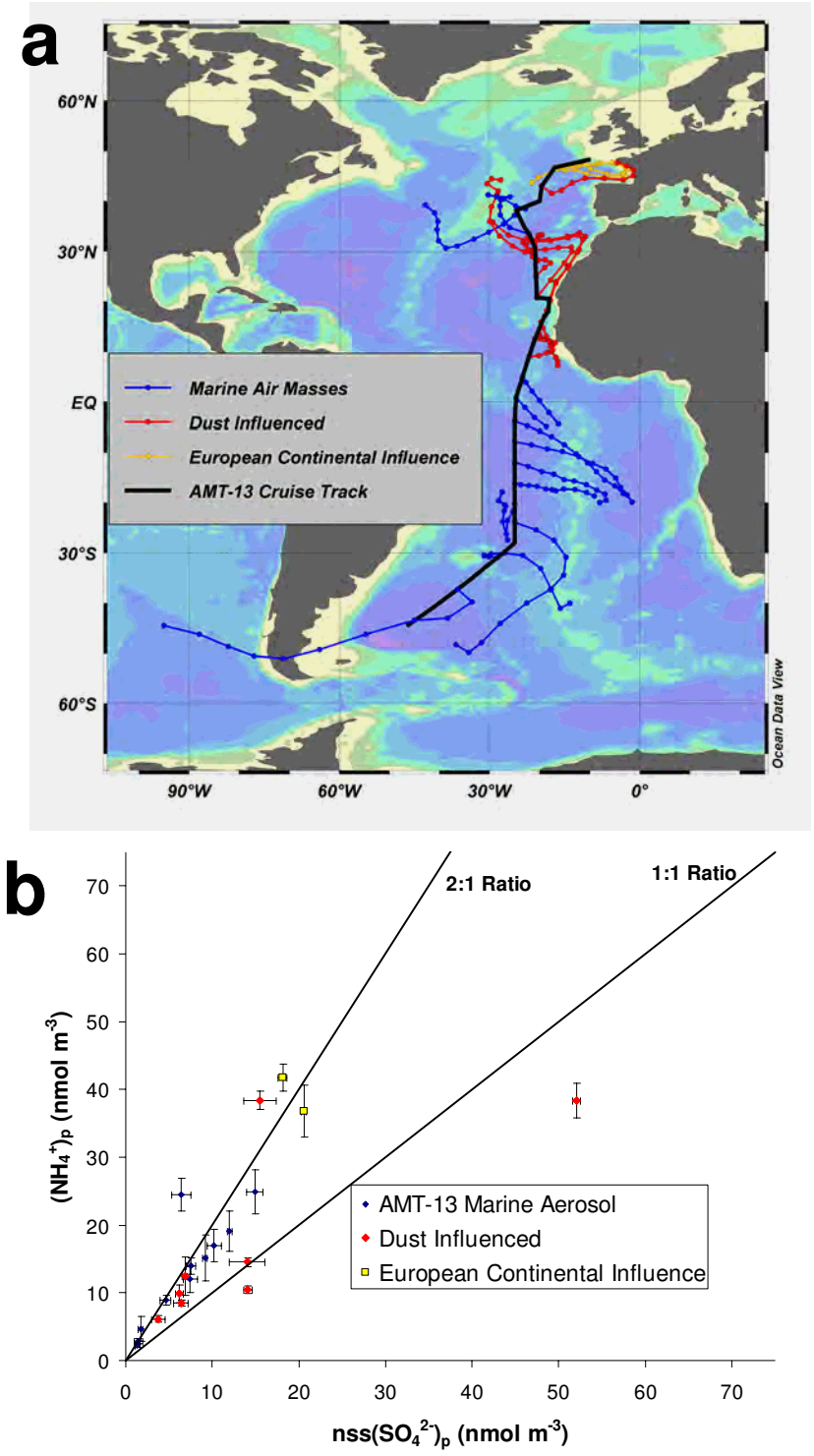

Figure 6.13 Part (a) displays 5-day air mass back trajectories at 15 m above mean sea level for AMT-13 samples, each dot representing half a day. Samples are colour-coded depending on whether they were deemed 'Marine' (blue), Saharan 'Dust' influenced (red), or 'European Continental' influenced (yellow) using the criterion defined in Section 6.2.4. Part (b) displays the concentration of particulate $nssSO_4^{2-}$ vs. NH_4^+ in each (<1 µm) sample, colour-coded as in (a). Error bars represent one standard deviation. Solid lines are the aerosol composition lines for $(NH_4)_2SO_4$ (2:1) and NH_4HSO_4 (1:1).

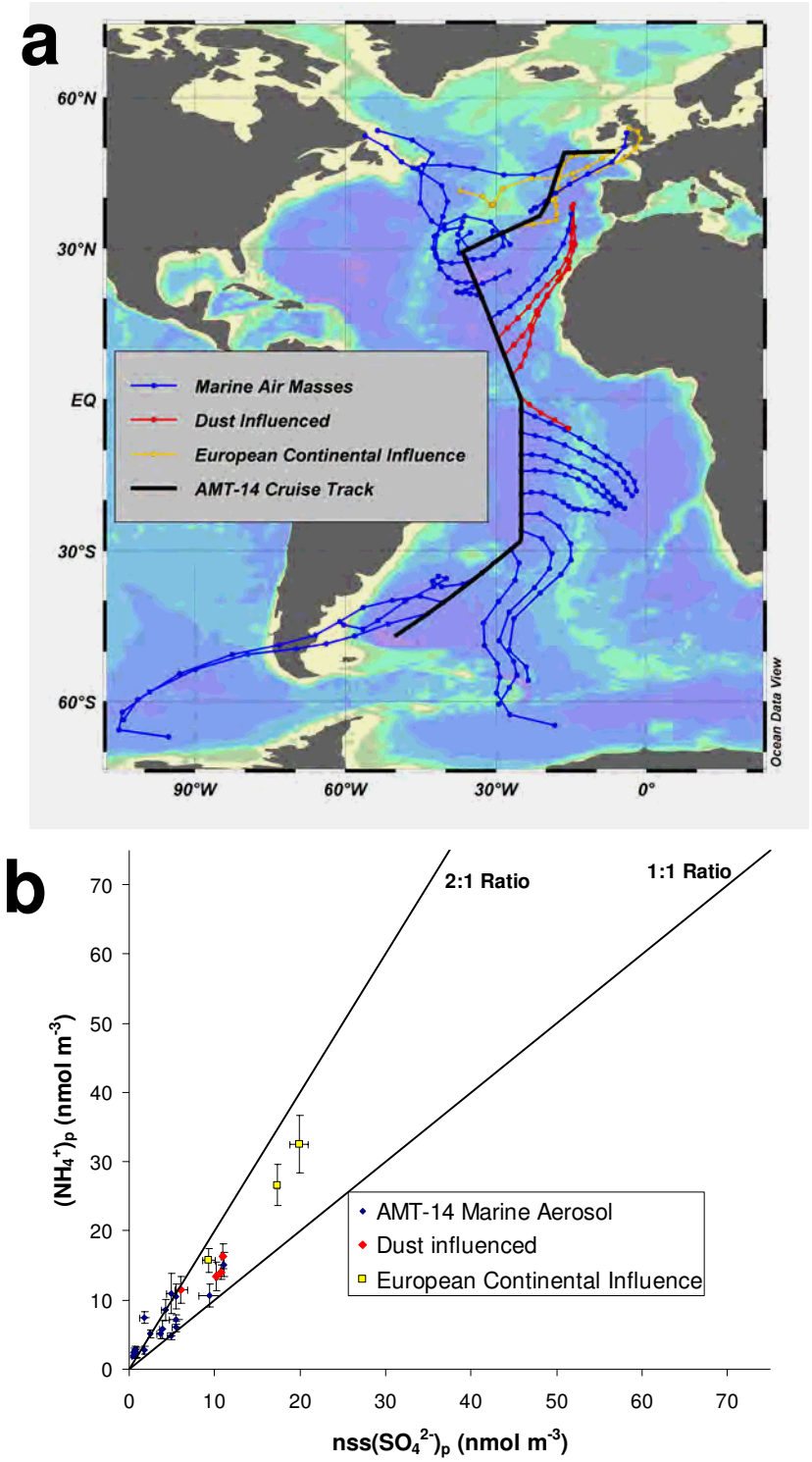

Figure 6.14 Part (a) displays 5-day air mass back trajectories at 15 m above mean sea level for AMT-14 samples, each dot representing half a day. Samples are colour-coded depending on whether they were deemed 'Marine' (blue), Saharan 'Dust' influenced (red), or 'European Continental' influenced (yellow) using the criterion defined in Section 6.2.4. Part (b) displays the concentration of particulate $nssSO_4^{2-}$ vs. NH_4^+ in each (<1 µm) sample, colour-coded as in (a). Error bars represent one standard deviation. Solid lines are the aerosol composition lines for $(NH_4)_2SO_4$ (2:1) and NH_4HSO_4 (1:1).

As can be seen, the majority of air masses sampled during AMT cruises -12, -13 and -14 could be defined as 'Marine' (Figure 6.12, Figure 6.13 and Figure 6.14). When addressing the concept that the nitrogen and sulphur cycles may be linked in remote marine regions, we are really only interested in these air masses. To aid interpretation, the fine mode NH_4^+:$nssSO_4^{2-}$ ratios of all remote air masses have therefore been plotted on the same graph (Figure 6.15), leaving aside any air masses with a terrestrial influence (i.e. European continent or Saharan Dust). Inset on Figure 6.15 are the results from Quinn et al. (1990) for comparison; on this plot, the remote air mass samples (labelled as **3**) can be seen to fall between the 2:1 and 1:1 composition lines. In contrast, the AMT results tend to fall closer to the 2:1 composition line, while the mean (± 1 standard error) fine mode NH_4^+:$nssSO_4^{2-}$ ratio for all marine AMT air masses is 2.4 ± 0.6.

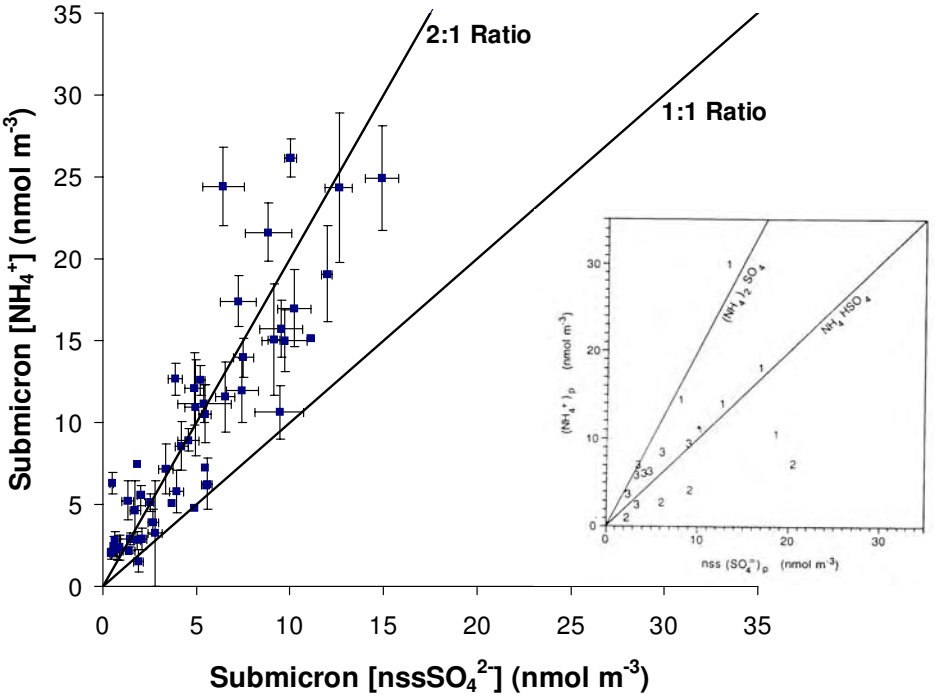

Figure 6.15 Particulate, sub-micron concentrations of $nssSO_4^{2-}$ versus NH_4^+ in each marine sample from AMT cruises -12, -13 and -14. Error bars represent one standard deviation. Solid lines indicate the aerosol composition lines for $(NH_4)_2SO_4$ (2:1) and NH_4HSO_4 (1:1). Inset is Figure 8 from Quinn et al. (1990), which has the same axes, scales and aerosol composition lines. The equivalent remote marine samples were labelled as **3** on this plot (Quinn et al., 1990).

From Figure 6.15, it appears that the Atlantic marine aerosol has a reasonably consistent NH_4^+:$nssSO_4^{2-}$ ratio and a lot of the points plot close to the 2:1 ratio line, indicating almost complete neutralisation of sulphate acidity. This is in contrast to the Pacific data of Quinn

et al. (1990), which suggest only partial neutralisation of the sulphate aerosol. However, as indicated by the average AMT ratio, a substantial number of data points plot above the 2:1 ratio line. On Figure 6.15 this is less obvious as many of the points are at the low end of both axes and therefore do not immediately appear distant from the 2:1 composition line. A more informative plot is a boxplot of the ratios, as this presents the data without the influence of high or low concentrations misleading the eye; Figure 6.16 presents all the AMT data (including terrestrially influenced samples) in this manner, with the data divided by source region as described in Section 6.2.4.

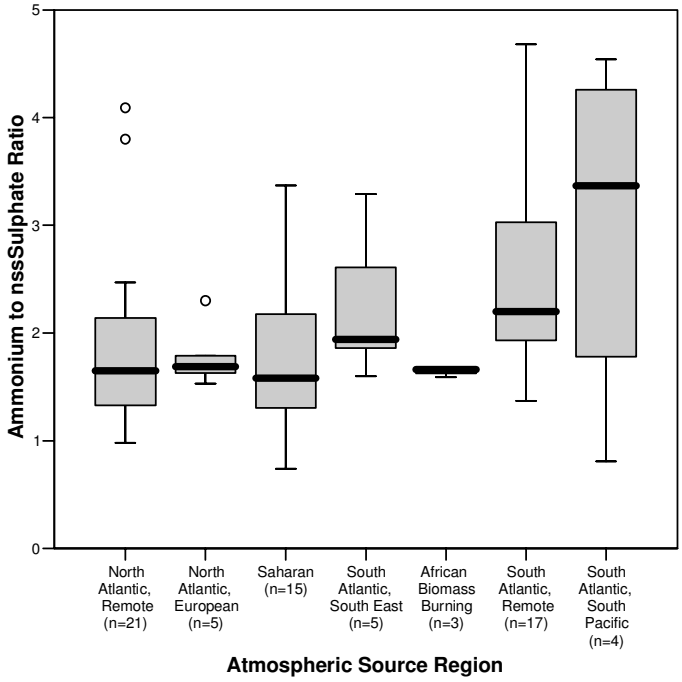

Figure 6.16 Boxplot of fine mode (<1 µm) NH_4^+:nssSO_4^{2-} ratios for the seven source regions along the AMT transect for AMT cruises -12, -13 and -14. Bold lines represent the median value; box length represents the interquartile range (IQR); error bars represent the data range excluding outliers. Circles represent outlying data, defined as 1.5 times the IQR or greater. (**n**) represents the number of samples per source region. On this plot, one extreme case is not shown for the *South Atlantic Remote* source region (value = 12.91).

Interestingly, many of the different source region median values are equal to or below a 2:1 ratio, i.e. an incomplete neutralisation of acidic sulphate aerosol (Figure 6.16). Another critical point is that, in general, values increase for data collected in the southern hemisphere, with error bars (representing the data range excluding outliers) extending as high as 4.5 in these regions. The *African Biomass Burning* and *South Atlantic / South Pacific* source region plots can, to some extent, be explained by the fact that there are very

few data points from these regions, but this explanation cannot be used for the *South Atlantic, Remote* source region (17 samples). To understand Figure 6.16 better, it is useful to examine equivalent boxplots of NH_4^+ and $nssSO_4^{2-}$ concentrations (Figure 6.17a&b). From these, it is evident that very little NH_4^+ or $nssSO_4^{2-}$ was present in aerosol for the *South Atlantic, Remote* air masses. Therefore only small changes in concentration would be required to produce a large change in aerosol composition ratio.

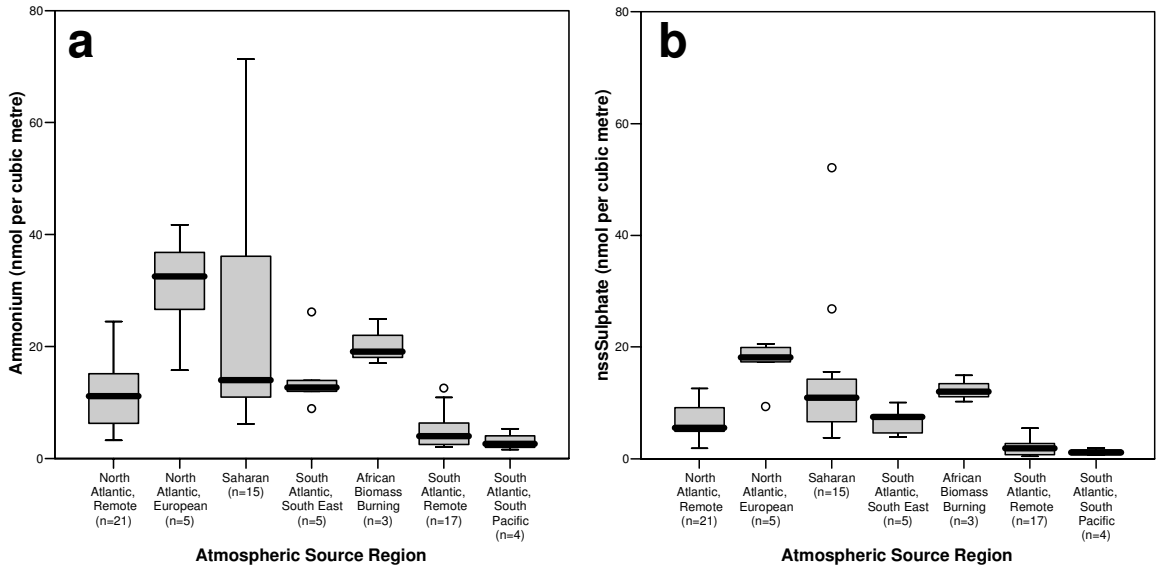

Figure 6.17 Boxplots of fine mode (<1 µm) concentrations of NH_4^+ (a) and $nssSO_4^{2-}$ (b) for the seven source regions along the AMT transect for AMT cruises -12, -13 and -14. Bold lines represent the median value; box length represents the interquartile range (IQR); error bars represent the data range excluding outliers. Circles represent outlying data, defined as greater than 1.5 times the IQR. (**n**) represents the number of samples per source region.

In summary, the AMT data collected appears to have a higher NH_4^+:$nssSO_4^{2-}$ ratio than that observed by Quinn et al. (1990), with many aerosols samples' fine mode $nssSO_4^{2-}$ acidity fully neutralised by NH_4^+. In addition, many truly remote air masses sampled from the *South Atlantic, Remote* and *South Atlantic / South Pacific* source regions demonstrate ratios greater than 2:1. Whilst this may in part be driven by the lower NH_4^+ and $nssSO_4^{2-}$ concentrations present in these aerosol samples creating more extreme ratio values, it also suggests an additional source of acidity in order to prevent loss of NH_3. It was therefore decided to investigate the fine mode net acidity of the AMT samples (see next section).

Net acidity in aerosol

It is currently impossible to measure the pH of an aerosol directly, and an ion balance approach (whereby H^+ concentration is estimated based on the charge balance) is difficult as it is unlikely that all chemical species have been measured. As a result, the basic formulation used for calculating net acidity (units = charge equivalents) in an aerosol is as follows:

$$Net\ Acidity = \sum Major\ Acid\ Species - \sum Major\ Alkaline\ Species$$

Equation 6.2

The major acidic species used are: hydrochloric acid, HCl, represented by $nssCl^-$ concentration; nitric acid, HNO_3, represented by NO_3^- concentration; and sulphuric acid, H_2SO_4, represented by $nssSO_4^{2-}$ concentration. Further to *Equation 6.2*, a correction had to be made for the following acid-displacement reaction (Brimblecombe and Clegg, 1988):

$$NaCl_{(s)} + HNO_{3(g)} \leftrightarrow NaNO_{3(s)} + HCl_{(g)}$$

Equation 6.3

If the sum of $nssCl^-$ and NO_3^- (*X*) was negative (i.e. more HCl was displaced than was replaced by $HNO_{3(g)}$), it could be assumed that there was no net contribution to acidity from either HNO_3 or HCl. If the sum of $nssCl^-$ and NO_3^- (*X*) was positive (i.e. after the displacement process, some HCl still existed in aerosol), then there is a net contribution to acidity. In this case, *X* is added to the contribution of $nssSO_4^{2-}$ to calculate net acidity. It should be noted that an equivalent reaction to *Equation 6.3* can occur between NaCl and H_2SO_4 but this is far less dominant (Seinfeld and Pandis, 1998). It is likely that either this reaction and/or the error propagated in calculating *X* are the causes for negative values of *X*.

The major basic species used in *Equation 6.2* are ammonia, NH_3, represented by NH_4^+ concentration; carbonate (CO_3^{2-}) from calcium carbonate in dust, represented by $2\times nssCa^{2+}$ concentration (this assumes that all $nssCa^{2+}$ is from $CaCO_3$); and bicarbonate (HCO_3^-) from seawater, represented by *Equation 6.4*:

$$\left[HCO_3^-\right]_{SW} = \left[Na^+\right] \times \left(\frac{\left[HCO_3^-\right]}{\left[Na^+\right]} \right)_{SW}$$

Equation 6.4

where the subscript *SW* represents 'in seawater'. This assumes that all sodium (Na^+) in the atmosphere is from the ocean and that the HCO_3^- to Na^+ ratio in the sea salt aerosol formed is the same as in the ocean, 4.915×10^{-3} (taken from Libes, 1992).

Some of the species and processes described above are mainly in the aerosol coarse mode ($nssCa^{2+}$ from dust, sea salt displacement of HCl, and sea salt contribution of sea salt HCO_3^-). However, only the sub-micron aerosol is focussed on here as the NH_4^+:$nssSO_4^{2-}$ ratio presented is also for sub-micron aerosol. The coarse mode processes are still relevant however, as the <1 µm cut off size inevitably results in some coarse mode collection because the size distribution peaks of coarse and fine mode aerosol overlap.

Using the information and equations above, the net acidity was calculated for the fine mode (<1 µm) aerosol during AMT cruises -12, -13 and -14. As can be seen, the variability in acidity was much greater in the northern part of each cruise transect and more balanced at the southern end (Figure 6.18).

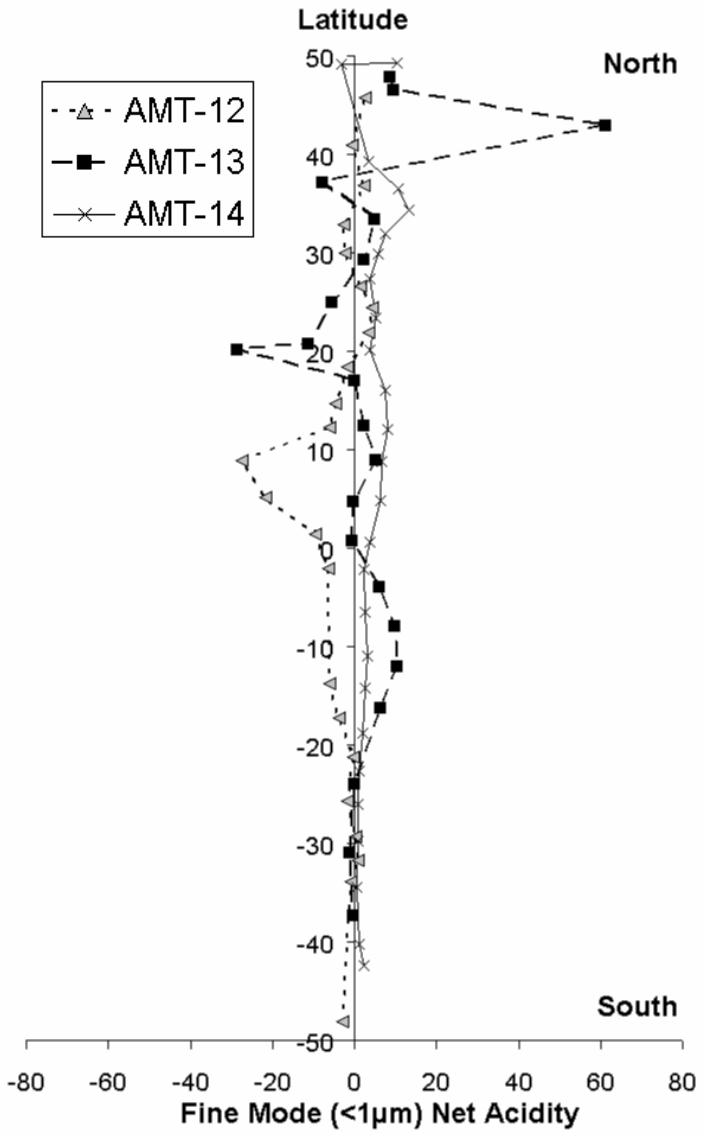

Figure 6.18 Latitudinal distribution of net fine mode (<1 µm) acidity in charge equivalents, calculated using *Equation 6.2* and *Equation 6.4* for AMT-12 (grey triangles); AMT-13 (filled squares); and AMT-14 (crosses).

The data shown in Figure 6.18 has been re-plotted in boxplot form with the air mass source regions distinguished (Figure 6.19). Although Figure 6.19 does not help us to understand the data much more, it does confirm that the net acidity of aerosol samples from the *South Atlantic, Remote* and *South Atlantic / South Pacific* source regions was relatively close to zero. These samples had a NH_4^+:$nssSO_4^{2-}$ ratio greater than two, but it is likely that once $nssSO_4^{2-}$ was fully neutralised, any excess NH_4^+ reacted with HNO_3 to form NH_4NO_3 (Seinfeld and Pandis, 1998). This has implications for the ability of aerosol to attract moisture and form cloud condensation nuclei (CCN) and demonstrates that, should the sea-to-air flux of DMS and thus $nssSO_4^{2-}$ increase, there is NH_3 available to react and form

more effective CCN. Finally, although the *African Biomass Burning* source region had an NH_4^+:nssSO_4^{2-} ratio greater than 2:1, this aerosol also appears to be net acidic (Figure 6.19). It should be noted that the true net acidity in this air mass is likely to also have been influenced by organic acids from biomass burning (Lacaux et al., 1995; Andreae and Merlet, 2001), and these are unaccounted for in *Equation 6.2*.

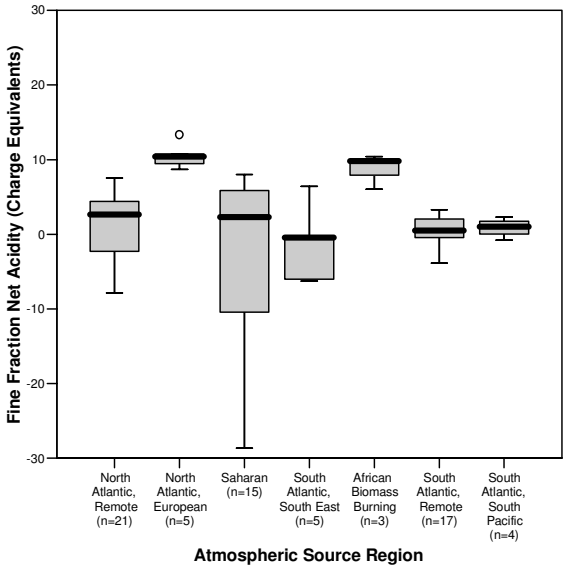

Figure 6.19 Boxplot of fine mode (<1 µm) net acidity for the seven source regions along the AMT transect for AMT cruises -12, -13 and -14. Bold lines represent the median value; box length represents the interquartile range (IQR); error bars represent the data range excluding outliers. Circles represent outlying data, defined as 1.5 times the IQR or greater. (n) represents the number of samples per source region. On this plot, one extreme case is not shown for the *Saharan* source region (value = +61.31).

6.5.1 Global NH_4^+:$nssSO_4^{2-}$ ratios

As mentioned earlier, numerous atmospheric studies have measured the composition of marine aerosol. This section attempts to synthesise as much of this information as possible to improve understanding of the remote marine NH_4^+:$nssSO_4^{2-}$ ratio in aerosol. Initially, the focus was on the Atlantic, combining the AMT-12-14 data already presented with measurements made as part of the following research cruises: AMT-9 (McKee, 2001); JCR 2001 (Baker, A., unpublished, *Pers. Comm.*); Meteor 2002 (Baker, A., unpublished, *Pers. Comm.*); Polarbjörn 1992/93 (Leck et al., 2002a); and Aerosols99 (Norman and Leck, 2005). With the exception of Meteor 2002, which traversed from 60°W to 10°W at 10/11°N in the Atlantic, all of these cruises followed a North-South transect similar to the AMT cruise tracks shown in Section 1.5 (Figure 1.18). For more detail, see the relevant references; for cruises JCR 2001 and Meteor 2002, cruise details can be found in Baker et al. (2003) and Croot et al. (2004) respectively.

As in the previous section, the data was subdivided by source region and it is possible to see how the results are influenced by the additional data (Figure 6.20a&b). When comparing the two plots, the obvious difference is that the 'new' samples have brought the NH_4^+:$nssSO_4^{2-}$ ratio down slightly, although the majority of marine aerosol in the Atlantic still has a ratio between 1:1 and 2:1. The biggest difference between (a) and (b) in Figure 6.20 is that the boxplot of the ratio for the *South Atlantic, Remote* source region has dropped substantially so that the median ratio is now also between 1:1 and 2:1.

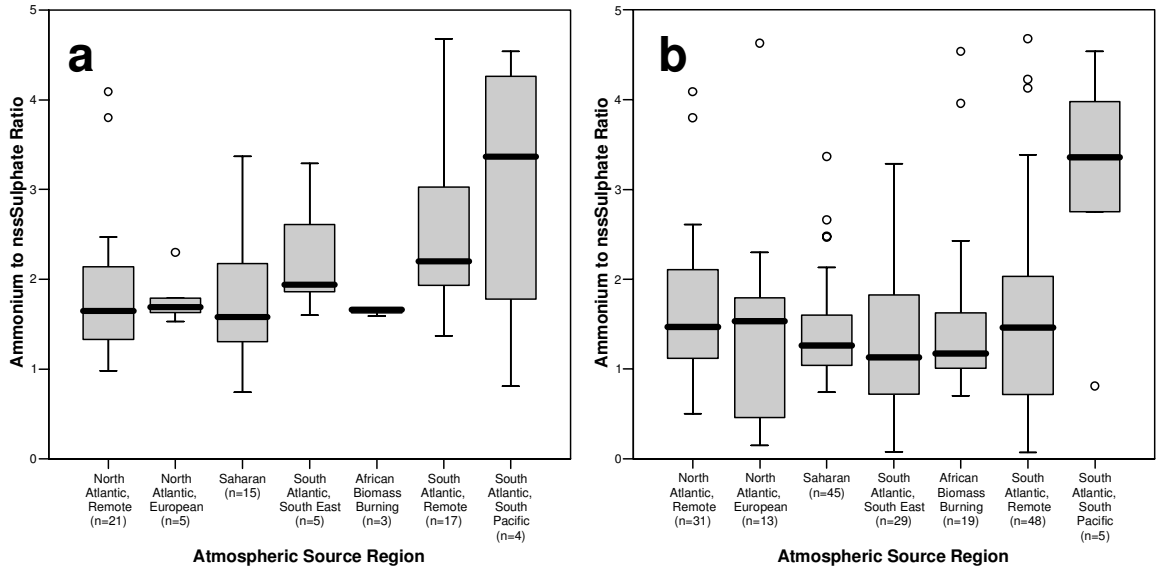

Figure 6.20 Boxplots of fine mode (<1 µm) NH_4^+:nssSO_4^{2-} ratios for seven source regions in the Atlantic using (a) AMT-12-14 data; and (b) AMT-12-14 data plus atmospheric measurements made during the following research cruises: AMT-9 (McKee, 2001); JCR 2001 (Baker, A., unpublished, *Pers. Comm.*); Meteor 2002 (Baker, A., unpublished, *Pers. Comm.*); Polarbjörn 1992/93 (Leck et al., 2002a); and Aerosols99 (Norman and Leck, 2005). Bold lines represent the median value; box length represents the interquartile range (IQR); error bars represent the data range excluding outliers. Circles represent outlying data, defined as 1.5 times the IQR or greater. (**n**) represents the number of samples per source region.

It is possible that a difference in methodology is the reason why the 'new' data reduced the ratio for many of the source regions. Throughout AMT-12-14, the aerosol data collected was filter-fractionated into fine (<1 µm) and coarse (>1 µm) mode. In contrast, during AMT-9 (McKee, 2001), the Polarbjörn 1992/93 cruise and the Aerosols99 campaign, the data was collected using a cascade impactor with a cyclone filter at the inlet to eliminate the larger mode aerosol. Estimates of the size fraction eliminated using such a method vary from > 0.6µm (Quinn et al., 1990) to > 0.9µm (Leck et al., 2002a; Norman and Leck, 2005). Regardless, it is clear that there is the potential to eliminate a greater proportion of the coarse mode marine aerosol using cascade impactor compared to high volume filter-fractionation. As we are interested in the ratio of two chemical species, this might be expected to have little impact upon our results. The conversion of gaseous DMS to SO_4^{2-} aerosol is thought to result predominantly in a sub-micron particle, but there is also evidence that the oxidation of SO_2 by ozone on the surface of coarse mode sea-salt particles may play a role (Sievering et al., 1992; O'Dowd et al., 1997b). In addition, the neutralisation of acidic SO_4^{2-} particles by NH_3 is indiscriminate of particle size and therefore may not display exactly the same size distribution. Thus, methodological

differences resulting in the collection of different size aerosol particles may also impact upon the NH_4^+:$nssSO_4^{2-}$ ratio.

Whilst boxplots such as Figure 6.20 are useful summaries of a large dataset, an examination of all data points within the dataset can provide an alternative perspective (Figure 6.21). What is immediately obvious is that the South Atlantic has significantly lower atmospheric NH_4^+ and $nssSO_4^{2-}$ concentrations (Figure 6.21a&b), likely due to reduced terrestrial influence (both anthropogenic and natural). Despite this, as much if not more scatter is present in the NH_4^+:$nssSO_4^{2-}$ ratios in the South Atlantic compared to the North Atlantic (Figure 6.21c), suggesting that the reduced sulphur and nitrogen cycles in remote regions are not that closely coupled.

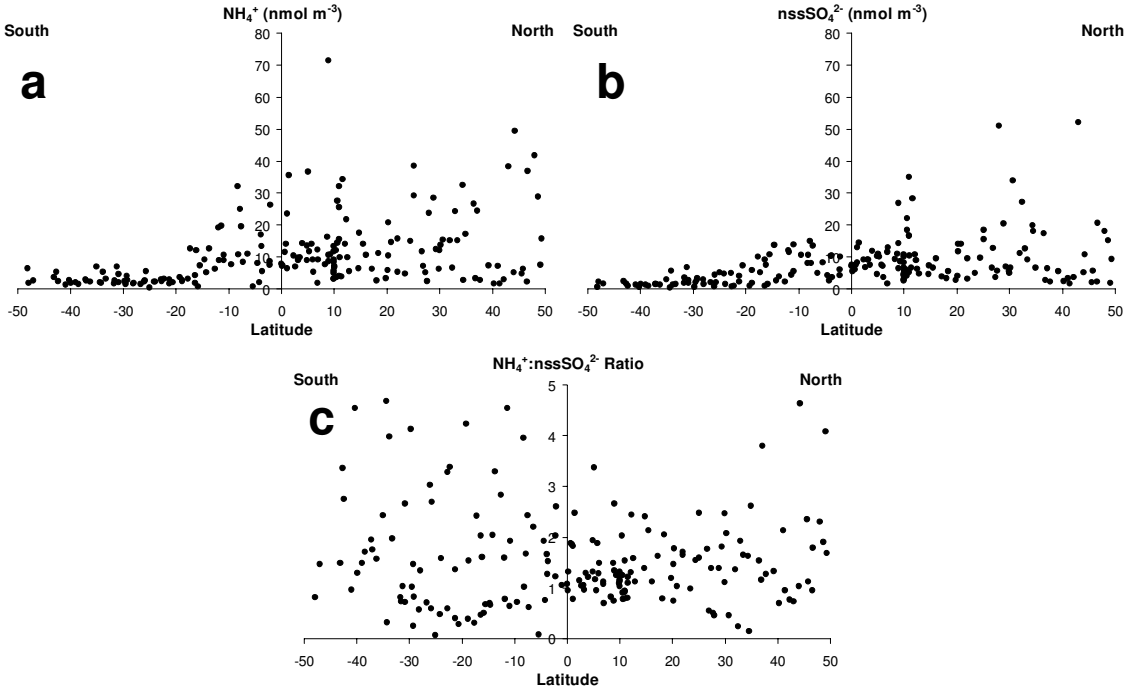

Figure 6.21 Latitudinal distribution of fine fraction (<1 µm) atmospheric concentrations of (a) NH_4^+; (b) $nssSO_4^{2-}$; and (c) the resulting NH_4^+:$nssSO_4^{2-}$ ratio for measurements made as part of the following research cruises in the Atlantic ocean: AMT-9 (McKee, 2001); AMT-12, -13 and -14 (this work); JCR 2001 (Baker, A., unpublished, *Pers. Comm.*); Meteor 2002 (Baker, A., unpublished, *Pers. Comm.*); Polarbjörn 1992/93 (Leck et al., 2002a); and Aerosols99 (Norman and Leck, 2005).

Having looked at the Atlantic data, the subsequent step was to analyse all available data in order to investigate the global NH_4^+:$nssSO_4^{2-}$ composition ratio in remote marine aerosol. Some publications present an inferred NH_4^+:$nssSO_4^{2-}$ ratio, but it was decided to focus only upon those that made direct measurements of NH_4^+:$nssSO_4^{2-}$ concentrations. As a result,

no data was utilised from physical aerosol characterisation methods that have been used to indirectly infer aerosol composition (e.g. Clarke and Porter, 1993; O'Dowd et al., 1997a). Table 6.1 provides a summary of the data used with some brief details about the region sampled and the method of sampling; in total, this data represents more than 1,300 samples from different regions of the global ocean.

In Table 6.1, the second column from the left refers to the size classification of the data and it is immediately apparent that some samples were size-fractionated (via cascade impactor or Moudi sampler), while the majority of data represents bulk samples. As discussed earlier in this section, size-fractionation method differences and differences with bulk sampling could potentially influence the NH_4^+:$nssSO_4^{2-}$ ratio. However, it should be noted that, as gas-to-particle conversion results in sub-micron particles, it is likely that the majority of $nssSO_4^{2-}$ will be in the fine mode aerosol. For the purposes of a global synthesis, it was deemed reasonable to assume that size fractionated and bulk samples could be compared.

Table 6.1 Summary table of data used in global synthesis of the NH_4^+:nssSO_4^{2-} ratio in marine aerosol.

Data Source	Size Classification	Region Sampled	Comment
Allen et al. (1997)	Pre-filter (50% removal of 3.5µm fraction)	Baring Head, South Pacific	
Andreae et al. (1995)	Fractionated with cascade impactor (<1 µm)	Tropical South Atlantic	
Baker, A. (unpublished, *Pers. Comm.*)	Fractionated with cascade impactor (<1 µm)	Atlantic Ocean	5 Cruises (JCR 2001; Meteor 2002; AMT-12; AMT-13; AMT-14)
Berresheim et al. (1991)	Bulk Sample	Western North Atlantic	
Cainey, J. (unpublished, *Pers. Comm.*)	Bulk Sample	Cape Grim, Australia	Routine samples taken by Melita Keywood
Cainey, J. (unpublished, *Pers. Comm.*)	Size Fractionated (Moudi sampler)	Cape Grim, Australia	
Harrison et al. (1996a)	Bulk Sample	North-East Atlantic	Aircraft data (Low Level)
Harrison et al. (1996b)	Bulk Sample	Santa Maria, Azores, Atlantic Ocean	
Huebert et al. (1996)	Bulk Sample	Santa Maria, Azores, Atlantic Ocean	
Huebert et al. (1998)	Bulk Sample	South Pacific / Southern Ocean Cape Grim, Australia	Aircraft data (Boundary Layer)
Leck et al. (2002a)	Cascade impactor and cyclone filter	Atlantic Ocean	
Legrand et al. (1998)	Bulk Sample	Antarctica	
McKee (2001)	Cascade impactor and cyclone filter	Atlantic Ocean (AMT-9) Halley, Antarctica	
Norman and Leck (2005)	Cascade impactor and cyclone filter	Atlantic and southern Indian Ocean	Median Values Used (from Figure 2 in paper)
Quinn et al. (1990)	Cascade impactor and cyclone filter	Central Pacific Ocean	
Savoie et al. (1993)	Bulk Sample	Mawson, Antarctica	
Silvente and Legrand (1993)	Bulk Sample	Antarctica	

One of the dominant issues encountered during the data synthesis was that many of the publications containing aerosol composition data only present the mean ratio from that campaign and do not publish the concentration data for each sample. In addition, depending on the sensitivity of the instrument used to analyse the data, the method of collection, and the air mass sampled, aerosol samplers are often run for highly variable periods of time (e.g. between 12 hours and 48 hours). In the true sense, an aerosol sample ought to be defined as the composition of a single aerosol particle. In practise this is difficult to achieve with present-day instrumentation and detection limits. As a result,

defining a single 'aerosol sample' is difficult and a single sample from one study could therefore represent the equivalent of an average of numerous individual samples from another study.

For the above reasons, the global analysis of aerosol NH_4^+:nssSO_4^{2-} ratio was restricted to classifying the mean ratio from each study into different ratio groups or 'bins' (Figure 6.22). The ratio bin size was chosen to be 0.3 units as this was small enough to identify the variation in average ratio between studies but big enough to encompass multiple studies in many of the bins. From Figure 6.22, it can be seen that the peak number of studies centred on the *0.91 - 1.20* ratio bin, although there is substantial range in the mean study ratios from 0.3 (Huebert et al., 1998) to 2.99 (Harrison et al., 1996a). From the graph, it appears that a second mode might exist for the *2.11 - 2.40* ratio bin but, relative to the peak ratio bin, the number of samples is too few to be conclusive.

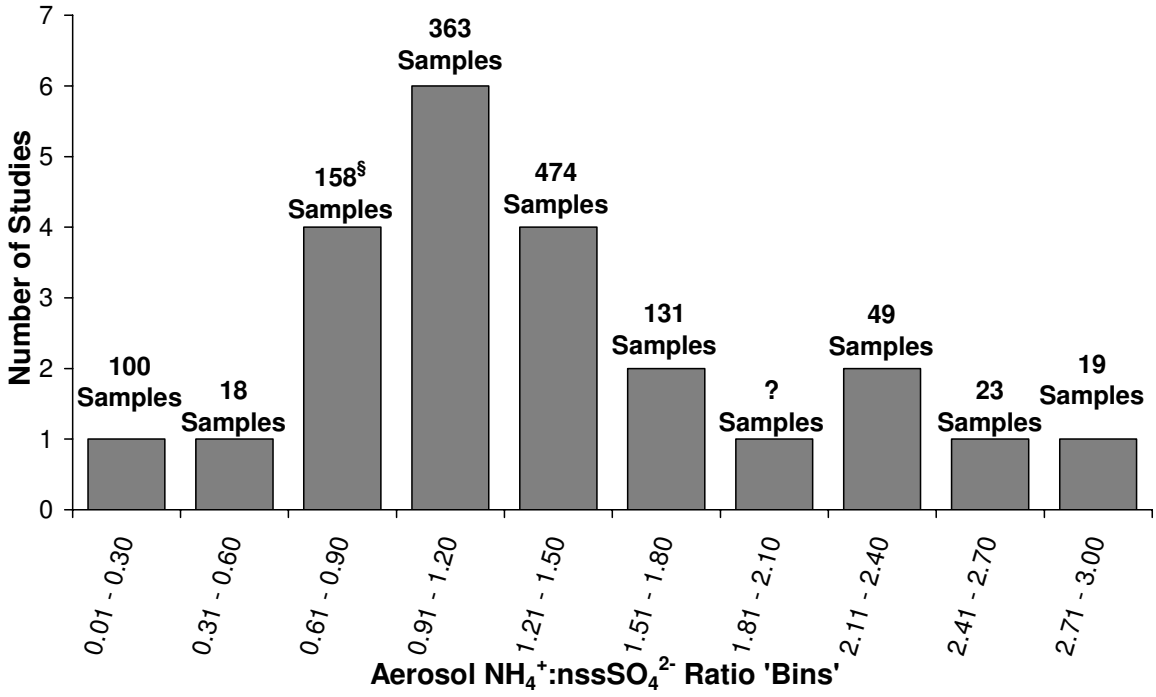

Figure 6.22 The total number of studies in each NH_4^+:nssSO_4^{2-} ratio bin. To aid interpretation, the total number of samples involved in each ratio bin is stated above each category bar. § indicates that one study in this category (Norman and Leck, 2005) did not state how many samples were collected. The same is true for the single study in the *1.81 - 2.10* ratio bin (Legrand et al., 1998).

The data presented in Figure 6.22 are representative of atmospheric measurements from various marine regions, and at this juncture no attempt was made to distinguish between air masses that might have been continentally influenced. The main reason for this was that different studies used different procedures to identify continentally-influenced samples, some more rigorous than others. In addition, when studies or samples known to be influenced by continental sources (e.g. AMT samples influenced by Saharan dust) were removed from the global analysis, a similar pattern could still be seen in the equivalent plot to Figure 6.22 (data not shown).

In an attempt to identify whether any of the substantial variations in NH_4^+:$nssSO_4^{2-}$ ratio relate to sampling region, the majority of the data was classified into broad categories. Table 6.2 presents the study average NH_4^+:$nssSO_4^{2-}$ ratio for aerosol and the range for each category. As much of the data from the AMT programme and other cruises sampled Atlantic air masses, a separate category represents this data. Only the average value from each study was used so the Atlantic data could not be subdivided between hemispheres. Hence in Table 6.2 this data was not used for a second time in the *Northern Hemisphere* category. For comparison, a new category was added with typical NH_4^+:$nssSO_4^{2-}$ data from an *Urban/Continental* environment (Warneck, 1988).

Table 6.2 Aerosol NH_4^+:$nssSO_4^{2-}$ ratio data (mean, median and range) for sample region categories. The data from Quinn et al. (1990) could not be placed in any of the sample region categories and is the only study from Table 6.1 not included in this analysis. The study by Legrand et al. (1998) was part of the *High Latitude* category and thus the true number of samples is greater than presented; this is marked by §. The same principle applies for the *Atlantic Ocean* category, which contains the study by Norman and Leck (2005) and is marked by ¥. Certain studies did not define the number of samples collected so it was not possible to weight the mean NH_4^+:$nssSO_4^{2-}$ ratio using the number of samples per study. Data representing the *Urban/Continental* category was taken from (Warneck, 1988).

Region	***Aerosol NH_4^+:$nssSO_4^{2-}$ Ratio***				***Number of Samples***
	Mean	*Median*	*Max*	*Min*	
High Latitude (Antarctica/Cape Grim/Greenland)	1.08	1.00	2.05	0.30	758 §
Atlantic Ocean	1.59	1.50	2.64	0.66	251 ¥
Northern Hemisphere	1.43	1.13	2.99	0.70	298
Urban/Continental	2.10	2.19	2.24	1.87	Unknown

From the data presented in Figure 6.22 and Table 6.2 it is clear that the majority of marine aerosol samples have a NH_4^+:$nssSO_4^{2-}$ ratio > 1 and thus the acidity from $nssSO_4^{2-}$ is at least partially neutralised. However, as Table 6.2 demonstrates, the ratio in high latitude regions (Antarctica, Cape Grim and Greenland) is lower than that observed in other regions of the world. In particular, the NH_4^+:$nssSO_4^{2-}$ ratio for Cape Grim is often substantially less than one; average study ratios of 0.32 (Huebert et al., 1998), 0.45 (Cainey, J., *Pers. Comm.*; routine sampling) and 0.96 (Cainey, J., *Pers. Comm.*; Moudi sampling) have been observed. As the $nssSO_4^{2-}$ concentrations are very low in these samples, it is unlikely that the low ratio is driven by an excess in $nssSO_4^{2-}$ and, by definition, this means that the source of NH_4^+ ($NH_{3(g)}$) must therefore be very low. In remote regions, atmospheric and oceanic concentrations often combine to facilitate the transfer of $NH_{3(g)}$ from the ocean to the atmosphere, although temperature has also been shown to significantly influence this flux (Johnson, 2004). As the remote, high latitude waters around Antarctica and Cape Grim are cold, it is possible that the sea-to-air flux is reduced and the consequence of this is very little atmospheric NH_3 to react with the small amounts of SO_4^{2-} acidity in aerosol. However, it should be noted that this theory is clearly in opposition to the higher latitude samples from AMT-12-14, which had NH_4^+:$nssSO_4^{2-}$ ratios consistently > 2.

6.5.2 Theoretical discussion of links between nitrogen and sulphur cycles

Having considered the data from AMT-12-14 as well as the global synthesis of many other studies, a number of discussions with Dr. Martin Johnson stimulated the following theoretical concept. As has been previously discussed, the flux of NH_3 is dependent upon atmospheric and oceanic concentrations and is encouraged out of the ocean when ocean temperatures are high (Johnson, 2004). A flux out of the ocean tends to be observed in remote regions away from anthropogenic influences (Quinn et al., 1988). Meanwhile, the AMT-14 data demonstrates that the NH_3 flux is often finely balanced in remote sub-tropical and tropical regions (Section 6.4).

The dominant source of aerosol acidity in remote regions is $nssSO_4^{2-}$ (Quinn et al., 1990) and this rapidly scavenges gas phase NH_3 to form ammonium sulphate. The preferred form of ammonium sulphate is $(NH_4)_2SO_4$ (solid or aqueous) and this has a very low vapour pressure (Seinfeld and Pandis, 1998). The reaction can therefore be treated as essentially irreversible for natural systems and as such is effectively a removal process from the atmosphere for gaseous NH_3. As the NH_3 flux is dependent upon atmospheric and oceanic concentrations, an increase in acidic particles is likely to reduce atmospheric NH_3 concentrations and could therefore encourage a flux out of the ocean. The DMS flux from the ocean is unidirectional due to the large and consistent concentration gradient caused by the oxidation of atmospheric DMS to $nssSO_4^{2-}$. This process provides a constant flux of acidity to the remote marine aerosol and changes in its magnitude may therefore influence the flux of NH_3. In addition, the advection of $nssSO_4^{2-}$ plumes (either anthropogenic or DMS-derived) may also affect the spatial and temporal variability of the oceanic NH_3 flux. In warm waters, an increase in the flux of DMS may therefore facilitate a flux of NH_3 from the ocean, while in cold waters an equivalent change in flux may reduce the magnitude of the NH_3 flux into the ocean.

The theoretical concept outlined above is difficult to prove conclusively without a modelling study as the timescales involved will have a significant impact upon how tightly coupled the sulphur-nitrogen cycle could be. In addition, the behaviour of other chemical species (both acidic and basic) will also have some impact. In the context of the AMT results, while remote samples appear to tend towards complete neutralisation, it is clear that the NH_4^+:$nssSO_4^{2-}$ ratio can still be quite variable. Globally, the ratio is typically between one and two and the range in values is even greater. As discussed in Section

6.5.1, the higher latitude studies have consistently observed lower ratios and this may well be linked to the effect of cooler waters reducing the air-sea flux of NH_3 and thus limiting the acid-neutralising capacity of the atmosphere, with clear implications for the acidity of marine aerosol. Finally, it is worth noting that despite consistently low NH_4^+:$nssSO_4^{2-}$ aerosol ratios, the NH_4^+, $nssSO_4^{2-}$ and MSA atmospheric seasonal cycles in Mawson, Antarctica, are remarkably coherent, with distinct peaks in the austral summer (Savoie et al., 1993).

An alternative explanation has been made to at least partially explain the NH_4^+:$nssSO_4^{2-}$ ratio observed in remote marine aerosol and it is linked to the recent discovery that a proportion of aerosol might originate from the process of bubble bursting introducing organic particles into the atmosphere (O'Dowd et al., 2004; Leck and Bigg, 2005). Based on this, the breakdown of organic material in the aerosol itself has been suggested as a source of NH_4^+ (Leck et al., 2002b). If this process does indeed take place, it may well introduce another level of complexity in trying to understand what controls the NH_4^+:$nssSO_4^{2-}$ ratio.

6.6 Summary

As discussed in Section 6.3, the trend in atmospheric MSA concentrations along the AMT-14 cruise transect follows that of surface ocean DMS, and the latitudinal trend in the MSA:nssSO_4^{2-} ratio is primarily driven by temperature. This broad trend corroborates the results of earlier studies (Bates et al., 1992b; Leck et al., 2002a), although there appear to be differences between the trend for each study, which suggests that other factors are also likely to be playing a role.

The atmospheric NH_3 flux throughout the sub-tropics and tropics of AMT-14 was finely balanced between a flux into the ocean and a flux out (Section 6.4). This is in part driven by atmospheric and oceanic concentrations, but it is clear from these results that the effect of temperature on the NH_3 flux should not be underestimated. From this perspective, the concept of climate change and a warming ocean may have implications for nitrogen cycling in such environments. A final point to make is that, in remote marine regions, the sampling of oceanic NH_4^+ and atmospheric NH_3 is quite difficult because of rapidly changing oceanic concentrations and low atmospheric concentrations. This introduces substantial error into the NH_3 flux calculation, making it difficult to quantify the direction and magnitude of many low-latitude air-sea fluxes.

When investigating the AMT data for any possible linkages between the nitrogen and sulphur cycles (Section 6.5), no significant correlations were observed between NH_4^+ and either DMS, DMSPd or DMSPp. In addition, no obvious and consistent links existed between the NH_3 and DMS flux strengths. The NH_4^+:nssSO_4^{2-} ratio for fine mode (<1 µm) aerosol samples collected throughout AMT-12-14 was reasonably consistent. However, many of the sample ratios were greater than the results presented by Quinn et al. (1990) and had a mean (± 1 standard error) of 2.4 ± 0.6. Presenting these results using boxplots was more informative than a scatter diagram and revealed that many samples with low NH_4^+ and nssSO_4^{2-} concentrations had ratios substantially greater than 2. It is likely that any excess NH_4^+ exists in these aerosol particles as NH_4NO_3 (Seinfeld and Pandis, 1998) and this has implications for the ability of such particles to form effective CCN. If the aerosol is internally mixed, it also means that there is the potential to form more effective CCN as the addition of fresh nssSO_4^{2-} will preferentially combine with NH_4^+ to form $(NH_4)_2SO_4$ (Seinfeld and Pandis, 1998).

A theoretical calculation of the fine mode aerosol net acidity for the AMT-12-14 dataset suggests that remote aerosol particles are well balanced while particles influenced by terrestrial sources (e.g. pollution, biomass burning) are either much more acidic or have additional basic species not accounted for by *Equation 6.2*.

Having incorporated other Atlantic datasets into the dataset from AMT (Section 6.5.1), the average ratio for different source regions was found to be lower and a possible explanation for this is the differences between collection methods. Comparing scatter plots of all Atlantic data versus latitude suggests that the nitrogen and sulphur cycles are not well coupled because large variations in ratio can be seen at all latitudes and concentration levels. Scaling up to the entire globe, an analysis of numerous studies confirmed that the majority of marine aerosols are somewhere between partially and fully neutralised with respect to sulphate acidity (i.e. between a 1:1 and 2:1 ratio). When broadly divided by source region, it is noticeable that the high latitude studies from Cape Grim and Antarctica often have lower NH_4^+:nssSO_4^{2-} ratios. This is possibly related to reduced NH_3 source strength and a NH_3 flux hindered by lower temperatures.

Section 6.5.2 outlined a theoretical concept proposed as a result of extensive discussion with Dr. Martin Johnson. In brief, it is suggested that changes in a DMS-derived flux of SO_4^{2-} might actually help to control the direction and magnitude of the NH_3 flux by varying the amount of available NH_3 in the atmosphere. To take this work further forward, it would be necessary to devise a proof-of-concept model to identify whether the rates of reaction involved could facilitate such a process. Finally, it has been suggested that an alternative source of NH_4^+ in aerosol could come from the breakdown of organic matter injected into the atmosphere by bubble bursting at the sea surface (Leck et al., 2002b).

7 Conclusions

This concluding chapter draws together the findings of the preceding chapters before identifying areas that the scientific community should address and discussing how future work should progress.

7.1 Summary

In this PhD thesis the four results chapters contain relatively discrete conclusions, which are below:

- Synthesis of the entire AMT dataset produced a number of strong positive correlations between carbon fixation rate (primary production) and DMS and DMSPp (see Chapter 3), suggesting that in oligotrophic regions primary production might be a better predictor of DMS(P) than biomass (chlorophyll *a*).
- Correlations were also observed between DMSP (dissolved and particulate) and violaxanthin, an accessory pigment known to be part of a photoprotective xanthophyll cycle. The AMT cruises progressed through waters exposed to relatively high light levels that are predominantly nutrient-limited. In this context, the AMT dataset is of interest because of the proposed anti-oxidative function for DMS(P).
- Principal components analysis (PCA) indicated that pigment concentrations were not that useful for explaining DMS(P) concentration trends in oligotrophic waters. This was primarily due to the substantial covariance between different pigments. Once such covariance was accounted for, the correlations with DMS(P) were not as strong as when individual pigments were considered.
- Whilst the North and South Atlantic gyres are identifiable regions of low biological productivity, they are not homogeneous biological communities with distinct boundaries such as those proposed by Longhurst (1995). They appear to demonstrate seasonal variation in community composition and production (ANOVA tests in Section 3.3.3), and their boundaries are indistinct (as shown by the differences between the AMT-5 and AMT-12-14 cruise tracks; Section 3.3.1). Caution is therefore needed when extrapolating from studies in one region of the northern or southern gyre to the entire oligotrophic Atlantic.
- The results of Chapter 4 (see also Bell et al., 2006b) indicate that current predictive models for DMS generally overestimate surface concentrations in the oligotrophic Atlantic. The most recent algorithm based upon the mixed layer depth (MLD) is that

produced by Aranami and Tsunogai (2004) and this is the best predictive algorithm for the AMT dataset. In its AMT-optimised form, this follows as DMS×MLD = 40 µmol m^{-2}. However, it is not advisable that this algorithm be adopted on a global scale as there are many processes, potentially unaccounted for by **AT04**, that influence DMS concentrations and may have caused the scatter observed in the AMT dataset (Figure 4.5c).

- The DMSP-lyase activity (DLA) results from Chapter 5 (see also Bell et al., 2006a) include the first measurements made in the South Atlantic and present an intriguing picture. Despite some ancillary measurements suggesting a link between DLA and oxidative stress, these results are not strong enough to be fully conclusive that DLA operates as part of a complex anti-oxidant cascade mechanism. Part of the problem is the nature of oxidative stress, which can be due to numerous factors (e.g. nutrient limitation, high light intensity, iron limitation, etc.), and is thus problematic when deciding upon an appropriate measurement technique to identify the level of oxidative stress experienced by the phytoplankton community.
- The MSA:nssSO_4^{2-} results presented in Chapter 6 (Section 6.3) demonstrate that the trend in the ratio (increasing with increasing latitude) is consistent with other results (Bates et al., 1992a; Leck et al., 2002a). Despite the multitude of influences upon atmospheric MSA concentrations, the AMT data appears to co-vary with its ultimate source – surface ocean DMS concentrations.
- The direction of the NH_3 flux throughout AMT-14 is uncertain due to the degree of error involved in the calculation, but it appears to be finely balanced between INTO and OUT of the ocean in low latitude regions (see Section 6.4). The potential for a flux out of the ocean is somewhat surprising given the low oceanic NH_4^+ concentrations in such regions.
- For the AMT dataset, the submicron NH_4^+:nssSO_4^{2-} ratio in aerosol was consistently greater than 1:1 (see Section 6.5) and the nssSO_4^{2-} was therefore more neutralised than the remote marine air masses sampled by Quinn et al. (1990) in the Pacific. Extreme ratio values (i.e. > 3:1) for high latitude air masses in the southern hemisphere may be due to the presence of a $NH_4^+ – NO_3^-$ component after complete neutralisation of nssSO_4^{2-}.
- Although aerosol NH_4^+:nssSO_4^{2-} ratios were relatively consistent in remote marine air masses, there was little apparent linkage between the sea-to-air fluxes of DMS and NH_3 (see Section 6.5).

- Despite the AMT dataset suggesting a higher NH_4^+:$nssSO_4^{2-}$ aerosol ratio than observed by Quinn et al. (1990), a global synthesis indicates that the submicron ratio is generally between 1:1 and 2:1 (Section 6.5.1). The degree of variation in the global NH_4^+:$nssSO_4^{2-}$ ratio suggests that it may be driven purely by variations in source strengths of NH_3 and $nssSO_4^{2-}$.
- Whilst the cycles of reduced nitrogen and sulphur may operate independently, it is suggested in Section 6.5.2 that these cycles may still have an influence upon each other and that this might help explain the relatively consistent NH_4^+:$nssSO_4^{2-}$ ratios observed in marine air masses. Potentially, variations in the flux of DMS could indirectly influence the flux of NH_3 in low latitude regions.

7.2 Future Work

Over the past few decades, current understanding of the many aspects of the CLAW hypothesis and climate regulation has progressed substantially due to great endeavour in the fields of biogeochemical oceanography and atmospheric chemistry. However, there is always room for further advances, whether technological or theoretical. The following section proposes what areas of our understanding need improving, based initially upon the results and conclusions of this thesis. Subsequently, a more general comment is made on the current state of DMS(P) research and how it should develop.

The correlations identified between DMS(P) concentrations and the rate of primary production demand further work. A recent publication suggests that the rate of carbon fixation in the surface ocean can now be determined via satellite using parameters such as light, nutrients and mixed layer depth (Behrenfeld et al., 2005). A further development of the results in Chapter 3 (Section 3.3.1) would be to test how well DMS(P) concentrations can be predicted in oligotrophic regions using such information.

The DMSP-lyase activity (DLA) measurements from the South Atlantic presented in Chapter 5 interesting and more measurements are required from this region, with greater spatial (both vertical and horizontal) resolution. In an ideal world with no time or personnel constraints, the DLA measurement should also be refined by size-fractionating each sample and testing the *in vivo* activity of the community. Size fractionation would help to identify which organisms were responsible for the majority of DLA (although this would not identify if particle-attached bacteria were responsible for the DLA). An *in vivo*

activity measurement represents the activity of the enzyme(s) without removal from a living organism and is clearly more representative of true enzyme activity (i.e. under true pH and temperature conditions) than *in vitro* activity.

An improved method for atmospheric NH_3 (in terms of frequency and sensitivity) is required to further investigate low latitude sea-air NH_3 fluxes. The current filter-pack method, whilst adequate for some air masses over certain regions of the ocean, is not sensitive enough after blank correction to determine remote marine atmospheric NH_3 concentrations. Norman and Leck (2005) recently demonstrated a method that facilitated an atmospheric NH_3 measurement every 10 minutes, even for air masses over the remote Atlantic (detection limit = ~0.2 nmol m^{-3}). Meanwhile, the aerosol data collected during AMT indicates that future work should focus on the isotopic signature of the NH_4^+ and $nssSO_4^{2-}$ contained in the remote submicron aerosol as an indication of their respective sources. In terms of the NH_4^+:$nssSO_4^{2-}$ ratio in aerosol, it has previously been assumed that all fine mode NH_4^+ in remote marine aerosol is associated with $nssSO_4^{2-}$, but the results in Chapter 6 suggest otherwise. Finally, the concept that the DMS flux might control the NH_3 flux in certain regions warrants further investigation; the best approach would be via a simple box model.

There was a plethora of ancillary data collected during AMT and this enabled substantial statistical analysis, which has shed some light on the regulation of DMS(P) concentrations in oligotrophic regions. However, in retrospect, coordination between different research groups could be improved. Despite the presence of both research groups on the same ship, data was often not collected from the same depth, limiting the number of data 'pairs' that could be analysed statistically. For example, throughout AMT-12-14 a total of 538 individual DMS(P) measurements and 1637 individual bacterial density measurements were made. Despite this, the total number of paired DMS(P)/bacterial density measurements was only 358. In an ideal world with no time constraints, improved planning and communication could have increased this number considerably. As the research on DMS and related compounds relies upon various biological community and process measurements, the responsibility for making them arguably lies with those involved in DMS(P) research.

Despite the comments above, the dataset collected during AMT represents a significant achievement by many different research groups and should not be underestimated. The results from this work are novel and useful to the DMS(P) community. It is, however, debateable how useful a repeat of such an experiment would be. DMS and DMSP concentrations in the surface ocean can effectively be described as the net product of a complex biological system that rapidly consumes and produces the compound of interest. Arguably, measuring ambient concentrations is of limited use and the equivalent of measuring ambient macro-nutrient concentrations. To understand the natural environment better, emphasis must also be placed upon rate measurements as these can be incorporated into current global models. If these models can be parameterised to accurately model the current system, they can then be used to give an improved indication of how net production of DMS in the surface ocean might alter with future climate change. In addition, the molecular cell processes involved in DMSP production should be thoroughly investigated and understood in the laboratory as these will provide clues as to how organisms may act in the natural environment.

Appendix

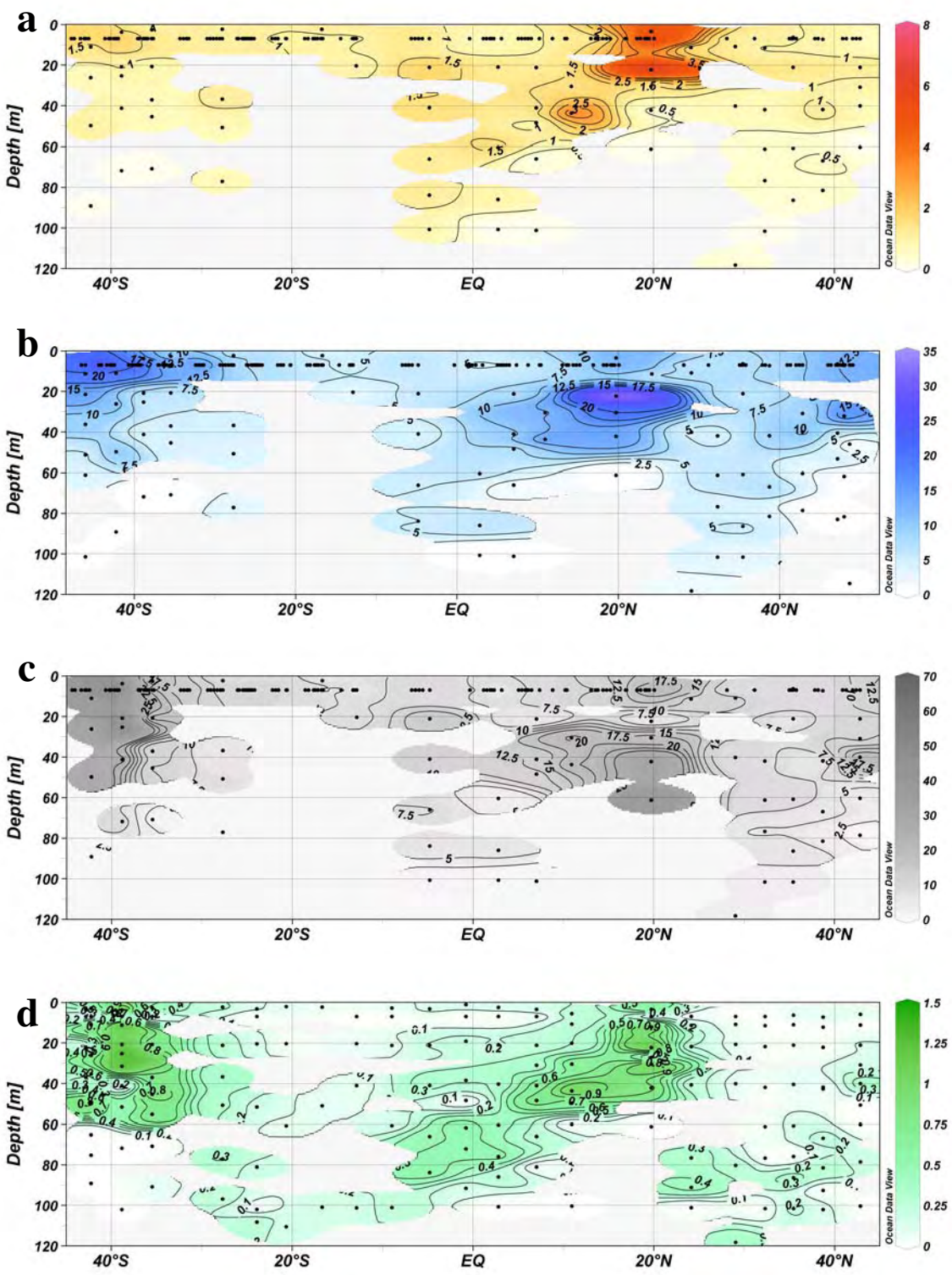

Figure I Depth contour plots of (a) DMS (red); (b) DMSPd (blue); (c) DMSPp (grey); and (d) TChl a (green) along AMT-5 (the green cruise track on Figure 3.1). Sample points are indicated (black dots). Contour lines are set at intervals of 0.5 nM; 2.5 nM; 2.5 nM; and 0.1 µg L^{-1} for DMS, DMSPd, DMSPp and TChl a respectively.

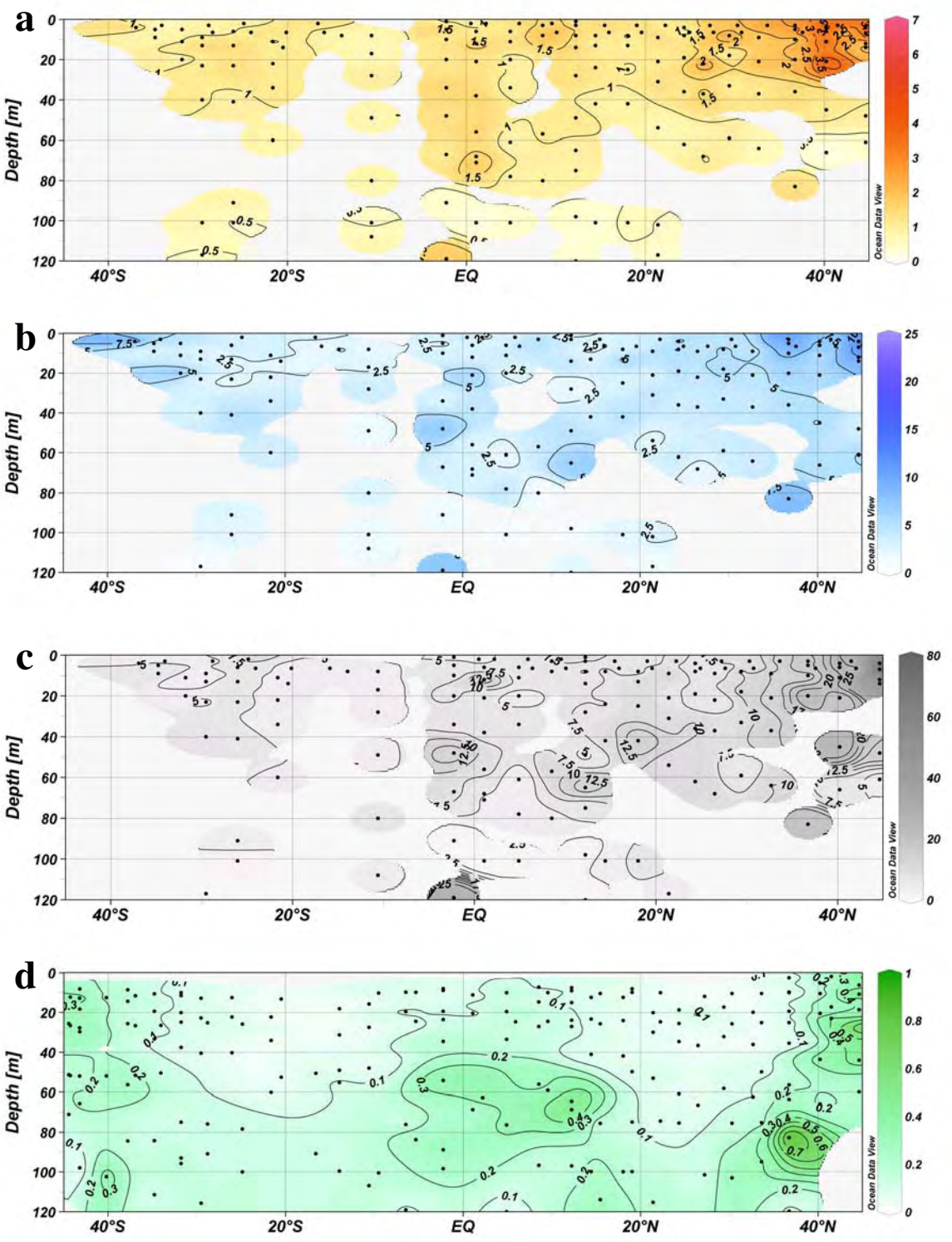

Figure II Data from AMT-12 (the blue cruise track on Figure 3.1). Otherwise, legend is as for Figure I.

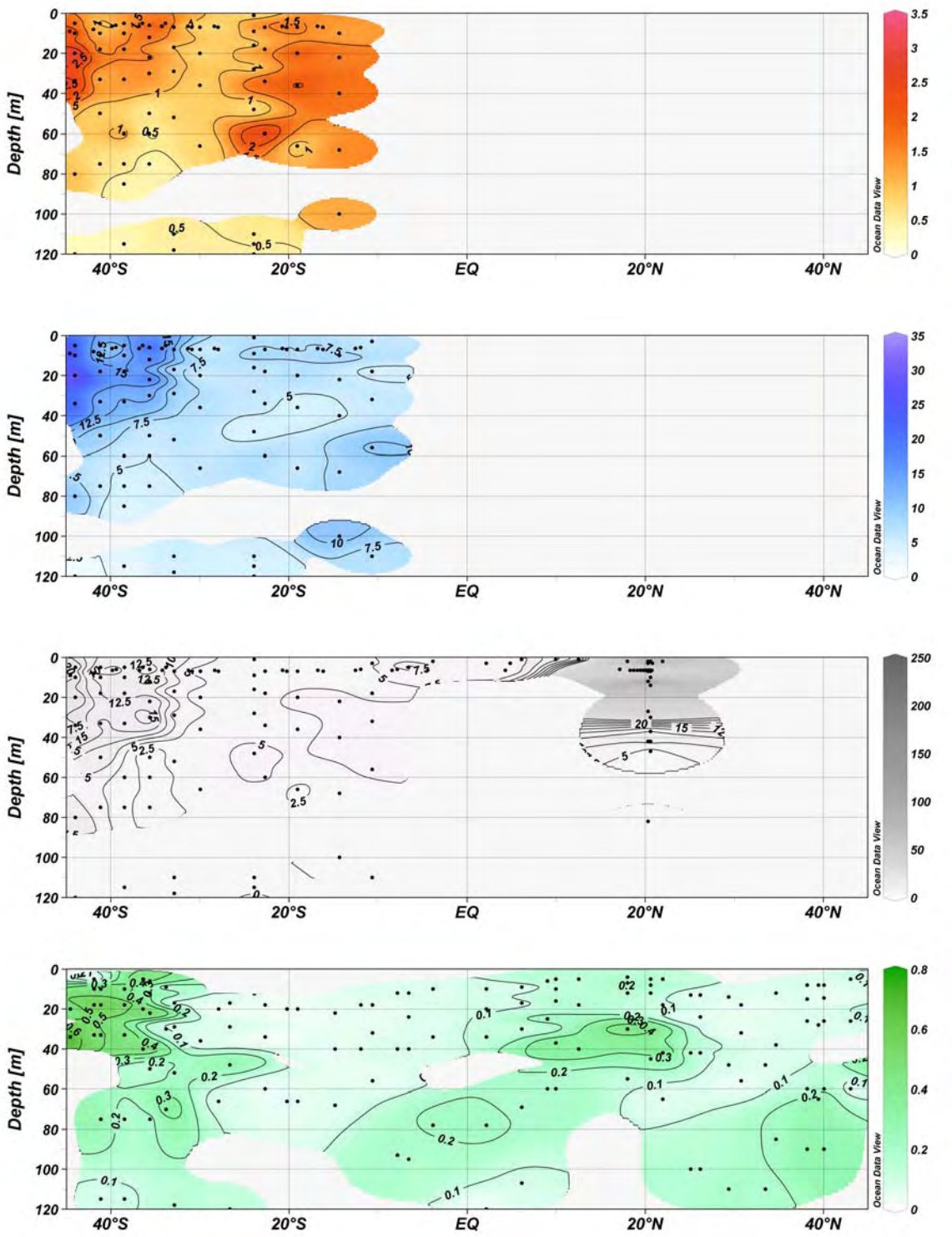

Figure III Data from AMT-13 (the white cruise track on Figure 3.1). North of 14°S, no DMS and DMSPd data was collected due to equipment malfunction. DMSPp data between the upwelling region (approximately 20°N) and 14°S were collected and stored until the equipment was fixed. Otherwise, legend is as for Figure I.

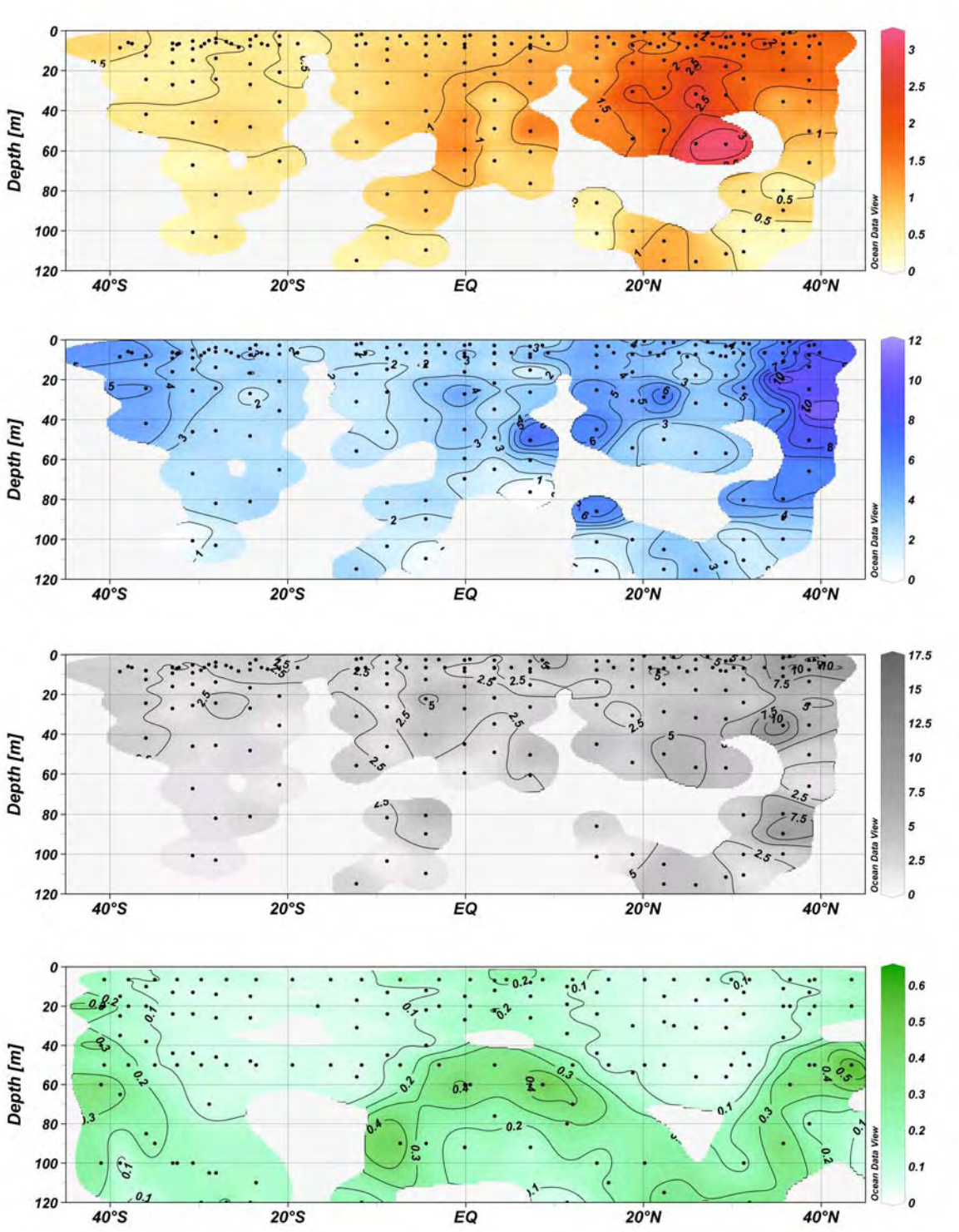

Figure IV Data from AMT-14 (the red cruise track on Figure 3.1). Otherwise legend is as for Figure I.

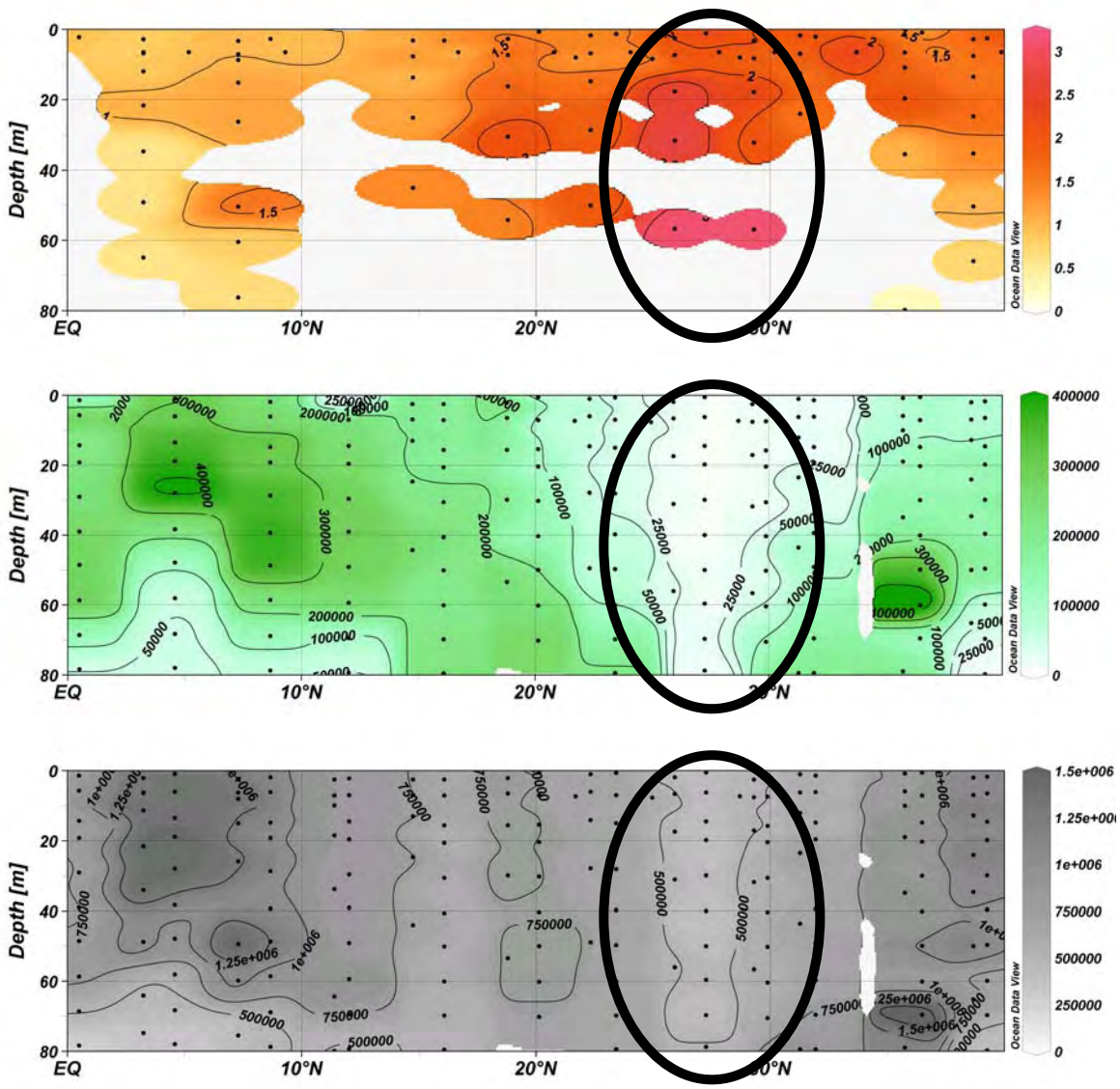

Figure V Depth contour plots of (a) DMS (red); (b) Prochlorococcus density in number ml^{-1} (green); and (c) heterotrophic bacterial density in number ml^{-1} (grey) during the northern section of AMT-14 (the red cruise track on Figure 3.1, equator to 40°N). Sample points are indicated (black dots) and the location of the DMS 'hotspot' circled on each section. Contour lines are set at intervals of 0.5 nM and 250,000 cells ml^{-1} for DMS and heterotrophic bacterial density respectively. For Prochlorococcus density, contour lines were set at 100,000 cells ml^{-1} with extra contours for 50,000 and 25,000 cell ml^{-1}.

References

Allen, A.G., Dick, A.L. and Davison, B.M., 1997. Sources of atmospheric methanesulphonate, non-sea-salt sulphate, nitrate and related species over the temperate South Pacific. Atmospheric Environment, 31(2): 191-205.

Anderson, T.R., Spall, S.A., Yool, A., Cipollini, P., Challenor, P.G. and Fasham, M.J.R., 2001. Global fields of sea surface dimethylsulfide predicted from chlorophyll, nutrients and light. Journal of Marine Systems, 30(1-2): 1-20.

Andreae, M.O., Elbert, W. and Demora, S.J., 1995. Biogenic sulfur emissions and aerosols over the tropical South-Atlantic 3. Atmospheric dimethylsulfide, aerosols and cloud condensation nuclei. Journal of Geophysical Research-Atmospheres, 100(D6): 11335-11356.

Andreae, M.O. and Merlet, P., 2001. Emission of trace gases and aerosols from biomass burning. Global Biogeochemical Cycles, 15(4): 955-966.

Aranami, K. and Tsunogai, S., 2004. Seasonal and regional comparison of oceanic and atmospheric dimethylsulfide in the northern North Pacific: Dilution effects on its concentration during winter. Journal of Geophysical Research-Atmospheres, 109(D12): art. no.-D12303.

Archer, S.D., Stelfox-Widdicombe, C.E., Malin, G. and Burkill, P.H., 2003. Is dimethyl sulphide production related to microzooplankton herbivory in the southern North Sea? Journal of Plankton Research, 25(2): 235-242.

Atkinson, A. and Whitehouse, M.J., 2001. Ammonium regeneration by Antarctic mesozooplankton: an allometric approach. Marine Biology, 139(2): 301-311.

Atkinson, R., Pitts, J.N. and Aschmann, S.M., 1984. Tropospheric reactions of dimethyl sulfide with NO_3 and OH radicals. Journal of Physical Chemistry, 88(8): 1584-1587.

Aumont, O., Belviso, S. and Monfray, P., 2002. Dimethylsulfoniopropionate (DMSP) and dimethylsulfide (DMS) sea surface distributions simulated from a global three-dimensional ocean carbon cycle model. Journal of Geophysical Research-Oceans, 107(C4): art. no.-3029.

Ayers, G.P. and Gras, J.L., 1980. Ammonia gas concentrations over the Southern Ocean. Nature, 284(5756): 539-540.

Ayers, G.P., Gras, J.L., Adriaansen, A. and Gillett, R.W., 1984. Solubility of ammonia in rainwater. Tellus Series B-Chemical and Physical Meteorology, 36(2): 85-91.

Ayers, G.P., Ivey, J.P. and Gillett, R.W., 1991. Coherence between seasonal cycles of dimethyl sulfide, methanesulfonate and sulfate in marine air. Nature, 349(6308): 404-406.

Ayers, G.P., Gillet, R.W., Ivey, J.P., Schafer, B. and Gabric, A., 1995. Short-term variability in marine atmospheric dimethylsulfide concentration. Geophysical Research Letters, 22(18): 2513-2516.

Ayers, G.P., Cainey, J.M., Granek, H. and Leck, C., 1996. Dimethylsulfide oxidation and the ratio of methanesulfonate to non sea-salt sulfate in the marine aerosol. Journal of Atmospheric Chemistry, 25(3): 307-325.

Ayers, G.P. and Gillett, R.W., 2000. DMS and its oxidation products in the remote marine atmosphere: implications for climate and atmospheric chemistry. Journal of Sea Research, 43(3-4): 275-286.

Azam, F., Fenchel, T., Field, J.G., Gray, J.S., Meyerreil, L.A. and Thingstad, F., 1983. The ecological role of water-column microbes in the sea. Marine Ecology-Progress Series, 10(3): 257-263.

Bacic, M.K. and Yoch, D.C., 1998. *In vivo* characterization of dimethylsulfoniopropionate lyase in the fungus *Fusarium lateritium*. Applied and Environmental Microbiology, 64(1): 106-111.

Baker, A.R., Kelly, S.D., Biswas, K.F., Witt, M. and Jickells, T.D., 2003. Atmospheric deposition of nutrients to the Atlantic Ocean. Geophysical Research Letters, 30(24): art. no.-2296.

Barnes, I., Hjorth, J. and Mihalopoulos, N., 2006. Dimethyl sulfide and dimethyl sulfoxide and their oxidation in the atmosphere. Chemical Reviews, 106(3): 940-975.

Bates, T.S., Calhoun, J.A. and Quinn, P.K., 1992a. Variations in the methanesulfonate to sulfate molar ratio in submicrometer marine aerosol particles over the South-Pacific Ocean. Journal of Geophysical Research-Atmospheres, 97(D9): 9859-9865.

Bates, T.S., Lamb, B.K., Guenther, A., Dignon, J. and Stoiber, R.E., 1992b. Sulfur emissions to the atmosphere from natural sources. Journal of Atmospheric Chemistry, 14(1-4): 315-337.

Behrenfeld, M.J., Boss, E., Siegel, D.A. and Shea, D.M., 2005. Carbon-based ocean productivity and phytoplankton physiology from space. Global Biogeochemical Cycles, 19(1): art. no.-GB1006.

Bell, T.G., Malin, G., Kim, Y.N. and Steinke, M., 2006a. Spatial variability in DMSP-lyase activity along an Atlantic meridional transect. Aquatic Sciences *Submitted*.

Bell, T.G., Malin, G., McKee, C.M. and Liss, P.S., 2006b. A comparison of dimethylsulphide (DMS) data from the Atlantic Meridional Transect (AMT) programme with proposed algorithms for global surface DMS concentrations. Deep-Sea Research Part Ii-Topical Studies in Oceanography, 53(14-16): 1720-1735.

Belviso, S., Claustre, H. and Marty, J.C., 2001. Evaluation of the utility of chemotaxonomic pigments as a surrogate for particulate DMSP. Limnology and Oceanography, 46(4): 989-995.

Belviso, S., Bopp, L., Moulin, C., Orr, J.C., Anderson, T.R., Aumont, O., Chu, S., Elliott, S., Maltrud, M.E. and Simo, R., 2004a. Comparison of global climatological maps of sea surface dimethyl sulfide. Global Biogeochemical Cycles, 18(3): art. no.-GB3013.

Belviso, S., Moulin, C., Bopp, L. and Stefels, J., 2004b. Assessment of a global climatology of oceanic dimethylsulfide (DMS) concentrations based on SeaWiFS imagery (1998-2001). Canadian Journal of Fisheries and Aquatic Sciences, 61(5): 804-816.

Berges, J.A., Cochlan, W.P. and Harrison, P.J., 1995. Laboratory and field responses of algal nitrate reductase to diel periodicity in irradiance, nitrate exhaustion, and the presence of ammonium. Marine Ecology-Progress Series, 124(1-3): 259-269.

Berges, J.A., 1997. Algal nitrate reductases. European Journal of Phycology, 32(1): 3-8.

Berman, T. and Bronk, D.A., 2003. Dissolved organic nitrogen: a dynamic participant in aquatic ecosystems. Aquatic Microbial Ecology, 31(3): 279-305.

Berresheim, H., Andreae, M.O., Iverson, R.L. and Li, S.M., 1991. Seasonal variations of dimethylsulfide emissions and atmospheric sulfur and nitrogen species over the western North Atlantic Ocean. Tellus Series B-Chemical and Physical Meteorology, 43(5): 353-372.

Blomquist, B.W., Fairall, C.W., Huebert, B.J., Kieber, D.J. and Westby, G.R., 2006. DMS sea-air transfer velocity: Direct measurements by eddy covariance and parameterization based on the NOAA/COARE gas transfer model. Geophysical Research Letters, 33(7): art. no.-L07601.

Brainerd, K.E. and Gregg, M.C., 1995. Surface mixed and mixing layer depths. Deep-Sea Research Part I-Oceanographic Research Papers, 42(9): 1521-1543.

Brimblecombe, P., 1984. Henry's Law confounded. Nature, 310(5972): 11-12.

Brimblecombe, P. and Shooter, D., 1986. Photooxidation of dimethylsulfide in aqueous solution. Marine Chemistry, 19(4): 343-353.

Brimblecombe, P. and Clegg, S.L., 1988. The solubility and behavior of acid gases in the marine aerosol. Journal of Atmospheric Chemistry, 7(1): 1-18.

Brugger, A., Slezak, D., Obernosterer, I. and Herndl, G.J., 1998. Photolysis of dimethylsulfide in the northern Adriatic Sea: Dependence on substrate concentration, irradiance and DOC concentration. Marine Chemistry, 59(3-4): 321-331.

Brzezinski, M.A., 1988. Vertical distribution of ammonium in stratified oligotrophic waters. Limnology and Oceanography, 33(5): 1176-1182.

Burgermeister, S., Zimmermann, R.L., Georgii, H.W., Bingemer, H.G., Kirst, G.O., Janssen, M. and Ernst, W., 1990. On the biogenic origin of dimethylsulfide - Relation between chlorophyll, ATP, organismic DMSP, phytoplankton species, and DMS distribution in Atlantic surface-water and atmosphere. Journal of Geophysical Research-Atmospheres, 95(D12): 20607-20615.

Bushaw, K.L., Zepp, R.G., Tarr, M.A., SchulzJander, D., Bourbonniere, R.A., Hodson, R.E., Miller, W.L., Bronk, D.A. and Moran, M.A., 1996. Photochemical release of biologically available nitrogen from aquatic dissolved organic matter. Nature, 381(6581): 404-407.

Cachier, H., Liousse, C., Buatmenard, P. and Gaudichet, A., 1995. Particulate content of savanna fire emissions. Journal of Atmospheric Chemistry, 22(1-2): 123-148.

Cainey, J. and Harvey, M., 2002. Dimethylsulfide, a limited contributor to new particle formation in the clean marine boundary layer. Geophysical Research Letters, 29(7): art. no.-1128.

Capone, D.G., Zehr, J.P., Paerl, H.W., Bergman, B. and Carpenter, E.J., 1997. Trichodesmium, a globally significant marine cyanobacterium. Science, 276(5316): 1221-1229.

Charlson, R.J. and Rodhe, H., 1982. Factors controlling the acidity of natural rainwater. Nature, 295(5851): 683-685.

Charlson, R.J., Lovelock, J.E., Andreae, M.O. and Warren, S.G., 1987. Oceanic phytoplankton, atmospheric sulfur, cloud albedo and climate. Nature, 326(6114): 655-661.

Chu, S.P., Elliott, S. and Maltrud, M.E., 2003. Global eddy permitting simulations of surface ocean nitrogen, iron, sulfur cycling. Chemosphere, 50(2): 223-235.

Clarke, A.D. and Porter, J.N., 1993. Pacific marine aerosol 2. Equatorial gradients in chlorophyll, ammonium, and excess sulfate during SAGA 3. Journal of Geophysical Research-Atmospheres, 98(D9): 16997-17010.

Claustre, H., 1994. The trophic status of various oceanic provinces as revealed by phytoplankton pigment signatures. Limnology and Oceanography, 39(5): 1206-1210.

Claustre, H. and Marty, J.C., 1995. Specific phytoplankton biomasses and their relation to primary production in the tropical North Atlantic. Deep-Sea Research Part I-Oceanographic Research Papers, 42(8): 1475-1493.

Coffman, D.J. and Hegg, D.A., 1995. A preliminary study of the effect of ammonia on particle nucleation in the marine boundary layer. Journal of Geophysical Research-Atmospheres, 100(D4): 7147-7160.

Cohen, J., 1988. Statistical power analysis for the behavioural sciences. Lawrence Erlbaum Associates, Inc., Hillsdale, New Jersey.

Corn, M., Belviso, S., Partensky, F., Simon, N. and Christaki, U., 1995. Origin and importance of picoplanktonic DMSP. In: R.P. Kiene, P.T. Visscher, M.D. Keller and G.O. Kirst (Editors), Biological and environmental chemistry of DMSP and related sulfonium compounds. Plenum Press, New York, Mobile, Alabama, pp. 191-201.

Covert, D.S., 1988. North Pacific marine background aerosol: Average ammonium to sulfate molar ratio equals 1. Journal of Geophysical Research-Atmospheres, 93(D7): 8455-8458.

Croot, P.L., Streu, P. and Baker, A.R., 2004. Short residence time for iron in surface seawater impacted by atmospheric dry deposition from Saharan dust events. Geophysical Research Letters, 31(23): art. no.-L23S08.

Dacey, J.W.H., Wakeham, S.G. and Howes, B.L., 1984. Henry law constants for dimethylsulfide in fresh water and seawater. Geophysical Research Letters, 11(10): 991-994.

Dacey, J.W.H. and Wakeham, S.G., 1986. Oceanic dimethylsulfide: Production during zooplankton grazing on phytoplankton. Science, 233(4770): 1314-1316.

Dacey, J.W.H. and Blough, N.V., 1987. Hydroxide decomposition of dimethylsulfoniopropionate to form dimethylsulfide. Geophysical Research Letters, 14(12): 1246-1249.

Dacey, J.W.H., Howse, F.A., Michaels, A.F. and Wakeham, S.G., 1998. Temporal variability of dimethylsulfide and dimethylsulfoniopropionate in the Sargasso Sea. Deep-Sea Research Part I-Oceanographic Research Papers, 45(12): 2085-2104.

Dalsgaard, T., Canfield, D.E., Petersen, J., Thamdrup, B. and Acuna-Gonzalez, J., 2003. N_2 production by the anammox reaction in the anoxic water column of Golfo Dulce, Costa Rica. Nature, 422(6932): 606-608.

Dasgupta, P.K. and Dong, S., 1986. Solubility of ammonia in liquid water and generation of trace levels of standard gaseous ammonia. Atmospheric Environment, 20(3): 565-570.

de Souza, M.P. and Yoch, D.C., 1995. Purification and characterization of dimethylsulfoniopropionate lyase from an *Alcaligenes*-like dimethyl sulfide-producing marine isolate. Applied and Environmental Microbiology, 61(1): 21-26.

DiTullio, G.R. and Smith, W.O., 1995. Relationship between dimethylsulfide and phytoplankton pigment concentrations in the Ross Sea, Antarctica. Deep-Sea Research Part I-Oceanographic Research Papers, 42(6): 873-892.

Donelan, M.A. and Wanninkhof, R., 2002. Gas transfer at water surfaces - concepts and issues. In: M.A. Donelan, W.M. Drennan, E.S. Saltzman and R. Wanninkhof (Editors), Gas Transfer at Water Surfaces. American Geophysical Union, Washington, D.C.

Dortch, Q., 1990. The interaction between ammonium and nitrate uptake in phytoplankton. Marine Ecology-Progress Series, 61(1-2): 183-201.

Draxler, R.R. and Rolph, G.D., 2003. HYSPLIT (HYbrid Single-Particle Lagrangian Integrated Trajectory) Model access via NOAA ARL READY Website (http://www.arl.noaa.gov/ready/hysplit4.html). NOAA Air Resources Laboratory, Silver Spring, MD.

Duce, R.A., Liss, P.S., Merrill, J.T., Atlas, E.L., Buatmenard, P., Hicks, B.B., Miller, J.M., Prospero, J.M., Arimoto, R., Church, T.M., Ellis, W., Galloway, J.N., Hansen, L., Jickells, T.D., Knap, A.H., Reinhardt, K.H., Schneider, B., Soudine, A., Tokos, J.J., Tsunogai, S., Wollast, R. and Zhou, M., 1991. The atmospheric input of trace species to the world ocean. Global Biogeochemical Cycles, 5(3): 193-259.

Dugdale, R.C. and Goering, J.J., 1967. Uptake of new and regenerated forms of nitrogen in primary productivity. Limnology and Oceanography, 12(2): 196-206.

Eppley, R.W. and Peterson, B.J., 1979. Particulate organic matter flux and planktonic new production in the deep ocean. Nature, 282(5740): 677-680.

Falkowski, P.G. and Raven, J.A., 1997. Aquatic photosynthesis. Blackwell Science, Oxon.

Fasham, M.J.R., Ducklow, H.W. and McKelvie, S.M., 1990. A nitrogen-based model of plankton dynamics in the oceanic mixed layer. Journal of Marine Research, 48(3): 591-639.

Franklin, M.P., McDonald, I.R., Bourne, D.G., Owens, N.J.P., Upstill-Goddard, R.C. and Murrell, J.C., 2005. Bacterial diversity in the bacterioneuston (sea surface microlayer): the bacterioneuston through the looking glass. Environmental Microbiology, 7(5): 723-736.

Galloway, J.N., Schlesinger, W.H., Levy, H., Michaels, A. and Schnoor, J.L., 1995. Nitrogen fixation: Anthropogenic enhancement-environmental response. Global Biogeochemical Cycles, 9(2): 235-252.

Georgii, H.W. and Gravenhorst, G., 1977. Ocean as source or sink of reactive trace gases. Pure and Applied Geophysics, 115(3): 503-511.

Gibb, S.W., 1994. Trace determination of ammonia and methylamines by flow injection extraction - ion chromatography in estuarine and marine environments, University of East Anglia, Norwich.

Gibb, S.W., Mantoura, R.F.C. and Liss, P.S., 1999a. Ocean-atmosphere exchange and atmospheric speciation of ammonia and methylamines in the region of the NW Arabian Sea. Global Biogeochemical Cycles, 13(1): 161-177.

Gibb, S.W., Mantoura, R.F.C., Liss, P.S. and Barlow, R.G., 1999b. Distributions and biogeochemistries of methylamines and ammonium in the Arabian Sea. Deep-Sea Research Part Ii-Topical Studies in Oceanography, 46(3-4): 593-615.

Gibb, S.W., Barlow, R.G., Cummings, D.G., Rees, N.W., Trees, C.C., Holligan, P. and Suggett, D., 2000. Surface phytoplankton pigment distributions in the Atlantic Ocean: An assessment of basin scale variability between 50°N and 50°S. Progress in Oceanography, 45(3-4): 339-368.

Goldman, J.C., Dennett, M.R. and Frew, N.M., 1988. Surfactant effects on air-sea gas exchange under turbulent conditions. Deep-Sea Research Part a-Oceanographic Research Papers, 35(12): 1953-1970.

Gondwe, M., Krol, M., Klaassen, W., Gieskes, W. and de Baar, H., 2004. Comparison of modeled versus measured MSA:nss$SO_4^=$ ratios: A global analysis. Global Biogeochemical Cycles, 18(2): art. no.-GB2006.

Gonzalez, J.M., Kiene, R.P. and Moran, M.A., 1999. Transformation of sulfur compounds by an abundant lineage of marine bacteria in the α-subclass of the class *Proteobacteria*. Applied and Environmental Microbiology, 65(9): 3810-3819.

Gorsuch, R.L., 1983. Factor analysis. Lawrence Erlbaum Associates, New Jersey.

Hales, J.M. and Drewes, D.R., 1979. Solubility of ammonia in water at low concentrations. Atmospheric Environment, 13(8): 1133-1147.

Harada, H., Rouse, M.A., Sunda, W. and Kiene, R.P., 2004. Latitudinal and vertical distributions of particle-associated dimethylsulfoniopropionate (DMSP) lyase activity in the western North Atlantic Ocean. Canadian Journal of Fisheries and Aquatic Sciences, 61(5): 700-711.

Hardy, J.T., 1997. Biological effects of chemicals in the sea-surface microlayer. In: P.S. Liss and R.A. Duce (Editors), The Sea Surface and Global Change. Cambridge University Press, Cambridge, pp. 339-370.

Harrison, R.M. and Kitto, A.M.N., 1992. Estimation of the rate constant for the reaction of acid sulfate aerosol with NH_3 gas from atmospheric measurements. Journal of Atmospheric Chemistry, 15(2): 133-143.

Harrison, R.M., Peak, J.D. and Kaye, A.D., 1996a. Atmospheric aerosol major ion composition and cloud condensation nuclei over the northeast Atlantic. Journal of Geophysical Research-Atmospheres, 101(D2): 4425-4434.

Harrison, R.M., Peak, J.D. and Msibi, M.I., 1996b. Measurements of airborne particulate and gaseous sulphur and nitrogen species in the area of the Azores, Atlantic Ocean. Atmospheric Environment, 30(1): 133-143.

Hatton, A.D., Malin, G., Turner, S.M. and Liss, P.S., 1996. DMSO: A significant compound in the biogeochemical cycle of DMS. In: R.P. Kiene, P.T. Visscher, M.D. Keller and G.O. Kirst

(Editors), Biological and environmental chemistry of DMSP and related sulphonium compounds. Plenum Press, New York, pp. 405-412.

Hatton, A.D., Malin, G. and Liss, P.S., 1999. Distribution of biogenic sulphur compounds during and just after the southwest monsoon in the Arabian Sea. Deep-Sea Research Part Ii-Topical Studies in Oceanography, 46(3-4): 617-632.

Hatton, A.D., 2002. Influence of photochemistry on the marine biogeochemical cycle of dimethylsulphide in the northern North Sea. Deep-Sea Research Part Ii-Topical Studies in Oceanography, 49(15): 3039-3052.

Hatton, A.D., Darroch, L. and Malin, G., 2005. The role of dimethylsulphoxide in the marine biogeochemical cycle of dimethylsulphide, Oceanography and Marine Biology: An Annual Review, Vol 42, pp. 29-55.

Heywood, J.L., Zubkov, M.V., Tarran, G.A., Fuchs, B.M. and Holligan, P.M., 2006. Prokaryoplankton standing stocks in oligotrophic gyre and equatorial provinces of the Atlantic Ocean: Evaluation of inter-annual variability. Deep-Sea Research Part Ii-Topical Studies in Oceanography, 53(14-16): 1530-1547.

Ho, D.T., 1997. The effect of rain on air-water gas-exchange. Tellus Series B-Chemical and Physical Meteorology, 49B(1): 149-158.

Ho, D.T., Asher, W.E., Bliven, L.F., Schlosser, P. and Gordan, E.L., 2000. On mechanisms of rain-induced air-water gas exchange. Journal of Geophysical Research-Oceans, 105(C10): 24045-24057.

Holmes, R.M., Aminot, A., Kerouel, R., Hooker, B.A. and Peterson, B.J., 1999. A simple and precise method for measuring ammonium in marine and freshwater ecosystems. Canadian Journal of Fisheries and Aquatic Sciences, 56(10): 1801-1808.

Holm-Hansen, O., Lorenzen, C.J., Holmes, R.W. and Strickland, J.D.H., 1965. Fluorometric determination of chlorophyll. J. Cons. Perm. Int. Explor. Mer, 30: 3-15.

Hood, E.M., Wanninkhof, R. and Merlivat, L., 2001. Short timescale variations of $f(CO_2)$ in a North Atlantic warm-core eddy: Results from the Gas-Ex 98 carbon interface ocean atmosphere (CARIOCA) buoy data. Journal of Geophysical Research-Oceans, 106(C2): 2561-2572.

Hooker, S.B., Rees, N.W. and Aiken, J., 2000. An objective methodology for identifying oceanic provinces. Progress in Oceanography, 45(3-4): 313-338.

Huebert, B.J., Zhuang, L.Z., Howell, S., Noone, K. and Noone, B., 1996. Sulfate, nitrate, methanesulfonate, chloride, ammonium, and sodium measurements from ship, island, and aircraft during the Atlantic Stratocumulus Transition Experiment Marine Aerosol Gas Exchange. Journal of Geophysical Research-Atmospheres, 101(D2): 4413-4423.

Huebert, B.J., Howell, S.G., Zhuang, L., Heath, J.A., Litchy, M.R., Wylie, D.J., Kreidler-Moss, J.L., Coppicus, S. and Pfeiffer, J.E., 1998. Filter and impactor measurements of anions and cations during the First Aerosol Characterization Experiment (ACE 1). Journal of Geophysical Research-Atmospheres, 103(D13): 16493-16509.

Huebert, B.J., Blomquist, B.W., Hare, J.E., Fairall, C.W., Johnson, J.E. and Bates, T.S., 2004. Measurement of the sea-air DMS flux and transfer velocity using eddy correlation. Geophysical Research Letters, 31(23): art. no.-L23113.

Huisman, J., Thi, N.N.P., Karl, D.M. and Sommeijer, B., 2006. Reduced mixing generates oscillations and chaos in the oceanic deep chlorophyll maximum. Nature, 439(7074): 322-325.

Hunter, K.A., 1997. Chemistry of the sea-surface microlayer. In: P.S. Liss and R.A. Duce (Editors), The Sea Surface and Global Change. Cambridge University Press, Cambridge, pp. 287-320.

Hynes, A.J., Wine, P.H. and Semmes, D.H., 1986. Kinetics and mechanism of OH reactions with organic sulfides. Journal of Physical Chemistry, 90(17): 4148-4156.

Jenkins, W.J., 1998. Studying subtropical thermocline ventilation and circulation using tritium and ^{3}He. Journal of Geophysical Research-Oceans, 103(C8): 15817-15831.

Jickells, T.D., Kelly, S.D., Baker, A.R., Biswas, K., Dennis, P.F., Spokes, L.J., Witt, M. and Yeatman, S.G., 2003. Isotopic evidence for a marine ammonia source. Geophysical Research Letters, 30(7): art. no.-1374.

Jickells, T.D., An, Z.S., Andersen, K.K., Baker, A.R., Bergametti, G., Brooks, N., Cao, J.J., Boyd, P.W., Duce, R.A., Hunter, K.A., Kawahata, H., Kubilay, N., laRoche, J., Liss, P.S., Mahowald, N., Prospero, J.M., Ridgwell, A.J., Tegen, I. and Torres, R., 2005. Global iron connections between desert dust, ocean biogeochemistry, and climate. Science, 308(5718): 67-71.

Johansson, O. and Wedborg, M., 1980. Ammonia-ammonium equilibrium in seawater at temperatures between 5 and 25°C. Journal of Solution Chemistry, 9(1): 37-44.

Johnson, M., 2004. The air-sea flux of ammonia, University of East Anglia, Norwich.

Keller, M.D., Bellows, W.K. and Guillard, R.R.L., 1989. Dimethyl sulphide production in marine phytoplankton. In: E.S. Saltzman and C.W. J. (Editors), Biogenic sulphur in the environment. American Chemical Society, Washington DC, pp. 167-182.

Keller, M.D., Kiene, R.P., Matrai, P.A. and Bellows, W.K., 1999. Production of glycine betaine and dimethylsulfoniopropionate in marine phytoplankton. II. N-limited chemostat cultures. Marine Biology, 135(2): 249-257.

Kettle, A.J., Andreae, M.O., Amouroux, D., Andreae, T.W., Bates, T.S., Berresheim, H., Bingemer, H., Boniforti, R., Curran, M.A.J., DiTullio, G.R., Helas, G., Jones, G.B., Keller, M.D., Kiene, R.P., Leck, C., Levasseur, M., Malin, G., Maspero, M., Matrai, P., McTaggart, A.R., Mihalopoulos, N., Nguyen, B.C., Novo, A., Putaud, J.P., Rapsomanikis, S., Roberts, G., Schebeske, G., Sharma, S., Simo, R., Staubes, R., Turner, S. and Uher, G., 1999. A global database of sea surface dimethylsulfide (DMS) measurements and a procedure to predict sea surface DMS as a function of latitude, longitude, and month. Global Biogeochemical Cycles, 13(2): 399-444.

Kettle, A.J. and Andreae, M.O., 2000. Flux of dimethylsulfide from the oceans: A comparison of updated data seas and flux models. Journal of Geophysical Research-Atmospheres, 105(D22): 26793-26808.

Khoo, K.H., Culberson, C.H. and Bates, R.G., 1977. Thermodynamics of dissociation of ammonium ion in seawater from 5 to 40°C. Journal of Solution Chemistry, 6(4): 281-290.

Kieber, D.J., Jiao, J.F., Kiene, R.P. and Bates, T.S., 1996. Impact of dimethylsulfide photochemistry on methyl sulfur cycling in the equatorial Pacific Ocean. Journal of Geophysical Research-Oceans, 101(C2): 3715-3722.

Kiene, R.P., Linn, L.J., Gonzalez, J., Moran, M.A. and Bruton, J.A., 1999. Dimethylsulfoniopropionate and methanethiol are important precursors of methionine and protein-sulfur in marine bacterioplankton. Applied and Environmental Microbiology, 65(10): 4549-4558.

Kiene, R.P. and Linn, L.J., 2000. The fate of dissolved dimethylsulfoniopropionate (DMSP) in seawater: Tracer studies using ^{35}S-DMSP. Geochimica Et Cosmochimica Acta, 64(16): 2797-2810.

Kiene, R.P., Linn, L.J. and Bruton, J.A., 2000. New and important roles for DMSP in marine microbial communities. Journal of Sea Research, 43(3-4): 209-224.

Kirchman, D.L., 1994. The uptake of inorganic nutrients by heterotrophic bacteria. Microbial Ecology, 28(2): 255-271.

Koga, S. and Tanaka, H., 1993. Numerical study of the oxidation process of dimethylsulfide in the marine atmosphere. Journal of Atmospheric Chemistry, 17(3): 201-228.

Koga, S. and Tanaka, H., 1996. Simulations of seasonal variations of sulfur compounds in the remote marine atmosphere. Journal of Atmospheric Chemistry, 23(2): 163-192.

Koga, S. and Tanaka, H., 1999. Modeling the methanesulfonate to non-sea-salt sulfate molar ratio and dimethylsulfide oxidation in the atmosphere. Journal of Geophysical Research-Atmospheres, 104(D11): 13735-13747.

Korhonen, P., Kulmala, M., Laaksonen, A., Viisanen, Y., McGraw, R. and Seinfeld, J.H., 1999. Ternary nucleation of H_2SO_4, NH_3, and H_2O in the atmosphere. Journal of Geophysical Research-Atmospheres, 104(D21): 26349-26353.

Kraemer, H.C. and Thiemann, S., 1987. How many subjects? Statistical power analysis in research. SAGE Publications, London.

Kuypers, M.M.M., Sliekers, A.O., Lavik, G., Schmid, M., Jorgensen, B.B., Kuenen, J.G., Damste, J.S.S., Strous, M. and Jetten, M.S.M., 2003. Anaerobic ammonium oxidation by anammox bacteria in the Black Sea. Nature, 422(6932): 608-611.

Lacaux, J.P., Brustet, J.M., Delmas, R., Menaut, J.C., Abbadie, L., Bonsang, B., Cachier, H., Baudet, J., Andreae, M.O. and Helas, G., 1995. Biomass burning in the tropical savannas of Ivory Coast: An overview of the field experiment Fire of Savannas (FOS/DECAFE 91). Journal of Atmospheric Chemistry, 22(1-2): 195-216.

Leck, C., Heintzenberg, J. and Engardt, M., 2002a. A meridional profile of the chemical composition of submicrometre particles over the East Atlantic Ocean: regional and hemispheric variabilities. Tellus Series B-Chemical and Physical Meteorology, 54(4): 377-394.

Leck, C., Norman, M., Bigg, E.K. and Hillamo, R., 2002b. Chemical composition and sources of the high Arctic aerosol relevant for cloud formation. Journal of Geophysical Research-Atmospheres, 107(D12): art. no.-4135.

Leck, C. and Bigg, E.K., 2005. Biogenic particles in the surface microlayer and overlaying atmosphere in the central Arctic Ocean during summer. Tellus Series B-Chemical and Physical Meteorology, 57(4): 305-316.

Lee, P.A. and de Mora, S.J., 1999. Intracellular dimethylsulfoxide (DMSO) in unicellular marine algae: Speculations on its origin and possible biological, role. Journal of Phycology, 35(1): 8-18.

Lee, P.A., Haase, R., de Mora, S.J., Chanut, J.P. and Gosselin, M., 1999. Dimethylsulfoxide (DMSO) and related sulfur compounds in the Saguenay Fjord, Quebec. Canadian Journal of Fisheries and Aquatic Sciences, 56(9): 1631-1638.

Lee, P.A., de Mora, S.J., Gosselin, M., Levasseur, M., Bouillon, R.C., Nozais, C. and Michel, C., 2001. Particulate dimethylsulfoxide in Arctic sea-ice algal communities: The cryoprotectant hypothesis revisited. Journal of Phycology, 37(4): 488-499.

Legrand, M., Fenietsaigne, C., Saltzman, E.S., Germain, C., Barkov, N.I. and Petrov, V.N., 1991. Ice-core record of oceanic emissions of dimethylsulfide during the last climate cycle. Nature, 350(6314): 144-146.

Legrand, M., Ducroz, F., Wagenbach, D., Mulvaney, R. and Hall, J., 1998. Ammonium in coastal Antarctic aerosol and snow: Role of polar ocean and penguin emissions. Journal of Geophysical Research-Atmospheres, 103(D9): 11043-11056.

Legrand, M.R., Delmas, R.J. and Charlson, R.J., 1988. Climate forcing implications from Vostok ice-core sulfate data. Nature, 334(6181): 418-420.

Levitus, S., 1982. Climatological atlas of the world ocean, *NOAA Prof. Pap. 13*, 173 pp. U.S. Govt. Printing Off., Washington D.C.

Libes, S.M., 1992. An introduction to marine biogeochemistry. John Wiley and Sons, Inc., New York.

Liss, P.S. and Slater, P.G., 1974. Flux of gases across the air-sea interface. Nature, 247(5438): 181-184.

Liss, P.S. and Merlivat, L., 1986. Air-sea gas exchange rates: introduction and synthesis. In: P. Buatmenard (Editor), The role of air-sea exchange in geochemical cycling. Reidel, pp. 113-127.

Liss, P.S. and Galloway, J.N., 1993. Air-sea exchange of sulphur and nitrogen and their interaction in the marine atmosphere. In: R. Wollast, Mackenzie, F.T. and Chou, L. (Editor), Interactions of C, N, P and S biogeochemical cycles and global change. Springer-Verlag, Berlin Heidelberg, pp. 259-281.

Longhurst, A., 1995. Seasonal cycles of pelagic production and consumption. Progress in Oceanography, 36(2): 77-167.

Malin, G., Turner, S.M., Liss, P.S. and Aiken, 1992. Sulfur: the plankton/climate connection. Journal of Phycology, 28(5): 590-597.

Malin, G., Liss, P.S. and Turner, S.M., 1994. Dimethylsulfide: Production and atmospheric consequences. In: J.C. Green and B.S.C. Leadbeater (Editors), The Haptophyte Algae. Clarendon Press, Oxford, pp. 303-320.

Malin, G., Wilson, W.H., Bratbak, G., Liss, P.S. and Mann, N.H., 1998. Elevated production of dimethylsulfide resulting from viral infection of cultures of *Phaeocystis pouchetii*. Limnology and Oceanography, 43(6): 1389-1393.

Malmstrom, R.R., Kiene, R.P., Vila, M. and Kirchman, D.L., 2005. Dimethylsulfoniopropionate (DMSP) assimilation by *Synechococcus* in the Gulf of Mexico and northwest Atlantic Ocean. Limnology and Oceanography, 50(6): 1924-1931.

Mantoura, R.F.C., Jeffrey, S.W., Llewellyn, C.A., Claustre, H. and Morales, C.E., 1997. Comparison between spectrophotometric, fluorometric and HPLC methods for chlorophyll analysis. In: S.W. Jeffrey, R.F.C. Mantoura and S.W. Wright (Editors), Phytoplankton pigments in oceanography. UNESCO, Paris.

McArdle, N., Liss, P. and Dennis, P., 1998. An isotopic study of atmospheric sulphur at three sites in Wales and at Mace Head, Eire. Journal of Geophysical Research-Atmospheres, 103(D23): 31079-31094.

McArdle, N.C. and Liss, P.S., 1995. Isotopes and atmospheric sulfur. Atmospheric Environment, 29(18): 2553-2556.

McClain, C.R., Signorini, S.R. and Christian, J.R., 2004. Subtropical gyre variability observed by ocean-color satellites. Deep-Sea Research Part Ii-Topical Studies in Oceanography, 51(1-3): 281-301.

McKee, C.M., 2001. Biogeochemical cycles of ammonia and dimethylsulphide in the marine environment, University of East Anglia, Norwich, 223 pp.

Montegut, C.D., Madec, G., Fischer, A.S., Lazar, A. and Iudicone, D., 2004. Mixed layer depth over the global ocean: An examination of profile data and a profile-based climatology. Journal of Geophysical Research-Oceans, 109(C12): art. no.-C12003.

Moore, C.M., Suggett, D.J., Hickman, A.E., Kim, Y.N., Tweddle, J.F., Sharples, J., Geider, R.J. and Holligan, P.M., 2006. Phytoplankton photoacclimation and photoadaptation in response to environmental gradients in a shelf sea. Limnology and Oceanography, 51(2): 936–949.

Nightingale, P.D., Liss, P.S. and Schlosser, P., 2000a. Measurements of air-sea gas transfer during an open ocean algal bloom. Geophysical Research Letters, 27(14): 2117-2120.

Nightingale, P.D., Malin, G., Law, C.S., Watson, A.J., Liss, P.S., Liddicoat, M.I., Boutin, J. and Upstill-Goddard, R.C., 2000b. In situ evaluation of air-sea gas exchange parameterizations using novel conservative and volatile tracers. Global Biogeochemical Cycles, 14(1): 373-387.

Niki, T., Kunugi, M. and Otsuki, A., 2000. DMSP-lyase activity in five marine phytoplankton species: its potential importance in DMS production. Marine Biology, 136(5): 759-764.

Norman, M. and Leck, C., 2005. Distribution of marine boundary layer ammonia over the Atlantic and Indian Oceans during the Aerosols99 cruise. Journal of Geophysical Research-Atmospheres, 110(D16).

O'Dowd, C.D., Lowe, J.A., Smith, M.H., Davison, B., Hewitt, N. and Harrison, R.M., 1997a. Biogenic sulphur emissions and inferred non-sea-salt-sulphate cloud condensation nuclei in and around Antarctica. Journal of Geophysical Research-Atmospheres, 102(11D): 12839-12854.

O'Dowd, C.D., Smith, M.H., Consterdine, I.E. and Lowe, J.A., 1997b. Marine aerosol, sea-salt, and the marine sulphur cycle: A short review. Atmospheric Environment, 31(1): 73-80.

O'Dowd, C.D., Facchini, M.C., Cavalli, F., Ceburnis, D., Mircea, M., Decesari, S., Fuzzi, S., Yoon, Y.J. and Putaud, J.P., 2004. Biogenically driven organic contribution to marine aerosol. Nature, 431(7009): 676-680.

Owens, N.J.P., Galloway, J.N. and Duce, R.A., 1992. Episodic atmospheric nitrogen deposition to oligotrophic oceans. Nature, 357(6377): 397-399.

Parkhill, J.P., Maillet, G. and Cullen, J.J., 2001. Fluorescence-based maximal quantum yield for PSII as a diagnostic of nutrient stress. Journal of Phycology, 37(4): 517-529.

Patris, N., Mihalopoulos, N., Baboukas, E.D. and Jouzel, J., 2000. Isotopic composition of sulfur in size-resolved marine aerosols above the Atlantic Ocean. Journal of Geophysical Research-Atmospheres, 105(D11): 14449-14457.

Pilcher, H., 2005. Microbiology: Pipe dreams. Nature, 437(7063): 1227-1228.

Porra, R.J., Pfundel, E.E. and Engel, N., 1997. Metabolism and function of photosynthetic pigments. In: S.W. Jeffrey, R.F.C. Mantoura and S.W. Wright (Editors), Phytoplankton pigments in oceanography. UNESCO, Paris.

Poulton, A.J., Holligan, P.M., Hickman, A.E., Kim, Y.N., Adey, T.R., Stinchcombe, M.C., Holeton, C., Root, S. and Woodward, E.M.S., 2006. Phytoplankton carbon fixation, chlorophyll-biomass and diagnostic pigments in the Atlantic Ocean. Deep-Sea Research Part Ii-Topical Studies in Oceanography, 53(14-16): 1593-1610.

Pryor, S.C. and Sorensen, L.L., 2002. Dry deposition of reactive nitrogen to marine environments: recent advances and remaining uncertainties. Marine Pollution Bulletin, 44(12): 1336-1340.

Putaud, J.P. and Nguyen, B.C., 1996. Assessment of dimethylsulfide sea-air exchange rate. Journal of Geophysical Research-Atmospheres, 101(D2): 4403-4411.

Quinn, P.K., Charlson, R.J. and Zoller, W.H., 1987. Ammonia, the dominant base in the remote marine troposphere: a review. Tellus, 39(B): 413-425.

Quinn, P.K., Charlson, R.J. and Bates, T.S., 1988. Simultaneous observations of ammonia in the atmosphere and ocean. Nature, 335(6188): 336-338.

Quinn, P.K., Bates, T.S., Johnson, J.E., Covert, D.S. and Charlson, R.J., 1990. Interactions between the sulfur and reduced nitrogen cycles over the central Pacific Ocean. Journal of Geophysical Research-Atmospheres, 95(D10): 16405-16416.

Quinn, P.K., Asher, W.E. and Charlson, R.J., 1992. Equilibria of the marine multiphase ammonia system. Journal of Atmospheric Chemistry, 14(1-4): 11-30.

Quinn, P.K., Barrett, K.J., Dentener, F.J., Lipschultz, F. and Six, K.D., 1996. Estimation of the air sea exchange of ammonia for the North Atlantic Basin. Biogeochemistry, 35(1): 275-304.

Raes, F., Van Dingenen, R., Vignati, E., Wilson, J., Putaud, J.P., Seinfeld, J.H. and Adams, P., 2000. Formation and cycling of aerosols in the global troposphere. Atmospheric Environment, 34(25): 4215-4240.

Rees, A.P., Malcolm, E., Woodward, S., Robinson, C., Cummings, D.G., Tarran, G.A. and Joint, I., 2002. Size-fractionated nitrogen uptake and carbon fixation during a developing coccolithophore bloom in the North Sea during June 1999. Deep-Sea Research Part Ii-Topical Studies in Oceanography, 49(15): 2905-2927.

Rees, A.P., Woodward, E.M.S. and Joint, I., 2006. Concentrations and uptake of nitrate and ammonium in the Atlantic Ocean between 60°N and 50°S. Deep-Sea Research Part Ii-Topical Studies in Oceanography, 53(14-16): 1649-1665.

Roberts, M.J. and Russo, R., 1999. A student's guide to analysis of variance. Routledge, London.

Robinson, C., Poulton, A.J., Holligan, P., Baker, A.R., Forster, G., Gist, N., Jickells, T.D., Malin, G., Upstill-Goddard, R.C., Williams, R.G., Woodward, E.M.S. and Zubkov, M., 2006. The Atlantic Meridional Transect Programme (AMT): A contextual view 1995 - 2005. Deep-Sea Research Part Ii-Topical Studies in Oceanography, 53(14-16): 1485-1515.

Rodrigues, R.M.N.V., 1998. Interaction between the bacterial and phytoplanktonic inorganic nitrogenous nutrition, University of Wales, Bangor.

Saigne, C. and Legrand, M., 1987. Measurements of methanesulfonic acid in Antarctic ice. Nature, 330(6145): 240-242.

Saltzman, E.S., King, D.B., Holmen, K. and Leck, C., 1993. Experimental determination of the diffusion coefficient of dimethylsulfide in water. Journal of Geophysical Research-Oceans, 98(C9): 16481-16486.

Savoie, D.I., Prospero, J.M., Larsen, R.J., Huang, F., Izaguirre, M.A., Huang, T., Snowdon, T.H., Custals, L. and Sanderson, C.G., 1993. Nitrogen and sulfur species in Antarctic aerosols at Mawson, Palmer Station, and Marsh (King George Island). Journal of Atmospheric Chemistry, 17(2): 95-122.

Scarratt, M., Cantin, G., Levasseur, M. and Michaud, S., 2000. Particle size-fractionated kinetics of DMS production: where does DMSP cleavage occur at the microscale? Journal of Sea Research, 43(3-4): 245-252.

Schlesinger, W.H., 1991. Biogeochemistry: An analysis of global change. Academic Press, Inc., San Diego.

Sciare, J., Mihalopoulos, N. and Dentener, F.J., 2000. Interannual variability of atmospheric dimethylsulfide in the southern Indian Ocean. Journal of Geophysical Research-Atmospheres, 105(D21): 26369-26377.

Seinfeld, J.H. and Pandis, S.N., 1998. Atmospheric chemistry and physics: From air pollution to climate change. John Wiley and Sons, Inc., Canada.

Sieburth, J.M., 1960. Acrylic acid, an antibiotic principle in *Phaeocystis* blooms in Antarctic waters. Science, 132(3428): 676-677.

Sievering, H., Boatman, J., Gorman, E., Kim, Y., Anderson, L., Ennis, G., Luria, M. and Pandis, S., 1992. Removal of sulfur from the marine boundary layer by ozone oxidation in sea-salt aerosols. Nature, 360(6404): 571-573.

Silvente, E. and Legrand, M., 1993. Ammonium to sulfate ratio in aerosol and snow of Greenland and Antarctic regions. Geophysical Research Letters, 20(8): 687-690.

Simo, R., Hatton, A.D., Malin, G. and Liss, P.S., 1998. Particulate dimethyl sulphoxide in seawater: production by microplankton. Marine Ecology-Progress Series, 167: 291-296.

Simo, R. and Pedros-Alio, C., 1999. Role of vertical mixing in controlling the oceanic production of dimethyl sulphide. Nature, 402(6760): 396-399.

Simo, R., 2001. Production of atmospheric sulfur by oceanic plankton: biogeochemical, ecological and evolutionary links. Trends in Ecology & Evolution, 16(6): 287-294.

Simo, R., Archer, S.D., Pedros-Alio, C., Gilpin, L. and Stelfox-Widdicombe, C.E., 2002. Coupled dynamics of dimethylsulfoniopropionate and dimethylsulfide cycling and the microbial food web in surface waters of the North Atlantic. Limnology and Oceanography, 47(1): 53-61.

Simo, R. and Dachs, J., 2002. Global ocean emission of dimethylsulfide predicted from biogeophysical data. Global Biogeochemical Cycles, 16(4): art. no.-1078.

Simo, R., 2004. From cells to globe: approaching the dynamics of DMS(P) in the ocean at multiple scales. Canadian Journal of Fisheries and Aquatic Sciences, 61(5): 673-684.

Slezak, D., Brugger, A. and Herndl, G.J., 2001. Impact of solar radiation on the biological removal of dimethylsulfoniopropionate and dimethylsulfide in marine surface waters. Aquatic Microbial Ecology, 25(1): 87-97.

Slezak, D.M., Puskaric, S. and Herndl, G.J., 1994. Potential role of acrylic acid in bacterioplankton communities in the sea. Marine Ecology-Progress Series, 105(1-2): 191-197.

Smethie, W.M., Takahashi, T. and Chipman, D.W., 1985. Gas-Exchange and CO_2 Flux in the Tropical Atlantic-Ocean Determined from ^{222}Rn and pCO_2 Measurements. Journal of Geophysical Research-Oceans, 90(NC4): 7005-7022.

Smith, S.D., 1988. Coefficients for sea surface wind stress, heat flux, and wind profiles as a function of wind speed and temperature. Journal of Geophysical Research-Oceans, 93(C12): 15467-15472.

Spokes, L.J., Yeatman, S.G., Cornell, S.E. and Jickells, T.D., 2000. Nitrogen deposition to the eastern Atlantic Ocean. The importance of south-easterly flow. Tellus Series B-Chemical and Physical Meteorology, 52(1): 37-49.

Stefels, J. and van Boekel, W.H.M., 1993. Production of DMS from dissolved DMSP in axenic cultures of the marine phytoplankton species *Phaeocystis* sp. Marine Ecology-Progress Series, 97(1): 11-18.

Stefels, J., 2000. Physiological aspects of the production and conversion of DMSP in marine algae and higher plants. Journal of Sea Research, 43(3-4): 183-197.

Steinke, M., Wolfe, G.V. and Kirst, G.O., 1998. Partial characterisation of dimethylsulfoniopropionate (DMSP) lyase isozymes in 6 strains of *Emiliania huxleyi*. Marine Ecology-Progress Series, 175: 215-225.

Steinke, M., Malin, G., Archer, S.D., Burkill, P.H. and Liss, P.S., 2002a. DMS production in a coccolithophorid bloom: evidence for the importance of dinoflagellate DMSP lyases. Aquatic Microbial Ecology, 26(3): 259-270.

Steinke, M., Malin, G., Gibb, S.W. and Burkill, P.H., 2002b. Vertical and temporal variability of DMSP lyase activity in a coccolithophorid bloom in the northern North Sea. Deep-Sea Research Part II-Topical Studies in Oceanography, 49(15): 3001-3016.

Steinke, M., Malin, G. and Liss, P.S., 2002c. Trophic interactions in the sea: An ecological role for climate relevant volatiles? Journal of Phycology, 38(4): 630-638.

Steinke, M., Evans, C., Lee, G.A. and Malin, G., 2006a. Substrate kinetics of DMSP-lyases in axenic cultures and mesocosm populations of *Emiliania huxleyi*. Aquatic Sciences *Submitted*.

Steinke, M., Stefels, J. and Stamhuis, E., 2006b. Dimethyl sulfide (DMS) triggers search behaviour in copepods. Limnology and Oceanography.

Strom, S., Wolfe, G., Holmes, J., Stecher, H., Shimeneck, C., Lambert, S. and Moreno, E., 2003a. Chemical defense in the microplankton I: Feeding and growth rates of heterotrophic protists on the DMS-producing phytoplankter *Emiliania huxleyi*. Limnology and Oceanography, 48(1): 217-229.

Strom, S., Wolfe, G., Slajer, A., Lambert, S. and Clough, J., 2003b. Chemical defense in the microplankton II: Inhibition of protist feeding by *ß*-dimethylsulfoniopropionate (DMSP). Limnology and Oceanography, 48(1): 230-237.

Stumm, W. and Morgan, J.J., 1981. Aquatic chemistry. Wiley Interscience, New York.

Sunda, W., Kieber, D.J., Kiene, R.P. and Huntsman, S., 2002. An antioxidant function for DMSP and DMS in marine algae. Nature, 418(6895): 317-320.

Suttle, C.A., Fuhrman, J.A. and Capone, D.G., 1990. Rapid ammonium cycling and concentration-dependent partitioning of ammonium and phosphate: Implications for carbon transfer in planktonic communities. Limnology and Oceanography, 35(2): 424-433.

Tanaka, N., Rye, D.M., Xiao, Y. and Lasaga, A.C., 1994. Use of stable sulfur isotope systematics for evaluating oxidation reaction pathways and in-cloud-scavenging of sulfur dioxide in the atmosphere. Geophysical Research Letters, 21(14): 1519-1522.

Tans, P.P., Fung, I.Y. and Takahashi, T., 1990. Observational constraints on the global atmospheric CO_2 budget. Science, 247(4949): 1431-1438.

Toole, D.A., Kieber, D.J., Kiene, R.P., Siegel, D.A. and Nelson, N.B., 2003. Photolysis and the dimethylsulfide (DMS) summer paradox in the Sargasso Sea. Limnology and Oceanography, 48(3): 1088-1100.

Toole, D.A. and Siegel, D.A., 2004. Light-driven cycling of dimethylsulfide (DMS) in the Sargasso Sea: Closing the loop. Geophysical Research Letters, 31(9): art. no.-L09308.

Trevena, A.J., Jones, G.B., Wright, S.W. and van den Enden, R.L., 2003. Profiles of dimethylsulphoniopropionate (DMSP), algal pigments, nutrients, and salinity in the fast ice of Prydz Bay, Antarctica. Journal of Geophysical Research-Oceans, 108(C5): art. no.-3145.

Tupas, L. and Koike, I., 1991. Simultaneous Uptake and Regeneration of Ammonium by Mixed Assemblages of Heterotrophic Marine-Bacteria. Marine Ecology-Progress Series, 70(3): 273-282.

Turner, S.M., Malin, G., Liss, P.S., Harbour, D.S. and Holligan, P.M., 1988. The seasonal variation of dimethyl sulfide and dimethylsulfoniopropionate concentrations in nearshore waters. Limnology and Oceanography, 33(3): 364-375.

Turner, S.M., Malin, G., Bagander, L.E. and Leck, C., 1990. Interlaboratory calibration and sample analysis of dimethyl sulfide in water. Marine Chemistry, 29(1): 47-62.

Turner, S.M., Nightingale, P.D., Broadgate, W. and Liss, P.S., 1995. The distribution of dimethyl sulfide and dimethylsulphoniopropionate in Antarctic waters and sea ice. Deep-Sea Research Part Ii-Topical Studies in Oceanography, 42(4-5): 1059-1080.

Twomey, S., 1977. Influence of pollution on shortwave albedo of clouds. Journal of the Atmospheric Sciences, 34(7): 1149-1152.

Upstill-Goddard, R.C., Frost, T., Henry, G.R., Franklin, M., Murrell, J.C. and Owens, N.J.P., 2003. Bacterioneuston control of air-water methane exchange determined with a laboratory gas exchange tank. Global Biogeochemical Cycles, 17(4): art. no.-1108.

Van Alstyne, K.L. and Houser, L.T., 2003. Dimethylsulfide release during macroinvertebrate grazing and its role as an activated chemical defense. Marine Ecology-Progress Series, 250: 175-181.

van Leeuwe, M.A. and Stefels, J., 1998. Effects of iron and light stress on the biochemical composition of Antarctic *Phaeocystis* sp. (Prymnesiophyceae). II. Pigment composition. Journal of Phycology, 34(3): 496-503.

van Rijssel, M. and Buma, A.G.J., 2002. UV radiation induced stress does not affect DMSP synthesis in the marine prymnesiophyte *Emiliania huxleyi*. Aquatic Microbial Ecology, 28(2): 167-174.

von Glasow, R. and Crutzen, P.J., 2004. Model study of multiphase DMS oxidation with a focus on halogens. Atmospheric Chemistry and Physics, 4: 589-608.

Wadleigh, M.A., 2004. Sulphur isotopic composition of aerosols over the western North Atlantic Ocean. Canadian Journal of Fisheries and Aquatic Sciences, 61(5): 817-825.

Wanninkhof, R., 1992. Relationship between wind speed and gas exchange over the ocean. Journal of Geophysical Research-Oceans, 97(C5): 7373-7382.

Wanninkhof, R. and McGillis, W.R., 1999. A cubic relationship between air-sea CO_2 exchange and wind speed. Geophysical Research Letters, 26(13): 1889-1892.

Warneck, P., 1988. Chemistry of the natural atmosphere. International Geophysics Series, 41. Academic Press, San Diego, California.

Watson, A.J., Upstill-Goddard, R.C. and Liss, P.S., 1991. Air-sea gas exchange in rough and stormy seas measured by a dual-tracer technique. Nature, 349(6305): 145-147.

Wheeler, P.A. and Kokkinakis, S.A., 1990. Ammonium recycling limits nitrate use in the oceanic sub-Arctic Pacific. Limnology and Oceanography, 35(6): 1267-1278.

Whung, P.Y., Saltzman, E.S., Spencer, M.J., Mayewski, P.A. and Gundestrup, N., 1994. Two-hundred-year record of biogenic sulfur in a South Greenland ice core (20D). Journal of Geophysical Research-Atmospheres, 99(D1): 1147-1156.

Wolfe, G.V. and Steinke, M., 1996. Grazing-activated production of dimethyl sulfide (DMS) by two clones of *Emiliania huxleyi*. Limnology and Oceanography, 41(6): 1151-1160.

Wolfe, G.V., Steinke, M. and Kirst, G.O., 1997. Grazing-activated chemical defence in a unicellular marine alga. Nature, 387(6636): 894-897.

Wolfe, G.V., Strom, S.L., Holmes, J.L., Radzio, T. and Brady Olson, M., 2002. Dimethylsulfoniopropionate cleavage by marine phytoplankton in response to mechanical, chemical, or dark stress. Journal of Phycology, 38: 948-960.

Wolff, E.W., Fischer, H., Fundel, F., Ruth, U., Twarloh, B., Littot, G.C., Mulvaney, R., Rothlisberger, R., de Angelis, M., Boutron, C.F., Hansson, M., Jonsell, U., Hutterli, M.A., Lambert, F., Kaufmann, P., Stauffer, B., Stocker, T.F., Steffensen, J.P., Bigler, M., Siggaard-Andersen, M.L., Udisti, R., Becagli, S., Castellano, E., Severi, M., Wagenbach, D., Barbante, C., Gabrielli, P. and Gaspari, V., 2006. Southern Ocean sea-ice extent, productivity and iron flux over the past eight glacial cycles. Nature, 440(7083): 491-496.

Wong, P.K. and Wang, Y.H., 1997. Determination of the Henry's Law constant for dimethyl sulfide in seawater. Chemosphere, 35(3): 535-544.

Woodward, E.M.S. and Rees, A.P., 2001. Nutrient distributions in an anticyclonic eddy in the northeast Atlantic Ocean, with reference to nanomolar ammonium concentrations. Deep-Sea Research Part Ii-Topical Studies in Oceanography, 48(4-5): 775-793.

Wright, S.W. and Jeffrey, S.W., 1997. High-resolution HPLC system for chlorophylls and carotenoids of marine phytoplankton. In: S.W. Jeffrey, R.F.C. Mantoura and S.W. Wright (Editors), Phytoplankton pigments in oceanography. UNESCO, Paris.

Yin, F.D., Grosjean, D., Flagan, R.C. and Seinfeld, J.H., 1990a. Photooxidation of dimethyl sulfide and dimethyl disulfide 2. Mechanism evaluation. Journal of Atmospheric Chemistry, 11(4): 365-399.

Yin, F.D., Grosjean, D. and Seinfeld, J.H., 1990b. Photooxidation of dimethyl sulfide and dimethyl disulfide 1. Mechanism development. Journal of Atmospheric Chemistry, 11(4): 309-364.

Zeyer, J., Eicher, P., Wakeham, S.G. and Schwarzenbach, R.P., 1987. Oxidation of dimethyl sulfide to dimethylsulfoxide by phototrophic purple bacteria. Applied and Environmental Microbiology, 53(9): 2026-2032.

Zhao, F.J., Hawkesford, M.J. and McGrath, S.P., 1999. Sulphur assimilation and effects on yield and quality of wheat. Journal of Cereal Science, 30(1): 1-17.

Zinder, S.H. and Brock, T.D., 1978. Production of methane and carbon dioxide from methane thiol and dimethyl sulfide by anaerobic lake sediments. Nature, 273(5659): 226-228.

Zubkov, M., Linn, L.J., Amann, R. and Kiene, R.P., 2004. Temporal patterns of biological dimethylsulfide (DMS) consumption during laboratory-induced phytoplankton bloom cycles. Marine Ecology-Progress Series, 271: 77-86.

Zubkov, M.V., Sleigh, M.A., Burkill, P.H. and Leakey, R.J.G., 2000. Picoplankton community structure on the Atlantic Meridional Transect: a comparison between seasons. Progress in Oceanography, 45(3-4): 369-386.

Zubkov, M.V., Fuchs, B.M., Archer, S.D., Kiene, R.P., Amann, R. and Burkill, P.H., 2001. Linking the composition of bacterioplankton to rapid turnover of dissolved dimethylsulphoniopropionate in an algal bloom in the North Sea. Environmental Microbiology, 3(5): 304-311.

Zubkov, M.V., Fuchs, B.M., Archer, S.D., Kiene, R.P., Amann, R. and Burkill, P.H., 2002. Rapid turnover of dissolved DMS and DMSP by defined bacterioplankton communities in the stratified euphotic zone of the North Sea. Deep-Sea Research Part Ii-Topical Studies in Oceanography, 49(15): 3017-3038.

Then I woke up and it was all a dream! The end.